Fall 2020

MANIPULATING SINGLE POLYMER MOLECULES FOR APPLICATIONS IN NANOMATERIALS

Ruiwen Chen
University of New Hampshire, Durham

MANIPULATING SINGLE POLYMER MOLECULES FOR APPLICATIONS IN NANOMATERIALS

BY

RUIWEN CHEN

B.S., Zhejiang Sci-Tech University, 2013

DISSERTATION

Submitted to the University of New Hampshire
in Partial Fulfillment of
the Requirements for the Degree of

Doctor of Philosophy
in
Chemistry

September, 2020

This dissertation was examined and approved in partial fulfillment of the requirements for the degree of Doctor of Philosophy in Chemistry by:

Dissertation Director, Dr. Erik Berda, Professor of Chemistry and Materials Science

Dr. John Tsavalas, Associate Professor of Chemistry and Materials Science

Dr. Marc Boudreau, Assistant Professor of Chemistry

Dr. Patricia Wilkinson, Affiliate Assistant Professor of Chemistry

Dr. Ashley Hanlon, Product Development Engineer, Formosa Plastics Corporation

On July 31st, 2020

Approval signatures are on file with the University of New Hampshire Graduate School.

ACKNOWLEDGEMENTS

I would like to express my deepest appreciation and gratitude to my advisor Dr. Erik Berda, for the patient guidance he provided me, all the way from when I applied for the program, through to the completion of this degree. Dr. Berda has been extremely supportive of my career goals and has worked actively to provide me with the resources to pursue those goals. As my teacher and mentor, he has taught me more than I could ever give him credit for here. He has shown me, by his example, what a good scientist and person should be. I am truly fortunate to have had the opportunity to work with him.

I would like to thank Dr. Ashley Hanlon who extended a great amount of assistance since I entered the group. Ashley taught me everything, from the English names of glassware and techniques to setup and workup experiments, to the maintenance of instruments and writing of quarterly reports. The completion of my studies would not have been possible without the help of Ashley.

I would like to extend my sincere thanks to my committee, Dr. Pat Wilkinson for training me NMR operations and helping me with NMR problems all the time, Dr. John Tsavalas and Dr. Marc Boudreau for your insightful comments and suggestions for my research projects.

Special thanks to Dr. Jesse Ambrose for the relentless help with pumps, glove box and GC. Many thanks to Cindi Rowher, Laura Bicknell and Kristen Blackwell for their all-the-time kind help. I very much appreciate Karen who prefers to be called KareBear, for the company and candies she gave me when working late nights in Parsons.

I would like to thank my parents, whose love and guidance are with me in whatever I pursue. Thanks also to my loving and supportive boyfriend Ding Tian for your continuous encouragement over the years.

在 UNH 的博士生生涯即将走入尾声，回想起五年前初次踏上这片土地，波士顿机场外明媚的阳光穿过立交桥的缝隙投下斑驳的影子，忙碌的大巴车在候机楼外走走停停，彼时的兴奋和紧张还历历在目。回首往事，感谢命运对我的眷顾，让我在异国他乡结识了诸多可爱的人儿。感谢那些在我生活中画下浓墨重彩的同事同学和亲朋好友，也感谢那些擦肩而过时对我善意微笑的陌生人，谢谢你们以各种各样的方式装点了我的生活。

我可爱的博导 Berda 老师在我对化学一窍不通时接纳我入组，多年来从未嫌弃我的愚钝，帮我夯实基础，教我分析问题，培养我成为一名独立的科研人。Berda 带我参加会议拓展人脉，替我宣传物色合适的工作机会，传授给我许多宝贵的职场和人生经验，是我的良师益友。学业上的挑战和落差导致我读博期间心态起起伏伏，若不是老师持续不断的关切和鞭策，我断然无法走到今天。回首往事，感激之情不胜言表。能成为您的学生，是我的荣幸和骄傲。

我亲爱的师姐 Ashley 从我进实验室的第一天开始手把手地教我，从每一件玻璃仪器的英文名称，到每一项实验操作的要点，从如何写好季度工作汇报，到如何进行仪器的维护保养，都是师姐一点点耐心地教给我。师姐人美心善，学业优异还是一名优秀的管理者，这些年来一直是我努力的榜样。

感谢 Pat 老师帮我解决核磁上各种各样的问题，培训我每台仪器的使用，教我谱图处理的技巧，我参加过很多次 Pat 办过的核磁小讲堂，在家工作期间的小测验和练习题都让我收获良多。

感谢我其他的答辩委员会成员，Tsavalas 老师和 Boudreau 老师还有曾经在我委员会的李老师，都曾在科研上给过我许多宝贵的建议和指导。

感谢 Jesse, 帮我修泵,修加热台，教我如何维护手套箱的检测器，教我如何换氢气瓶。

感谢 Cindi，Laura 和 Kristen，我有很多很多的琐事麻烦过她们，她们不厌其烦地帮了我很多。

感谢可爱的 Karen （她更喜欢被称作 KareBear），在我加夜班做实验时常常和我唠唠家常，还经常给我咖啡糖吃，末了总会叮嘱我保重。

感谢我的师弟刘祥庚，常常和我讨论实验，解答了我有机化学上的好多问题。感谢我温暖的室友和好朋友黄佩佩，常常开导我，带我走近花花草草的世界。我们一起养了一只可爱的豚鼠团子，这只能吃能睡、胆小又常跃跃欲试的团子同学给我们带来了很多不一样的乐趣。感谢曾经共处一间办公室的 Ian 赵培远、董德军和徐邵晨，还有常常来串门的任天宇和李周丹阳，给枯燥的实验生活带来了许多欢声笑语。

感谢辛勤维护 Parsons 后花园的园丁们，虽然我不知道是谁，但这个美丽的院子是我放空自己的小乐园，我爱这里的一草一木。

最后，感谢我亲爱的爸爸妈妈，无条件支持我做的每一个决定，我爱你们。感谢我的男朋友田丁五年来的爱与陪伴，蒲苇韧如丝，磐石无转移。

Table of Contents

LIST OF FIGURES

LIST OF TABLES

LIST OF SCHEMES

ABSTRACT

MANIPULATING SINGLE POLYMER MOLECULES FOR APPLICATIONS IN NANOMATERIALS

by

Ruiwen Chen

University of New Hampshire

Polymeric nanoparticles have been utilized in an increasing number of fields over the past two decades due to their unique properties such as design flexibility and good biocompatibility. Despite various techniques available to produce polymer nanoparticles, the preparation of small nanoparticles with customized functions in the sub 20 nm dimension remains challenging. Inspired by the self-organizing behavior of natural biomacromolecules, a class of single-chain nanoparticles (SCNP) are synthesized featuring biomimicry and ultrafine size. These nanoparticles are prepared from self-folding of polymer precursors bearing reactive pendant groups by intramolecular cross-linking reactions. A variety of cross-linking chemistries are available including covalent, dynamic covalent and non-covalent chemistries. Among these methods intramolecular polymerization is of particular importance as it allows for easy control of an SCNP's degree of cross-linking, and lead to SCNP with tunable level of compaction.

The aim of this dissertation is to 1) provide a comprehensive overview of recent advances in the field of single-chain folding; 2) investigate the synthesis of SCNP by intramolecular polymerizations, and 3) study the synthetic variations relating to the efficiency of a polymer's self-folding by intramolecular polymerization.

Chapter 2 of this work discusses the synthesis of poly(oxanorbornene imide) single-chain nanoparticles by intrachain radical polymerization of pendant methacryloyl units. Structure/ property relationships related to methacryloyl pendant length and percent incorporation were studied. Chapter 3 investigates the synthesis of an epoxide-maleimide bifunctional monomer, and its ring-opening polymerization to afford polyethyleneglycol based polymer precursor. The polymer precursor could undergo intramolecular radical polymerization to afford SCNP, and the cross-linked moiety could potentially be isolated for the study of degree of intrachain polymerization. Chapter 4 expands the scope of intrachain polymerization and explores the synthesis of SCNP by intramolecular ring-opening metathesis polymerization (ROMP). A series of poly(pentafluoro-methacrylate)s containing pendant norbornene imide groups was synthesized and subjected to intrachain ROMP. The efficiency of chain folding was explored relating to norbornene content on the polymer precursor, species and feed ratio of Grubbs catalysts, as well as doping effects of fluorinated aromatic comonomer.

Chapter 1. Introduction

1.1 Nanoparticles based on single polymer molecules

Since the emergence of nanotechnology in the past decades, the development of nanomaterials has become an important field of research. An emerging component in this field is polymeric nanoparticles (PNPs) which provide a broad range of medical, mechanical and electronic applications due to their unique properties including design flexibility, good biocompatibility, bio-mimetic characters, etc.[1-4] Although PNPs with sizes ranging from 50 nm to several micrometers are commercially available, these PNPs are mainly in the form of multi-chain nanostructures, e.g., micelles and polymersomes.[5-7] The preparation of smaller PNPs with customized functions in the sub 20 nm dimension, however, remains a challenging research goal. An effort toward this goal involves the manipulation of polymers on a single molecule level and gives access to PNPs with ultrafine size. These nano sized objects originate from cross-linking of single polymer molecules and exhibit novel properties and functions.

Single-polymer PNPs can be divided into two categories based on the preparation methods. Those synthesized from direct polymerization of multi-functional monomers are named single-chain cyclized/knotted polymeric nanoparticles or nanogels (SCKNPs, SCKPs or SCNGs), and those taking advantage of preformed polymer precursors are termed single-chain nanoparticles (SCNP or SCPN).

1.1.1 Single-chain cyclized/knotted polymeric nanoparticles/nanogels

Single-chain cyclized/knotted polymeric nanoparticles or nanogels (SCKNPs, SCKPs, SCNGs) are prepared from kinetically controlled homopolymerization of multivinyl monomers (MVMs).[8-10](Figure 1.1)

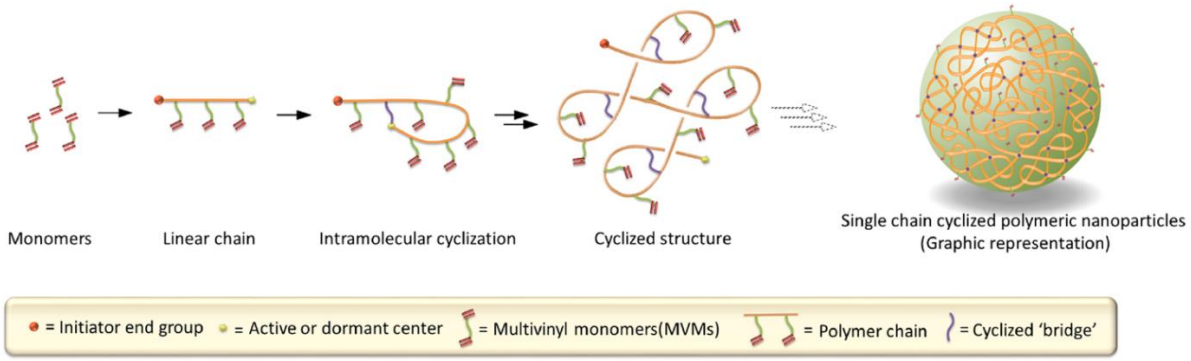

Figure 1.1 Illustration of the formation process of SCKPs. The intramolecular cyclization is promoted due to the small kinetic chain length and the high local vinyl concentration near the active center.[9] *Reprinted with permission from Ref. 9. Copyright 2015 American Chemical Society.*

Direct homopolymerization of MVMs is very challenging since each MVM is a potential crosslinker. According to the classical Flory-Stockmayer theory, the polymerization of MVMs would inevitably lead to gelation even at low monomer conversion due to significant intermolecular cross-linking reactions.[8-11] Recent development of controlled radical polymerization (CRP) including RAFT polymerization and Cu^0 mediated CRP allows unprecedented kinetic and spatial manipulation of chain propagation and can promote intramolecular cyclization while suppressing intermolecular cross-linking under proper conditions. These methods allow significant delay in reaching the gel point, and a single-chain cyclized/knotted nanoparticle can be achieved from one-pot *in situ* intramolecular reaction and self-cyclization of the propagating MVM polymer chain.[8-11]

SCKPs prepared by this approach contain large numbers of residual vinyl groups within the cyclized nanoparticles and can be further functionalized *via* Michal additional. Zheng and coworkers[8] synthesized SCKPs from RAFT polymerization of ethylene glycol dimethacrylate (EGDMA) and successfully functionalized the SCKPs through thiol-Michael addition with 2-mercaptoethanol. Huang et al[12] showed that SCKPs with multiple pendant vinyl groups can be used as a core to prepare star polymers *via* a grafting-onto approach. When an acid cleavable

divinyl monomer was used, the resulting SCKPs were degradable in acidic conditions. The degraded product was highly branched but showed little reduction in the hydrodynamic volume, confirming the internal cyclized architecture.[8] SCNGs can also be made from supramolecular divinyl monomers, assembled *via* host-guest complexation of vinyl-adamantane and vinyl-β-cyclodextrin, as demonstrated by Chen and coworkers.[13] These SCNGs undergo stimuli-induced cleavage of intra-chain crosslinks and can be unfolded by adding free competitive guest agent.

1.1.2 Single-chain nanoparticles (SCNP or SCPN)

Single-chain polymeric nanoparticles (SCNP) are another category of PNPs synthesized from single polymer molecules. Unlike SCKPs which are prepared from one pot *in situ* intramolecular cyclization of multivinyl monomers, SCNP take advantage of preexisting polymer precursors that are functionalized in the side chains with cross-linking sites. (Figure 1.2A)[14] After intramolecular cross-linking, the polymer folds into a well-defined nanosized object with potential functions such as catalysis and sensing. In that sense, SCNP partially mimic the folding of biomacromolecules, but can be made using a variety of monomers and polymerization techniques available. An immense number of synthetic methodologies have been applied to the formation of SCNP, including covalent, dynamic covalent and noncovalent cross-linking.[14-17] The main approaches to achieve chain folding can be classified into homofunctional cross-linking, heterobifunctional cross-linking and cross-linker mediated chain collapse. (Figure 1.2B)[18]

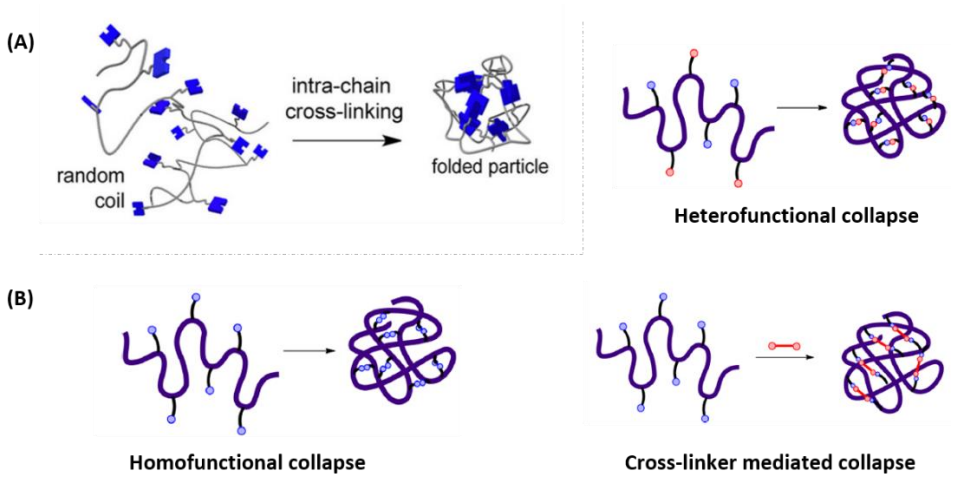

Figure 1.2 (A) Schematic representation of SCNP synthesis;[14] (B) Modes for intramolecular cross-linking of a polymer chain.[18] Adapted with permission from Ref. 18. Copyright 2015 American Chemical Society.

The history of intramolecular crosslinking of polymer molecules dates back to the 1950s.[19] Early work involving both experimental and theoretical studies of the process set the ground for the rapid development of SCNP.[20-24] Over the past decade, due to the advancement of controlled polymerization techniques as well as utilization of efficient synthetic strategies such as photo-mediated reactions and organometallic reactions, the scientific community has witnessed a surge in the studies of SCNP. New characterization methods also contribute significantly to the expansion of SCNP studies: triple-detection size exclusion chromatography (SEC), dynamic light scattering (DLS) and diffusion ordered nuclear magnetic resonance (DOSY-NMR) offer more accurate size evaluation;[14, 25-26] High-resolution mass spectroscopy and matrix-assisted laser desorption/ionization-time of flight (MALDI-TOF) show chemistries of intramolecular cross-linking;[27-28] Small-angle X-ray scatter (SAXS) and small-angle neutron scattering (SANS) reveal the inner structure of SCNP;[29-32] Scanning tunneling microscope (STM) and atomic force microscopy (AFM) provide direct visualization of the molecular structures and folding process of single polymer chains;[33-34] Other instrumentations are also available depending on the specific

chemistry and end use of SCNP. The synthesis, characterization, and potential use of SCNP were extensively covered in a handful of review articles[15, 17-18, 35-42] and will not be the focus of this chapter. The rest of this chapter will highlight a selection of recent SCNP examples involving programmed folding of single polymer precursors, intramolecular cross-linking of non-linear polymer precursors, and novel topologies of SCNP.

1.2 Programmed folding of linear polymer precursors

Programmed folding of macromolecules is a phenomenon frequently encountered in living process, such as protein formation. Remarkably, Nature manipulates the process creating numerous proteins, each with unique function with only 20 different amino acids. Synthesizing SCNP by intramolecular cross-linking of synthetic polymers is seen as a rudimentary model of the chain folding process of biomacromolecules. Despite the vast number of synthetic techniques available, it remains a formidable challenge to manipulate polymers on a single molecule level and fold them into designated conformations equally complex as a biomacromolecule. The process requires a high level of precision control in the intramolecular cross-linking process between reactive groups along the same chain.

1.2.1 Selective point folding

The simplest case of selective point folding is the synthesis of single ring polymers: Binding partners are installed at each end of the linear polymer chain and are connected *via* ring closure reactions. Cyclization of linear polymers by this approach is well-known in the polymer chemistry field and a lot of highly efficient linking reactions have been exploited, such as copper(I)-catalyzed alkyne-azide cycloaddition (CuAAC)[43] and olefin metathesis condensation reactions[44]. The synthesis of cyclic polymers by ring closure usually becomes less efficient as chain length increases, since the probability of an individual chain's end groups having sufficient proximity to

react and cyclize decreases.[45] This problem was addressed in a recent example reported by Konomoto and coworkers.[46] They synthesized zwitterionic polystyrene and poly(THF) telechelics having a pair of cyclic ammonia groups and a carboxylate end groups. Unimolecular electrostatic self-assembly under dilution and subsequent covalent fixation (ESA-CF) transforms the linear precursor to a cyclic polymer. (Figure 1.3A) Because the ionic chain-ends were brought together by electrostatic association prior to covalent fixation, local concentration of reactive chain end units becomes higher, and the inherent kinetic suppression of the conventional ring closure process under dilution could be circumvented.

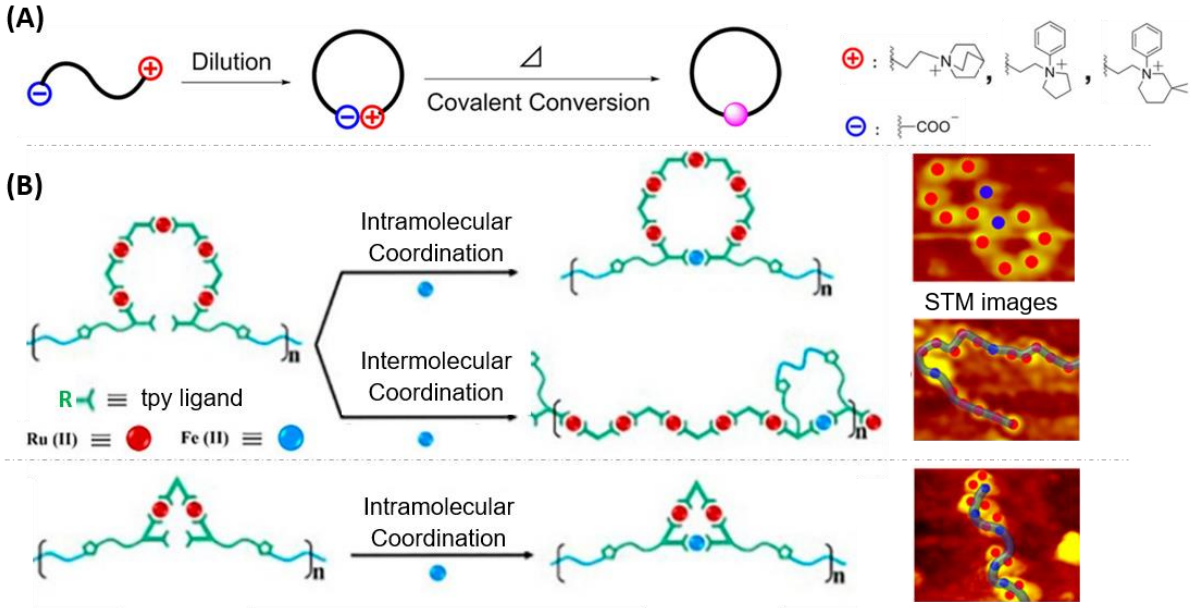

Figure 1.3 Examples of selective-point folding of single polymer molecules. (A) Cyclization of zwitterionic telechelic polymer precursors by unimolecular electrostatic self-assembly and covalent fixation;[46] (B) Ring-close metalation within open-form repeat units of a metallo-polymer.[34] Adapted with permission from Ref. 46 and Ref. 34. Copyright 2019 and 2020 American Chemical Society.

Internal cyclization can also occur within repeat units of a single polymer chain. As shown in Figure 1.3B, Li et al [34] synthesized a copolymer of polyethylene glycol with supramolecular metallo-monomers. The hexameric monomer consists of six pairs of terpyridine ligands and five

of them were strongly coordinated with Ru(II). The open-form monomeric units could be ring-closed *via* further coordination with Fe(II) in diluted solution (0.2 mg/mL). It was found that the polymer not only underwent ring-closure within each repeat unit and formed hexagons, it also formed linear chains by coordination with the ligand on neighboring repeat unit. Apart from hexameric metallo-monomers, the researchers also synthesized copolymers with trimeric metallo-monomers, and those exclusively underwent intramolecular coordination within repeat units under the same conditions. The different results were attributed to the size and rigidity of the repeat units (tri- vs hexa-). These results showed that reactive groups on a single polymer chain prefer to react with those in closer proximity instead of bending over to find a binding partner with larger spatial distance. In the meantime, the exclusive intramolecular ring-closure of trimetric monomers suggests that in the synthesis of SCNP, intramolecular cross-linking could potentially be controlled by tuning the size and rigidity of internal cycles since each intramolecular cross-linking reaction can be viewed as a ring-close reaction. This study also provides a new strategy to visualize single polymer molecules by STM: The random coil conformation of amorphous single polymer chains is often hard to address due to the variability and low atomic resolution. However, by introducing metal ions with high electron density into the polymer chains as "staining reagent", the single polymer chains could be directly visualized by STM.

Selective-point folding of linear-chain single polymers becomes more complicated with an increased number of reactive sites since the different combinations of these reactive sites lead to a variety of constitutional isomers. For polymers with two reactive sites located on the chain ends, the only topology resulting from intramolecular folding is single ring. The number of constitutional isomers drastically increases when four reactive sites are installed along the polymer chain. Figure 1.4A shows possible topologies originated from folding a linear polymer precursor having four

linking units.[47] Harnessing the folding process of such a polymer and understanding the conformations of the resulting constitutional isomers is a joint subject of both synthetic and topological polymer chemistry.

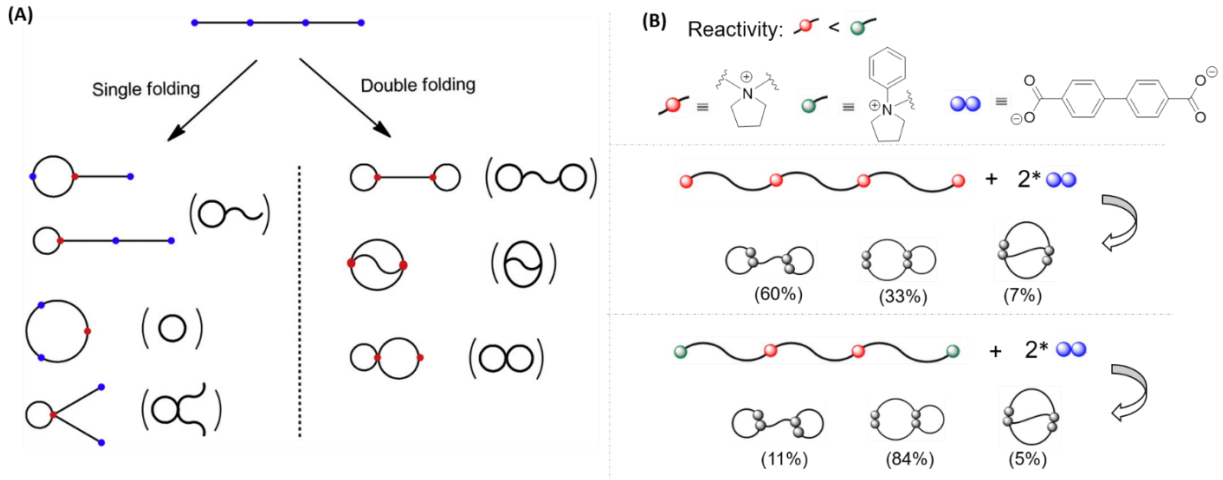

Figure 1.4 (A) Single (left) and double (right) polymer folding with a linear polymer precursor having four nodal units (two blue nodal points are linking together to form a red nodal point by the polymer folding)[47]; Reprinted with permission from Ref. 47. Copyright 2020 Elsevier. (B) Construction of dicyclic polymer topologies (manacle-form, 8-form and θ-form through the folding of a tetrafunctional telechelic precursor.[48]Adapted with permission from Ref. 48. Copyright 2019 American Chemical Society.

Recently, programmed folding of a pair of linear polymer precursors having four linking units was reported by Kyoda and coworkers.[48] (Figure 1.4B) The first polymer contains four linking units with equal reactivity. By adding two equivalents of the difunctional crosslinker, the linear polymer folds into dicyclic isomers of manacle-, 8-, and θ-forms with a ratio of 60:33:7. This composition indicates that although reactive sites along a polymer chain are of identical chemical reactivity, they don't undergo random combination. Rather, cross-linking between two adjacent positions of the spatially closer distance is preferred. This finding is consistent with early theoretical studies of intramolecular cross-linking reaction,[22, 49-50] as well as simulations by Pomposo et al[51]. Another linear polymer precursor was studied with end groups exhibiting higher chemical reactivity than the internal reactive sites. Folding of this polymer lead to a dominant formation of the 8-shaped

isomer, resulting from initial coupling of the chain ends due to their higher reactivity, followed by subsequent coupling of the two residual reactive sites at interior positions. The results indicated that the polymer folding process is directed either by spatial distance between functional points, or by the chemical reactivity of the functional points in the telechelic precursor. These findings provide insight into the bottom up synthesis of topologically controlled single-chain nanoparticles, and are crucial for the structure design and property tuning of SCNP.

The idea of selective point folding is also extensively applied in the field of synthetic peptide chemistry. Topologically controlled folding of synthetic linear peptides into multicyclic peptides has received significant interest since they are promising candidates as drug compounds with a wide therapeutic window. Recently, topologically controlled bicyclic and tricyclic peptide scaffolds were reported to be fabricated from linear peptides through intramolecular selenoether cyclization followed by disulfide or thioether cyclization.[52] Isomerically pure tricyclic peptides were also synthesized from one-pot ligation/cyclization of linear peptides.[53] Kale and coworkers[54] made a library of macrocyclic peptides through two chemical bridges that connect two pairs of cysteines of a peptide chain. The linear precursors in these examples are all synthetic peptides with a precise sequence of amino acids. Programmed folding of these molecules, although more synthetically challenging, largely mimics the behaviors of natural biomacromolecule and are promising biomimetic nanomaterials.

1.2.2 Protein-mimetic folding

The synthesis of SCNP is often seen as the development of simplified tertiary protein mimics. Tertiary protein structures originate from intramolecular folding single peptide chains among secondary structural elements, such as α-helices and β-sheets. Apart from random intramolecular

cross-linking of reactive groups to afford SCNP, a new direction emerges that simultaneous incorporates secondary structural elements into SCNP.

Nishimura and coworkers[55] demonstrated a water-soluble multiblock copolymer that folds into an SCNP with internal β-sheet domains. (Figure 1.5) The copolymer consists of hydrophobic and β-sheet forming tetra-lecune (Leu) blocks equally distributed within a thermo-responsive and water-soluble glycine (Gly)-derived vinyl polymer PNAGMe. The polymer exhibits lower critical solution temperature (LCST) behavior in water and transforms from an extended chain to a collapsed conformation upon heating. The repeated conformational transition induced by thermal cycles promoted the non-covalent interaction among the hydrophobic tetra-Leu peptide block, which self-assembles to isolate themselves from the hydrophilic PNAGMe blocks to minimize contact with water. As a result, the polymer folds into a single-chain nanoparticle with interior β-sheet domains.

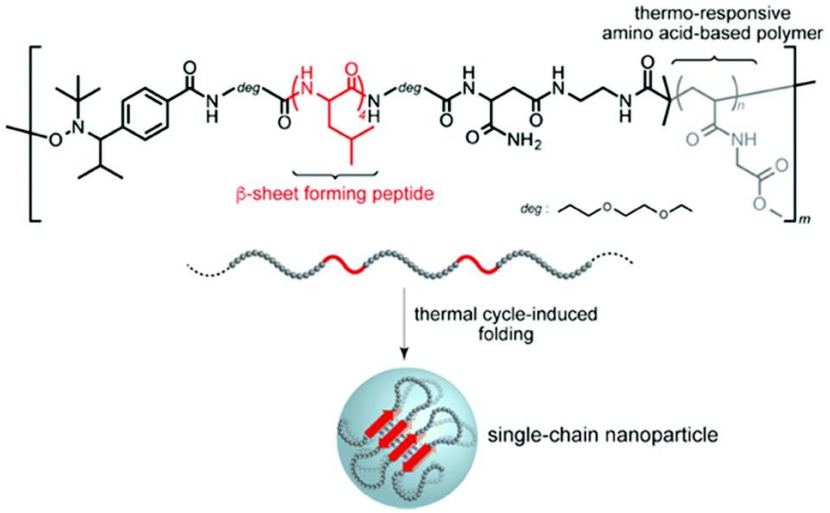

Figure 1.5 Chemical structure of a multiblock hybrid polymer composed of an alternating aligned tetraleucine β-sheet and a thermo-responsive glycine-derived vinyl polymer (top), and schematic illustration of the folding process to form single-chain nanoparticles via intramolecular cross-links among the peptide multiblocks (bottom).[55] Reproduced with permission from Ref. 55 from The Royal Society of Chemistry.

The formation of SCNP with internal helical substructures was achieved by the incorporation of a benzene-1,3,5-tricarboxamide (BTA) moiety. This approach was first reported, and then extensively studied by the Meijer group. BTA exhibits three-fold hydrogen bonding and could self-assemble into helical supramolecules. (Figure 1.6) Therefore, using BTA to induce the folding of a polymer chain will result in SCNP with internal helical structure.[56] This approach was first carried out in organic media on poly(isobornyl methacrylate) carrying o-nitrobenzyl-protected BTA groups.[56] Removal of the photo-label protecting group allowed BTA to self-assemble into their helical stacks and fold the polymer to SCNP. A later study revealed that the folded polymer chain does not contain a single BTA stack, but instead it's composed of multiple segregated stacks.[57] Incorporating other cross-linking motifs together with BTA in the polymer backbone such as 2-ureido-pyrimidinone (UPy),[58] Hamilton wedges with cyanuric acids,[59] or coumarins[60] allows orthogonal folding of polymers. Other parameters relating to the BTA-directed folding process were also explored, including the sequence distribution[61] and graft composition of the polymer,[62] structural constraints by covalent cross-links and order of cross-linking events in an orthogonal regime.[60] These studies show that SCNP with internal helical structure are accessible *via* intramolecular H-bonding of BTA, and the resulting nanostructures can be tuned by synthetic variations.

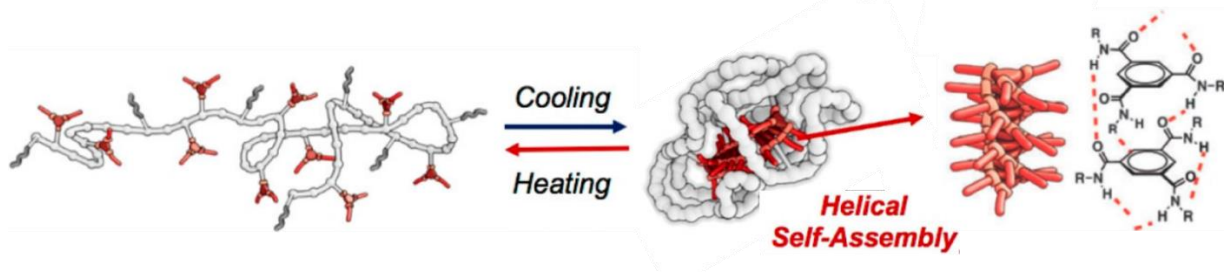

Figure 1.6 Self-folding and self-assembly of BTA-functionalized copolymers with different sequence distribution.[61] Reprinted with permission from Ref. 61. Copyright 2016 American Chemical Society.

The compartmentalized nanostructure inside SCNP can be functionalized and utilized as catalytic pockets for enzyme-mimetic applications. Enzymes are efficient biocatalysts that regulate a broad variety of reactions in aqueous environments. Their catalytic capability originates from the guided folding of single protein molecules which brings amino acid residues together, forming the inner compartments that act as "active sites".[63] The controlled single-chain folding of synthetic polymers leads to SCNP with compartmentalized nanostructures around crosslinking points. When catalytic functional groups are placed in these polymeric pockets, SCNP can exhibit features that resemble natural enzymes. This idea is widely applied in the synthesis of metal-containing SCNP that mimic biological metallo-enzymes. Two approaches have been developed to incorporate metal complexes in SCNP matrix.[38] Coordination-driven self-folding is based on a polymer precursor with ligand-functionalized side chains. The addition of metal ions collapses the polymer through intra-molecular metal-ligand coordination, and simultaneously imparts catalytic functions to the polymeric architecture. Another approach is to fold the polymer into an SCNP first, then incorporate the metal-ions in a separate step.

Studies have shown that metallo-folded SCNP catalysts are advantageous over their molecular catalyst counterparts that are not immobilized in a polymer matrix. Metallo-folded SCNP's inner compartment results from polymer folding, that creates shielded catalytic pockets with a specific local environment and will allow selective substrates to enter the cavity, increasing selectivity of the catalyst.[64] The small size of SCNP enables relatively high local concentration of the catalytic sites, leading to high efficiency of the catalyst. Having too many catalytic sites in SCNP may lower the efficiency of the catalyst due to dense packing of metal complexes and lower flexibility of the folded polymer. But the number of catalytic sites per polymer can be easily tuned synthetically.[65] The polymer backbone, side chains, and metal centers are also adjustable depending on

applications of the catalyst. Metals including Cu, Ru, Pd, Ti, Pt, Rh, Ag and Ir ions were successfully employed in the synthesis of artificial metal-enzymes targeting catalysis of a variety of reactions including reduction, oxidation, coupling and click reactions.[38, 66-73] Some SCNP catalysis reactions were performed in organic media while some were able to function in aqueous media which more closely mimic the biological environment. Activity of SCNP catalysts were also studied in living cells and showed excellent biocompatibility and catalytic activity.[74-75]

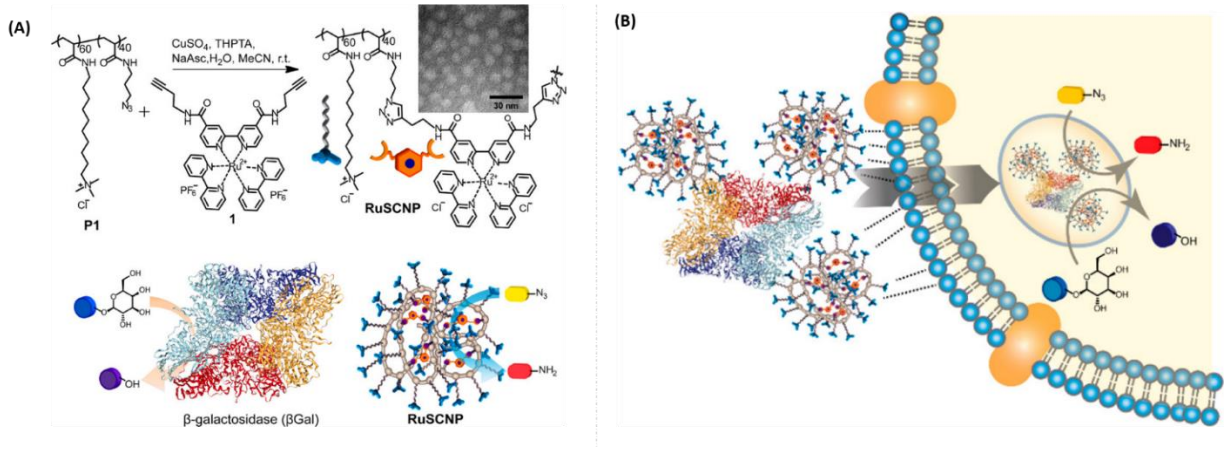

Figure 1.7 (A) Illustration of RuSCNP preparation and dual catalysis with βGal. (B) Illustration of SCNP-enzyme codelivery and dual catalysis.[76] Reprinted with permission from Ref. 76. Copyright 2020. American Chemical Society.

A recent study by Chen and coworkers[76] codelivered an SCNP catalyst and an exogenous enzyme into cells and performed bioorthogonal reactions intracellularly. They prepared a water-soluble polymer and intramolecularly cross-linked it with $Ru(bpy)_3$ diyne to form SCNP that was able to catalyze reduction of azido groups and produce highly fluorescent rhodamine. (Figure 1.7A) *β*-Galactosidase (*β*Gal) was chosen as a model exogenous enzyme that catalyzes the hydrolysis of *β*-galactosides. The SCNP catalyst was bound to *β*Gal enzyme surface through electrostatic and hydrophobic interactions. The SCNP-enzyme pair was then delivered across cell membranes and performed concurrent and tandem intracellular catalysis. (Figure 1.7B)

1.2.3 Sequential folding

Sequential folding of polymer precursors with orthogonal linkers lead to smaller and more spherical SCNP.[51] Liu et al [77] reported a method to form SCNP with denser cores through sequential intrachain photodimerization of anthracene groups. The first irradiation partially folded the polymer chain. By adding a poor solvent for the anthracene groups, the unreacted functionalities were brought closer together. A subsequent irradiation enables further cross-linking of the anthracene groups and lead to SCNP with a more compact core. Frisch and coworkers[78] reported the stepwise folding of a single polymer chain by two photocycloaddition reactions initiated by different colors of visible light (Figure 1.8) The polymer carries styrylpyrene and anthracene pendants that undergo [2+2] and [4+4] photocycloaddition respectively. Irradiation with blue light selectively triggers the intramolecular cross-linking of styrylpyrene, whereas subsequent irradiation with violet light induces the photoreaction of anthracene, fully compacting the dual photoreactive polymer into an SCNP. Both styrylpyrene and anthracene groups undergo photocycloaddition when irradiated with violet light, hence an SCNP was synthesized by direct irradiation of violet light, which triggers cross-linking of both groups in a parallel manner. It was found that SCNP synthesized by stepwise folding was smaller compared to the parallel folded SCNP. Such differences could result from the overall faster folding of parallel folding or from the loss of the strict separation of both cross-linking steps. Other chemistries were also employed to sequentially fold a linear polymer precursor into an SCNP, including sequential photo- and radical coupling,[79] orthogonal photoreaction and supramolecular interactions,[60] etc.[58-60, 71, 80]

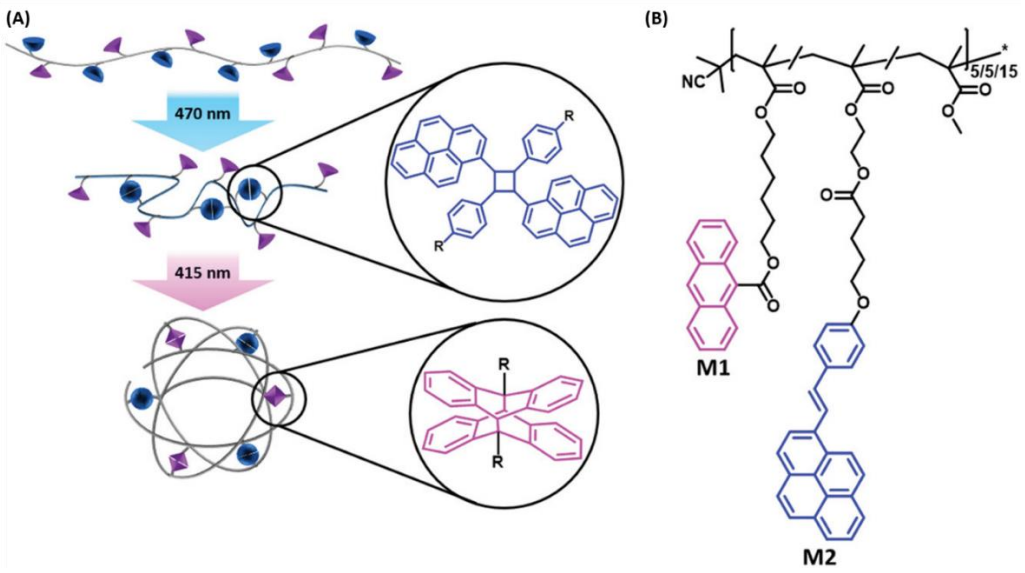

Figure 1.8 (A) Schematic representation of the wavelength selective SCNP folding, induced by the [2+2] photocycloaddition of styrylpyrene (blue) and [4+4] photocycloaddition of anthracene (violet); (B) Chemical structure of the dual photoreactive polymer.[78] *Reprinted with permission from Ref. 78. Copyright 2020 Wiley.*

1.3 SCNP from cyclic, brush/comb and star polymer precursors

1.3.1 Cyclic polymer precursor

Conventional SCNP from random intramolecular cross-linking of linear polymer precursors often exhibit a sparse, non-globular conformation in solution, as revealed by both SAXS, SANS data and computer simulations.[81] A recent molecular dynamics simulation study by Formanek and Moreno[82] predicted that using cyclic polymers as precursors would enhance intramolecular cross-linking of distant functional groups and lead to SCNP with more compact and globular conformation. Experimental work by Rubio-Cervilla and coworkers[83] validated this prediction. As shown in Figure 1.9, a linear polymer was first folded to a single ring polymer *via* hetero Diels-Alder reaction of chain ends. The resulting cyclic polymer was subsequently activated by azidation, then subjected to collapse *via* CuAAC in the presence of an external dialkyne crosslinker. As a comparison, an SCNP from direct cross-linking of the linear polymer precursor was synthesized

using the same reaction sequence without the ring-closing step (Step II). It was found that the SCNP from ring polymer precursor had a higher compaction degree than the SCNP from linear precursor. This phenomenon was attributed to the conformation of the polymer precursors: In the case of linear polymer precursor, cross-linking of functional groups pre-aligned within the chain contributes little to the level of compaction. By cyclization, the chain conformation has a distinct rearrangement, resulting in a higher degree of compaction upon collapse. The synthesis of SCNP from cyclic polymer precursors also introduced new strategies for the preparation of artificial cyclotide mimetics exploiting the versatility of synthetic polymers and orthogonal collapse chemistries.

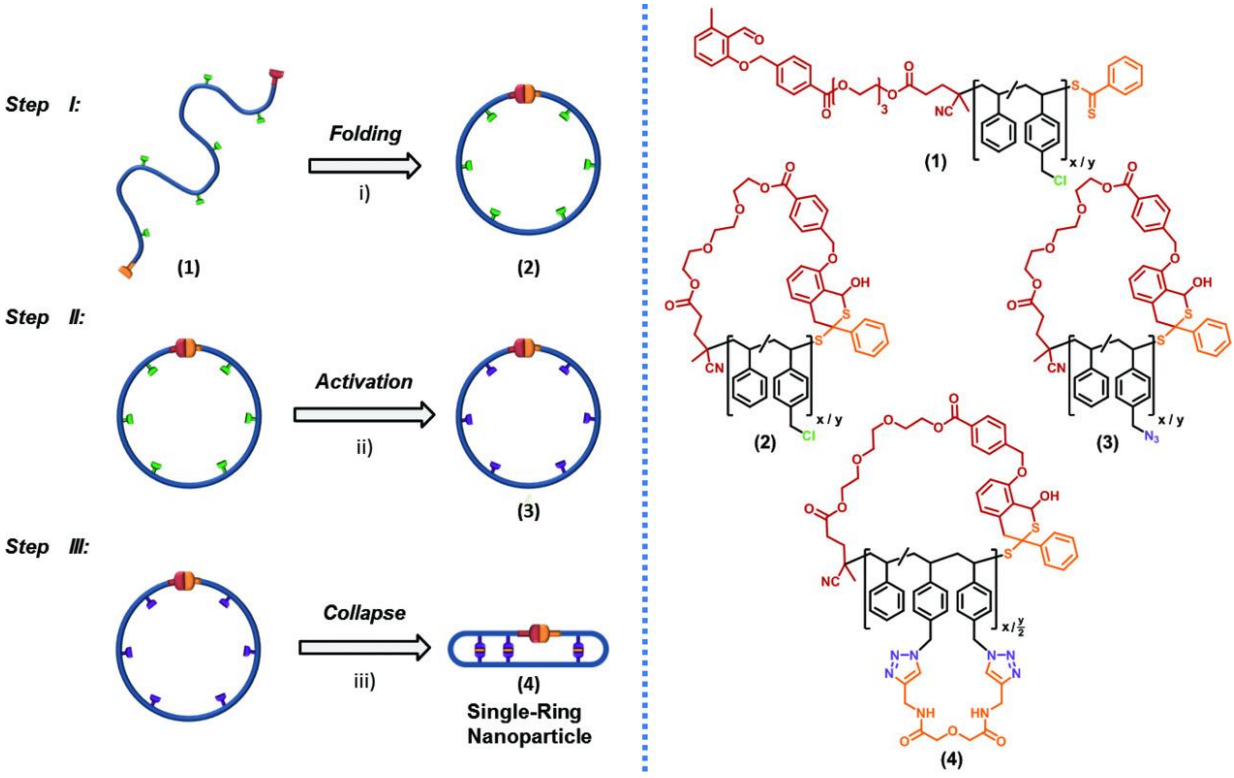

Figure 1.9 Schematic illustration of the synthetic route toward single-ring nanoparticles as cyclotide mimetics by a stepwise folding-activation-collapse process.[83] *Reprinted with permission from Ref. 83. Copyright 2018 Wiley.*

1.3.2 Brush/comb/graft polymer precursor

Some SCNP were synthesized from linear polymer precursors with long side chains, i.e., polymer grafts. Polymer grafts carrying cross-linkable functional groups may aid the intramolecular reaction, since the increased length and flexibility of side chains allows cross-linking of sites separated by long contour distance. This design is widely found in literature but a quantitative evaluation of graft length on polymer folding is not yet available. A recent study in our group[84] (detailed in Chapter 2) explored the length of methacryloyl-functionalized side chain in relation to the folding of a poly(oxanorbornene) polymer precursor. Our results showed that within the length scales we synthesized, side chain length does not significantly affect polymer folding by intramolecular radical polymerization.

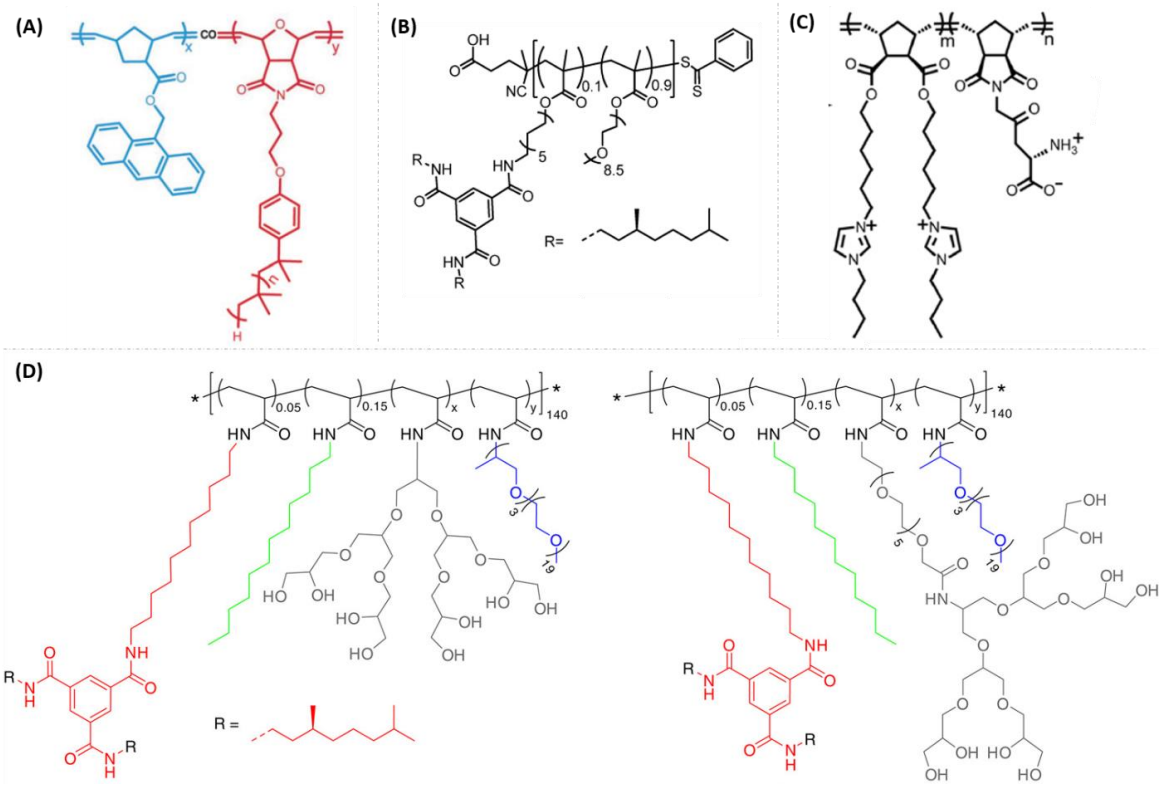

Figure 1.10 Examples of polymer precursors with grafted side chains that promote solubilities. (A) polyisobutylene side chains soluble in THF and hexanes;[77] (B) water soluble linear PEG grafts;[85] (C) water soluble alkyl side chains containing imidazolium groups;[68] (D) water soluble dendritic polyglycerol side chains.[86]

Polymer grafts that are not functionalized with cross-linkable groups can contribute to the overall solubility of SCNP. During the synthesis of SCNP, intramolecular cross-linking of the functional groups leads to collapsed inner compartments. Polymer grafts not carrying functional groups could be made solvophilic or hydrophilic. They exhibit an extended conformation in solution, shielding the core of SCNP and stabilize the SCNP solution by repulsive forces between coronas. A study by Liu and coworkers[77] reported intramolecular cross-linking of comb polymers with large aliphatic polyisobutylene grafts, which have affinity for non-polar aliphatic solvents. (Figure 1.10A) They found that switching the solvent from THF to hexanes has pronounced effect on the chain collapse, indicating that disparate solvency could be a choice to tune chain collapse of a single comb copolymer. Besides hydrophobic polymer grafts, hydrophilic grafts are widely applied in the synthesis of water soluble SCNP. These hydrophilic grafts on the polymers could be water soluble PEG chains,[85] or ionic species embedded in an alkyl chain.[68] (Figure 1.10B,C) A study by ter Huurne and coworkers[86] substituted the linear PEG grafts with dendritic polyglycerol grafts on an amphiphilic heterograft copolymer (Figure 1.10D) and found that branching of the hydrophilic pendants affected the local structure of the folded polymer but does not influence the overall conformation and single-chain character of the folded copolymers in solution. The hydrophilic grafts can also provide steric stabilizing effect to efficiently isolate the cross-linking groups, preventing interparticle coupling events. As a result, the synthesis of SCNP could be carried out at concentrations as high as 100 mg/mL.[87]

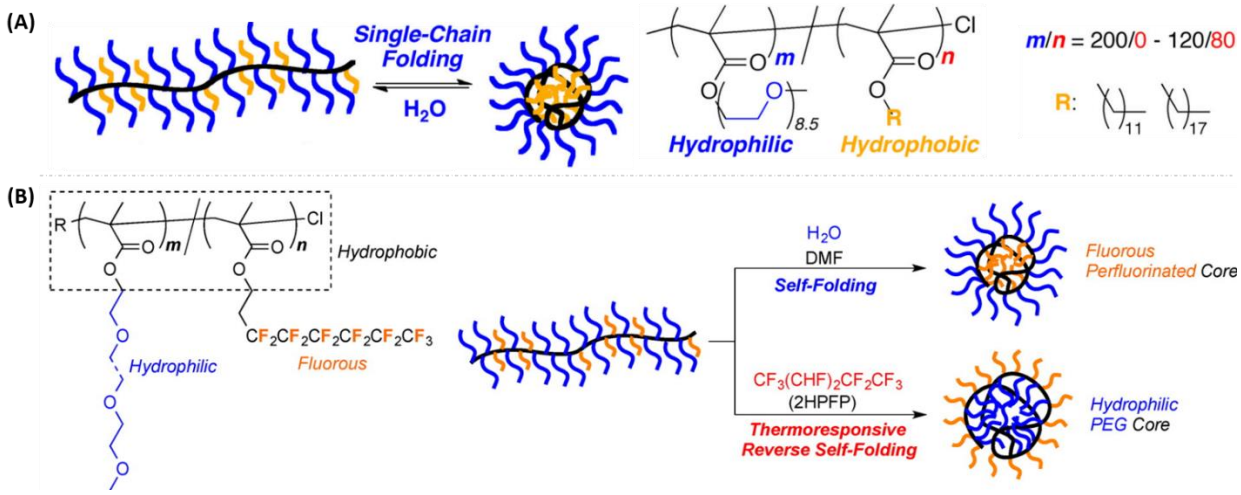

*Figure 1.11 (A) Single-chain folding of amphiphilic copolymer in water;[88] (B) Reversible and thermo-responsive folding properties of the copolymers in water, DMF and 2*H,3H*-perfluoro-pentane (2HFP).[89]Adapted with permission from Ref. 88 and 89. Copyright 2014 and 2016 American Chemical Society.*

Comb-like amphiphilic random copolymers can undergo single-chain self-folding in water by purely hydrophobic interaction without any additional covalent or H-bonding of functional groups on the polymer precursor.[90] The resulting nanoparticles are commonly referred to as unimer micelles. The synthesis of unimer micelles by this approach is well studied by Sawamoto and Terashima. As shown in Figure 1.11A,[88] a series of graft polymers were synthesized consisting of PEG and hydrophobic alkyl pendant groups. The hydrophobic segments avoid contacting water, residing in the interior of a self-folded structure and thereby creating hydrophobic nanocompartments. They found that single-chain folding occurs with 20-40 mol% of hydrophobic units where relatively long and/or large alkyl groups (e.g., R = $C_{12}H_{25}$, $C_{18}C_{37}$) are especially effective. The folded-unfolded transition is reversible and occurs upon addition of methanol or by elevating solution temperature. In several follow-up studies, they showed that the intra- and intermolecular self-assembly could be tuned by a few parameters, including hydrophilic /hydrophobic balance,[91] degree of polymerization,[91] sequence distributions of the polymer precursor,[92] length of hydrophilic PEGs and hydrophobic alkyl pendants,[93] etc. Substituting the

alkyl pendants with perfluorinated pendants allows various self-assembly modes by changing solvents.[89] In water or DMF, the polymer self-fold into unimer micelles with fluorous/hydrophobic cores while in perfluoropentane they form reverse unimer micelles with hydrophilic PEG cores. (Figure 1.11B)[89]

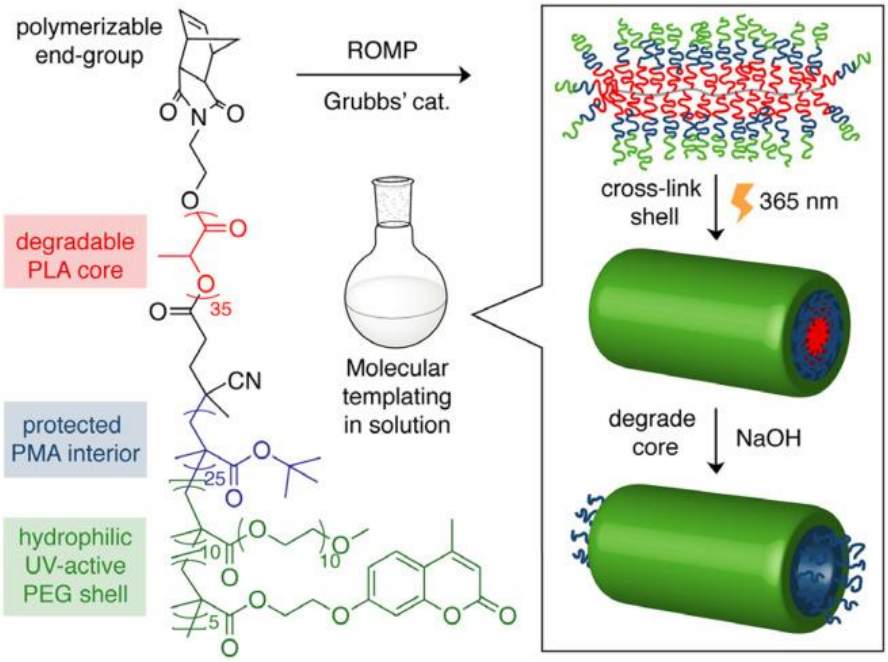

Figure 1.12 Synthesis of PEG nanotubes with inner functionalities from tricomponent bottlebrush copolymers.[94] Reprinted with permission from Ref. 94. Copyright 2017 Wiley.

Another advantage of using graft polymers as precursors for intramolecular cross-linking is that they could be used as templates for the preparation of nanotubes. Comb-like polymer precursors with densely grafted polymeric branches adopt a persistent cylindrical shape in solution, when the polymeric side chains are much shorter than the backbone.[95-96] The Rzayev group developed a series of core-shell bottlebrush copolymers that exhibit cylindrical shape in solution and used them as single molecule templates.[94, 97-101] The polymer precursors were subjected to intramolecular cross-linking of the shell layer followed by selective removal of the core. The size and shape of the polymer precursor was preserved after these transformations, leading to organic nanotubes.

The polymer backbone could be methacrylate or norbornene-based, and a variety of cross-linking chemistries have been utilized, including photodimerization of coumarin functionalities,[94, 97] oxidative coupling of mercapto groups,[98] cross metathesis of olefin groups,[99, 101] and oxidative polymerization of pyrrole groups.[100] Figure 1.12 shows an example of nanotube preparation by this approach.[94] The bottlebrush copolymer template was synthesized from ROMP of the shown macromonomer and served as a cylindrical template. Cross-linking of the coumarin groups in the outer shell was performed under UV irradiation in dilute chloroform solution. SEC analysis of the shell-cross-linked product exhibited a small shift toward higher elution volume without any high molecular weight shoulders, indicating intramolecular reactions. The PLA core was subsequently etched out by treatment with methanolic NaOH, leading to cylindrical nanoparticles.

1.3.3 Star and dendritic polymer precursor

Intramolecular cross-linking of star-shaped polymer precursors was first reported by Van Renterghem and coworkers in 2008.[102] They synthesized star-shaped poly(isobornyl acrylate) precursors with methacrylate end groups and converted them to unimolecular nanoparticles by intramolecular polymerization. The nanoparticles were used as viscosity modifiers in the polymerization of acrylate monomers and changed the visco-elastic properties of the polymer by noncovalent chain entanglements. Ding and colleagues[103] synthesized polymer nanoparticles from intramolecular cross-linking of reactive azo-containing star polymer precursors. The nanoparticles show circular transformations when the azo chromophores undergo trans-cis isomerization cycles. A porphyrin-cored four-arm star polymer was synthesized by Rodriguez et al[104] and transformed to a nanoparticle by intramolecular anthracene dimerization. The resulting porphyrin-cored polymer nanoparticle displayed redox and ligand-binding reactivity and was used as a macromolecular model for heme proteins.

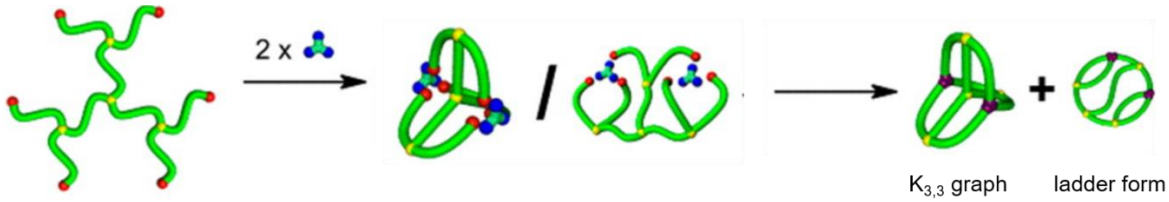

Figure 1.13 Construction of a K3,3 graph polymer topology and its isomeric ladder-form topology carrying six reactive end groups.[105] Reprinted in part with permission from Ref. 105. Copyright 2014 American Chemical Society.[*]

Topologically controlled folding of a dendritic polymer precursor having six reactive end groups was demonstrated by Suzuki and coworkers.[105] Reacting the polymer with two equivalents of the trifunctional cross-linkers led to nanoparticles of $K_{3,3}$ graph topology and another constitutional isomer having a tetracyclic ladder form. (Figure 1.13) The $K_{3,3}$ graph isomer was found to be remarkably contracted in comparison with the ladder form isomer in solution.

Dendrimers with a high degree of branching adopt a three-dimensional globular conformation with a large number of functional groups at the periphery.[106] Intramolecular cross-linking of high-generation ($g \geq 3$) dendronized polymer precursor was scarcely reported in the literature. In 2002 Zimmerman and coworkers[107] reported the synthesis of macromolecular hosts for porphyrin guests based on dendrimer precursors. (Figure 1.14A) An allyl-functionalized dendrimer was synthesized containing a porphyrin core as the templating agent. The dendrimer was subjected to intramolecular ring-closing metathesis of the peripheral allyl groups, leading to a cross-linked unimolecular nanoparticle. Subsequent removal of the porphyrin template from the rigid nanoparticle left behind spatially arranged functional groups that act as recognition sites for porphyrin derivatives. A subsequent study by Lemcoff et al[108] showed that a dendrimer's size

*Link to the article: https://pubs.acs.org/doi/10.1021/ja504891x. Request for further reuse of this figure should go to the ACS for permission.

reduction is linearly dependent on the extent of intramolecular cross-linking, irrespective of the number of dendrons used. Encapsulating a hydrophobic, fluorescent dye inside the core of a water-soluble shell-crosslinked dendrimer provides solubility of the dye in aqueous media.[109] The cross-linked dendritic shell of the small and rigid nanoparticle enhanced the photostability of the fluorescent dye in water. A similar approach of solubilizing and stabilizing fluorophores was applied on linear dendronized polymers.[110] (Figure 1.14B) Linear dendronized polymers contain densely packed dendrons along the polymer backbone and adopt a semi-rod-like structure, hence intramolecular cross-linking occurs primarily on short range, leading to lower degree of compaction. The fluorophores embedded in the cross-linked dendronized polymer exhibited high aqueous solubility and improved brightness and photostability. (Figure 1.14C)

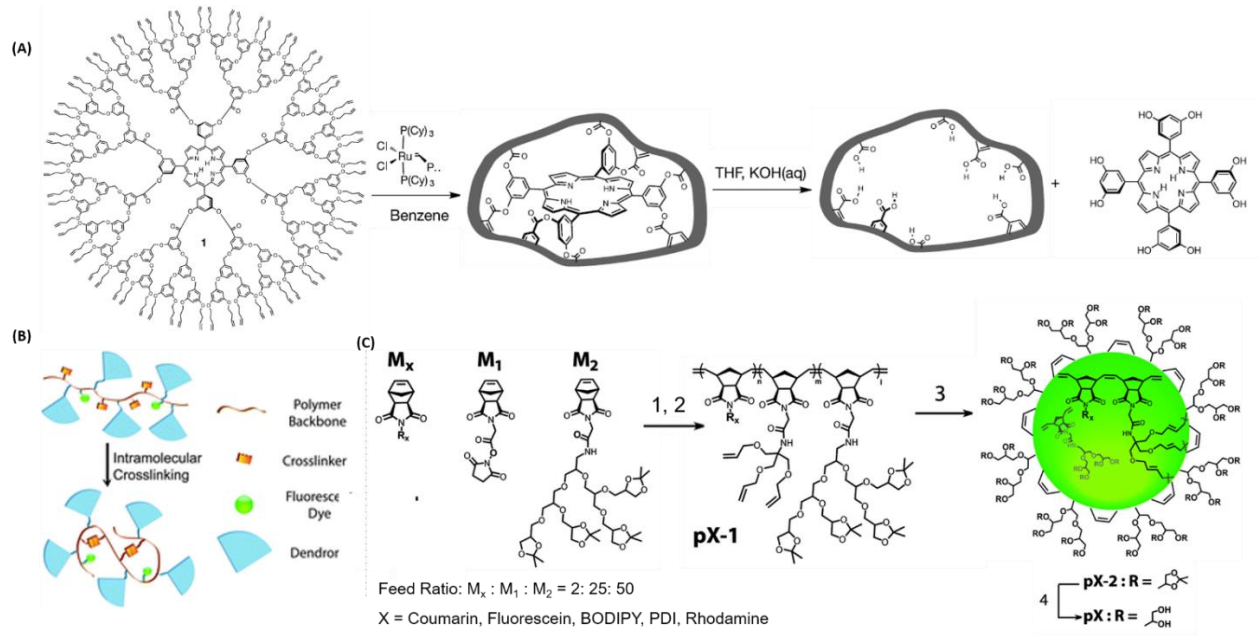

Figure 1.14 (A) Schematic illustration of the preparation of imprinted dendrimer;[107] Adapted with permission from Ref. 107. Copyright 2002 Springer. (B) Schematic illustration of crosslinked dendronized polyols incorporated with fluorophores;[110] (C) Synthesis of the crosslinked dendronized polymer pX.[110] Adapted with permission from Ref. 110 from The Royal Society of Chemistry.

1.4 SCNP with novel topologies

1.4.1 Tadpole

Tadpole-shaped SCNP are composed of a flexible polymer attached to an intramolecularly folded SCNP. They are commonly synthesized from diblock linear polymer precursors containing a reactive block and an inert block. A mathematical study by Asenjo-Sanz and coworkers[111] demonstrated that the size of a tadpole-shaped SCNP is related to its tail length and could be predicted prior to the synthesis of SCNP. Tadpole-shaped SCNP exhibit surfactant-mimicking structures and have been used as nano building blocks to self-assemble to higher ordered structure.[112-117]

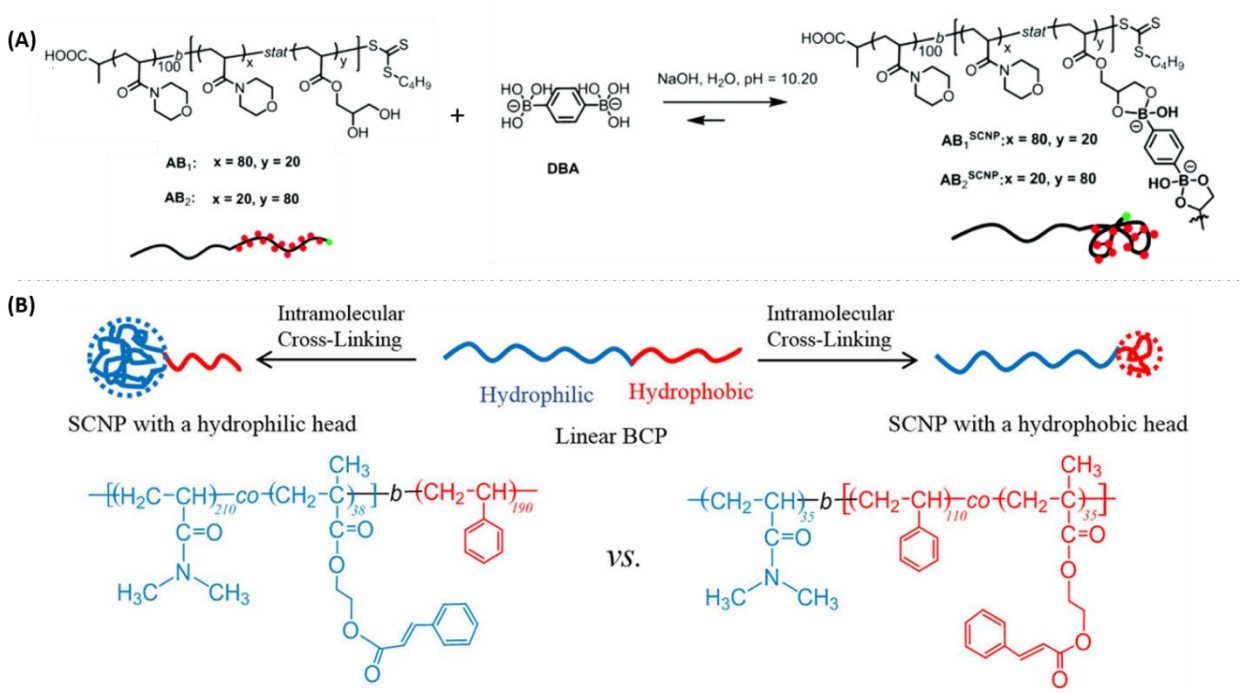

Figure 1.15 (A) Synthesis of the tadpole-like SCNP from intramolecular cross-linking of 1,2-diol pendants;[118]Reprinted in part with permission from Ref. 118 from The Royal Society of Chemistry. (B) Preparation of tadpole-shaped SCNP by intramolecular photo-cross-linking reaction of cinnamoyl groups.[119] Reprinted with permission from Ref. 119. Copyright 2019 American Chemical Society.

Zhang and coworkers[118] synthesized linear diblock copolymers with diol pendants, and used a boronic acid crosslinker to afford tadpole-shaped SCNP. (Figure 1.15A) The crosslinker exhibited an isoelectric point so the head of the tadpole undergoes hydrophobic/hydrophilic transition based on pH. The SCNP self-assembled into spherical multimeric morphology and the assembly could be dissociated by varying the environmental pH or adding glucose. Thanneeru et al[119] prepared amphiphilic diblock copolymers poly(PDMA-*b*-PS) from N,N'-dimethylacrylamide and styrene monomers. (Figure 1.15B) Photo-crosslinkable cinnamoyl groups reside in either the hydrophilic PDMA block or the hydrophobic PS block. Intramolecular photo-cross-linking of cinnamoyl groups led to the formation of tadpole-shaped SCNP containing either a hydrophobic or hydrophilic self-collapsed head. It was found that in both cases, the size and morphology of the self-assembled SCNP are related to the degree of intramolecular cross-linking and could be controlled from a single polymer precursor. A systematic study on the self-assembly behavior of tadpole-shaped SCNP consisting liquid crystalline (LC) properties was reported by Wen and coworkers.[120] By varying the UV irradiation time or hydrophilic block chain length, a library of assembled morphologies were afforded, including tubular assemblies, bowl-like particles, saddle-shaped lamellae and spheres. (Figure 1.16)

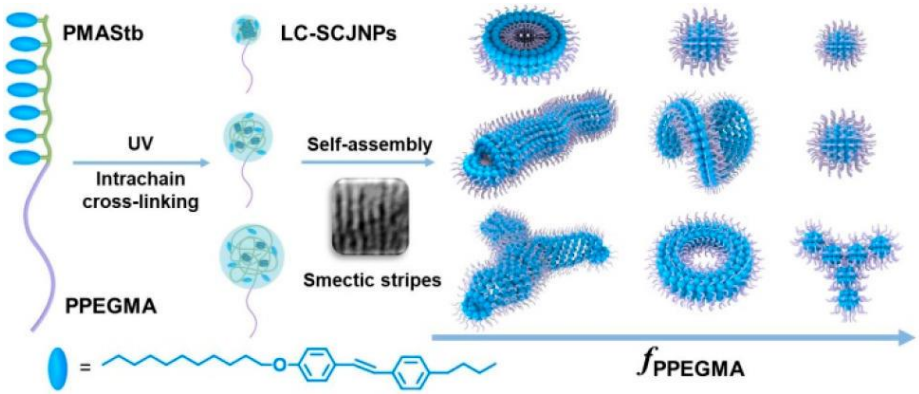

Figure 1.16 Synthesis of SCNP with tunable liquid crystalline properties via intrachain photo-cross-linking stilbene-containing amphiphilic block copolymers, and the self-assembly behavior of SCNP in solution.[120] Reprinted with permission from Ref. 120. Copyright 2019 American Chemical Society.

Another pathway to tadpole-shaped SCNP is to synthesize a self-cross-linked nanoparticle first, then attach a tail in a separate step. Recently, a set of photoligations that can be carried out orthogonally either by a sequence of decreasing or increasing wavelengths was reported by the Barner-Kowollik group.[121] As shown in Figure 1.17, the polymer precursor contains 9-triazolylanthracene units distributed along the backbone and a styrylpyrene chain end. The polymer can be ligated with a PEG chain through [2+2] cycloaddition of styrylpyrene at the chain ends and folded into an SCNP through [4+4] cycloaddition of the anthracene units along the polymer backbone. The two sets of reactions could occur in either order controlled by irradiation wavelength, and both lead to tadpole shaped SCNP.

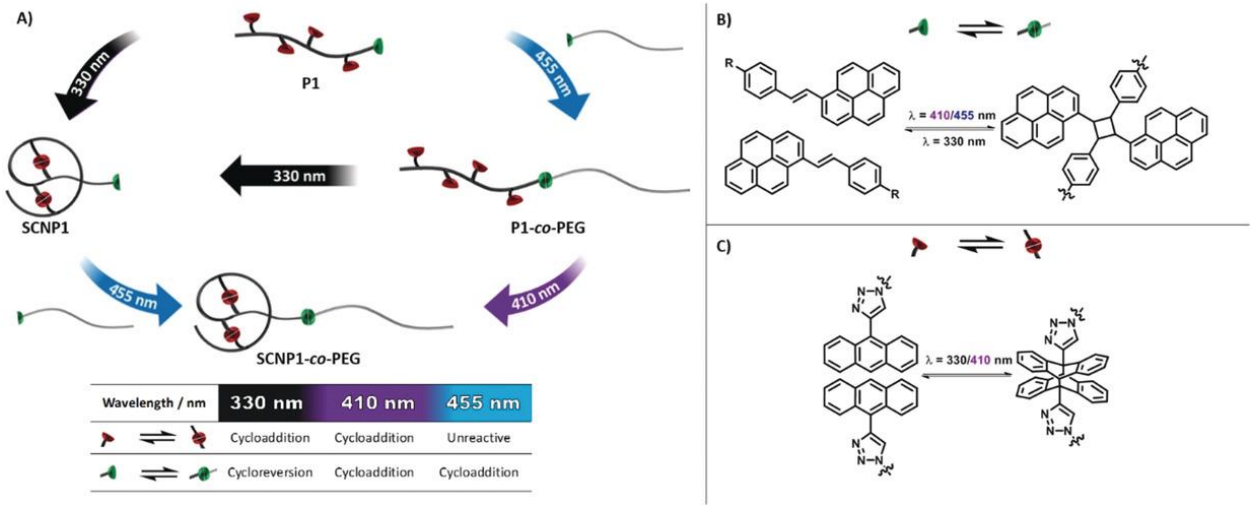

Figure 1.17 Schematic representation of the light-induced intrachain crosslinking and single-chain ligation pathways of P1 (A). The dual photoreactive parent polymer P1 can be ligated with a PEG chain through [2+2] cycloaddition of styrylpyrene (B) and folded into an SCNP through the [4+4] cycloaddition of 9-triazolylanthracene units distributed along the backbone (C).[121] *Reprinted with permission from Ref. 121. Copyright 2019 Wiley.*

1.4.2 Compartmentalized/Dumbbell

Orthogonal self-folding of a diblock copolymer bearing reactive groups within each block leads to a double compartment SCNP. Matsumoto and coworkers[122] synthesized an amphiphilic random block copolymer containing PEG and hydrophobic dodecyl, benzyl and olefin pendants. The

copolymer undergoes orthogonal self-assembly of hydrophobic dodecyl and benzyl pendants in water, followed by covalent crosslinking, forming an SCNP carrying double yet distinct hydrophobic nanocompartments. (Figure 1.18A) Another study by Kozawa and coworkers[123] used amphiphilic ABA random triblock copolymers as precursors bearing PEG and hydrophobic dodecyl pendants as the A-segments, and a hydrophilic poly(ethylene oxide) (PEO) as the middle B-segment. It was found that the copolymers could self-assemble into PEO-linked double core unimer micelles, PEO-looped unimer or dimer micelles, or multimeric micelles, depending on the composition of the polymer precursor. (Figure 1.18B)

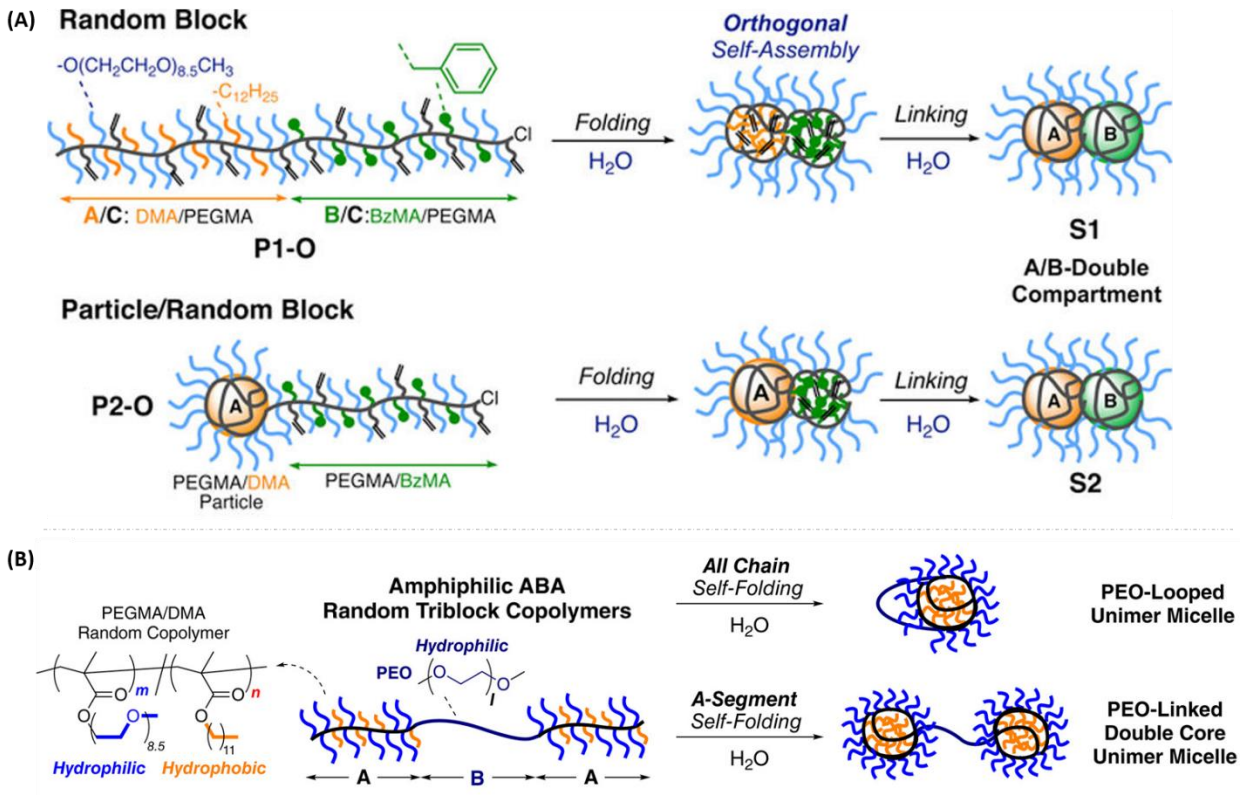

Figure 1.18 (A) Nanocompartment polymers created via the self-folding and cross-linking of amphiphilic random/block copolymers in water;[122] Reprinted in part with permission from Ref. 122. Copyright 2017 American Chemical Society. (B) Self-assembly and self-folding of amphiphilic ABA random block copolymers into micelles linked with poly(ethylene oxide) (PEO) in water.[123] Reprinted in part with permission from Ref. 123. Copyright 2019 Wiley.

Claus and coworkers[124] employed a PMMA-based ABC triblock copolymer precursor to form dual compacted SCNP. The middle B-block was a nonfunctional spacer block. The outer A- and C-blocks carry phenacyl sulfide and α-methylbenzaldehyde moieties respectively and could be sequentially compacted with external dithiol or diacrylate cross-linkers within each block. It was found that the hydrodynamic diameter of the polymer was significantly reduced after the first compaction. The second compaction revealed a far less pronounced reduction in size, due to the reduced degrees of freedom available after the first compaction. A dumbbell-shaped SCNP was synthesized by Cui and coworkers[125] using an ABC triblock copolymer bearing protonated imidazolium motifs in the A- block, NH_3^+ motifs in the C-block, and hydroxyl motifs in the B-block. The outer blocks underwent stepwise coordination to copper ions, taking advantage of the difference in the basicity and coordination of imidazole and NH_2 motifs. (Figure 1.19A) In a follow-up study[126], the dumbbell-shaped SCNP was subjected to ascorbic acid reduction and air oxidation. Unidirectional molecule shuttling between discrete double heads was found, leading to dumbbell-*to*-tadpole-*to*-dumbbell configurational transition and the intake of oxidized ascorbic acid into as-reassembled heads. (Figure 1.19B)

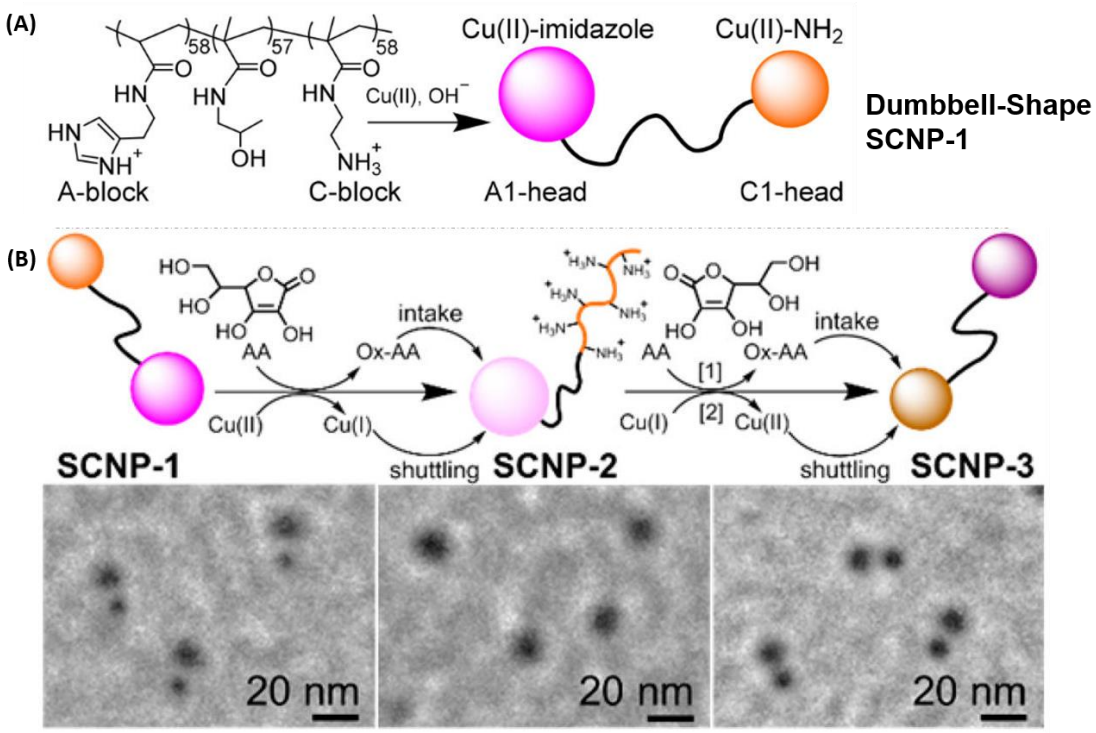

Figure 1.19 (A) Schematic illustration of the formation of dumbbell-shaped SCNP-1; (B) Suggested molecular shuttling mechanism and TEM images of SCNP.[126] *Adapted with permission from Ref. 126. Copyright 2018 American Chemical Society.*

Multi-block SCNP were synthesized by Zhang and coworkers[127] using a stepwise folding-chain extension-folding process. As shown in Figure 1.20, a multi-block copolymer was polymerized by RAFT polymerization containing hydroxyl pendants. The hydroxyl groups were cross-linked using isocyanate cross-linkers, leading to compaction of the block. Subsequent chain extension added a spacer block and a further hydroxyl-decorated block, and folding was repeated to generate SCNP with segregated compacted domains. A pentablock copolymer was synthesized by this approach bearing three individually folded subdomains with an overall dispersity of 1.21.

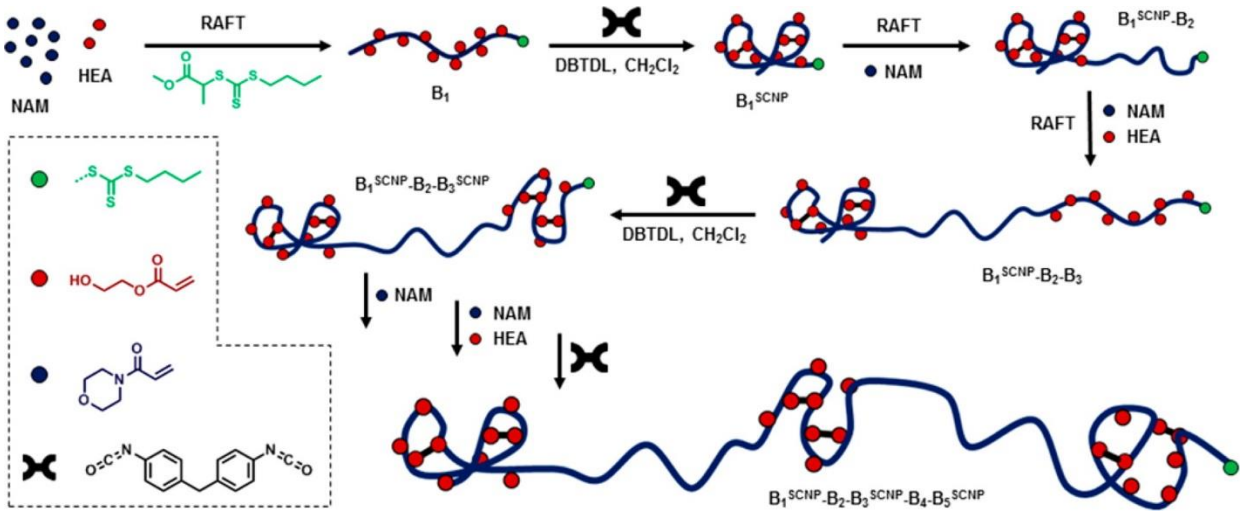

Figure 1.20 Schematic representation of the synthesis of the multiblock single-chain nanoparticles by a repeated folding-chain extension-folding process.[127] *Reprinted with permission from Ref. 127. Copyright 2016 American Chemical Society.*

1.4.3 Janus

Janus SCNP are prepared from double cross-linking of A-*b*-B diblock polymer precursors. They are a type of compartmented SCNP with distinct hydrophilicities between the compartments. Ji and coworkers[128] reported the synthesis of an amphiphilic Janus twin SCNP by two-step intramolecular cross-linking reactions including anthracene photodimerization and atom transfer radical coupling reaction. (Figure 1.21) The amphiphilic nanoparticles possess surfactant properties and reduced the surface tension of water. In aqueous solution, the nanoparticles self-assemble into vesicles with hydrophobic moieties in the inner walls and hydrophilic parts on the surface. Self-assembly behavior of the double cross-linked Janus SCNP was different from its linear precursor polymer.

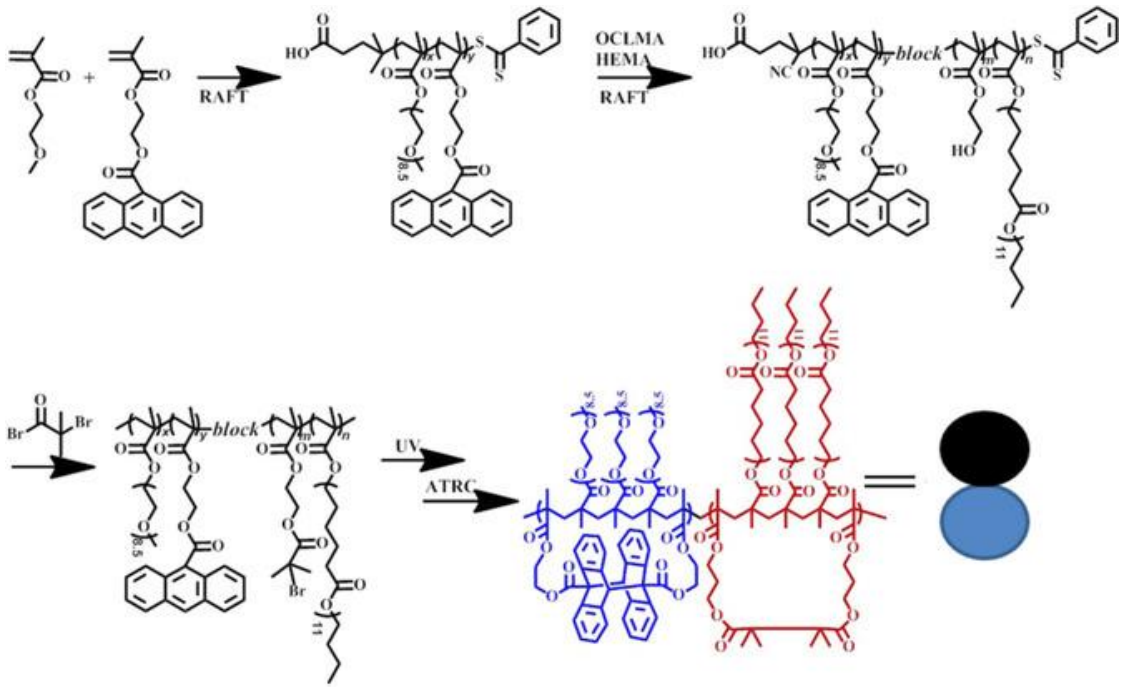

Figure 1.21 Synthesis of poly(OEGMA-co-AnMA)-block-poly(OCLMA-co-BIEMA) block copolymer, and Janus twin SCNP by two-step intramolecular cross-linking reactions.[128] *Reprinted with permission from Ref. 128. Copyright 2018 Wiley.*

The fabrication of pure Janus-type SCNP is reported by Jiang et al.[129] They synthesized a diblock copolymer A-*b*-B containing alkyne and tertiary amine pendants within the A- and B-blocks. Two-step intramolecular cross-linking *via* Glaser coupling and amine quaternization led to a mixture of single chain Janus nanoparticles, multichain particles and irregular single-chain particles. Under appropriate conditions, the single-chain Janus nanoparticles in the mixture exclusively self-assembled to form regularly structured macroscopic assemblies that crystallized out of the suspension. The exclusive self-assembly behavior of pure Janus SCNP is rationalized by the highly uniform size, shape and surface structures matching those of the surrounding SCNP. (Figure 1.22)

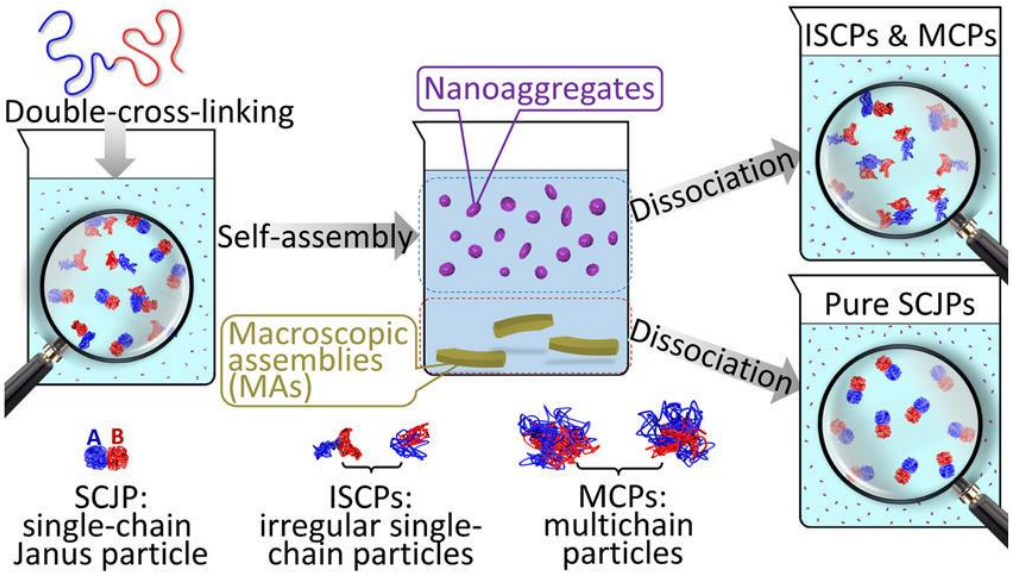

Figure 1.22 Fabrication of pure single-chain Janus particles through their exclusive self-assembly in mixtures with their analogues.[129] *Reprinted with permission from Ref. 129. Copyright 2018 American Chemical Society.*[†]

Another type of Janus SCNP was reported by Xiang and coworkers[130] and contains a cross-linked core with hydrophilic and hydrophobic tails on the opposite sides of the core. As shown in Figure 1.23, a linear polymer of polyethylene oxide-*block*-poly(2-vinylpyridine)-*block*-polystyrene (PEO-*b*-P2VP-*b*-PS) was first pretreated with $Co_2(CO)_8$ to introduce positive charges to the P2VP chain. It is crucial to introduce of electrostatic interaction along the polymer chain to allow intramolecular cross-linking at high polymer concentration.[131] The pretreated polymer was then cross-linked by metal complexation (step 1), followed by thermolysis to afford Janus SCNP containing cobalt within the core (step 2). The amphiphilic Janus nanoparticles worked as functional emulsifiers that could deliver metallic cobalt toward emulsion interfaces. They also

[†] Link to the article: https://pubs.acs.org/doi/10.1021/acsmacrolett.8b00503. Request for further reuse of this figure should go to the ACS for permission.

exhibit high catalytic capability and recyclability in the reduction of nitrobenzene to aniline at the oil-water emulsion interface.

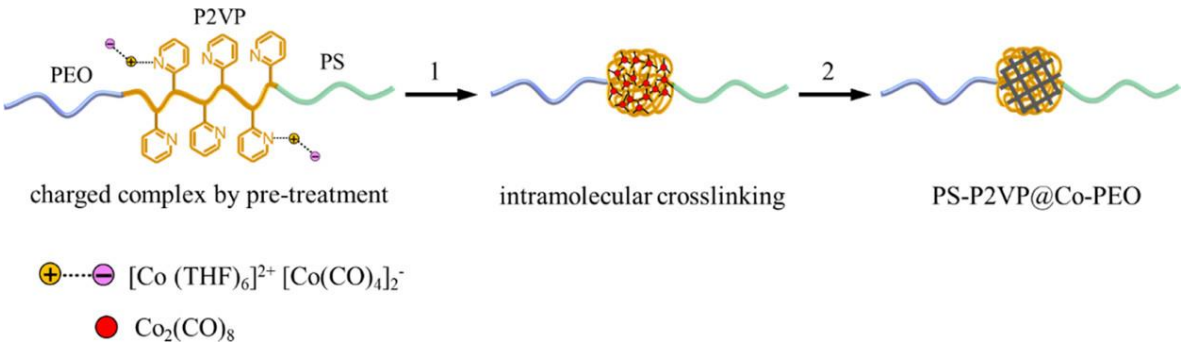

Figure 1.23 Intramolecular crosslinking of PEO-b-P2VP-b-PS by cobalt complexation and thermolysis forming single-chain Janus Composite Nanoparticle.[130] Reprinted in part with permission from Ref. 130. Copyright 2020 American Chemical Society.

1.5 Summary and outlook

Back in 2016, Hanlon et al[16] published a perspective article titled "What is next in single-chain nanoparticles?". The paper covered key challenges of the field including complex synthetic design of SCNP, obtaining folding control of polymers, SCNP functionalization, scalability, hierarchical self-assembly, characterization, and need for in-depth computer simulations. Over the past few years, we have witnessed a great amount of work devoted in these directions and significant advancement has been made in the field. In this chapter we highlighted recent examples of SCNP synthesis that afford controlled folding of linear polymer precursors, complex non-linear polymer precursors for intramolecular cross-linking, and novel conformations of SCNP. The programmed intramolecular cross-linking of polymers led to SCNP with ordered internal structure that mimic those of natural biomaterials. When catalysts were embedded in SCNP, they could be used as nanoreactors targeting a variety of reactions. SCNP with novel conformations were studied as nanostructured building blocks for higher ordered structures. New characterization techniques helped to unveil the polymer collapse process as well as the morphology of the final SCNP. And

a great number of computational studies were reported targeting the physical aspects of polymer folding. The rapid development of SCNP has shown that manipulation of single polymer molecules not only mimics the complexity of natural biomacromolecules, but also generates promising candidates for nanomaterials with practical applications.

So far, the scalability of SCNP synthesis is still a challenge requiring attention from researchers. Some new strategies have been developed targeting intramolecular cross-linking at higher concentrations such as continuous addition strategy,[132] steric stabilization by polymer brushes,[87] introducing electrostatic interaction along polymer chains,[131] and internalizing the cross-linking groups.[133] These approaches allow SCNP synthesis at higher concentrations but they are case-specific. More often SCNP synthesis still requires ultra-dilute condition which limits the scalability of SCNP. Generalized methods for efficient SCNP synthesis at higher concentration is still required. Topological purity of SCNP is another topic of concern. Due to the random conformation of polymer chains in solution and the kinetically controlled cross-linking process[129, 134], there are large structural and conformational deviations among SCNP produced in the same cross-linking system. The mixture of SCNP of different size and morphology may lead to unpredictable properties of the material. Characterization and purification of the topologically impure SCNP is needed to achieve the same level of precision and complexity as natural biomacromolecules.

Chapter 2. Assessing structure/property relationships and processing conditions in the fabrication of poly(oxanorbornene imide) single-chain nanoparticles[‡]

2.1 Introduction

Biomacromolecules have been a source of inspiration to polymer chemists in the design of well-defined materials with advanced functionalities. Perhaps the most fundamental and universal example is protein structure, where linear polypeptide chains fold into specific three-dimensional structures with precision and fidelity. This intricate process requires both a precise amino-acid sequence and self-assembly of its component molecular structures, and results in nanomaterials with unique biological activities such as recognition and catalysis.[17, 135] Progress in controlled radical polymerization has enabled the synthesis of polymers with narrow dispersity and diverse functionalities.[136-139] However, construction of materials with structural hierarchies comparable to those in nature remains a challenging research goal. A technique that represents a step towards these ends is the self-folding of single polymer chains in dilute solution to create globular nanoparticles, referred to as single-chain nanoparticles (SCNP).[16-18, 25, 33, 36, 40, 104] The concept is simple: synthesize linear polymers decorated with pendant groups that are able to form covalent or supramolecular bonds. Following intra-chain cross-linking of these pendant groups, the individual polymer chains compact into polymeric nanoparticles smaller than dimensions of the

[‡] This chapter is published in *European Polymer Journal*. Reproduced with permission from Elsevier.
Chen, R.; Benware, S. J.; Cawthern, S. D.; Cole, J. P.; Lessard, J. J.; Crawford-Eng, I. M.; Saxena, R.; Berda, E. B., Assessing structure/property relationships and synthetic protocols in the fabrication of poly(oxanorbornene imide) single-chain nanoparticles. *European Polymer Journal* **2019,** *112*, 206-213.

solvated coil, usually less than 20 nm in size and controllable based on the molecular weight of the parent chain.[15] SCNP offer a simplified route to crudely mimic protein tertiary structure[41] and show promise for applications in catalysis,[38, 68-69, 71, 75, 140] nanomedicine,[141-142] nanoreactors,[143-144] sensors,[145] etc.

A variety of crosslinking chemistries have been reported on the synthesis of SCNP, including covalent,[146-150] dynamic covalent [151] and noncovalent bonding.[16, 39, 152] High-yielding reactions with minimal side products are preferred as this promotes more efficient folding and simplified purification. Intrachain polymerization of reactive pendant groups is therefore an attractive crosslinking strategy since 1) it produces little or no byproduct, and 2) it offers a possibility to easily tune the compactness of an SCNP by controlling the degree of intrachain polymerization. Several groups have demonstrated this strategy: Miller and coworkers reported the synthesis of acrylic-functionalized poly(caprolactone). These pendant acrylic groups were initiated with AIBN under ultra-dilute conditions resulting in self-crosslinked nanoparticles.[153] Jiang and Thayumanavan prepared amine-functionalized polystyrene with pendant styryl moieties which were subsequently intrachain polymerized to yield SCNP.[154] Dirlam and coworkers used intramolecular oxidative polymerization of styrenic functional propylenedioxythiophene to afford SCNP.[155] Another example recently reported by Zhou et al displayed the synthesis of SCNP by intrachain ring-opening metathesis polymerization (ROMP) using polymers bearing furan-protected maleimides.[156] These methods, although involving intricate multi-step syntheses, highlight the versatility of intrachain polymerization techniques in the efficient fabrication of SCNP.

Our group recently investigated the use of ROMP of norbornene imides (NBI) to create linear chains that are functionalized for post-ROMP intrachain radical polymerization.[157] ROMP was

chosen as it is highly functional group tolerant, proceeds rapidly, and leads to easy access of functional materials. While simple in design, the intrachain crosslinking was more complicated than expected, presumably because the rigidity of the polymer backbone might inhibit pendant groups from finding nearby partners. This work also revealed that the ROMP of these monomers was sometimes plagued with side reactions leading to unwanted high molecular weight branched materials. Further, crosslinking under ambient conditions gave some ambiguous results due to the role of oxygen. We present a follow up to this study here, examining the effect of increasing the spacing between polymer backbone and pendant reactive groups. We prepared methacryloyl-functionalized oxanorbornene imide (ONBI) monomers with 2 carbon and 6 carbon spacers between ONBI and methacryloyl groups. These monomers were then subjected to ROMP conditions. We found that the presence of a radical inhibitor was necessary to ROMP methacryloyl-containing ONBI monomers in order to achieve well-defined linear polymers. The poly(ONBI) were then initiated with AIBN under ultra-dilute conditions with strict exclusion of oxygen to afford SCNP. We studied the length and flexibility of pendant groups in relation to the folding efficiency of poly(ONBI).

2.2 Results and discussion

2.2.1 Polymer design

We surmised it likely that due to the persistence length of poly(ONBI) backbone, coupling of reactive pendant groups is hindered by short contour distances. Increasing pendant lengths and flexibility will presumably increase the folding efficiency of this semi rigid polymer chain. In this work, we sought to demonstrate structural parameters of pendant groups, including pendant length and amount incorporation in relation to SCNP synthesis of poly(ONBI) *via* intrachain radical polymerization. Scheme 2.1 illustrates the chemical structures of our monomers and polymers. We

prepared methacryloyl-functionalized ONBI monomers with 2 carbons (n = 1, M2) and 6 carbons (n = 3, M3) as spacers between ONBI and methacryloyl groups. N-hexyl-ONBI (M1) was synthesized as a comonomer. Linear copolymers that contain various incorporations of M2 and M3 were obtained *via* ROMP. Subjecting the linear methacryloyl-containing copolymer to AIBN in dilute solution initiates intra-chain radical polymerization of pendant methacryloyl groups, leading to SCNP.

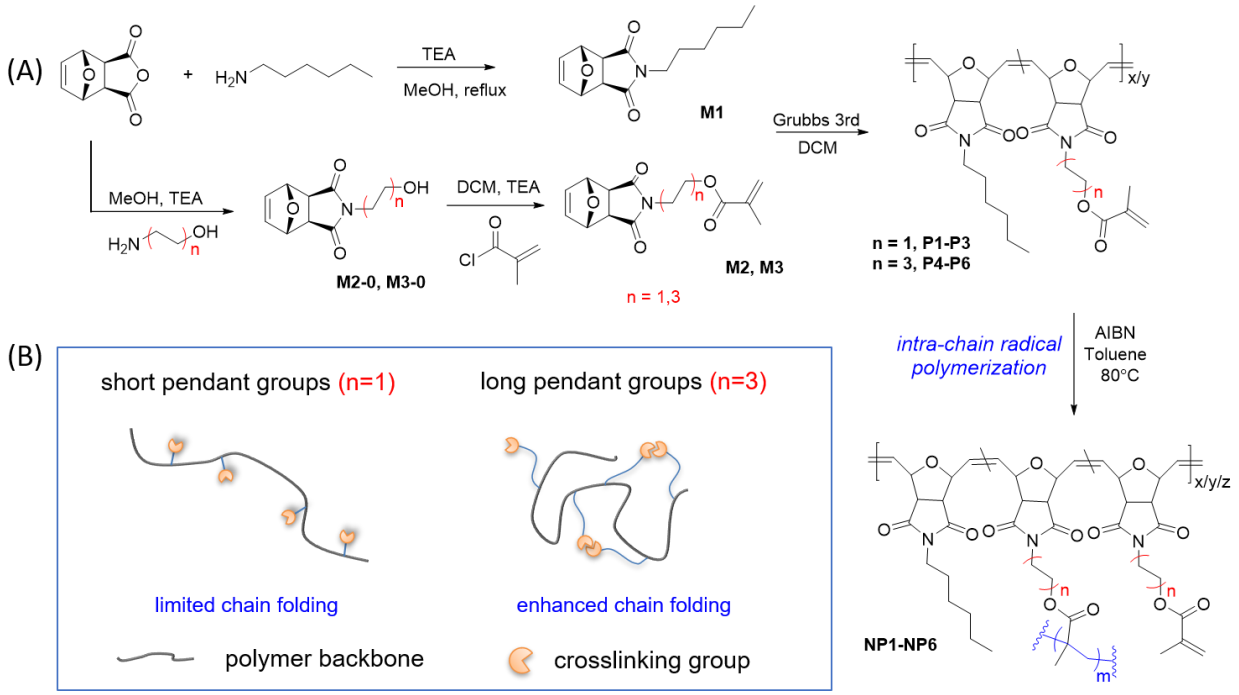

Scheme 2.1 (A) Synthetic route to poly(ONBI) SCNP by intrachain radical polymerization; (B) Proposed pendant effect on the efficiency of chain folding.

2.2.2 ROMP of methacryloyl-functionalized ONBI

ROMP is extensively used in the preparation of functional polymers since it allows for direct incorporation of a wide variety of functional groups into polymers with narrow dispersity and defined molecular weights.[158-159] While some reports show that methacryloyl groups can undergo cross metathesis in presence of Grubbs catalysts,[160-161] cross metathesis of electron deficient methacryloyl groups generally requires heating and long reaction time, [160-161] typically heating to

reflux in DCM or toluene for at least 12 hours. In this study, we are using the fast initiating Grubbs 3rd catalyst which leads to quantitative conversion of monomers in 3 minutes at room temperature. This design should have allowed for direct ROMP of methacryloyl-containing ONBI monomers to afford poly(ONBI) with pendant methacryloyl groups.

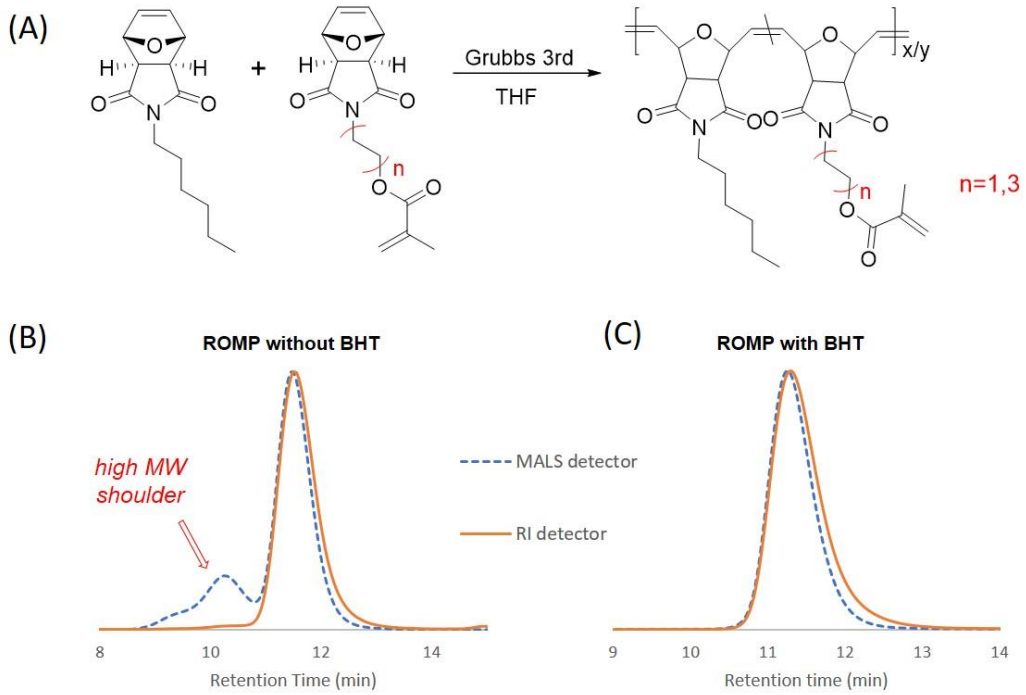

Figure 2.1 (A) Synthesis of methacryloyl-containing copolymers by ROMP; (B) SEC trace of copolymers polymerized without BHT, and (C) with BHT.

ROMP of M2 and M3 gave polymers that showed unimodal trace by RI detection when characterized with SEC. However by MALS detection a shoulder peak with shorter retention time often existed (Figure 2.1A, B). Since MALS detectors are sensitive to high molecular weight species while RI detectors are concentration-related, we attributed this shoulder peak to some byproduct with a high molecular weight but low concentration, presumably from interchain crosslinking.[162] We hypothesized that undesirable interchain reactivity during ROMP could be explained in one of three ways (Scheme 2.2). Option A is that the poly(ONBI) backbone undergoes

autoxidation/peroxidation, generating hydroperoxyl radicals that could result in interchain crosslinking *via* reactions with unsaturation sites on other chains. Option B is that cross metathesis of the methacryloyl units with ONBI groups is interfering with the linear ROMP reaction and forming branches and crosslinks in the polymer. Finally, option C is that radical oligomerization of the methacryloyl units is happening concurrently with ROMP, and that because the chains are in a relatively high concentration, interchain reactions occur.

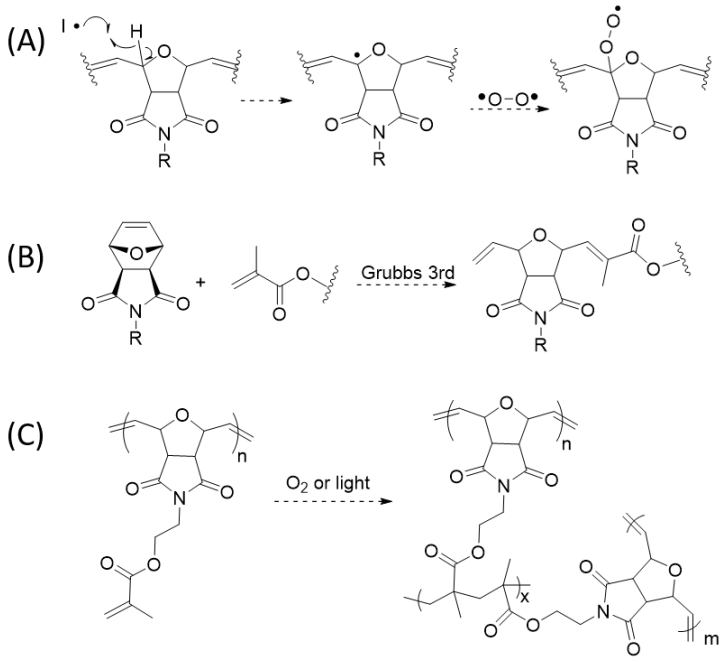

Scheme 2.2 Possible crosslinking side reactions during ROMP: (A) autoxidation on poly(oxanorbornene imide) backbone, (B) cross metathesis of pendant methacryloyl group, (C) interchain radical polymerization of pendant groups.

To test hypothesis A, we synthesized homopolymers of M1, M2 and M3. Although the three polymers shared the same poly(ONBI) backbone, we found that high MW shoulders only showed up in homopolymers of M2 and M3. This implies that the polymer backbone is not the cause of high MW shoulder, and that the presence of pendant methacryloyl group is the reason for high MW species. To test if methacryloyl groups interfere with ROMP by olefin metathesis, we added ethylene dimethacrylate during ROMP of M1. The dimethacrylate would act as a crosslinker

between two ONBIs if it participates in the metathesis, and lead to poor control of molecular weight. However, SEC results revealed that the presence of dimethacrylate during ROMP did not affect homopolymerization of M1. This leaves us with hypothesis C, a small amount of oligomerization of pendant methacryloyl groups. Since this is a radical side reaction, we simply added a radical inhibitor BHT during ROMP to prevent it. In this experiment the high MW shoulder peak did not show up (Figure 2.1C). It is now clear that the high MW shoulder peak was induced by interchain radical polymerization of pendant methacryloyl groups during ambient ROMP, and it can be prevented by adding a radical inhibitor such as BHT.

Using the BHT-modified ROMP procedure, we prepared a series of polymers with approximately 10, 20, and 50% incorporations of M2 and M3. P1-P3 were synthesized from copolymerization of M1 and M2. P4-P6 were made from copolymerization of M1 and M3. All polymers exhibited narrow molecular weight distributions with dispersities ranging from 1.03 to 1.10 and similar molecular weights of 45-55 kDa. ^{1}H NMR spectroscopy was used to determine the composition of each polymer. The mole fraction of methacryloyl-ONBI monomers were calculated from the ratio of the peak area around 3.79 ppm, corresponding to the methylene protons adjacent to oxygen on M2 and M3, to the area of peak at 0.87 ppm, which is attributed to the three methyl protons in M1 (Figure 2.7).

2.2.3 Synthesis of SCNP

We adopted a systematic nomenclature to describe these systems as follows: each parent linear polymer is assigned a number and given the prefix **P**. The corresponding nanoparticles obtained are labeled **NP** with the following number indicating which polymer precursor was used.

Single-chain nanoparticles were formed by subjecting the polymers to a radical initiator AIBN. We used 0.1 eq of AIBN to the amount of pendant methacryloyl groups on corresponding polymers.

The process was carried out in dilute solutions (1 mg/mL) to prevent intermolecular reaction and favor intrachain crosslinking. Freeze-pump-thaw cycles were performed to thoroughly exclude oxygen in the system, as autoxidation on allylic carbons generate peroxyl radicals that could crosslink the polymer through oxygen bridging or cause oxidative degradation of the backbone. Formation of each SCNP was confirmed by SEC, with a shift to longer retention time compared to its linear precursor, as well as a decrease in hydrodynamic radius (R_η) and intrinsic viscosity (η), indicating a more compact conformation.

As a control experiment, we prepared a homopolymer of M1, which contains no methacryloyl pendant group. When subjected to SCNP synthesis conditions, this polymer exhibited no change in its SEC trace (Figure 2.2), indicating that the poly(ONBI) backbone is not involved in the crosslinking reaction, and any change in SEC results could be attributed to reactions occuoccurringrred on pendant methacryloyl groups.

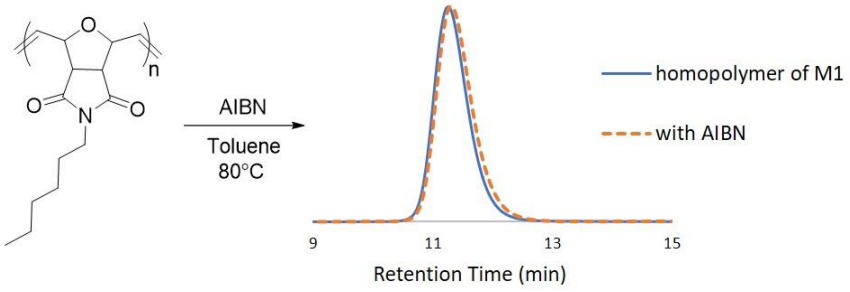

Figure 2.2 SEC traces of homopolymer M1 after exposed to SCNP synthesis condition.

Figure 2.3A shows an example of a successful SCNP synthesis. P2 contains around 20% incorporation of the functional monomer M2. When exposed to AIBN in dilute solution, the resulting NP2 shows an obvious shift to longer retention time in SEC, indicating the transition to a nanoparticle. A decrease in R_η from 5.9 nm to 4.5 nm, as well as a decrease in intrinsic viscosity

from 28.9 to 9.8 mL/g were also observed. (Table 2.1). The crosslinking chemistry was confirmed by ^{1}H NMR spectroscopy. As seen from Figure 2.3B, the peak labeled a at 5.6 ppm corresponds to a proton on the pendant methacryloyl group on P2. The intensity of peak "a" drastically decreased when the chain is folded into a nanoparticle. This indicates successful initiation and propagation of methacryloyl groups in parent polymers.

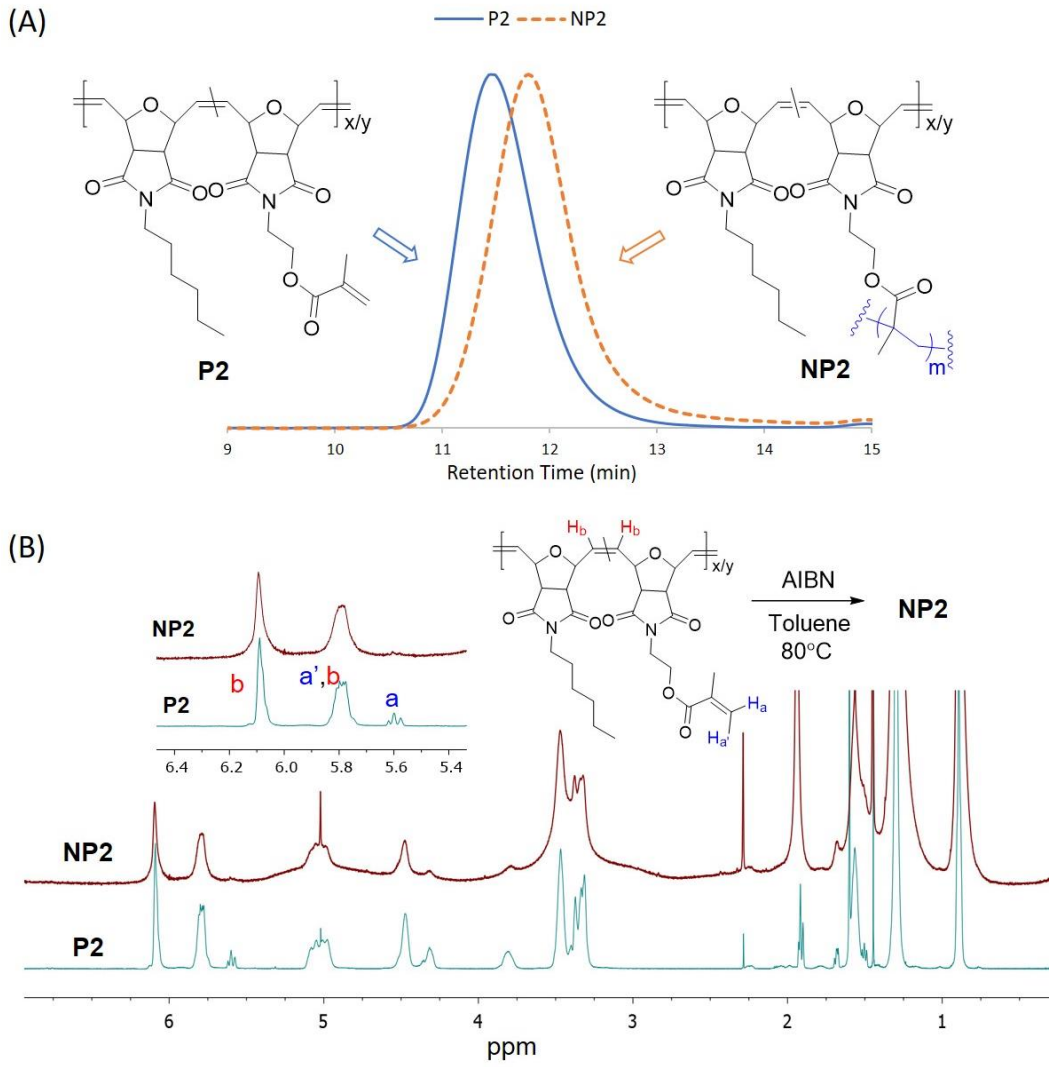

Figure 2.3 (A) SEC-MALS trace showing the transition from P2 to NP2; (B) ^{1}H NMR spectra of P2 and NP2 with olefin regions zoomed in.

The characteristic methacryloyl signals at 5.6 ppm and 5.8 ppm in ^{1}H NMR spectra partially overlap with the olefin peaks on the polymer backbone at 5.8 ppm and 6.1 ppm. Meanwhile, after chain folding, the resulting nanoparticles' peaks are broadened in ^{1}H NMR spectra and are sometimes difficult to interpret. To further corroborate that crosslinking took place on the pendant methacryloyl groups, we added styrene in the intrachain polymerization of methacryloyl groups. The resulting nanoparticles were labeled NP7. Styrene can copolymerize with methacryloyl groups, and with its distinguishable peaks, will be easily observed in ^{1}H NMR spectra. As seen in Figure 2.4, the yielded NP7 exhibits a broad peak at 7.0 -7.5 ppm, which belongs to the protons on styrene. SEC-UV traces of NP7 did not show any response that could be attributed to homopolymer of styrene, indicating that the styrene responses from ^{1}H NMR spectrum were solely from copolymerization with methacryloyl groups. These results confirmed that the SCNP formed under our reaction conditions were indeed from intrachain radical polymerization of pendant methacryloyl groups.

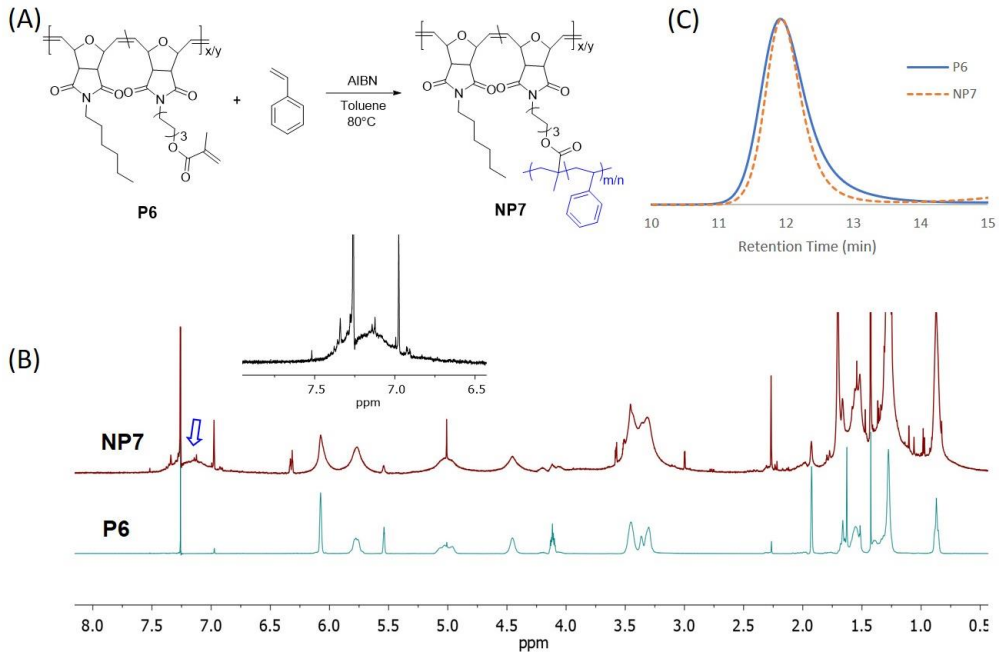

Figure 2.4 (A) Intrachain copolymerization of pendant methacryloyl group with styrene; (B) ^{1}H NMR spectra of P6 and NP6 with aromatic region zoomed in; (C) SEC-UV trace of P6 and NP7.

To study structural parameters in relation to chain folding, we initiated intrachain radical polymerizations on P1-P6. P1-P3 contains a shorter pendant group, with 2 carbons as a spacer between the methacryloyl group and poly(ONBI) backbone. We found that with around 10% incorporation of methacryloyl group, there was a shift to longer retention time in SEC, indicating a more compact structure upon chain folding (Figure 2.5). The decrease in hydrodynamic radius and intrinsic viscosity further confirms this finding (Table 2.1). When the incorporation of methacryloyl group is increased to around 20%, a more pronounced shift in retention time was observed as well as a greater extent of reduction in radius and intrinsic viscosity. When we continue to increase the incorporation of methacryloyl groups to 50%, the SEC-MALS trace of the resulting nanoparticle NP3 broadened and slightly shifted to shorter retention time. We attributed this observation to intermolecular reactions due to a higher concentration of methacryloyl groups.

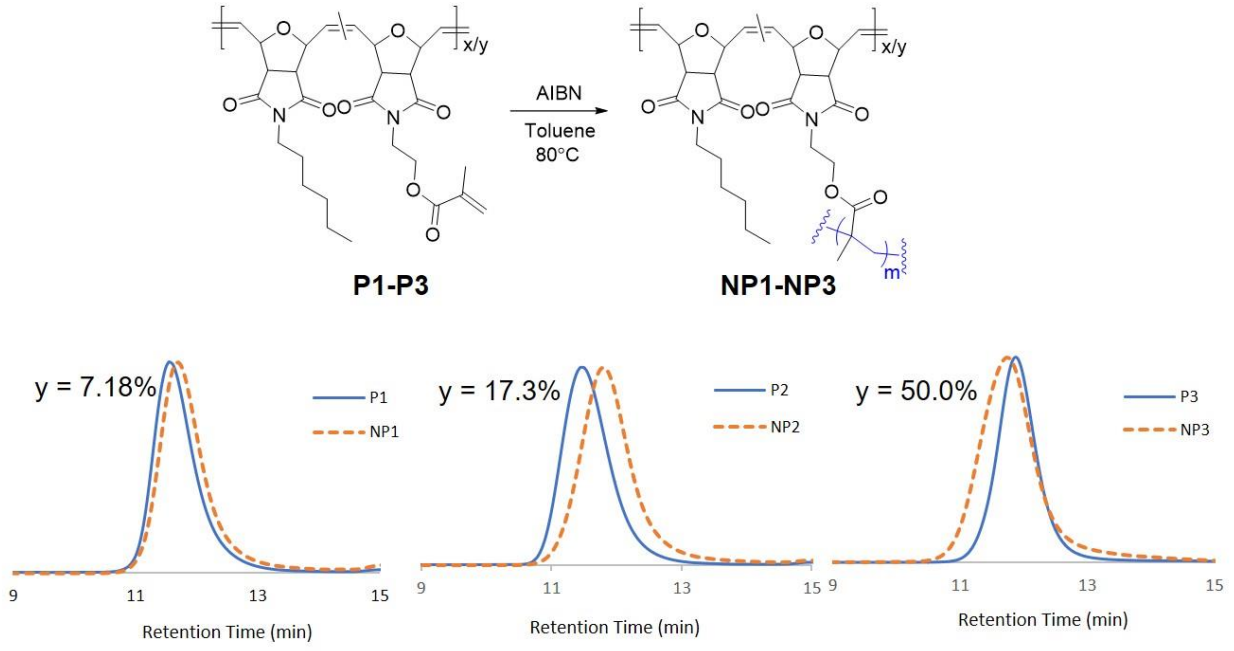

Figure 2.5 SEC-MALS of P1-P3 and corresponding NP1-NP3. y is percent incorporation of methacryloyl groups.

Table 2.1 SEC data for polymers P1-P6 and corresponding nanoparticles NP1-NP6

	Sample	Methacryloyl % incorp.	M_n [a] (kDa)	M_w [a] (kDa)	Đ [a]	R_η [a] (nm)	η [a] (mL/g)	dn/dc [a]	Peak retention time(min)
n = 1	P1	7.2	45.5	46.8	1.03	5.4	22.5	0.116	11.5
	NP1		46.0	50.4	1.10	4.8	15.8	0.109	11.6
	P2	17.3	45.7	47.5	1.04	5.9	28.9	0.119	11.4
	NP2		62.2	70.3	1.13	4.5	9.8	0.114	11.7
	P3	50.0	41.8	42.6	1.02	4.1	10.1	0.129	11.9
	NP3		123	141	1.15	4.7	6.6	0.076	11.8
n = 3	P4	6.6	59.4	65.4	1.10	6.1	26.1	0.119	11.3
	NP4		60.5	71.1	1.18	5.4	17.8	0.110	11.5
	P5	17.6	43.4	45.1	1.04	5.9	28.0	0.121	11.4
	NP5		53.9	59.6	1.11	4.2	9.0	0.113	11.8
	P6	45.5	55.3	57.4	1.04	4.0	7.9	0.121	11.8
	NP6		90.1	103	1.14	4.2	5.5	0.107	11.7

[a.] Obtained using triple detection SEC. See experimental section for more details. [b.] Calculated from MALS detector trace.

P4-P6 consist of a longer pendant group, with 6 carbons between the polymer backbone and pendant methacryloyl group. When subjecting P4-P6 to intrachain folding, a similar trend was found with P1-P3: Increasing the incorporation of methacryloyl units from 10% to 20% results in what we interpret as more efficient chain folding, but with 50% methacryloyl groups, a broadened MALS trace was found with a shift to shorter retention time, which is likely due to interchain reactions (Figure 2.6). When comparing NP1-NP3 with NP4-NP6, we found that increasing the space between polymer backbone to methacryloyl group from 2 carbons (n=1) to 6 carbons (n=3) did not make an observable difference in the efficiency of chain folding.

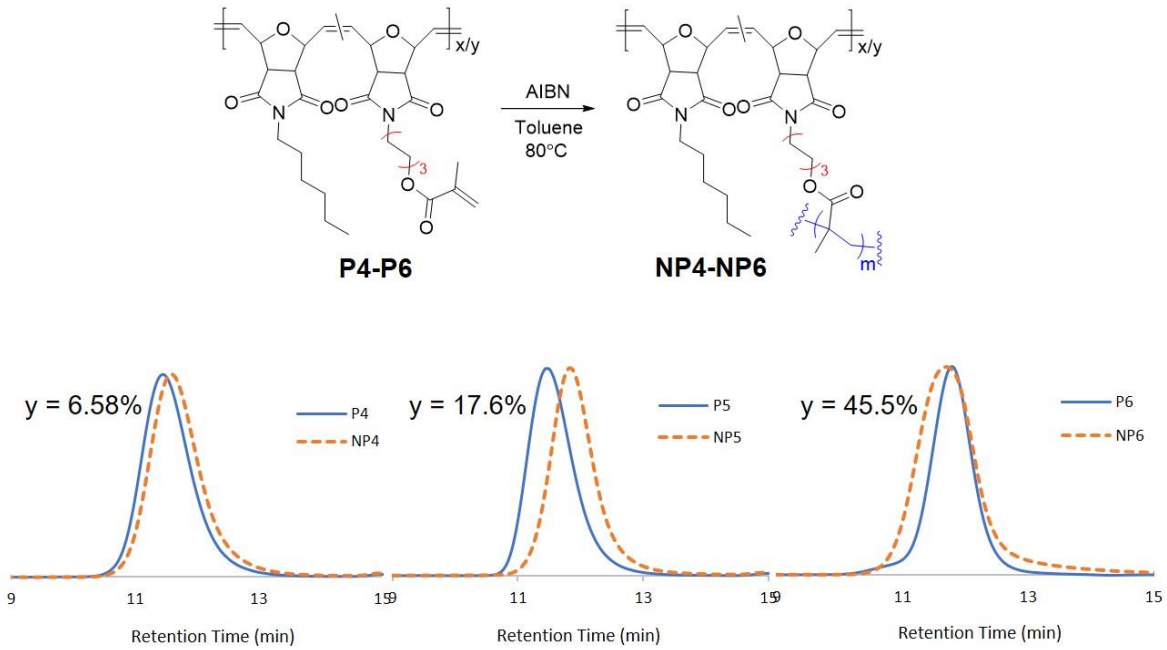

Figure 2.6 SEC-MALS of P4-P6 and corresponding NP4-NP6. y is percent incorporation of methacryloyl groups.

2.3 Conclusions

We have shown that synthesizing well-defined poly(ONBI) with methacryloyl-containing monomers in ambient environment through ROMP requires a radical inhibitor to prevent interchain crosslinking. Based on these findings we developed a method for fabricating single-chain nanoparticles through intrachain radical polymerization of pendant methacryloyl groups on poly(ONBI). Our results indicate that increasing pendant group length did not noticeably affect the efficiency in folding of a polymer chain at the length scales we synthesized. We also demonstrated that by changing the percent incorporations of pendant polymerizable unit in the parent polymer, the size of the resulting nanoparticles could be controlled consistent with our previous work.

2.4 Experimental

2.4.1 Materials

Reagents were obtained from the indicated commercial suppliers and used without further purification unless otherwise stated: exo-3,6-epoxy-1,2,3,6-tetrahydrophthalic anhydride (TCI), hexylamine (Sigma-Aldrich), triethylamine (TEA, Fisher Scientific), 2-aminoethanol (TCI), 6-amino-1-hexanol (Sigma-Aldrich), methacryloyl chloride (Sigma-Aldrich), hexanes (Fisher Scientific), ethyl acetate (Fisher Scientific), Grubbs catalyst 2nd generation (Sigma-Aldrich), 3-bromopyridine (Fisher Scientific), ethyl vinyl ether (Acros Organics), 2,2'-azobis(2-methylpropionitrile) (AIBN, Sigma-Scientific, recrystallized from methanol), butylated hydroxyltoluene (BHT, Sigma-Aldrich), styrene (Sigma-Aldrich, passed through a plug of basic alumina), silica gel (230 – 400 mesh, SiliCycle), THF (HPLC grade, Fisher Scientific, inhibited with BHT), sodium bicarbonate (Fisher Scientific), chloroform-d ($CDCl_3$, Cambridge Isotope Laboratories). Dry toluene, dichloromethane (DCM) and methanol (MeOH) were obtained from an Innovative Technology solvent purification system model SPS-400-.5.

2.4.2 Instrumentation

^{1}H and ^{13}C NMR spectra were acquired with a Varian Unity INOVA or Bruker Biospin 500 MHz or Varian Mercury 400 MHz spectrometer. Chemical shifts (δ) were reported in parts per million (ppm) relative to tetramethylsilane (TMS). Solvent ($CDCl_3$) contained 0.03% v/v TMS as an internal reference. Peak abbreviations are used as follows: s = singlet, d = doublet, t = triplet, q = quartet, m = multiplet, br = broad, Ar = Aryl).

SEC was performed on a Tosoh EcoSEC dual detection (RI and UV) SEC system coupled to an external Wyatt Technologies miniDAWN Treos multiangle light scattering (MALS) detector and a Wyatt Technologies ViscoStar II differential viscometer. Samples were run in THF at 40 °C at

a flow rate of 0.35 mL/min. The column set contained one Tosoh TSKgel SuperHM-M (6.0 mm ID × 15 cm) column, one Tosoh TSKgel SuperH2500 (6.0 mm ID × 15 cm) column and a Tosoh TSKgel SuperH5000-7000 guard column (4.6 mm ID × 3.5 cm). All polymer solutions characterized by SEC were 1.0 mg/mL in THF, stirred magnetically for at least 5 hours and filtered through 0.45 μm PTFE syringe filters before analysis.

2.4.3 dn/dc calculation

To calculate refractive index increment values (dn/dc), at least 3 injections were performed for each polymer sample with various injection mass. dn/dc values were calculated based on the slope of linear regression when plotting RI area versus injection mass.

The response from RI detector is proportional to instrument constant K_{RI}, sample concentration c (mg/mL), and dn/dc value of the sample. In the following equations (Eq 2.1, Eq 2.2) m_{inj} represents injected mass (μg), V_{inj} is the injection volume (μl).

$$RI_{signal} = K_{RI} * c * \frac{dn}{dc} \quad \text{(Eq 2.1)}$$

$$RI_{area} = K_{RI} * c * V_{inj} * \frac{dn}{dc} = K_{RI} * m_{inj} * \frac{dn}{dc} \quad \text{(Eq 2.2)}$$

When plotting RI area versus injected mass, and perform a linear regression, the slope was found to be:

$$Slope = K_{RI} * \frac{dn}{dc} \quad \text{(Eq 2.3)}$$

We first calculated K_{RI} with a narrow-dispersed polystyrene standard with known dn/dc (M_n = 30K, dn/dc = 0.185), then use the resulting K_{RI} to calculate the dn/dc of another PS standard (Mn=49K) using the abovementioned method. An expected dn/dc value was retrieved (calculated dn/dc=0.1850), proving that this is a reliable method to calculate dn/dc values.

2.4.4 Determination of copolymer composition

The mole fraction of methacryloyl-ONBI monomers M2 was calculated from the ratio of the NMR peak area of c to the area of peak f, as the equation shown in Figure 2.7.

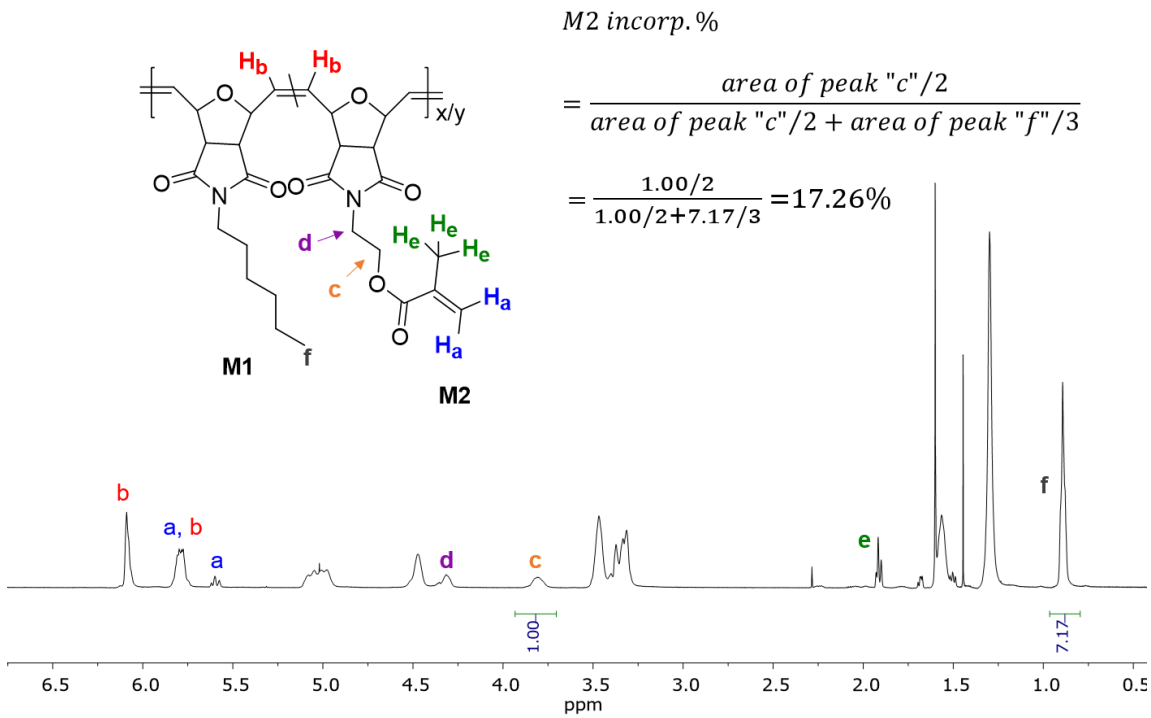

Figure 2.7 ^{1}H NMR spectrum of P2 with peak assignment.

2.4.5 Experimental procedures

2.4.5.1 Synthesis of N-hexyl oxanorbornene imide (M1)

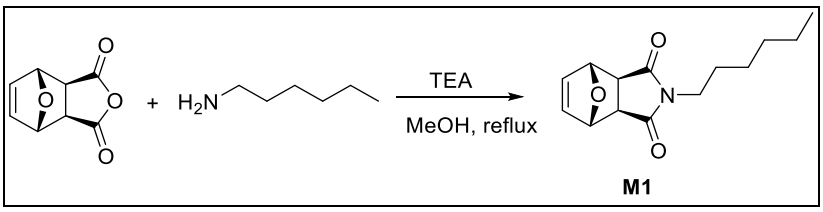

Exo-3,6-epoxy-1,2,3,6-tetrahydrophthalic anhydride (5 g, 30.1 mmol, 1 eq), hexylamine (4.37 mL, 33.1 mmol, 1.1 eq) and triethylamine (0.46 mL, 3.31mmol, 0.1 eq) were added to a round bottom flask with 50 mL of dry methanol. The mixture was stirred at reflux for 24 h and cool to room temperature. Methanol was removed through rotary evaporation. Crude product was dissolved in

30 mL of DCM, washed with 0.1 M HCl (50 mL × 2), Brine (50 mL × 2), and purified by column chromatograph using a 1:1 hexanes:ethyl acetate eluent to obtain pure product. (1.63 g, 21.73% yield) ^{1}H NMR (400 MHz, $CDCl_3$, δ, ppm): 6.50 (t, 2H), 5.25 (t, 2H), 3.45 (m, 2H), 2.82 (s, 2H), 1.47-1.57 (m, 2H), 1.20-1.33 (q, 6H), 0.79-0.90 (m, 3H). See appendix page 115 for full spectra.

2.4.5.2 Synthesis of OH-functionalized oxanorbornene imide (**M2-0**, **M3-0**)

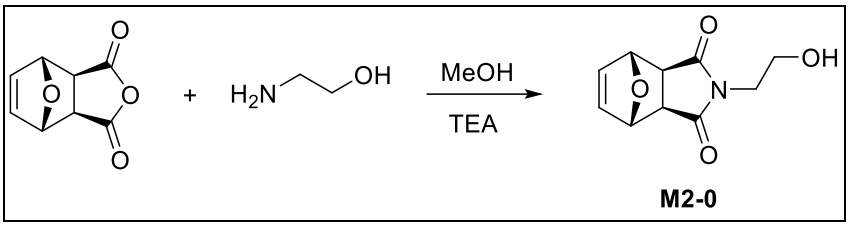

M2-0

M2-0: Exo-3,6-epoxy-1,2,3,6-tetrahydrophthalic anhydride (5 g, 30.1 mmol, 1 eq) and 2-aminoethanol (1.82 mL, 30.1 mmol, 1 eq) were added to a round bottom flask with 10 mL of dry methanol and brought to reflux. After 16 hours the mixture was cooled to room temperature then stored in freezer overnight to allow crystallization. Product was collected by vacuum filtration. (3.05 g, 48.41% yield) ^{1}H NMR (400 MHz, $CDCl_3$, δ, ppm): 6.53 (s, 2H), 5.29 (s, 2H), 3.78 (t, 2H), 3.71 (t, 2H), 2.90 (s, 2H), 2.22 (br, 1H). See appendix page 116 for full spectra.

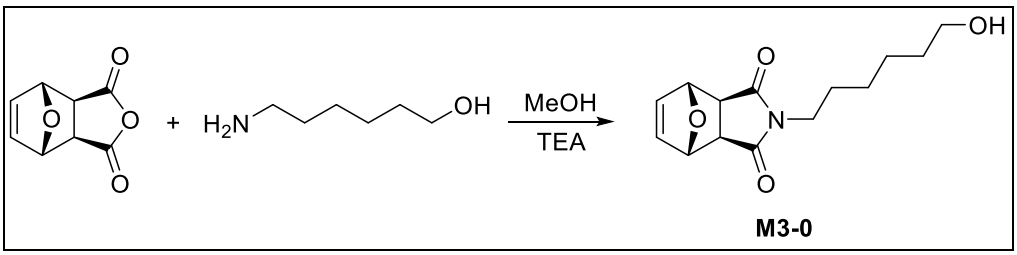

M3-0

M3-0: Exo-3,6-epoxy-1,2,3,6-tetrahydrophthalic anhydride (5 g, 30.1 mmol, 1 eq), 6-aminohexanol (3.88 g, 33.1 mmol, 1.1 eq) and triethylamine (0.46 mL, 3.31mmol, 0.1 eq) were added to a round bottom flask with 25 mL of dry methanol. The mixture was stirred at reflux for 24 and then cool to room temperature. Methanol was removed in vacuo. Crude product was

dissolved in 30 mL of DCM, washed with 0.1 M HCl (50 mL × 2), Brine (50 mL × 2) and purified by column chromatography. (Hex: EtOAc = 1:4, 2.06 g, 25.78% yield) ^{1}H NMR (400 MHz, $CDCl_3$, δ, ppm): 6.52 (s, 2H), 5.26 (s, 2H), 3.61 (t, 2H), 3.48 (t, 2H), 2.84 (s, 2H), 1.65 (br, 1H), 1.25-1.59 (m, 6H); ^{13}C NMR (400 MHz, $CDCl_3$, δ, ppm): 176.35, 136.50, 80,89, 62.55, 47.35, 38.76, 32.41, 27.43, 26.14, 25.02. See appendix page 117 for full spectra.

2.4.5.3 Synthesis of methacryloyl-functionalized oxanorbornene imide (**M2, M3**)

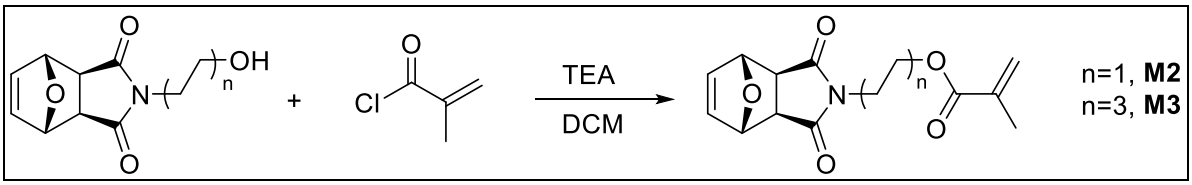

M2-0 or M3-0 (1 eq) was dissolved in dry DCM and added TEA (1.2 eq). The mixture was cooled over an ice bath and methacryloyl chloride (1.2 eq) was added dropwise. The mixture was stirred over ice for an additional 10 min before warmed up to room temperature. After 5 hours the reaction was quenched with saturated sodium bicarbonate (50 mL). Organic layer was washed with sodium bicarbonate (50 mL × 2) and Brine (50 mL × 2). Crude product purified by column chromatography. (Hex: EtOAc = 1:1, 60-90% yield) M2: ^{1}H NMR (400 MHz, $CDCl_3$, δ, ppm): 6.52 (s, 2H), 6.07 (s, 1H), 5.56 (s, 1H), 5.26 (s, 2H), 4.25-4.36 (m, 2H), 3.75-3.88 (m, 2H), 1.90 (s, 3H); M3: ^{1}H NMR (400 MHz, $CDCl_3$, δ, ppm): 6.51 (s, 2H), 6.09 (s,1H), 5.55 (s, 1H), 5.26 (s, 2H), 4.12 (t, 2H), 3.47 (t, 2H), 2.84 (s, 2H), 1.94 (s, 3H), 1.24-1.67 (m, 8H). See appendix page 118 and 119 for full spectra.

2.4.5.4 Synthesis of poly(oxanorbornene imide) via ROMP (**P1-P6**)

In a glovebox, monomers were dissolved in dry DCM in a scintillation vial. Grubbs' 3rd generation catalyst was dissolved in dry DCM in another scintillation vial. The monomer solution was added

to the catalyst solution while stirring. The reaction was run in the glovebox at room temperature for 3 min before quenched with excess ethyl vinyl ether, moved out of glovebox and added BHT (around 50 mg). After 12 hours the polymer was precipitated into methanol and isolated as a white solid with quantitative yield. The polymers were dried in the vacuum oven at 35 °C for 12 hours and stored in the freezer under Argon. See appendix page 120 through 125 for ^{1}H NMR spectra and GPC chromatograms of P1-P6.

2.4.5.5 SCNP synthesis *via* intra-chain radical polymerization (**NP1-NP6**)

Methacryloyl-decorated poly(oxanorbornene imide) (30 mg) was dissolved in dry toluene in a Schlenk flask to a concentration of 1 mg/mL. AIBN (0.1 eq to the methacryloyl groups) was added to the flask. The mixture was subjected to freeze-pump-thaw cycles until no visible bubble before being heated to 80 °C and stirred for 24 h. The solution was cooled to room temperature and BHT (around 10 mg) was added. Toluene was removed *via* rotary evaporation. Product was dissolved in a minimum amount of DCM, precipitated into cold hexanes, and dried in a vacuum oven at 40 °C overnight. Product was retrieved as a white solid with quantitative yield. See appendix page 126 through 131 for ^{1}H NMR spectra and GPC chromatograms of NP1-NP6.

2.4.5.6 Intra-chain copolymerization of methacryloyl pendants with styrene (**NP7**)

P6 (50mg) and styrene (20 μL, 2 eq to methacryloyl groups on P6) was dissolved in 50 mL of dry toluene in a Schlenk flask. AIBN (1.42 mg, 0.1 eq) was added. The mixture was subjected to free-pump-thaw cycles until no visible bubble before being heated to 80 °C and stirred for 24 h. Solution was cooled to room temperature and BHT (around 10 mg) was added. Toluene was removed via rotary evaporation. Product was dissolved in a minimum amount of DCM, precipitated into cold

hexanes, and dried in a vacuum oven at 40 °C overnight. (Yield: 49.42 mg) See appendix page 132 for for ^{1}H NMR spectra and GPC chromatograms of NP7.

Chapter 3. Fabrication of SCNP *via* intrachain radical polymerization: DP of intra-chain cross-links

3.1 Introduction

The creation of polymeric nanoparticles has been extensively studied over the past decade with appealing applications in drug delivery,[37, 163-164] nanoreactors,[144, 165-166] catalysis[68, 140] and so on. A number of different techniques have been developed for the synthesis of these polymer nanoparticles depending on the size, functionality and topology of the targeted materials, including emulsion-based polymerizations,[167-168] self-assembly of amphiphilic polymers,[123, 169-170] lithography,[171-172] etc. However, the preparation of well-defined globular polymeric nanoparticles with a sub-20 nm diameter remains challenging. Inspired by the self-organizing behavior of biomacromolecules, self-folding of single polymer chains was established to access nanoparticles of ultrafine size. These single-chain nanoparticles (SCNP) were synthesized *via* intramolecular crosslinking of linear polymer precursors and are generally in the size range of <20 nm.[15-16] A myriad of crosslinking chemistries has been reported utilizing covalent, dynamic covalent and noncovalent interactions.[17-18] Among these methods intramolecular polymerization of linear polymers carrying polymerizable pendants is of growing interest since it led to SCNP with tunable level of compaction.[173] A variety of intramolecular polymerization methods have been employed, including radical polymerization of methacrylate[84, 102, 157]/acrylate[153]/styryl[149, 154] groups, oxidation polymerization of thiophene,[155] ROMP of oxanorbornene,[156] ring-opening polymerization (ROP) of caprolactone[173-174]/glycidyl[175] groups, etc. These methods successfully transformed linear polymers to SCNP. However, the number of repeating units within each intra-chain linkage (i.e. degree of intra-chain polymerization) is yet to be explored.

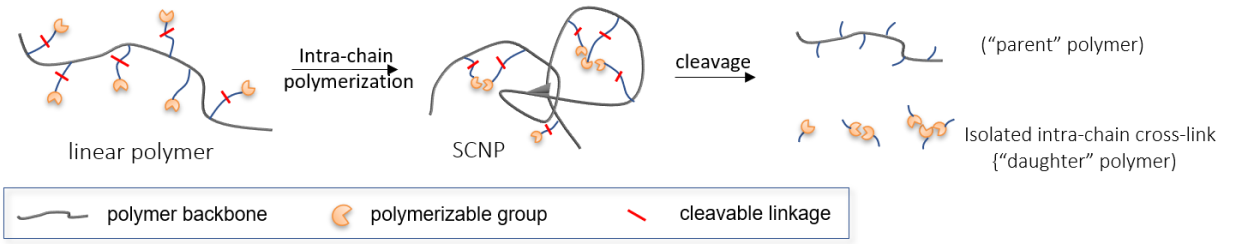

Figure 3.1 Synthesis of an SCNP by intra-chain polymerization and subsequent isolation of intra-chain cross-links.

Inspired by the templated polymerization technique where polymerization occurs in presence of a template which is removed at a later stage,[176-178] we aim to synthesize an SCNP *via* intramolecular polymerization and then isolate the intra-chain crosslinks from the linear precursor. (Figure 3.1) Direct characterization of these intra-chain crosslinks will provide insight into the degree of intra-chain polymerization that occurs in a sterically demanding environment. The strategy requires a monomer that could undergo two non-interfering polymerizations in a sequential fashion, one for the synthesis of a liner polymer chain, the other for the intra-chain polymerization that affords an SCNP. A cleavable unit must be present in order to efficiently separate the intra-chain cross-links (daughter polymer) from the linear chain (parent polymer).

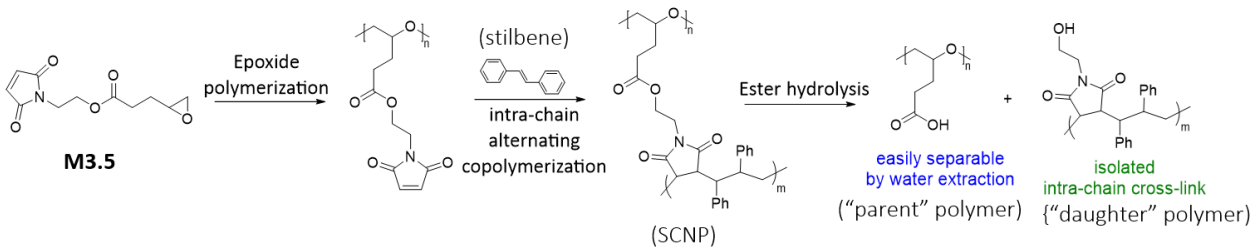

Scheme 3.1 Overall synthetic plan.

The overall synthetic plan is depicted in Scheme 3.1. Monomer **M3.5** contains an epoxide functional group that undergoes ring-opening polymerization (ROP), a maleimide group for radical polymerization, as well as an ester group as the cleavable linkage. ROP of the monomer

leads to a linear polymer with pendant maleimide groups. Under dilute conditions these maleimide groups copolymerize intramolecularly with external stilbene monomers and result in SCNP. The two polymers (parent and daughter) could be separated through hydrolytic cleavage of the ester linkage which has been successfully employed in previous reports.[176-177] After hydrolysis, the carboxylic acid derived polyethylene glycol linear polymer will likely be water soluble while the intra-chain cross-linked daughter polymer remains neutral and insoluble in water, resulting in easy separation.

3.2 Results and discussion

3.2.1 Monomer design

Quantitative cleavage and efficient separation of the intra-chain cross-links from the linear polymer is of particular importance as it allows for an accurate evaluation of the molecular weight and distributions of the daughter polymer. Bearing this in mind, we first attempted to synthesize **M3.0a** (Scheme 3.2A). This monomer, after intra-chain polymerization, forms an N-hydroxysuccinimide (NHS) active ester linkage between the parent and daughter polymers. NHS-esters have proved to be highly reactive toward nucleophilic attack as indicated by the relatively high acidity of NHS (pKa ~6 [179]), leading to efficient hydrolysis under mild conditions. Incorporating such NHS-ester linkages could potentially improve the separation of the intra-chain cross-links from the linear parent polymer.

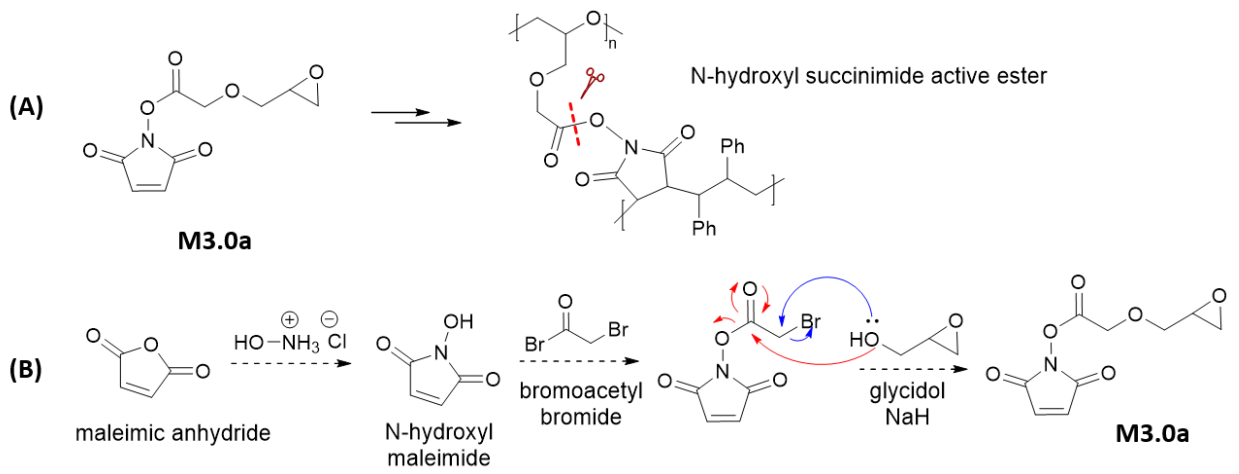

*Scheme 3.2 (A) Formation of NHS active ester after intra-chain polymerization from **M3.0a**; (B) synthesis of **M3.0a.** (Blue arrows: ideal pathway; red arrows: side reaction)*

The synthetic route to **M3.0a** begins with synthesis of N-hydroxyl maleimide from maleic anhydride (Scheme 3.2B), followed by esterification with bromoacetyl bromide, and a subsequent Williamson etherification to afford **M3.0a**. It is surprising that very few reports covered the synthesis of N-hydroxyl maleimide without substituents on the C=C double bond.[180] Similar compounds were found that contain either alkyl or phenyl substituents, or furan protecting groups.[181-183] Unfortunately following the literature procedures did not lead to successful synthesis of N-hydroxyl maleimide. In all cases the solutions turned black without formation of the desired compound. The Williamson etherification of glycidol is also envisioned to be problematic in presence of a carbonyl group. As shown in Scheme 3.2B, the alkyl bromide ideally undergoes S_N2 reaction and forms **M3.0a** (blue arrows). However the ester group is also highly susceptible to nucleophilic attack (red arrows) in presence of a strong $R\text{-}O^-$ nucleophile, leading to decomposition of the compound. Based on these results and hypothesis, we switched to synthesize monomer **M3.0b** instead (Scheme 3.3A).

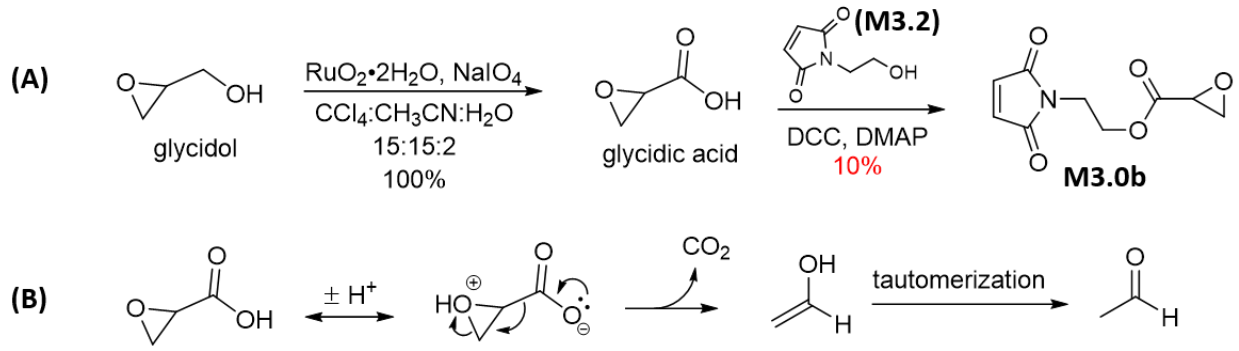

*Scheme 3.3 (A) Synthesis of **M3.0b**; (B) Decarboxylation of glycidic acid.*

The synthetic consideration of **M3.0b** differs from **M3.0a** in two major aspects: i) It begins with the synthesis of an acid-functionalized epoxide fragment. This avoids the use of bromoacetyl bromide and further prevents Williamson etherification in presence of a carbonyl group; ii) It replaces N-hydroxyl maleimide with N-hydroxyl ethyl maleimide (**M3.2**). Adding an ethyl spacer between maleimide and hydroxyl groups no longer leads to active esters after polymerization, which is negative for the separation of daughter and parent polymers. This presents a dilemma here: active esters are better choices for post-polymerization separations, but the highly reactive nature makes them difficult to survive the early stage multi-step monomer synthesis.

The oxidation of glycidol to glycidic acid using ruthenium tetroxide went smoothly with quantitative yield following the literature procedure.[184] Subsequent Steglich esterification of glycidic acid with **M3.2**, however, gave the desired product with a low yield (< 10%) with a dark red byproduct stuck on the top of the column during purification. Steglich esterification is very widely used in organic synthesis. It proceeds under mild conditions and is generally high yielding both found in the literature and from our previous work. We attributed the surprisingly low yield of this specific reaction to the stability of glycidic acid (Scheme 3.3B). It was reported that glycidic acid is not particularly stable even at room temperature.[185] It undergoes self-decarboxylation to

release CO_2 and generates an enol which tautomerize to its keto form in the presence of an acid or base catalyst. It is obvious that adding extra carbons between the epoxide ring and the carbonyl group would prevent decarboxylation and increase stability of the molecule. Therefore, we set out to synthesize **M3.5**. The added carbon spacers to the epoxide fragment will prevent the synthetic intermediate from undergoing decarboxylation, while keeping all structural requirements for the monomer: maleimide and epoxide as polymerizable groups and connected with an ester linkage.

3.2.2 Synthesis of monomer M3.5

As discussed above, Monomer **M3.5** contains three functionalities that need to be attached (Scheme 3.4): a maleimide group (blue); an ester group (green) and an epoxide group (red). These functional groups can be added in different orders. Scheme 3.4A is a convergent/branched synthesis that requires the syntheses of maleimide and epoxide functionalized precures separately, then bring them together with an ester group. Scheme 3.4B and C are both linear syntheses in the order of maleimide→ester→epoxide and ester→maleimide→epoxide, respectively.

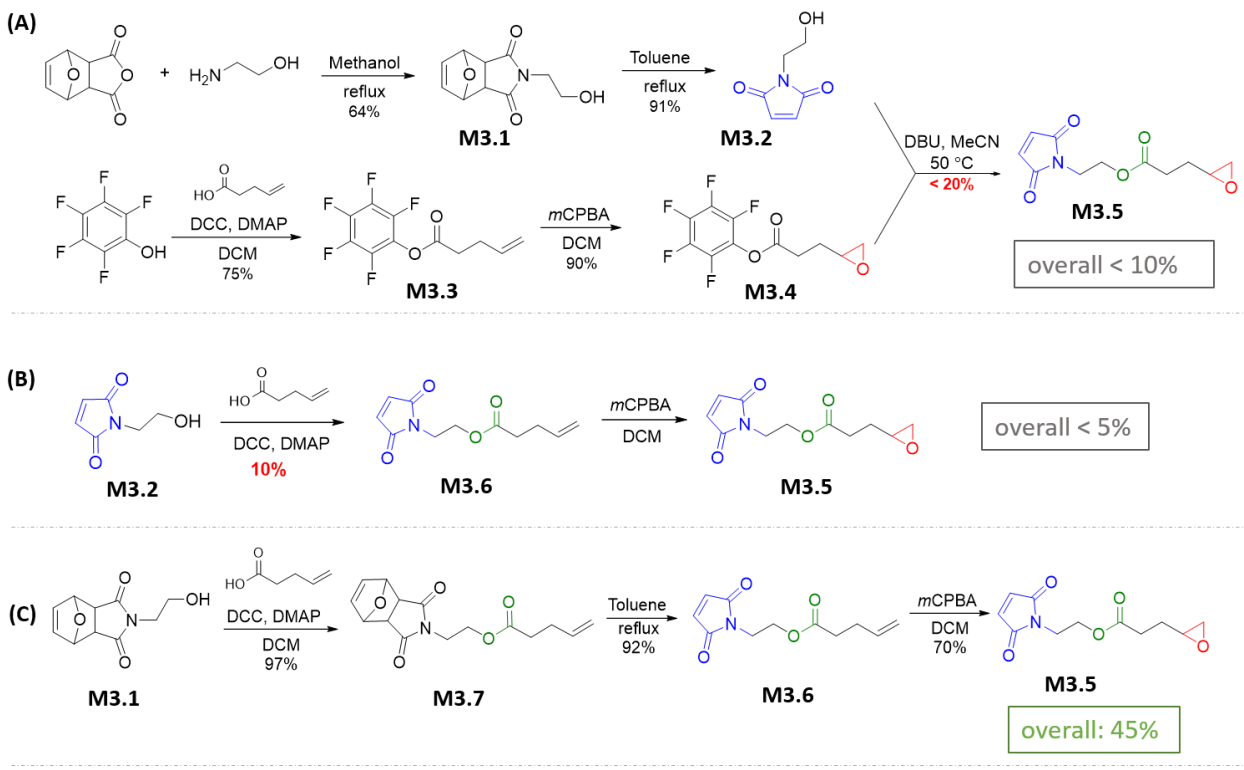

*Scheme 3.4 Synthetic routes to monomer **M3.5***

We first adopted the convergent synthetic strategy aiming to increase the overall efficiency of the multi-step synthesis (Scheme 3.4A). This includes independent synthesis of hydroxyl ethyl maleimide **M3.2** and a pentafluoroester masked epoxide fragment **M3.4**. A final transesterification step combines the two to afford the target molecule **M3.5**. **M3.2** was synthesized according to literature procedures.[186-187] **M3.4** was successfully made from Steglich esterification of pentafluorophenol with 4-pentenoic acid, followed by mCPBA epoxidation. All steps went well except for the final transesterification reaction: the yield was less than 20%, making the overall yield less than 10%, which is unacceptably low for a monomer synthesis since large quantities of monomers are required for the following polymerization steps. The inefficiency of this reaction was unexpected due to the high reactivity of pentafluoroesters as reported by several groups.[188-189] The reaction uses 1,8-diazabicyclo[5.4.0]undec-7-ene (DBU) as a base catalyst. The solution

turned dark red immediately upon addition of DBU but this phenomenon was not found reported in literature.

Linear synthesis shown in Scheme 3.4B was then adopted. The Steglich esterification of **M3.2** with 4-pentenoic acid produced again a dark red byproduct with only 10% yield of the target molecule **M3.6**. So far we have encountered three reactions that were haunted with the red byproduct along with a low yield (recall the Steglich esterification in Scheme 3.3A and the transesterification in Scheme 3.4A). It is not hard to find that these reactions all contain maleimide groups on the reagents, and those could be responsible for side reactions that lead to the colored species. The nature of this byproduct will be discussed in detail in the next section.

Based on the abovementioned observation and hypothesis, we adopted a synthetic route that kept the maleimide functionality protected with furan (**M3.1**) and subjected it to Steglich esterification with 4-pentenoic acid (Scheme 3.4C). This reaction proceeded well and yielded **M3.7** quantitatively. The maleimide functionality was unmasked through subsequent retro Diels-Alder reaction by heating to reflux in toluene resulting in **M3.6**. Radical inhibitor BHT was added during the process to prevent polymerization. mCPBA treatment with **M3.6** selectively oxidized the electron rich terminal olefin to an epoxide group and left the electron deficient maleimide olefin intact. This 4-step synthesis to **M3.5** gave an overall yield of 45% and is highly scalable.

3.2.3 Side reaction of maleimide groups

During the synthesis of **M3.5** we found that compounds with a maleimide group were sensitive to some organic bases even in catalytic amount, such as 4-dimethylaminopyridine (DMAP) and DBU. As shown in Scheme 3.5A, hydroxylethyl maleimide **M3.2** undergoes Steglich esterification with glycidic acid and 4-pentenoic acid with only 10% yield of the coupling products. In these reactions, some dark red byproduct was generated that stuck on the top of silica columns during purification.

The furan-protected counterpart **M3.1**, however, when subjected to the exact same reactants under the same conditions, led to the coupling products with 82% and 97% yield (Scheme 3.5B) and no sign of the colored species.

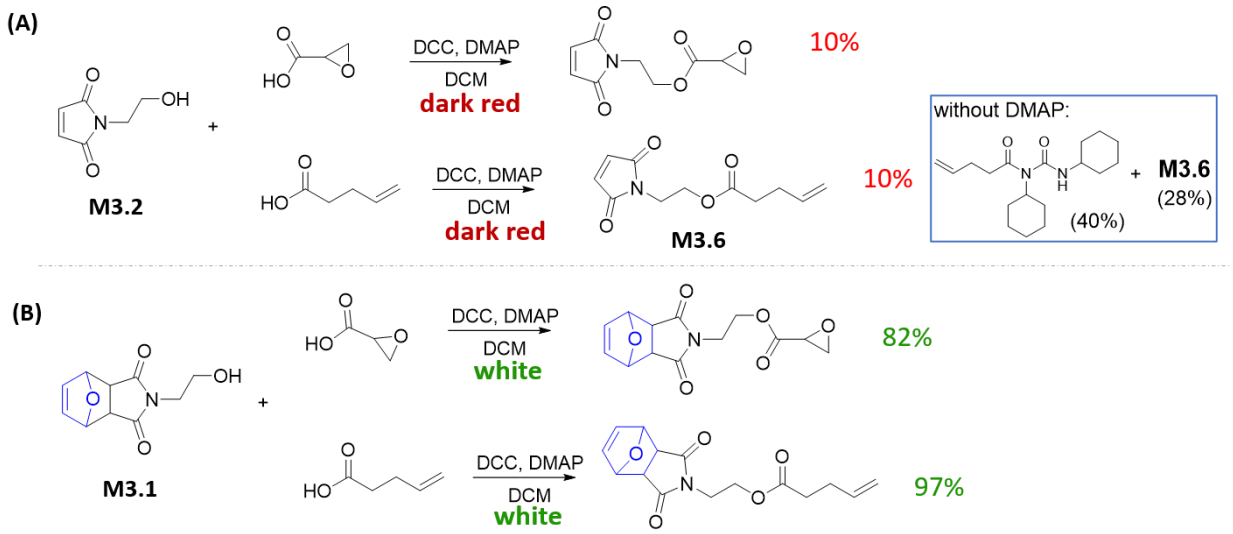

Scheme 3.5 Steglich esterifications of glycidic acid and 4-pentanoicacid with (A) ***M3.2*** *and (B)* ***M3.1****.*

Steglich esterification is an ester forming reaction between a carboxylic acid and an alcohol using DMAP as a catalyst and N,N'-dicyclohexylcarbodiimide (DCC) as a coupling agent. DMAP is a common catalyst for the activation of carbonyl groups – it acts as a good nucleophile to attack the carbonyl producing the acetylpyridium ion and becomes a good leaving group which lowers the reaction barrier for weaker nucleophiles such as alcohols. This allows the reaction to proceed at milder conditions. The coupling agent DCC first serves as an electrophile and then transforms into a good leaving group, producing a stable dicyclohexylurea (DCU) as byproduct. This makes the overall reaction thermodynamically favorable and can proceed to a higher extent. Compared with the classical acid-catalyzed Fisher esterification which features an unfavorable equilibrium that requires either excess of one of the reagents or removal of water, Steglich esterification occurs at

room temperature with high conversion, hence it has been frequently used by organic chemists. Given the fact that maleimides and esters are both key elements in our research plan, it is important to understand what side reactions they undergo under Steglich esterification conditions.

In order to confirm that the colored species was a result of treating maleimide compounds with base, we performed Steglich esterification of **M3.2** with 4-pentenoic acid without the addition of DMAP (Scheme 3.5A-box). Mechanistically this reaction could still proceed, but because of the low nucleophilicity of the hydroxyl group and hence slow addition to the O-acylurea intermediate, the intermediate undergoes a Mumm type rearrangement to the more thermodynamically stable N-acylurea which is no longer active toward nucleophilic addition, resulting in low yields. As expected, we observed the rearranged product (structure shown in Scheme 3.5A-box) with 40% yield and **M3.6** with 28% yield. More importantly, the dark red species was not observed without the addition of DMAP, which confirmed the incompatibility of maleimide group with DMAP.

A series of base tests were then performed on a model compound N-phenylmaleimide (NPhMI). When adding potassium carbonate (K_2CO_3), diisopropylethylamine (DIPEA), and triethylamine (TEA) to a solution of NPhMI in DCM at room temperature, no color change was observed. The solution turned red upon addition of DMAP, DBU and potassium *tert*-butoxide (*t*BuOK). This color disappeared after treatment with acetic acid. When treating NPhMI with sodium hydride (NaH) in dry THF under argon, no reaction was observed. However, NaH treatment in air using THF from the wash bottle resulted in red solution with bubbles evolved. ^{1}H NMR of the red product showed disappearance of the maleimide H-C=C-H protons at 7.2 ppm, as well as slight broadness of the peaks, suggesting polymerization of the maleimide groups.

Maleimide groups are better known to undergo radical polymerizations. Base-catalyzed anionic polymerization of maleimides is barely reported in the past two decades due to the lack of control

in the polymerizations. Early studies on base-catalyzed polymerization include the use of strong nucleophiles such as organolithium[190], organozinc[191] and Grignard reagent[192] as initiators, as well as milder initiators like tert-butoxides[193], alkylamines, even anilines[194]. These polymerizations typically proceed rapidly at -78°C except for the cases where amine initiators were used and those were reported to occur at 30°C. Since DMAP exhibits better nucleophilicity than amines, it is reasonable to assume that polymerization of **M3.2** is highly possible at room temperature under Steglich esterification condition and gave the red colored byproduct.

Poly(maleimides) were reported to exhibit a reversible color changes based on acid-base switching not only in solution[195] but also in the solid state when exposed to amine vapor[196]. These polymers are red colored in basic solvents and turned colorless in acidic solvents. The color change was considered to arise from the enolate anion tautomerization of the maleimide groups in basic solvent and/or in the presence of a basic reagent[195-197].

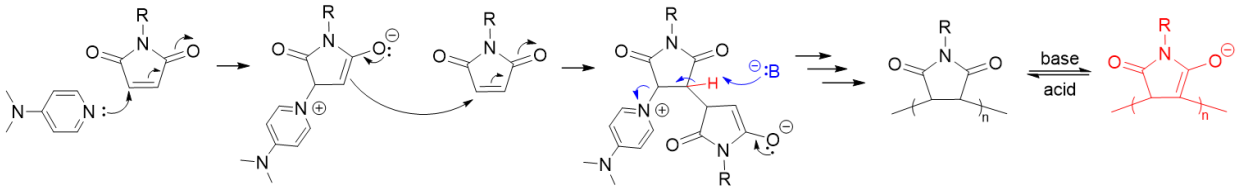

Scheme 3.6 Proposed mechanism of maleimide anionic polymerization with DMAP

Based on these findings we conclude that the side reactions that led to the dark red byproduct mentioned in Section 3.2.2 originated from the base-catalyzed anionic polymerization/ oligomerization of maleimide groups. The proposed mechanism of the reaction is sketched in Scheme 3.6. The initiation of the polymerization is a Michael addition of the nucleophilic base catalyst to the activated alkene to generate an enolate zwitterionic adduct. Propagation continues by enolate addition to another equivalent of the maleimide monomer. The base catalyst is recovered through elimination shown in blue arrows. The polymer/oligomer product undergoes

tautomerization that gave rise to the red colored byproduct. Based on our findings, maleimide groups are highly susceptible to this type of reaction. Attention needs to be paid when derivatizing molecules with maleimide groups, either by avoiding exposure to basic nucleophiles or by using protecting groups.

3.2.4 Ring-opening polymerization of M3.5 and M3.8

The selective ring-opening polymerization of glycidol methacrylate was previously reported by Carlotti and coworkers[198]. This technique uses tetraoctyammonium bromide (*i*-Bu_3Al)/ triisobutylaluminum ($NOct_4Br$) initiating system to selectively polymerize the epoxide groups while leaving the methacrylate polymerizable groups unscathed, which is potentially promising for polymerizing **M3.5**. However, attempts to polymerize **M3.5** following the reported procedure led to a crosslinked gel, with red byproduct forming in solution (Scheme 3.7A,B)

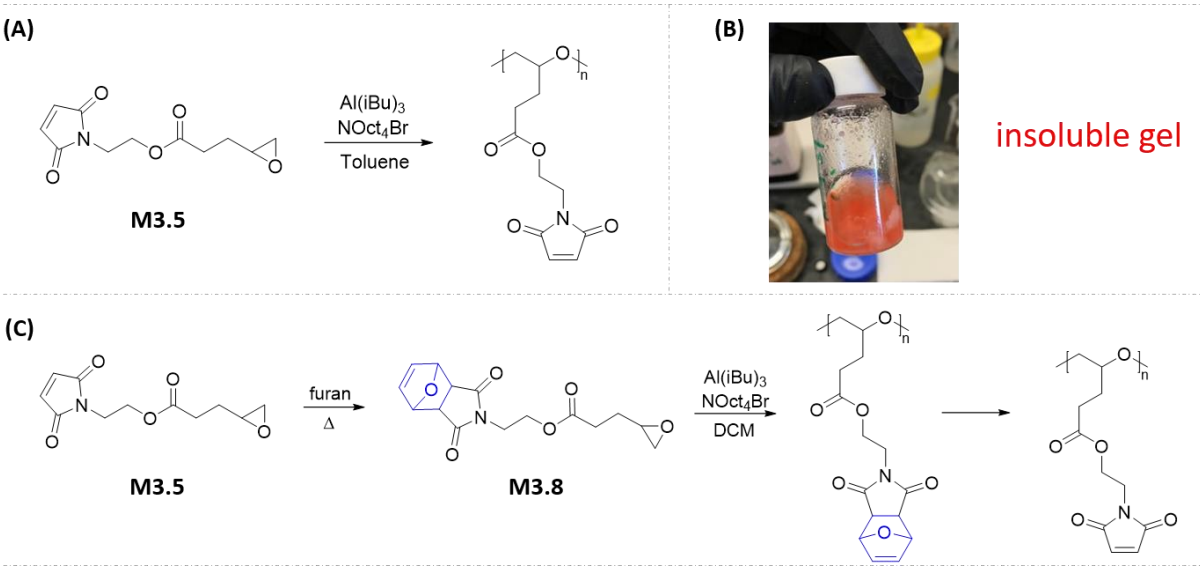

*Scheme 3.7 (A) Ring-opening polymerization of **M3.5** using the monomer-activated anionic approach; (B) Direct polymerization of **M3.5** led to an insoluble gel and red colored byproduct; (C) **M3.8** synthesis by Diels-Alder reaction of **M3.5** with furan, and subsequent polymerization and post-polymerization deprotection.*

The crosslinking reaction was attributed to maleimide groups participating in the polymerization. The Lewis acidic alkyl aluminum not only activated the epoxide oxygen but also activated maleimide carbonyls, which made them excellent Michael acceptors for the propagating anions to attack. Basicity of the aluminum species enabled the enolate tautomerization of the polymerized maleimides, which explains the red color. In order to prevent the crosslinking reaction from taking place, we sought to protect the maleimide functional group with furan (**M3.8**, Scheme 3.7C), and subject the monomer to ring-opening polymerization followed by a post-polymerization deprotection step.

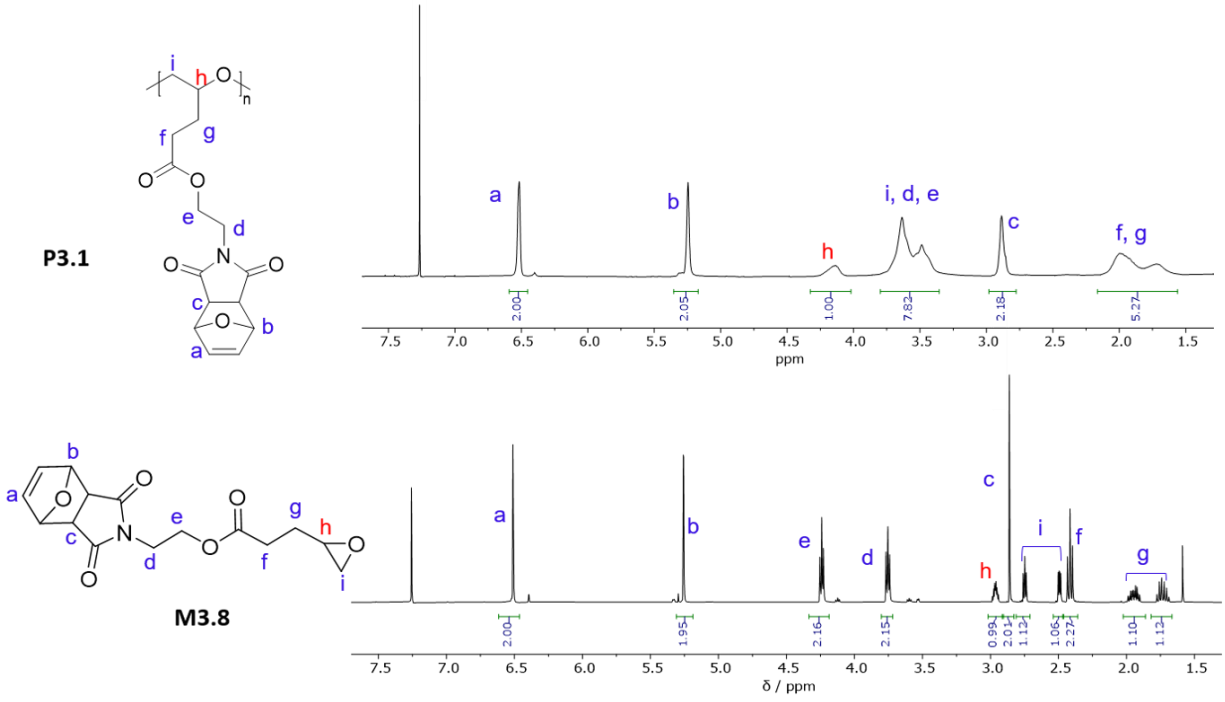

*Figure 3.2 ^{1}H NMR spectra of **M3.8** and **P3.1.***

The polymerization of epoxides by this approach requires the ratio of alkylaluminum to initiator to exceed unity ([i-Bu_3Al]/[$NOct_4Br$]>1) to ensure activation of the epoxide ring. [199-201] Monomers with more than one coordination sites require higher amount of the catalyst to overcome the strong interactions with the Lewis acid.[200] For example, [R_3Al]/[initiator] of 1.5 is reported to

successfully polymerize ethylene and propylene oxide.[202] But [R_3Al]/[initiator] as high as 3.4 is required to polymerize furfuryl glycidyl ether because all three oxygens on the monomer are able to coordinate with aluminum.[203] **M3.8** contains six oxygens capable of coordination with *i*-Bu_3Al, hence a large amount of *i*-Bu_3Al is needed for the reaction to take place. Polymerization of **M3.8** with [R_3Al]/[initiator]=12 went smoothly and gave product **P3.1**. ^1H NMR spectrums of the two are shown in Figure 3.2. **P3.1** exhibited all signals of the protected maleimide side chain, as well as peaks corresponding to the polyether backbone. The epoxide C-H proton of **M3.8** (peak h at 2.9 ppm) shifted downfield to 4.2 ppm after polymerization. This can be used to calculate monomer conversion of the polymerization.

*Table 3.1 Polymers **P3.1-P3.5** synthesized from ring-opening polymerization of **M3.8** [a]*

	[R_3Al]/[initiator]	Monomer conversion(%) [b]	Mn (kDa) [c]	Mw (kDa) [c]	Đ [c]
P3.1	12	100	5.0	16.2	3.24
P3.2	10	100	7.8	12.3	1.58
P3.3	8	85	10.2	13.7	1.35
P3.4	6	70	---------- not isolated ----------		
P3.5	4	0	------- no polymerization -------		

a. DCM, Ar, rt, 4 hr; b. Calculated from ^1H NMR; c. Obtained using triple detection GPC.

The polydispersity index of **P3.1** is 3.24. This is consistent with previous reports where broader distributions were seen with higher [R_3Al]/[initiator] ratios.[204-206] A series of polymerizations with smaller ratio of [R_3Al]/[initiator] (10, 8, 6 and 4, **P3.2-P3.5**) were performed to optimize the condition for narrower distribution of the polymers. The results are summarized in Table 3.1. Polymerization of **M3.8** successfully proceeded in the presence of *i*-Bu_3Al and $NOct_4Br$ at a ratio between 6 and 12. At a ratio of 4 no polymerization was observed. **P3.1** and **P3.2** reached full conversion within 4 hours at room temperature, **P3.3** and **P3.4** were 85% and 70% converted. The

polymers exhibited narrower distribution with smaller [R_3Al]/[initiator] ratio. **P3.3** shows a M_w/M_n value of 1.35. Unfortunately, we were unable to isolate **P3.4** for GPC analysis as it did not precipitate from methanol like other polymers did.

3.2.5 Post-polymerization deprotection

P3.1 – P3.3 were subjected to post-polymerization retro Diels-Alder reaction to deprotect the maleimide groups. The polymers were not soluble in toluene which is the most common solvent for retro D-A of similar structures. Stirring the polymer at reflux in chloroform for 2 days led to ~12.5% deprotection. Dissolving the polymer in DMF and heated at 130 ℃ resulted in a brown oil after workup. ^{1}H NMR of the product shows disappearance of the furan protons at 6.6 and 5.3 ppm, but the expected deprotected maleimide proton (~7 ppm) was missing, likely due to radical crosslinking of the deprotected maleimide group. Repeated the process in presence of a radical inhibitor (~4%wt BHT) shows disappearance of the furan protons and appearance of the maleimide protons as expected, but a lot of new peaks were present which might be degradation of the polyether backbone. (Figure 3.3) Lowering the temperature to 115 ℃ and increasing the amount of radical inhibitor to 20%wt BHT led to red polymers likely due to polymerization of the maleimide groups. Increasing the amount of BHT to 40%wt and heated at 115 ℃ gave the same result. Due to the susceptibility of maleimide groups to polymerization, the retro D-A condition needs to be further optimized, including simultaneous deprotection and intrachain crosslinking in one pot.

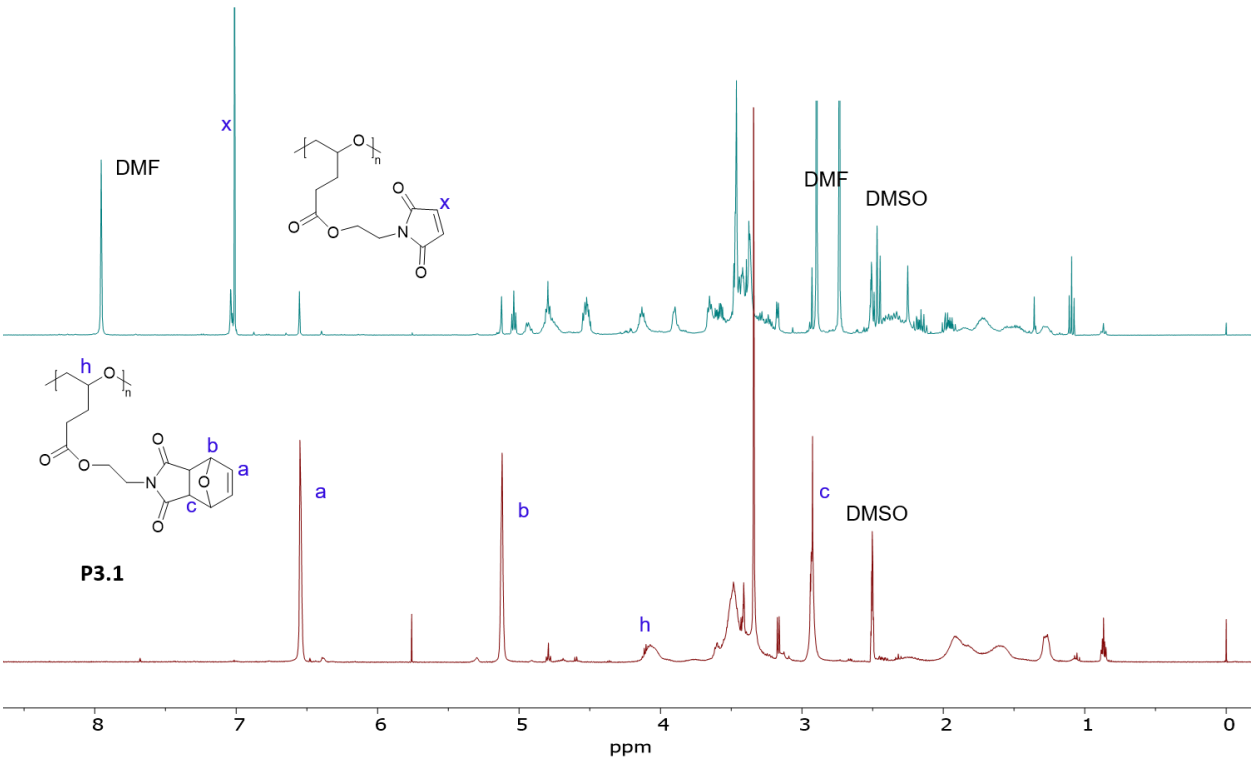

*Figure 3.3 ^{1}H NMR spectra of **P3.1**(bottom) and its post-polymerization deprotection product (top).*

3.2.6 Intramolecular cross-linking model reaction

SCNP are to be synthesized from intramolecular polymerization of pendant maleimide groups with external stilbene monomers. The reaction needs to run at ultra-dilute condition so that polymer coils are independent of each other and prefer intramolecular reaction. Calculating the critical concentration crossing over from dilute to concentrated solution regime will help the understanding of the physical aspects of SCNP synthesis. Additionally, despite the overall low concentration of polymer solution, maleimide groups are located within each solvated polymer coil and have a much higher local concentration than the overall polymer solution. Identifying the local concentration of maleimide groups and running a model polymerization reaction at that concentration will provide insight into the self-crosslinking process and the internal structure of SCNP.

The equilibrium concentration where intra- and inter-molecular reactions are equally probable is given by equation **Eq 3.1**.[207]

$$c^* = \frac{(1/N_A)*M}{V_h} = \frac{M}{N_A*V_h} \quad \textbf{(Eq 3.1)}$$

Where c* represents the critical concentration from dilute to semidilute regimes. Polymer coils are independent of each other below c* and start to touch each other above c*. M is the molecular weight of the polymer. V_h represents the hydrodynamic volume of a polymer coil. N_A is Avogadro's number.

C* can be related to the intrinsic viscosity of the polymer solution $[\eta]$ through Einstein's viscosity equation (**Eq 3.2**) if the polymer coils are treated as hard spheres.[208]

$$\eta = \eta_s(1 + 2.5\emptyset + 4\emptyset^2 + \cdots) \quad \textbf{(Eq 3.2)}$$

η and η_s are viscosities of the polymer solution and the solvent, respectively. $\emptyset$ is the volume fraction of the polymer solute, and can be derived from the concentration of the polymer solution through **Eq 3.3**.

$$\emptyset = (c/M) * N_A * V_h = \frac{c*N_A*V_h}{M} \quad \textbf{(Eq 3.3)}$$

Plotting Eq 3.3 into Eq 3.2:

$$\eta = \eta_s(1 + 2.5 * \frac{c*N_A*V_h}{M}) \quad \textbf{(Eq 3.4)}$$

Combining Eq 3.4, Eq 3.1 with calculation of intrinsic viscosity $[\eta]$:

$$[\eta] = \lim_{c\to 0} \frac{\eta/\eta_s - 1}{c} = \lim_{c\to 0} \frac{\eta - \eta_s}{c*\eta_s} = \lim_{c\to 0} \frac{2.5\eta_s \frac{c*N_A*V_h}{M}}{c*\eta_s} = 2.5\frac{N_A*V_h}{M} = \frac{2.5}{c^*} \quad \textbf{(Eq 3.5)}$$

Based on **Eq 3.5** and intrinsic viscosity of P3.2 from GPC, we calculated the overlap concentration c* of P3.2, as well as the local concentration of maleimide groups under c*. (Table 3.2)

Table 3.2 Overlap concentration c^* of P3.2

	Mn (kDa)	N (degree of polymerization)	$[\eta]$ [a] (mL/g)	c^* (mg/mL) [b]	c^* (mol/L) [c]	Local [c] of maleimide (mol/L) [d]
P3.2	7.76	25	5.67	441	0.06 M	1.5 M

a. Obtained from GPC viscometer using THF as eluent at 40°C; b. Calculated from $c^* = 2.5/[\eta]$; c. Calculated from $2.5/([\eta]\, M_n)$; d. Calculated from $N * c^*$.

A model reaction of maleimide-stilbene copolymerization was run at the calculated local [c] of 1.5 mol/L, targeting 25 repeating units of each monomer. The polymerization was performed in THF at 70°C using AIBN as an initiator. (Figure 3.4A) The reaction was quenched after 4 hours since the stir bar stopped working due to the high viscosity of the polymer solution. The copolymer showed broad distribution (Đ = 1.7) and much higher molecular weight than targeted. (Figure 3.4C)

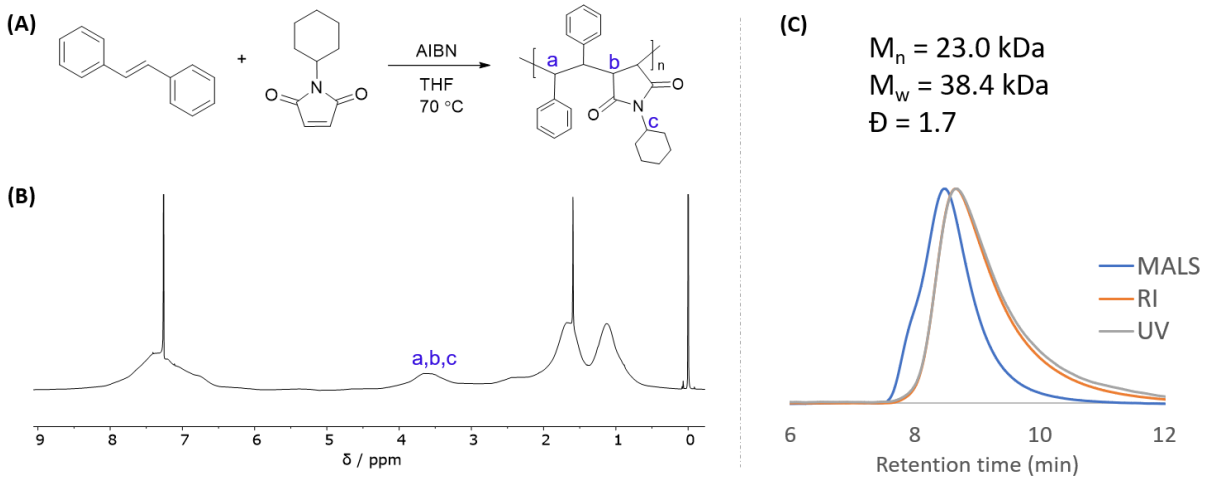

Figure 3.4 (A) Radical copolymerization of N-cyclohexylmaleimide and trans-stilbene; (B) ^1H NMR spectrum and (C) GPC chromatograms of the copolymer.

Apparently, this oversimplified model reaction performed at the calculated overlap concentration of P3.2 cannot represent the real case of intramolecular radical polymerization. The real process is

much more complicated and requires deeper understanding of polymer-solvent interaction and polymerization kinetics/thermodynamics in a confined space. Future work would require more viscometric studies to understand the conformation of polymers in ultra-dilute solution, as well as advanced characterization techniques to evaluate the internal structure of SCNP.

3.3 Conclusion

Monomers bearing an epoxide group and a maleimide group connected *via* an ester linkage were synthesized from a four-step reaction sequence. Some special care is required when synthesizing these monomers due to the sensitivity of maleimides to nucleophilic base. Although the monomer was proposed to undergo two mechanistically distinct polymerizations, the maleimide group turned out to interfere with the ring-opening polymerization of epoxides when using the activated monomer method. Having the maleimide group protected with furan led to the successful synthesis of polymers. The polymers exhibited lower molecular weight distribution when smaller [R_3Al]/[initiator] ratio was applied. Post-polymerization deprotection released the maleimide functionality but the polymer backbone may undergo degradation. Future work with this project includes the optimization of polymerization and post-polymerization deprotection steps, as well as intramolecular radical polymerization, and separation of the intra-chain cross-links from the linear polymer for further characterization.

3.4 Experimental

3.4.1 Materials

Reagents were obtained from the indicated commercial suppliers and used without further purification unless otherwise stated: exo-3,6-epoxy-1,2,3,6-tetrahydrophthalic anhydride (TCI), 2-aminoethanol (TCI), pentafluorophenol (Oakwood Products, Inc), 3-chloroperbenzoic acid (Sigma-Aldrich), 1,8-diazabicyclo[5.4.0]undec-7-ene (Acros Organics), 4-pentenoic acid (Sigma-

Aldrich), N,N'-dicyclohexylcarbodiimide (Sigma-Aldrich), 4-dimethylamino pyridine (Oakwood Products, Inc), glycidol (Sigma-Aldrich), ruthenium (IV) oxide (Acros Organics), sodium m-periodate (Sigma-Aldrich), triisobutylaluminum (1.0 M in hexanes, Sigma-Aldrich), tetraoctylammonium bromide (Sigma-Aldrich), hexanes (Fisher Scientific), ethyl acetate (Fisher Scientific), 2,2'-azobis(2-methylpropionitrile) (AIBN, Sigma-Scientific, recrystallized from methanol), butylated hydroxyltoluene (BHT, Sigma-Aldrich), silica gel (230 – 400 mesh, SiliCycle), N-phenyl maleimide (TCI), N-cyclohexyl maleimide (TCI), trans-stilbene (Acros Organics), THF (HPLC grade, Fisher Scientific, inhibited with BHT), sodium bicarbonate (Fisher Scientific), chloroform-d ($CDCl_3$, Cambridge Isotope Laboratories). Dry toluene was obtained by heating to reflux with sodium in presence of benzophenone as indicator. Dry dichloromethane (DCM) was obtained from heating to reflux with calcium hydride.

3.4.2 Instrumentation

^{1}H and ^{13}C NMR spectra were acquired with a Varian Unity INOVA or Bruker Biospin 500 MHz or Varian Mercury 400 MHz spectrometer. Chemical shifts (δ) were reported in parts per million (ppm) relative to tetramethylsilane (TMS). Solvent ($CDCl_3$) contained 0.03% v/v TMS as an internal reference. Peak abbreviations are used as follows: s = singlet, d = doublet, t = triplet, q = quartet, m = multiplet, br = broad, Ar = Aryl).

SEC was performed on a Tosoh EcoSEC dual detection (RI and UV) SEC system coupled to an external Wyatt Technologies miniDAWN Treos multiangle light scattering (MALS) detector and a Wyatt Technologies ViscoStar II differential viscometer. Samples were run in THF at 40 °C at a flow rate of 0.35 mL/min. The column set contained one Tosoh TSKgel SuperHM-M (6.0 mm ID × 15 cm) column, one Tosoh TSKgel SuperH2500 (6.0 mm ID × 15 cm) column and a Tosoh TSKgel SuperH5000-7000 guard column (4.6 mm ID × 3.5 cm). All polymer solutions

characterized by SEC were 1.0 mg/mL in THF, stirred magnetically for at least 5 hours and filtered through 0.45 μm PTFE syringe filters before analysis.

3.4.3 Experimental procedures

3.4.3.1 Synthesis of hydroxylethyl maleimide **M3.2**

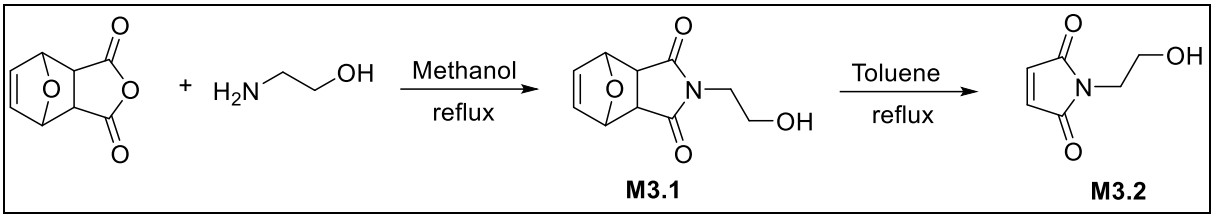

M3.1 was synthesized following the same procedure described in section 2.4.5.2. Hydroxylethyl oxanorbornene M3.1 (5g, 23.9 mmol) was stirred at reflux in toluene (15 mL) overnight. The mixture was cooled to room temperature and toluene removed by rotary evaporator. Crude product was purified by column chromatography. (Hex: EtOAc = 1:2, 1.56 g, 46.3%)); ^{1}H NMR (400 MHz, $CDCl_3$, δ, ppm): 6.75 (s, 2H), 3.79 (t, 2H), 3.73 (t, 2H), 2.20 (br, 1H); ^{13}C NMR (400 MHz, $CDCl_3$, δ, ppm): 170.78, 134.64, 59.86, 40.63. See appendix page 133 for full spectra.

3.4.3.2 Synthesis glycidic acid and **M3.0b**

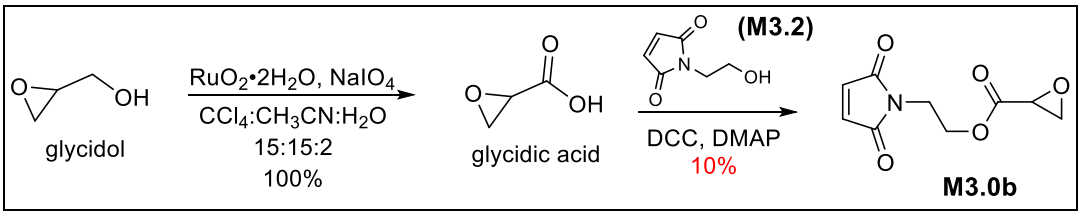

Glycidic acid:[184] To a 50 mL 3-neck flask was added glycidol (0.9 mL, 13.5 mmol, 1 eq), tetrachloromethane (7.5 mL), acetonitrile (7.5 mL) and water (1 mL). Ruthenium dioxide (55 mg, 0.41 mmol, 0.03 eq) was added and the mixture was stirred under argon for 5 min. Sodium periodate (11.57 g, 54.1 mmol, 4 eq) was added in small portions over 15 min. The mixture was

stirred at room temperature for another 2.5 hours then filter through celite. The filtrate was dry loaded with silica and elute through a short silica plug with EtOAc. (1.28 g, 100%);^{1}H NMR (400 MHz, $CDCl_3$, δ, ppm): 11.09 (br, 1H), 3.50 (t, 1H), 3.03 (d, 2H); ^{13}C NMR (400 MHz, $CDCl_3$, δ, ppm): 176.12, 46.89, 46.66. See appendix page 134 for full spectra.

M3.0b: Dissolve hydroxylethyl maleimide (M3.2, 1 g, 7.09 mmol, 1 eq), glycidic acid (0.75 g, 8.5 mmol, 1.2 eq), DCC (2.19 g, 10.63 mmol, 1.5 eq) and DMAP (95 mg, 0.71 mmol, 0.11 eq) in DCM (30 mL) and stir overnight. DCU byproduct was filtered off. Crude product was purified by column chromatography. (Hex: EtOAc = 1:1, 57 mg, 12.7%); ^{1}H NMR (400 MHz, $CDCl_3$, δ, ppm): 6.75 (s, 2H), 4.40 (m, 1H), 4.31 (m, 1H), 3.84 (m, 2H), 3.41 (dd, 1H), 2.96 (m, 2H); ^{13}C NMR (400 MHz, $CDCl_3$, δ, ppm): 170.75, 169.08, 135.57, 62.61, 47.97, 46.38, 36.67. See appendix page 135 for full spectra.

3.4.3.3 Synthesis of perfluorophenyl pent-4-enoate **M3.3**

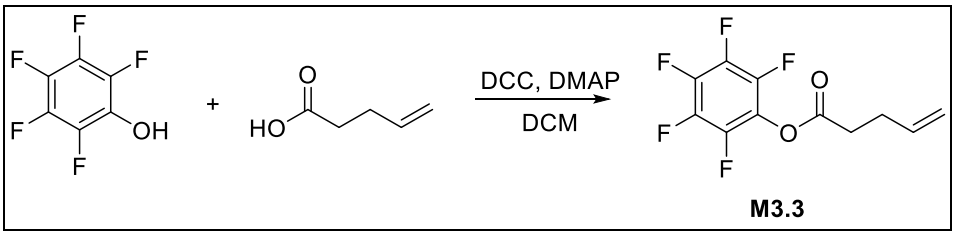

Pentafluorophenol (5g, 27.1 mmol, 1.2 eq), 4-pentenoic acid (2.31 mL, 22.6 mmol, 1 eq), DCC (7.0 g, 33.96 mmol, 1.5 eq), and DMAP (276 mg, 2.26 mmol, 0.11 eq) was dissolved in DCM (100mL) and stirred overnight. DCU salt was filtered off. Crude product was purified by column chromatography. (Hex: EtOAc = 7:1, 5.37 g, 89.2%); ^{1}H NMR (400 MHz, $CDCl_3$, δ, ppm): 5.86 (m, 1H), 5.13 (m, 2H), 2.80 (m, 2H), 2.52 (m, 2H); ^{13}C NMR (400 MHz, $CDCl_3$, δ, ppm): 168.85, 141.55, 140.57, 139.81, 139.11, 138.17, 136.25, 135.35, 116.45, 32.17, 27.21. See appendix page 136 for full spectra.

3.4.3.4 Synthesis of perfluorophenyl 3-(oxiran-2-yl)propanoate **M3.4**

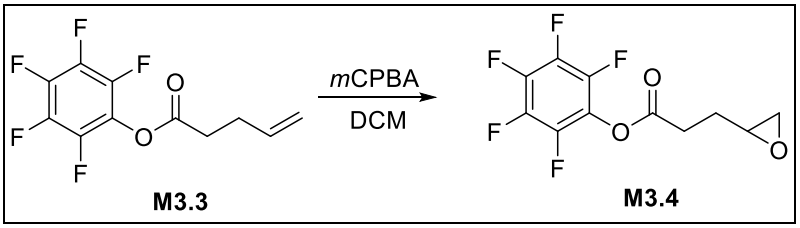

Perfluorophenyl pent-4-enoate (5g, 18.8 mmol, 1 eq) was dissolved in DCM (20 mL) in a 500 mL 3-neck flask. *m*CPBA (8.4 g, 48.8 mmol, 2 eq) was dissolved in 100 mL of DCM and added to the flask through an addition funnel over an ice bath. The mixture was warmed up to room temperature and stirred for 24 h. The benzoic acid byproduct was filtered off and the filtrate was washed with saturated sodium bisulfite, saturated $NaHCO_3$ until no bubbles, and Brine. Crude product was purified by column chromatography. (Hex: EtOAc = 7:1, 4.82 g, 91%); ^{1}H NMR (400 MHz, $CDCl_3$, δ, ppm): 2.97 (dtd, 1H), 2.75 (m, 3H), 2.49 (dd, 1H), 2.07 (dtd, 1H), 1.82 (m, 1H); ^{13}C NMR (400 MHz, $CDCl_3$, δ, ppm): 167.06, 142.28, 140.67, 139.77, 139.10, 138.19, 136.56, 50.55, 45.10, 28.49, 25.87. See appendix page 137 for full spectra.

3.4.3.5 Synthesis of **M3.5** by transesterification of M3.2 and M3.4

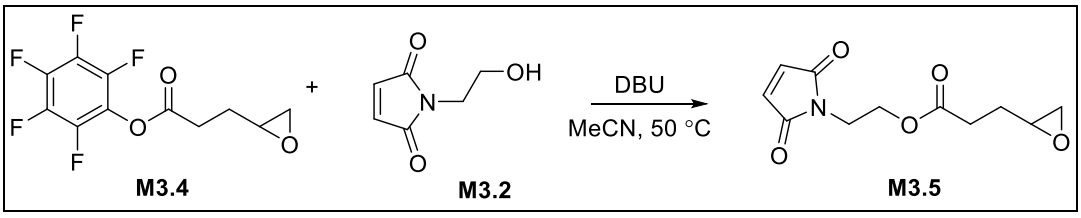

Perfluorophenyl 3-(oxiran-2-yl)propanoate (M3.4, 1 g, 3.53 mmol, 1 eq) and hydroxylethyl maleimide (M3.2, 1 g, 7.06 mmol, 2 eq) was dissolved in MeCN (40 mL), DBU (0.53 mL, 3.5 mmol, 1 eq) was added. The mixture was heated at 50 °C overnight. Crude product was purified by column chromatography. (Hex: EtOAc = 2:1, 160 mg, 20%); ^{1}H NMR (400 MHz, $CDCl_3$, δ,

ppm): 6.74 (s, 2H), 4.25 (t, 2H), 3.80 (t, 2H), 2.97 (m, 1H), 2.76 (m, 1H), 2.50 (dd, 1H), 2.43 (td, 2H), 1.96 (m, 1H), 1.74 (dq, 1H); ^{13}C NMR (400 MHz, $CDCl_3$, δ, ppm): 172.54, 170.40, 135.35, 62.17, 51.10, 46.96, 37.64, 30.09, 27.31. See appendix page 138 for full spectra.

3.4.3.6 Synthesis of **M3.6** from Steglich esterification of M3.2

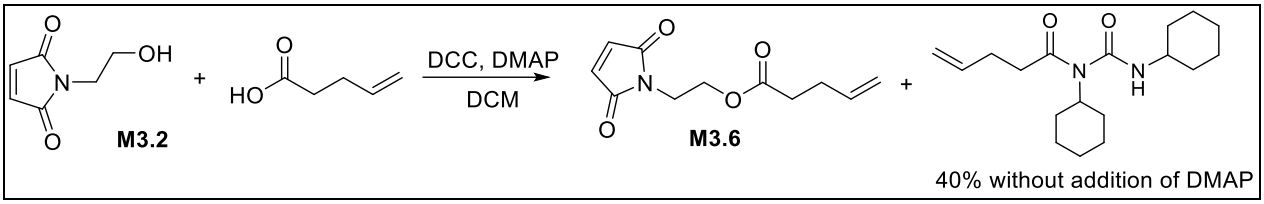

Hydroxylethyl maleimide (M3.2, 0.75 g, 5.3 mmol, 1 eq), 4-pentenoic acid (0.65 mL, 6.4 mmol, 1.2 eq), DCC (1.6 g, 7.9 mmol, 1.5 eq), and DMAP (65 mg, 0.5 mmol, 0.11 eq) was dissolved in DCM (35 mL) and stirred overnight. DCU byproduct was filtered off. Crude product was purified by column chromatography. (Hex: EtOAc = 3:1, 144 mg, 12.1%); ^{1}H NMR (400 MHz, $CDCl_3$, δ, ppm): 6.75 (s, 2H), 5.79 (m, 1H), 5.03 (m, 2H), 4.24 (t, 2H), 3.80 (t, 2H), 2.36 (m, 4H); ^{13}C NMR (400 MHz, $CDCl_3$, δ, ppm): 174.70, 169.67, 136.53, 134.21, 114.50, 61.93, 36.86, 33.14, 28.04. See appendix page 139 for full spectra.

The rearrangement product was observed with 40% yield when the reaction was repeated without the addition of DMAP. ^{1}H NMR (400 MHz, $CDCl_3$, δ, ppm): 6.98 (br, 1H), 5.84 (m, 1H), 5.06 (m, 2H), 3.92 (tt, 1H), 3.69 (dddd, 1H), 2.51 (m, 4H), 1.99-1.58 (m, 12H), 1.45-1.08 (m, 8H); ^{13}C NMR (400 MHz, $CDCl_3$, δ, ppm): 154.39, 137.63, 116.29, 49.77, 35.75, 32.72, 31.72, 29.34, 26.88, 25.55, 25.30, 24.70. See appendix page 140 for full spectrum.

3.4.3.7 Synthesis of **M3.7**

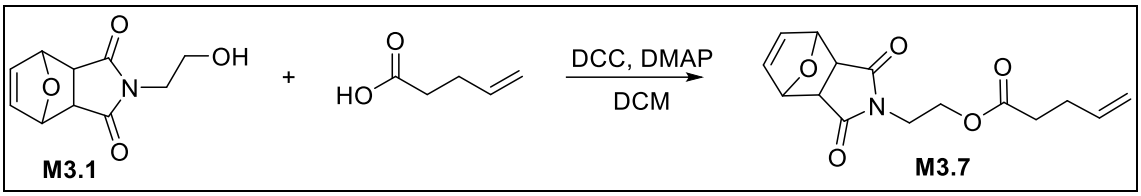

Hydroxylethyl oxanorbornene (M3.1, 1.5 g, 7.17 mmol, 1 eq), 4-pentenoic acid (0.88 mL, 8.6 mmol, 1.2 eq), DCC (2.22 g, 10.76 mmol, 1.5 eq), and DMAP (96 mg, 0.79 mmol, 0.11 eq) was dissolved in DCM (50 mL) and stirred overnight. DCU byproduct was filtered off. Crude product was purified by column chromatography. (Hex: EtOAc = 1:2, 2.03 g, 97%); ^{1}H NMR (400 MHz, $CDCl_3$, δ, ppm): 6.51 (s, 2H), 5.79 (m, 1H), 5.25 (m, 2H), 5.00 (m, 2H), 4.22 (t, 2H), 3.74 (t, 2H), 2.86 (d, 2H), 2.35 (m, 4H); ^{13}C NMR (400 MHz, $CDCl_3$, δ, ppm): 177.39, 172.74, 136.64, 136.54, 114.29, 80.90, 59.08, 48.24, 39.80, 33.21, 29.07. See appendix page 140 and 141 for full spectra.

3.4.3.8 Synthesis of **M3.6** from **M3.7**

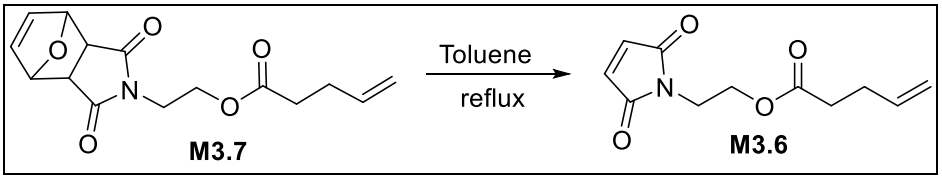

M3.7 (1.8 g, 6.18 mmol) was dissolved in toluene (30 mL) and stirred at reflux overnight. The condenser was removed and continued boiling for an additional 30 min. Toluene was removed on a rotary evaporator. Crude product was collected without further purification. (1.26 g, 91.3%); NMR characterization refer to section 3.4.3.6.

3.4.3.9 Synthesis of **M3.5** from **M3.6**

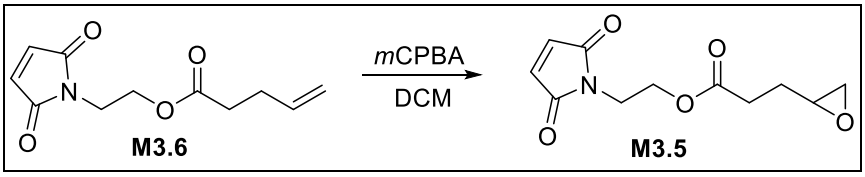

M3.6 (1.2 g, 5.38 mmol, 1 eq) was dissolved in DCM (10 mL) in a 3-neck flask. mCPBA (1.45 g, 6.45 mmol, 1.2 eq) was dissolved in DCM (20 mL) and added to the flask through an addition funnel over an ice bath. The mixture was warmed up to room temperature and stirred for 24 h. White precipitate was filtered off and filtrate was washed with sat. sodium bisulfite, sat. sodium bicarbonate and brine. Crude product was purified by column chromatography. (Hex: EtOAc = 1:1, 0.89 g, 69.0%); NMR characterization refer to section 3.4.3.5.

3.4.3.10 Synthesis of **M3.8** from M3.5

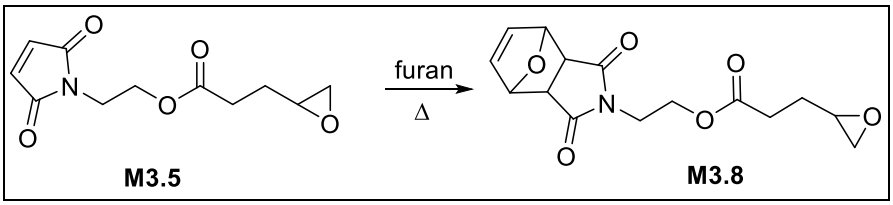

M3.5 (1 g, 4.18 mmol, 1 eq) and furan (3.0 mL, 8.36 mmol, 10 eq) was dissolved in toluene (30 mL) and stirred at reflux for 3 days. Solvent and excess furan was removed on a rotary evaporator. Crude product was purified by column chromatography. (Hex: EtOAc = 1:2, <50%, mixture of isomers); ^{1}H NMR (400 MHz, $CDCl_3$, δ, ppm): 6.52 (t, 2H), 5.28 (m, 2H), 4.25 (dd, 2H), 3.76 (dd, 2H), 2.97 (m, 1H), 2.87 (s, 2H), 2.76 (m, 1H), 2.50 (dd, 1H), 2.42 (td, 2H), 1.95 (m, 1H), 1.74 (m, 1H); ^{13}C NMR (400 MHz, $CDCl_3$, δ, ppm): 176.01, 172.54, 135.68, 81.48, 60.74, 51.17, 47.45, 47.00, 37.83, 30.97, 27.32. See appendix page 141 and 142 for full spectra.

3.4.3.11 Synthesis of **P3.1 – P3.5**

In a glovebox, M3.8 (500 mg) and $NOct_4Br$ was dissolved in dry DCM (2 mL) in a vial equipped with a stir bar. A solution of *i*-Bu_3Al was added while stirring and the solution turned orange. The mixture was stirred in the glovebox for 4 hrs before being moved out of the glovebox and quenched with 0.5 mL of ethanol. The solvents were removed on a rotary evaporator. The residual white

solid was dissolved in a small amount of DCM and precipitated from cold methanol. The solid was collected, redissolved in DCM and eluted through a plug of neutral alumina with DCM. Polymers were collected after removing DCM as a light yellow porous solid.

3.4.3.12 Post-polymerization deprotection

The polymer (P3.1 and P3.2) was dissolved in dry DMF in a vial capped with a septum, BHT (4-20%wt) was added. The mixture was heated to 115 °C under argon and stirred for 24 hrs. The solution slowly turned red upon heating. DMF was removed under vacuum. The residual solid was dissolved in a small amount of DCM and precipitated from cold methanol. Product was collected as a red powder.

3.4.3.13 N-cyclohexyl maleimide and trans-stilbene radical copolymerization

N-cyclohexyl maleimide (250 mg), trans-stilbene (250 mg) and AIBN (0.5 mg) was dissolved in dry THF (1.5 M) in a 10 mL Schlenk flask. The mixture was sparged with argon over an ice bath for 20 min. The flask was heated to 70 °C in an oil bath. After 4 hrs the stir bar stopped moving and the reaction was quenched by opening to air. The viscous product was diluted with THF and the polymer precipitated from hexanes. (0.32 g, M_n 23.0 kDa, M_w 38.4 kDa, Đ 1.7)

Chapter 4. Fabrication of SCNP *via* intra-chain ring-opening metathesis polymerization (ROMP)

4.1 Introduction

Single-chain nanoparticles are a class of nanoparticles obtained from self-folding of single polymer molecules. Linear polymer precursors bearing reactive pendant groups undergo intramolecular cross-linking when the solution concentration is below the polymer's overlap concentration c*.[15-17] This method mimics the natural folding process of peptide chains to afford complex hierarchical protein structures. It also provides a way to produce polymeric nanoparticles of ultrafine size. A variety of cross-linking chemistries have been explored, including covalent, dynamic covalent and non-covalent chemistries, among which intramolecular polymerization is of particular importance as it allows for easy control of an SCNP's degree of cross-linking.[173] Intramolecular radical polymerization, oxidation polymerization and ring-opening polymerization have been reported to successfully fold linear polymer precursors into SCNP. [149, 153-155, 157]

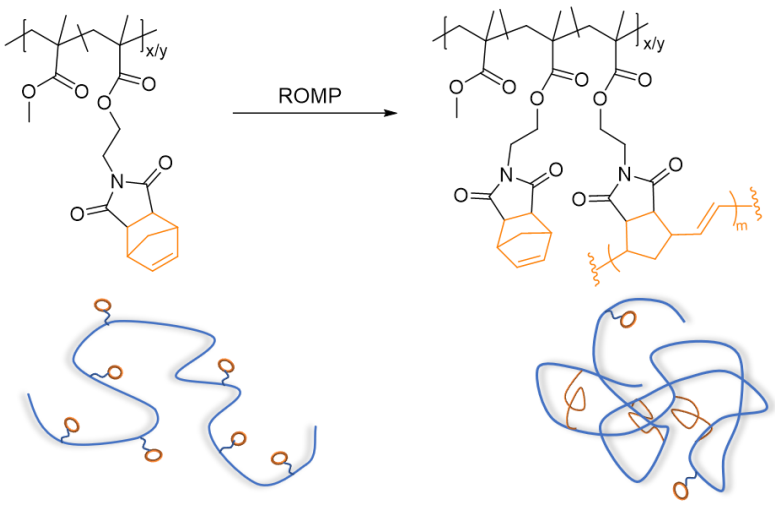

Figure 4.1 Schematic illustration of intramolecular ROMP of polymers bearing norbornene pendant groups.

The purpose of this project is to expand the scope of intramolecular polymerizations and fabricate SCNP from ROMP of norbornene pendants on linear polymers. (Figure 4.1) ROMP was chosen as it is highly functional group tolerant and proceeds rapidly, leading to fast access of nanoparticles. Intramolecular ROMP of a polymer bearing furan-protected maleimide moieties was recently reported by Zhou and coworkers.[156] Herein we provide a more detailed study on chain folding by ROMP. Our results showed that the efficiency of chain folding was related to norbornene content on the polymer precursor, species and feed ratio of Grubbs catalysts, as well as doping effects of fluorinated aromatic comonomers.

4.2 Results and discussion

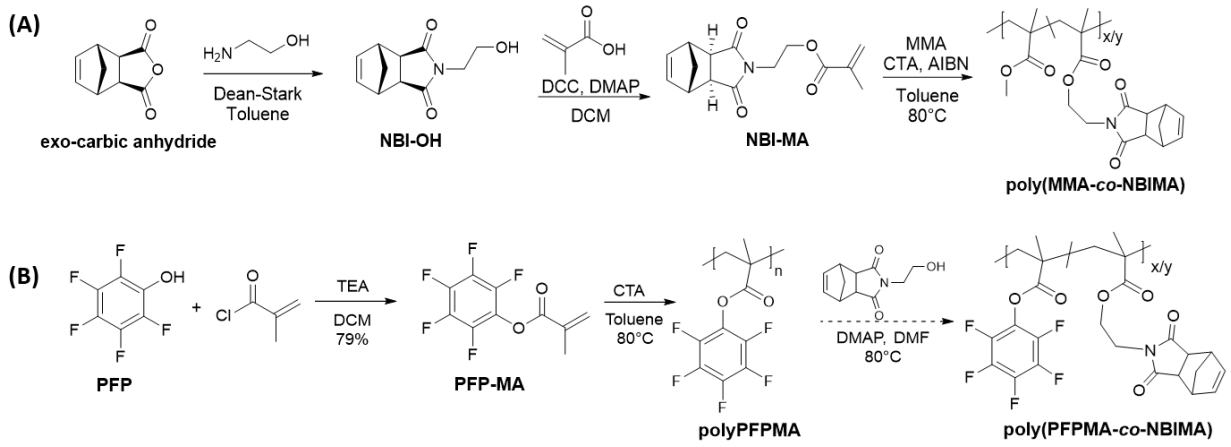

Scheme 4.1 Synthesis of norbornene-containing copolymers by (A) direct RAFT copolymerization and (B) post-polymerization transesterification.

We sought to synthesize a series of poly(MMA-co-NBIMA) polymers with various amount of norbornene incorporations. (Scheme 4.1A) Comonomer NBIMA was synthesized according to literature procedures.[157] Direct copolymerization of MMA and NBIMA by RAFT polymerization led to well-defined polymers only when low NBIMA incorporations were targeted. At higher NBIMA incorporation (≥40%) the polymers started to show higher molecular weight and broader distribution because of interchain cross-linking. The cross-linking reaction was attributed to

radical addition on the alkene functionality of norbornene during RAFT polymerization, or it may be caused by the retro Diels-Alder reaction of norbornene imide followed by radical polymerization of the maleimide group. In order to synthesize copolymers with higher NBIMA incorporation we adopted a post-polymerization functionalization strategy which was to attach NBIOH to the polymer after RAFT polymerization of PFPMA *via* a transesterification reaction. (Scheme 4.1B) Transesterification of polypentafluoroesters was previously reported using DMAP as a catalyst in DMF at 80 °C.[209] However, applying the referenced procedure to our reactants only led to ~15% transesterification of polyPFPMA when 100% was targeted. Meanwhile the DMAP catalyst was found to cause nucleophilic aromatic substitution of fluorobenzene under the employed condition.[210-212]

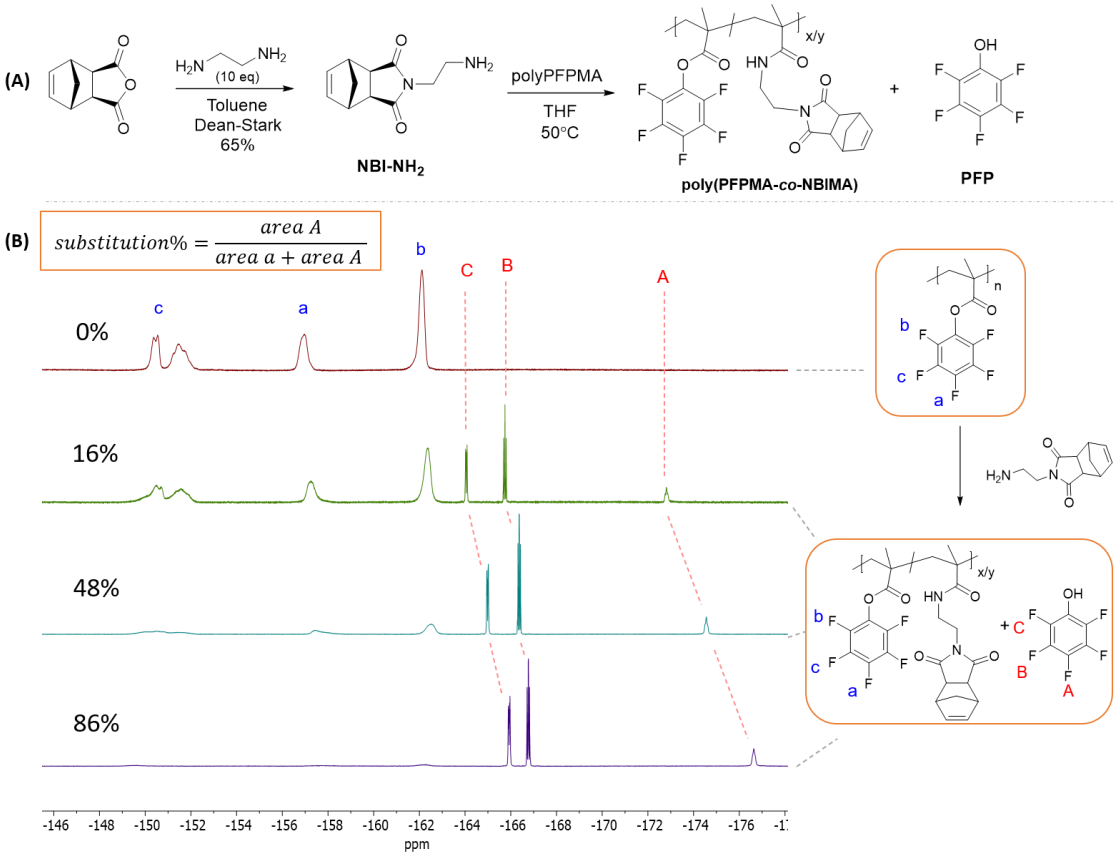

Figure 4.2 (A) Synthesis of poly(PFPMA-co-NBIMA) by amine-pentafluoroester substitution; (B) Stack of ^{19}F NMR spectrum showing various degree of substitution.

An amine-functionalized norbornene imide NBI-NH_2 was then synthesized and subjected to nucleophilic substitution of polyPFPMA. (Figure 4.2A) Due to the superior nucleophilicity of primary amine, the reaction proceeded at mild conditions and the degree of substitution could be monitored by ^{19}F NMR. (Figure 4.2B) The polyPFPMA homopolymer contained three broad peaks at -151, -157 and 162 ppm corresponding to the meta, para and ortho fluorine. The substitution produced pentafluorophenol which showed three new peaks in ^{19}F NMR and the degree of substitution could be calculated based on the ratio of peak integration. As shown in Figure 4.2B, the polymer peaks became smaller with higher degree of substitution while the pentafluorophenol peaks became larger. A homopolymer of polyNBIMA could be synthesized based on this method when the degree of substitution reached 100%. As seen from Figure 4.3, the broad fluorine peaks on polyPFPMA completely disappeared and all transformed to pentafluorophenol. After workup to remove pentafluorophenol, no fluorine peak was present indicating all pentafluoroesters substituted with NBI-NH_2.

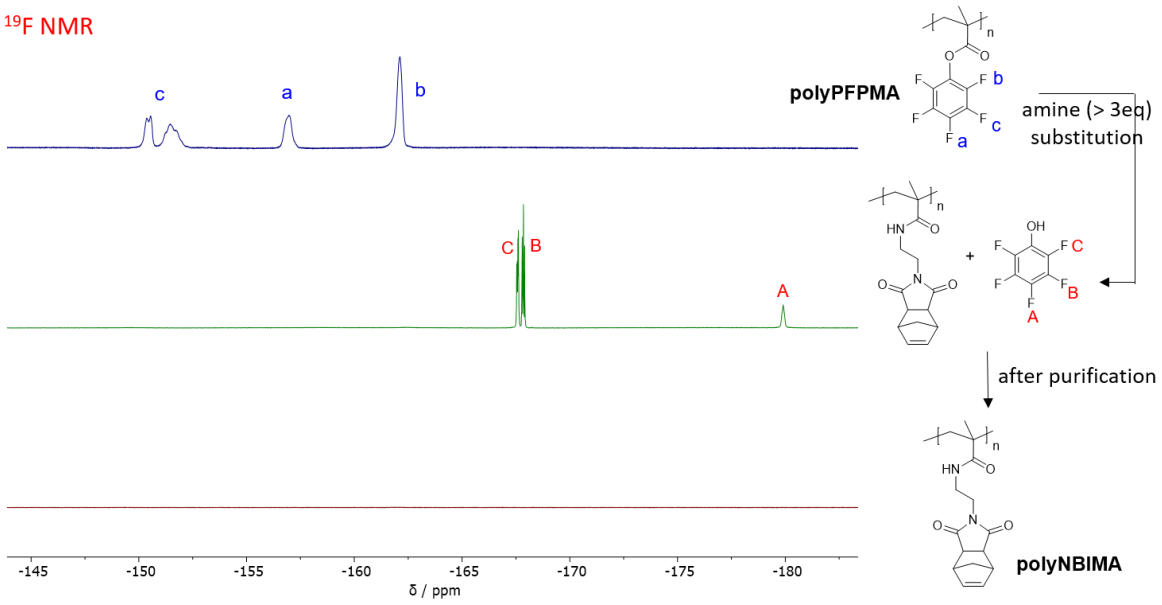

Figure 4.3 Synthesis of polyNBIMA from polyPFPMA and ^{19}F NMR spectrum of the polymers before and after complete substitution with NBI-NH_2.

A series of poly(PFPMA-co-NBIMA) were synthesized based on this method targeting 20%, 50%, 70% and 100% incorporation of NBIMA. It is worth mentioning that polyPFPMA was not soluble in room temperature DMF even after 72 hours of stirring, so we were not able to collect GPC data of this polymer using DMF as mobile phase. The molecular weight of polyPFPMA could be estimated from monomer conversion calculated from ^{19}F NMR, assuming each chain transfer agent constitutes the chain ends of a polymer molecule. The polymers became soluble in DMF after substitution with NBI-NH_2 and they were characterized by GPC using DMF containing 0.1%wt LiBr as a mobile phase. (Table 4.1)

Table 4.1 Molecular weight data of polymers P4.1-P4.4 and nanoparticles NP4.1-NP4.4

	NBIMA% [a]	M_n (kDa) [b]	M_w (kDa) [b]	Đ [b]	dn/dc [c]
P4.1	100%	47.8	75.0	1.56	0.130
NP4.1-DP5		57.0	140.0	2.46	0.136
NP4.1-DP30		109.6	6238.1	57.76	0.078
P4.2	76%	49.3	75.9	1.54	0.107
NP4.2-DP5		50.0	82.0	1.64	0.099
NP4.2-DP30		56.4	127.0	2.25	0.099
P4.3	56%	54.8	82.6	1.51	0.083
NP4.3-DP5		49.2	77.4	1.57	0.061
NP4.3-DP30		49.9	80.7	1.62	0.078
P4.4	22%	54.1	69.5	1.29	0.059
NP4.4-DP5		38.6	52.8	1.37	0.062
NP4.4-DP30		40.2	57.9	1.44	0.051

a. Calculated from ^{19}F NMR; b. Obtained from conventional calibration based on polystyrene standards; c. Obtained using triple detection GPC.

Polymers P4.1-P4.4 were treated with Grubbs 3rd generation catalyst to initiate intra-chain ROMP of pendant norbornene groups. (Figure 4.4A) Two series of reactions were attempted for each polymer, targeting intra-chain degree of polymerization of 5 and 30. The corresponding nanoparticles were denoted NP4.x-DP5 and NP4.x-DP30. In order to promote intra-chain

polymerization over inter-chain crosslinking, the reactions were run at a low concentration of 0.75 mg/mL before being quenched with vinyl ether. The nanoparticles obtained were analyzed by GPC and the results are summarized in Table 4.1 and Figure 4.4.

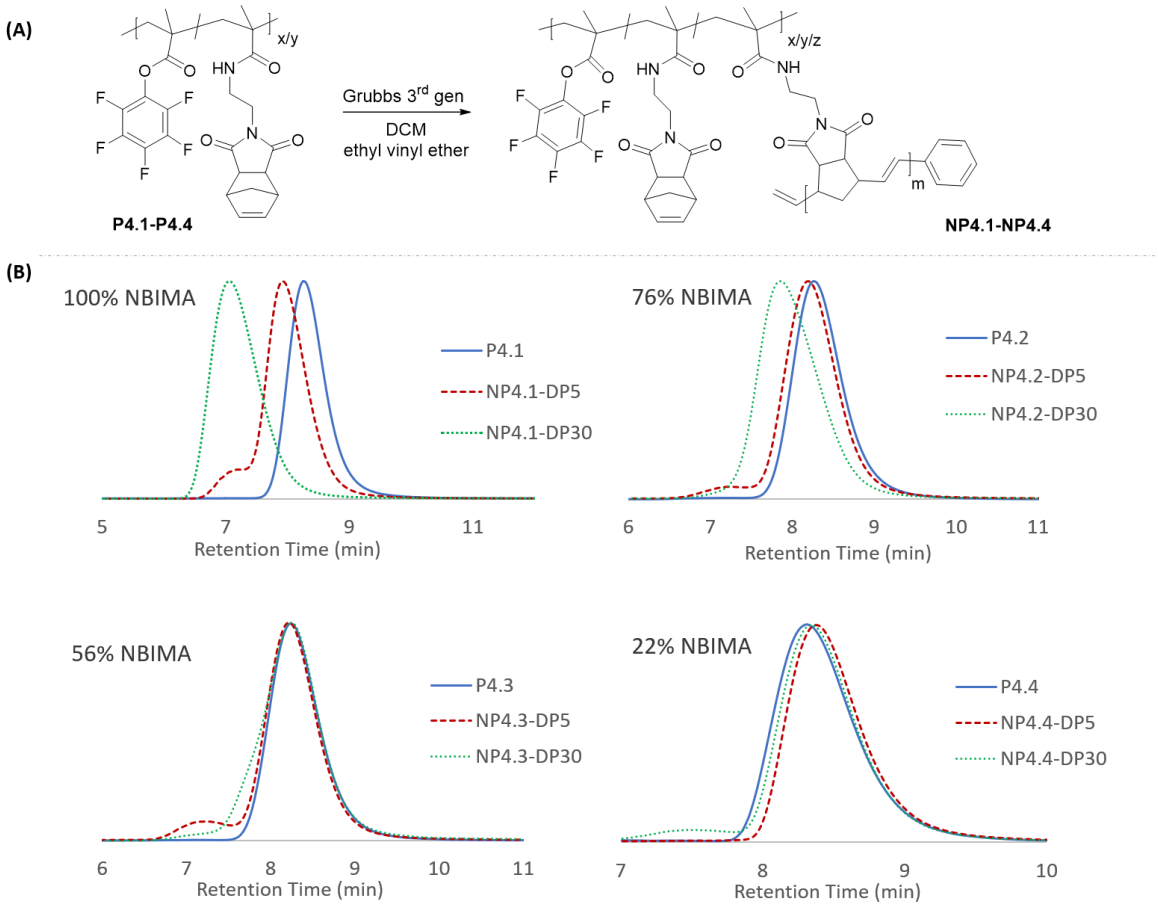

Figure 4.4 (A) Intra-chain ROMP of P4.1-P4.4; (B) GPC-MALS traces of P4.1-P4.4 and corresponding NP4.1-NP4.4.

The synthesis of SCNP by intra-chain cross-linking reactions is always in competition with inter-chain reactions which lead to a high molecular weight, cross-linked network. The two reactions are chemically equivalent, and the ratio of intra- versus inter- depends solely on the probability of pendant norbornene groups finding each other. When the polymers are dissolved in an ultra-dilute solution, each polymer coil is proposed to be independent. Reactive pendant groups have higher

probability of finding a reacting partner along the same chain, so intra-chain reactions within the solvated coil is enhanced. The conformation of a linear polymer precursor becomes denser as a result of intra-chain cross-linking reaction, leading to a nanoparticle with smaller hydrodynamic volume. Hence an SCNP shows longer retention time than its linear precursor when eluted in GPC. When inter-chain cross-linking reactions occur, the molecular weight of a polymer will grow by orders of magnitute. A light scattering detector is good at detecting inter-chain reactions because of its sensitivity to high molecular weight fractions. Compared with its linear polymer precursor, inter-chain cross-linked product often exhibits shorter retention times or a shoulder peak on the high molecular weight end. As shown in Figure 4.4B, when polymers P4.1 through P4.4 were subjected to intra-chain ROMP targeting 5 norbornene units per Grubbs catalyst, only P4.4 gave an SCNP NP4.4-DP5. The nanoparticle shows longer retention time than its polymer precursor, indicating smaller hydrodynamic volume resulting from intra-chain ROMP. Polymers with high incorporations of NBIMA including P4.1 and P4.2 encountered significant inter-chain cross-linking. The retention times of the resulting nanoparticles NP4.1-DP5 and NP4.2-DP5 were shorter than their linear precursors, indicating larger hydrodynamic volume. The GPC traces of P4.3 and NP4.3-DP5 were largely overlapped, except that the nanoparticle trace has a small shoulder peak with high molecular weight. This represents a small amount of inter-chain crosslinking during intra-chain ROMP. When the target degree of intra-chain polymerization is 30, similar results were found – only P4.4 gave single-chain nanoparticles while P4.1-P4.3 showed signs of high molecular weight product from inter-chain cross-linking. The degree of inter-chain cross-linking is more significant when the target intra-chain DP is 30, evidenced by the larger shift to short retention time in NP4.1-DP30 and NP4.2-DP30. This is attributed to the small feed amount of Grubbs catalyst and fewer propagating chains in the process of polymer folding. The relationship between

reactive group incorporation and single chain folding of linear polymer precursors is consistent with our previous findings: high incorporation of reactive pendant groups leads to inter-chain crosslinking and lowers the efficiency of SCNP synthesis. This is because polymer coils in dilute solutions are free to move, and collisions between polymer chains are unavoidable. When collisions occur between two polymer coils, those bearing less reactive groups have a smaller chance of having reactive groups in the correct orientation to react. A polymer containing more reactive groups is more likely to react with a coupling partner on another polymer chain during collision and form a dimer. This phenomenon is especially prominent for fast reactions such as radical coupling and ROMP.

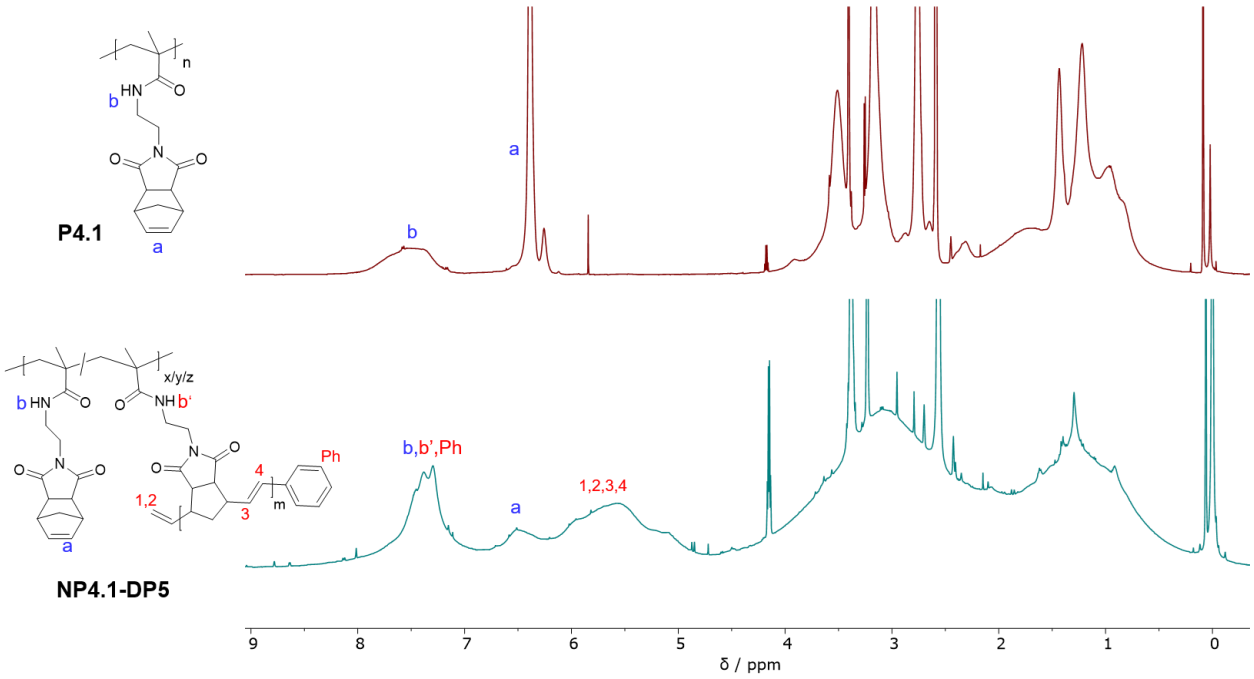

Figure 4.5 ^{1}H NMR spectra of P4.1 and NP4.1-DP5 in d6-DMSO.

The polymers and nanoparticles were characterized by ^{1}H NMR. (Figure 4.5) Amide protons on the polymers appear at 7.1-7.9 ppm. Olefin groups on pendant norbornene show up at 6.1-6.6 ppm. After ROMP of norbornene groups, some unreacted norbornene peaks remained. New peaks

showed up at a broad range of 4.9-6.2 ppm corresponding to the polymerized norbornene units, as well as vinyl end groups from quenching agent ethyl vinyl ether. Phenyl end groups from Grubbs initiator are overlapped within amide proton peaks. Although the degree of ROMP cannot be quantified from integration due to the broadness and overlap of peaks after crosslinking, the emergence of polymerized norbornene peaks confirms successful polymerization of pendant norbornene groups on linear polymer precursors.

We compared the efficiency of 1st, 2nd and 3rd generation Grubbs catalyst in the self-folding of polymer P4.4 by intra-chain ROMP. (Figure 4.6) Grubbs 3rd gen catalyst is the most used for ROMP of cyclic olefins. The dissociation of electron-deficient bromopyridine ligands is extremely rapid and rebinding is slow, leading to fast initiation of polymerization and narrow distribution of the resulting polymers. The N-heterocyclic carbene ligand on the catalyst improves the complex's selectivity for binding olefinic substrates in the presence of free phosphine ligands, hence increases the turnover of the intermediate. To investigate whether Grubbs 3rd gen catalyst exhibit superior behavior for intra-chain ROMP of norbornene pendants on linear polymer precursors, we subjected polymer P4.4 to 1st, 2nd and 3rd gen Grubbs catalysts under the same conditions. A shrinking factor defined as $[G] = M_{n(SCNP)} / M_{n(polymer)}$ was used to evaluate the level of compaction.[83] It was found that all three catalysts successfully initiated intra-chain ROMP and folded the linear polymers to smaller single-chain nanoparticles. The GPC peak retention and peak shape of the nanoparticles were about the same. The shrinking factors of the three SCNP were 0.74, 0.71 and 0.71, respectively. The nanoparticle synthesized from 1st gen Grubbs catalyst is slightly less compacted than the other two, but overall, the level of compaction from the linear polymer precursor were similar for all 3 catalysts.

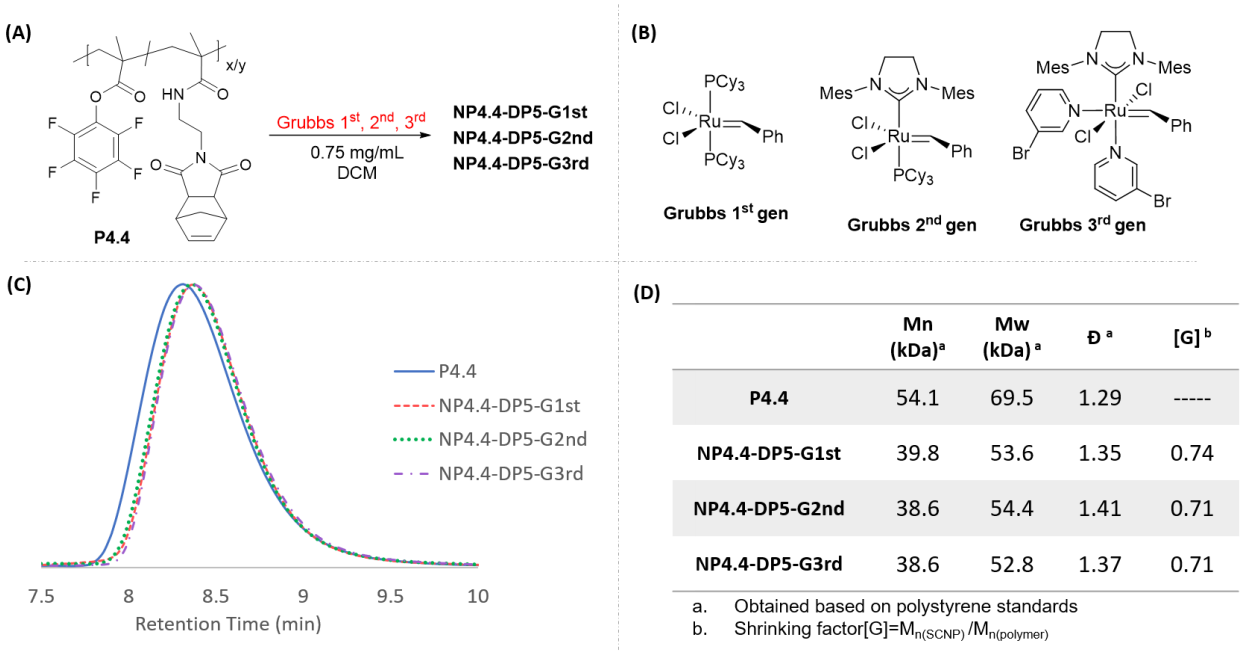

	Mn (kDa)[a]	Mw (kDa)[a]	Đ [a]	[G] [b]
P4.4	54.1	69.5	1.29	-----
NP4.4-DP5-G1st	39.8	53.6	1.35	0.74
NP4.4-DP5-G2nd	38.6	54.4	1.41	0.71
NP4.4-DP5-G3rd	38.6	52.8	1.37	0.71

a. Obtained based on polystyrene standards
b. Shrinking factor[G]=$M_{n(SCNP)}/M_{n(polymer)}$

Figure 4.6 Intra-chain ROMP of P4.4 by Grubbs 1st, 2nd and 3rd gen catalyst (A, B); GPC-MALS traces (C) and molecular weight data (D) of P4.4 and corresponding nanoparticles.

Researchers have found that fluorinated aromatic hydrocarbons (FAH) exhibit doping effects on second and third generation Grubbs' catalyst.[213-215] When a pentafluoroester moiety was attached to a sufficiently long spacer unit on a ROMP active monomer, Grubbs 2nd and 3rd gen catalysts demonstrated extremely fast and uncontrolled rates of propagation while Grubbs 1st gen catalyst gave well-controlled polymers. The actual mechanism of this phenomenon is under debate, but it is widely accepted that the doping effects of FAH on ruthenium centers is caused by strong, stabilizing π-π interactions. Since the norbornene-bearing copolymers we used contain pentafluoroesters, intra-chain ROMP might be affected by doping effects as well. The comparison between 3 generations of Grubbs catalysts on single chain folding of P4.4 revealed that all 3 catalysts led to SCNP with shrinking factors of around 0.7. Specific doping effects of FAH on 2nd and 3rd gen Grubbs catalysts were not obvious when performing ROMP intramolecularly. We further substituted the residual pentafluoesters on polymer P4.4 with n-hexylamine to afford

polymer P4.5. (Figure 4.7A) P4.5 was folded with 3rd gen Grubbs catalyst and the results were compared with P4.4. As shown in Figure 4.7B, from P4.5 to NP4.5 there was a very small shift to longer retention time indicating successful intramolecular folding of the linear polymer precursor by ROMP. Although P4.4 and P4.5 contain the same molar incorporation of the ROMP-active norbornene pendants, and the two polymers were subjected to the exact same procedures synthesizing SCNP, the resulting nanoparticles NP4.4 and NP4.5 showed different levels of compaction. The shrinking factor of NP4.5 was 0.94, larger than NP4.4 which was 0.71, indicating NP4.5 less compacted than NP4.4. This could be caused by the doping effects of pentafluoroesters on P4.4 to the 3rd gen Grubbs catalyst, causing a faster intra-chain propagation which led to a more compacted single-chain nanoparticle.

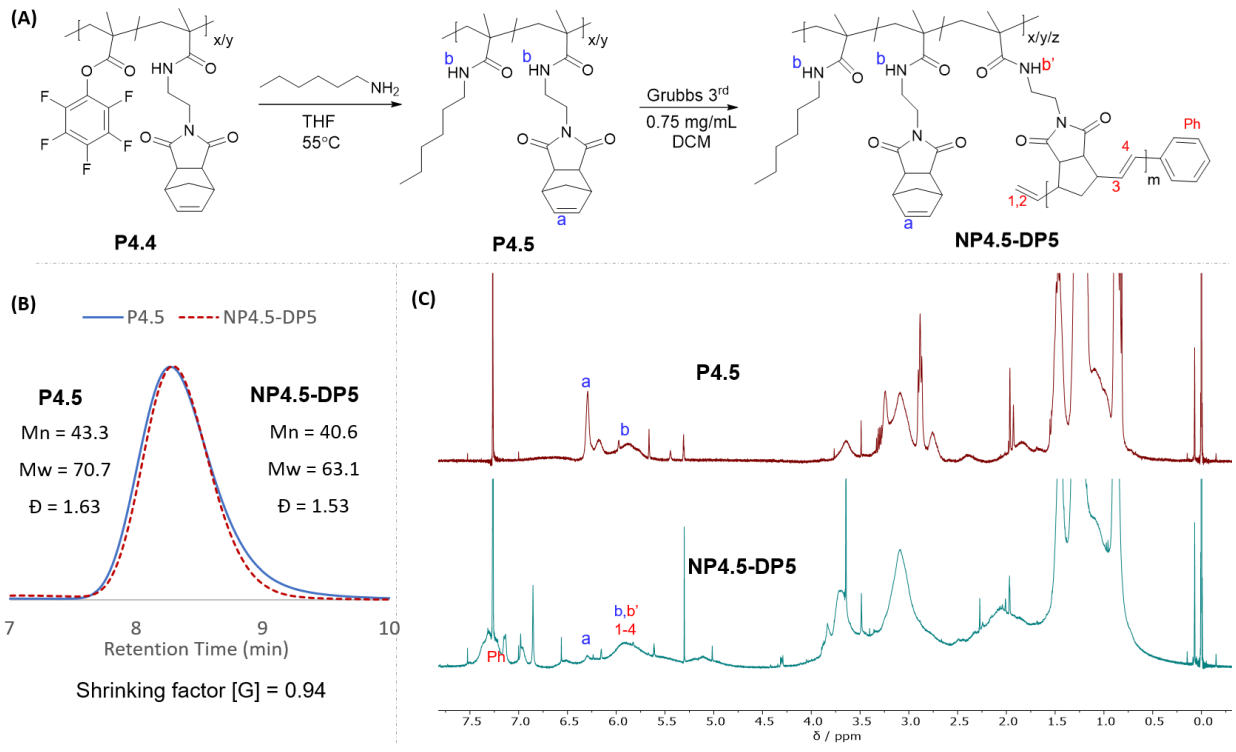

Figure 4.7 (A) Synthesis of P4.5 and NP4.5-DP5; (B) GPC-MALS traces of P4.5 and NP4.5-DP5; (C) ^{1}H NMR spectra of P4.5 and NP4.5-DP5.

4.3 Conclusion

A series of linear polymers containing various amount of norbornene pendant groups were synthesized by post-polymerization amine-pentafluoroester substitution reaction. The polymers were subjected to intramolecular ROMP with Grubbs catalysts in a dilute solution of 0.75 mg/mL (~1.5×10^{-5}M). It was found that when the polymer precursors contain high amount of norbornene groups (>50%mol), intermolecular reactions tend to take place and afford intermolecular cross-linked products. Polymers with low incorporations of pendant norbornene groups prefer intramolecular reactions and lead to SCNP. Grubbs 1st, 2nd and 3rd generation catalysts all successfully folded the 22% norbornene-containing polymer precursor into SCNP. Substituting the pentafluoroesters on the polymer with alkyl amine led to a polymer which after intrachain ROMP, afforded an SCNP less compacted than the pentafluoroester containing polymer. The difference is likely caused by the doping effect of pentafluoesters on the catalyst.

4.4 Experimental

4.4.1 Materials

Reagents were obtained from the indicated commercial suppliers and used without further purification unless otherwise stated: cis-5-Norbornene-endo-2,3-dicarboxylic anhydride, 97% (Sigma-Aldrich), 2-aminoethanol (TCI), pentafluorophenol (Oakwood Products, Inc), N,N'-dicyclohexylcarbodiimide (Sigma-Aldrich), 4-dimethylamino pyridine (Oakwood Products, Inc), methyl methacrylate (Sigma-Aldrich, eluted through basic alumina), methacryloyl chloride (Sigma-Aldrich), ethylenediamine (Acros Organics), Grubbs catalyst 1st generation (Materia), Grubbs catalyst 2nd generation (Materia), 3-bromopyridine (Sigma-Aldrich), 1,4-dichlorobenzene (Sigma-Aldrich), hexanes (Fisher Scientific), ethyl acetate (Fisher Scientific), 2,2'-azobis(2-methylpropionitrile) (AIBN, Sigma-Scientific, recrystallized from methanol), silica gel (230 – 400

mesh, SiliCycle), N,N'-dimethylformamide (HPLC grade, Fisher Scientific), dimethyl sulfoxide-d6 (Cambridge Isotope Laboratories), chloroform-d ($CDCl_3$, Cambridge Isotope Laboratories). Dry dichloromethane (DCM) were obtained by heating to reflux with calcium hydride.

4.4.2 Instrumentation

^{1}H and ^{13}C NMR spectra were acquired with a Varian Unity INOVA or Bruker Biospin 500 MHz or Varian Mercury 400 MHz spectrometer. Chemical shifts (δ) were reported in parts per million (ppm) relative to tetramethylsilane (TMS). Solvent ($CDCl_3$) contained 0.03% v/v TMS as an internal reference. Peak abbreviations are used as follows: s = singlet, d = doublet, t = triplet, q = quartet, m = multiplet, br = broad, Ar = Aryl).

GPC was performed on a Tosoh EcoSEC dual detection (RI and UV) SEC system coupled to an external Wyatt Technologies miniDAWN Treos multiangle light scattering (MALS) detector. The mobile phase was HPLC grade DMF containing 0.1%wt LiBr and filtered through 0.2 μm PTFE membrane filters. Samples were run at 50 °C at a flow rate of 0.45 mL/min. The column set contained one Tosoh TSKgel SuperH4000 (6.0 mm ID × 15 cm) column, one Tosoh TSKgel SuperH2500 (6.0 mm ID × 15 cm) column and a Tosoh TSKgel SuperH5000-7000 guard column (4.6 mm ID × 3.5 cm). All polymer solutions characterized by SEC were 1.0 mg/mL in DMF with 0.1%wt LiBr, stirred magnetically for at least 5 hours and filtered through 0.45 μm PTFE syringe filters before analysis.

4.4.3 Experimental procedures

4.4.3.1 Synthesis of exo-norbornene dicarboxylic anhydride

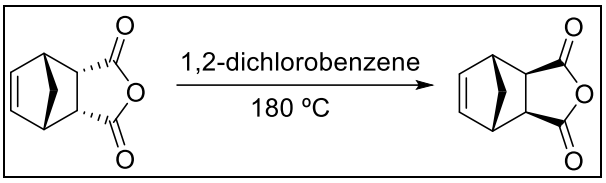

Carbic anhydride (170 g, 1.05 mol) was heated to reflux in 1,2-dichlorobenzene (170 mL) at 180 °C overnight. The brown solution was cooled to room temperature and further cooled over ice. Precipitate was collected by vacuum filtration and recrystallized from benzene 6 times. (33g,white crystals, 19.7%)); ^{1}H NMR (400 MHz, $CDCl_3$, δ, ppm): 6.35 (s, 2H), 3.45 (s, 2H), 3.01 (s, 2H), 1.66 (s, 1H), 1.44 (s, 1H);^{13}C NMR (400 MHz, $CDCl_3$, δ, ppm): 171.58, 137.95, 48.77, 46.87, 44.01. See appendix page 142 and 143 for full spectra.

4.4.3.2 Synthesis of NBI-NH_2 [216]

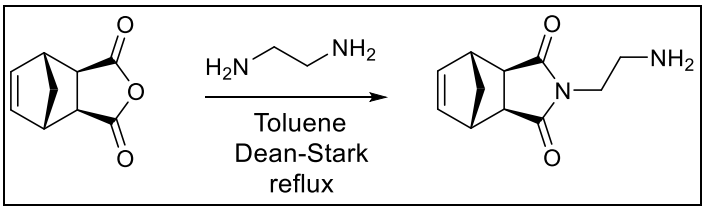

Exo-norbornene dicarboxylic anhydride (3 g, 18.27 mmol) was dissolved in toluene (100 mL). Ethylenediamine (12.21 mL, 182.7 mmol) was added dropwise with vigorous stirring. The mixture was heated to reflux with a Dean-Stark trap overnight under argon. The solvent and excess ethylenediamine was removed on a rotary evaporator. Crude product was purified by column chromatography. (5% MeOH in DCM, 2.58 g, 68.4%); ^{1}H NMR (400 MHz, $CDCl_3$, δ, ppm): 6.29 (s, 2H), 3.52 (t, 2H), 3.27 (s, 2H), 2.88 (t, 2H), 2.69 (s, 2H), 1.50 (d, 1H), 1.35 (d, 1H), 1.13 (br, 1H); ^{13}C NMR (400 MHz, $CDCl_3$, δ, ppm): 179.75, 137.80, 47.85, 45.19, 42.82, 41.45, 39.95. See appendix page 143 and 144 for full spectra.

4.4.3.3 Synthesis of PFP-MA

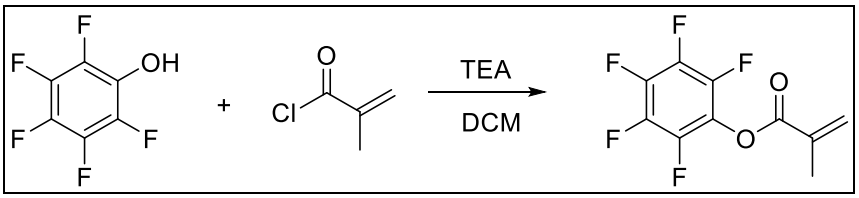

Pentafluorophenol (3 g, 16.30 mmol), triethylamine (2.73 mL, 19.56 mmol) and butylated hydroxytoluene (~10 mg) was dissolved in dry DCM (80 mL) and cooled over an ice bath. Methacryloyl chloride (1.91 mL, 19.56 mmol) was added dropwise. The mixture was stirred at room temperature overnight. TEA salt was filtered off and the filtrate and washed with 0.1 M HCL and Brine. Crude product was purified by column chromatography to afford a clear liquid. (5% ethyl acetate in hexanes, 2.53 g, 62%); ^{1}H NMR (400 MHz, $CDCl_3$, δ, ppm): 6.45 (s, 1H), 5.90 (s, 1H), 2.09 (s, 3H); ^{13}C NMR (400 MHz, $CDCl_3$, δ, ppm): 165.95, 142.79, 140.71, 138.90, 137.43, 133.71, 129.52, 20.07; ^{19}F NMR (400 MHz, $CDCl_3$, δ, ppm): -152.87, -158.29, -162.62. See appendix page 144 and 145 for full spectra.

4.4.3.4 Synthesis of polyPFPMA by RAFT polymerization

PFPMA, CTA and AIBN were dissolved in dry Toluene in a Schlenk flask and sparged with argon over an ice bath for 30 min. The mixture was heated to 80 °C and stirred for 24 hrs. Monomer conversion was calculated from ^{19}F NMR of the mixture. (Figure A 63) The product was precipitated from cold methanol and collected by vacuum filtration. The obtained polymers were purified by dissolving in THF and reprecipitating from cold methanol.

4.4.3.5 Synthesis of poly(PFPMA-*co*-NBINH2) by amine-pentafluoroester substitution

PolyPFPMA and NBI-NH_2 were dissolved in THF and stirred at 50°C. The reaction was monitored by ^{19}F NMR and shut off when the target degree of substitution was reached. The mixture was

concentrated and precipitated from cold methanol. The product was further washed by methanol a few times and collected by vacuum filtration.

4.4.3.6 General procedure of intrachain ROMP

Grubbs 3rd generation catalyst was synthesized following reported procedure.[217] The linear polymer precursor (30 mg) was dissolved in dry DMC (30 mL) in a round bottom flask under argon and stirred at room temperature for 2 hrs to ensure full dissolution. Grubbs catalyst was dissolved in 10 mL of dry DCM and added quickly to the polymer solution over an ice bath. The solution turned orange upon addition of the 3rd gen Grubbs catalyst solution. The mixture was stirred over ice for an additional hour before quenched with ethyl vinyl ether (1mL) and stirred at room temperature overnight. The solvent was removed on a rotary evaporator. Product was dissolved in a small amount of DCM and precipitated from methanol. This step was repeated 3-4 times for purification.

REFERENCES

(1) Xia, Y.; Gates, B.; Yin, Y.; Lu, Y. Monodispersed Colloidal Spheres: Old Materials with New Applications. *Adv. Mater.* **2000,** *12*, 693-713.

(2) Liu, X.; Yang, Y.; Urban, M. W. Stimuli-Responsive Polymeric Nanoparticles. *Macromol. Rapid Commun.* **2017,** *38*, 1700030.

(3) Astruc, D.; Lu, F.; Aranzaes, J. R. Nanoparticles as Recyclable Catalysts: The Frontier between Homogeneous and Heterogeneous Catalysis. *Angew. Chem. Int. Ed.* **2005,** *44*, 7852-72.

(4) Li, B.; Huang, X.; Liang, L.; Tan, B. Synthesis of Uniform Microporous Polymer Nanoparticles and Their Applications for Hydrogen Storage. *J. Mater. Chem.* **2010,** *20*, 7444.

(5) Lee, S.; Jang, S.; Kim, K.; Jeon, J.; Kim, S. S.; Sohn, B. H. Branched and Crosslinked Supracolloidal Chains with Diblock Copolymer Micelles Having Three Well-Defined Patches. *Chem. Commun.* **2016,** *52*, 9430-3.

(6) Crucho, C. I. C.; Barros, M. T. Polymeric Nanoparticles: A Study on the Preparation Variables and Characterization Methods. *Mater. Sci. Eng., C* **2017,** *80*, 771-784.

(7) Kamaly, N.; Yameen, B.; Wu, J.; Farokhzad, O. C. Degradable Controlled-Release Polymers and Polymeric Nanoparticles: Mechanisms of Controlling Drug Release. *Chem. Rev.* **2016,** *116*, 2602-63.

(8) Zheng, Y.; Newland, B.; Tai, H.; Pandit, A.; Wang, W. Single Cyclized Molecule Structures from Raft Homopolymerization of Multi-Vinyl Monomers. *Chem. Commun.* **2012,** *48*, 3085-7.

(9) Gao, Y.; Zhou, D.; Zhao, T.; Wei, X.; McMahon, S.; O'Keeffe Ahern, J.; Wang, W.; Greiser, U.; Rodriguez, B. J.; Wang, W. Intramolecular Cyclization Dominating Homopolymerization of Multivinyl Monomers Toward Single-Chain Cyclized/Knotted Polymeric Nanoparticles. *Macromolecules* **2015,** *48*, 6882-6889.

(10) Gao, Y.; Newland, B.; Zhou, D.; Matyjaszewski, K.; Wang, W. Controlled Polymerization of Multivinyl Monomers: Formation of Cyclized/Knotted Single-Chain Polymer Architectures. *Angew. Chem. Int. Ed.* **2017,** *56*, 450-460.

(11) Lyu, J.; Gao, Y.; Zhang, Z.; Greiser, U.; Polanowski, P.; Jeszka, J. K.; Matyjaszewski, K.; Tai, H.; Wang, W. Monte Carlo Simulations of Atom Transfer Radical (Homo)Polymerization of Divinyl Monomers: Applicability of Flory–Stockmayer Theory. *Macromolecules* **2018,** *51*, 6673-6681.

(12) Huang, X.; Zhou, D.; A, S.; Gao, Y.; Wang, X.; Li, X.; Xu, Q.; Greiser, U.; Yin, G.; Wang, W. Star Polymers from Single-Chain Cyclized/Knotted Nanoparticles as a Core. *Macromol. Chem. Phys.* **2018,** *219*, 1700473.

(13) Chen, X.; Li, R.; Wong, S. H. D.; Wei, K.; Cui, M.; Chen, H.; Jiang, Y.; Yang, B.; Zhao, P.; Xu, J.; Chen, H.; Yin, C.; Lin, S.; Lee, W. Y.; Jing, Y.; Li, Z.; Yang, Z.; Xia, J.; Chen, G.; Li, G.;

Bian, L. Conformational Manipulation of Scale-up Prepared Single-Chain Polymeric Nanogels for Multiscale Regulation of Cells. *Nat. Commun.* **2019,** *10*, 2705.

(14) Frank, P.; Prasher, A.; Tuten, B.; Chao, D.; Berda, E. Characterization of Single-Chain Polymer Folding Using Size Exclusion Chromatography with Multiple Modes of Detection. *Appl. Petrochem. Res.* **2014,** *5*, 9-17.

(15) Lyon, C. K.; Prasher, A.; Hanlon, A. M.; Tuten, B. T.; Tooley, C. A.; Frank, P. G.; Berda, E. B. A Brief User's Guide to Single-Chain Nanoparticles. *Polym. Chem.* **2015,** *6*, 181-197.

(16) Hanlon, A. M.; Lyon, C. K.; Berda, E. B. What Is Next in Single-Chain Nanoparticles? *Macromolecules* **2015,** *49*, 2-14.

(17) Cole, J. P.; Hanlon, A. M.; Rodriguez, K. J.; Berda, E. B. Protein-Like Structure and Activity in Synthetic Polymers. *J. Polym. Sci., Part A: Polym. Chem.* **2017,** *55*, 191-206.

(18) Mavila, S.; Eivgi, O.; Berkovich, I.; Lemcoff, N. G. Intramolecular Cross-Linking Methodologies for the Synthesis of Polymer Nanoparticles. *Chem. Rev.* **2016,** *116*, 878-961.

(19) Kuhn, V. W.; Majer, H. Die Selbstvernetzung Von Fadenmolekülen. *Angew. Chem.* **1956,** *18*, 239-253.

(20) Kuhn, W.; Balmer, G. Crosslinking of Single Linear Macromolecules. *J. Polym. Sci.* **1962,** *57*, 311-319.

(21) Longi, P.; Greco, F.; Rossi, U. Polymers Containing Intra-Molecular Crosslinks. *Angew. Chem.* **1969,** *129*, 157-164.

(22) Martin, J. E.; Eichinger, B. E. Dimensions of Intramolecularly Crosslinked Polymers. 2. Dilute Solution Thermodynamic Parameters and Photon Correlation Results on the Polystyrene/Cyclopentane System. *Macromolecules* **1983,** *16*, 1350-1358.

(23) Antonietti, M. Microgels—Polymers with a Special Molecular Architecture. *Angew. Chem. Int. Ed.* **1988,** *100*, 1813-1817.

(24) Antonietti, M.; Sillescu, H.; Schmidt, M.; Schuch, H. Solution Properties and Dynamic Bulk Behavior of Intramolecular Cross-Linked Polystyrene. *Macromolecules* **1988,** *21*, 736-742.

(25) Pomposo, J. A. *Single-Chain Polymer Nanoparticles: Synthesis, Characterization, Simulations, and Applications*, John Wiley & Sons: 2017.

(26) Engelke, J.; Brandt, J.; Barner-Kowollik, C.; Lederer, A. Strengths and Limitations of Size Exclusion Chromatography for Investigating Single Chain Folding – Current Status and Future Perspectives. *Polym. Chem.* **2019,** *10*, 3410-3425.

(27) Steinkoenig, J.; Rothfuss, H.; Lauer, A.; Tuten, B. T.; Barner-Kowollik, C. Imaging Single-Chain Nanoparticle Folding Via High-Resolution Mass Spectrometry. *J. Am. Chem. Soc.* **2017,** *139*, 51-54.

(28) Blasco, E.; Tuten, B. T.; Frisch, H.; Lederer, A.; Barner-Kowollik, C. Characterizing Single Chain Nanoparticles (Scnps): A Critical Survey. *Polym. Chem.* **2017,** *8*, 5845-5851.

(29) Arbe, A.; Rubio-Cervilla, J.; Alegría, A.; Moreno, A. J.; Pomposo, J. A.; Robles-Hernández, B.; Malo de Molina, P.; Fouquet, P.; Juranyi, F.; Colmenero, J. Mesoscale Dynamics in Melts of Single-Chain Polymeric Nanoparticles. *Macromolecules* **2019,** *52*, 6935-6942.

(30) González-Burgos, M.; Arbe, A.; Moreno, A. J.; Pomposo, J. A.; Radulescu, A.; Colmenero, J. Crowding the Environment of Single-Chain Nanoparticles: A Combined Study by Sans and Simulations. *Macromolecules* **2018,** *51*, 1573-1585.

(31) Oberdisse, J.; González-Burgos, M.; Mendia, A.; Arbe, A.; Moreno, A. J.; Pomposo, J. A.; Radulescu, A.; Colmenero, J. Effect of Molecular Crowding on Conformation and Interactions of Single-Chain Nanoparticles. *Macromolecules* **2019,** *52*, 4295-4305.

(32) Lo Verso, F.; Pomposo, J. A.; Colmenero, J.; Moreno, A. J. Simulation Guided Design of Globular Single-Chain Nanoparticles by Tuning the Solvent Quality. *Soft Matter* **2015,** *11*, 1369-75.

(33) Hosono, N.; Kushner, A. M.; Chung, J.; Palmans, A. R.; Guan, Z.; Meijer, E. W. Forced Unfolding of Single-Chain Polymeric Nanoparticles. *J. Am. Chem. Soc.* **2015,** *137*, 6880-8.

(34) Li, Z.; Li, Y.; Zhao, Y.; Wang, H.; Zhang, Y.; Song, B.; Li, X.; Lu, S.; Hao, X. Q.; Hla, S. W.; Tu, Y.; Li, X. Synthesis of Metallopolymers and Direct Visualization of the Single Polymer Chain. *J. Am. Chem. Soc.* **2020,** *142*, 6196-6205.

(35) Huurne, G. M. t.; Palmans, A. R. A.; Meijer, E. W. Supramolecular Single-Chain Polymeric Nanoparticles. *CCS Chem.* **2019,** *1*, 64-82.

(36) Gonzalez-Burgos, M.; Latorre-Sanchez, A.; Pomposo, J. A. Advances in Single Chain Technology. *Chem. Soc. Rev.* **2015,** *44*, 6122-42.

(37) Kroger, A. P. P.; Paulusse, J. M. J. Single-Chain Polymer Nanoparticles in Controlled Drug Delivery and Targeted Imaging. *J. Controlled Release* **2018,** *286*, 326-347.

(38) Rothfuss, H.; Knofel, N. D.; Roesky, P. W.; Barner-Kowollik, C. Single-Chain Nanoparticles as Catalytic Nanoreactors. *J. Am. Chem. Soc.* **2018,** *140*, 5875-5881.

(39) Altintas, O.; Barner-Kowollik, C. Single Chain Folding of Synthetic Polymers by Covalent and Non-Covalent Interactions: Current Status and Future Perspectives. *Macromol. Rapid Commun.* **2012,** *33*, 958-71.

(40) Altintas, O.; Barner-Kowollik, C. Single-Chain Folding of Synthetic Polymers: A Critical Update. *Macromol. Rapid Commun.* **2016,** *37*, 29-46.

(41) Latorre-Sánchez, A.; Pomposo, J. A. Recent Bioinspired Applications of Single-Chain Nanoparticles. *Polym. Int.* **2016,** *65*, 855-860.

(42) Verde-Sesto, E.; Blazquez-Martin, A.; Pomposo, J. A. Advances in the Phototriggered Synthesis of Single-Chain Polymer Nanoparticles. *Polymers* **2019,** *11*, 1903.

(43) Laurent, B. A.; Grayson, S. M. An Efficient Route to Well-Defined Macrocyclic Polymers Via "Click" Cyclization. *J. Am. Chem. Soc.* **2006,** *128*, 4238-4239.

(44) Tezuka, Y.; Komiya, R. Metathesis Polymer Cyclization with Telechelic Poly(THF) Having Allyl Groups. *Macromolecules* **2002,** *35*, 8667-8669.

(45) Edwards, J. P.; Wolf, W. J.; Grubbs, R. H. The Synthesis of Cyclic Polymers by Olefin Metathesis: Achievements and Challenges. *J. Polym. Sci., Part A: Polym. Chem.* **2018,** *57*, 228-242.

(46) Konomoto, T.; Nakamura, K.; Yamamoto, T.; Tezuka, Y. Synthesis and Unimolecular Esa-Cf Polymer Cyclization of Zwitterionic Telechelic Precursors. *Macromolecules* **2019,** *52*, 9208-9219.

(47) Tezuka, Y. Cyclic and Topological Polymers: Ongoing Innovations and Upcoming Breakthroughs. *React. Funct. Polym.* **2020,** *148*, 104489.

(48) Kyoda, K.; Yamamoto, T.; Tezuka, Y. Programmed Polymer Folding with Periodically Positioned Tetrafunctional Telechelic Precursors by Cyclic Ammonium Salt Units as Nodal Points. *J. Am. Chem. Soc.* **2019,** *141*, 7526-7536.

(49) Martin, J. E.; Eichinger, B. Dimensions of Intramolecularly Crosslinked Polymers. 1. Theory. *Macromolecules* **1983,** *16*, 1345-1350.

(50) Mita, I.; Horie, K. Diffusion-Controlled Reactions in Polymer Systems. *Journal of Macromolecular Science-Reviews in Macromolecular Chemistry and Physics* **1987,** *27*, 91-169.

(51) Moreno, A. J.; Lo Verso, F.; Sanchez-Sanchez, A.; Arbe, A.; Colmenero, J.; Pomposo, J. A. Advantages of Orthogonal Folding of Single Polymer Chains to Soft Nanoparticles. *Macromolecules* **2013,** *46*, 9748-9759.

(52) Yin, Y.; Fei, Q.; Liu, W.; Li, Z.; Suga, H.; Wu, C. Chemical and Ribosomal Synthesis of Topologically Controlled Bicyclic and Tricyclic Peptide Scaffolds Primed by Selenoether Formation. *Angew. Chem. Int. Ed.* **2019,** *58*, 4880-4885.

(53) Richelle, G. J. J.; Ori, S.; Hiemstra, H.; van Maarseveen, J. H.; Timmerman, P. General and Facile Route to Isomerically Pure Tricyclic Peptides Based on Templated Tandem Clips/Cuaac Cyclizations. *Angew. Chem. Int. Ed.* **2018,** *57*, 501-505.

(54) Kale, S. S.; Villequey, C.; Kong, X. D.; Zorzi, A.; Deyle, K.; Heinis, C. Cyclization of Peptides with Two Chemical Bridges Affords Large Scaffold Diversities. *Nat. Chem.* **2018,** *10*, 715-723.

(55) Nishimura, S. N.; Higashi, N.; Koga, T. A Novel Thermo-Responsive Multiblock Architecture Composed of a Sequential Peptide and an Amino Acid-Derived Vinyl Polymer: Toward Protein-Mimicking Single-Chain Folding. *Chem. Commun.* **2019,** *55*, 1498-1501.

(56) Mes, T.; van der Weegen, R.; Palmans, A. R.; Meijer, E. W. Single-Chain Polymeric Nanoparticles by Stepwise Folding. *Angew. Chem. Int. Ed.* **2011,** *50*, 5085-9.

(57) Hosono, N.; Palmans, A. R.; Meijer, E. "Soldier–Sergeant–Soldier" Triblock Copolymers: Revealing the Folded Structure of Single-Chain Polymeric Nanoparticles. *Chem. Commun.* **2014,** *50*, 7990-7993.

(58) Hosono, N.; Gillissen, M. A.; Li, Y.; Sheiko, S. S.; Palmans, A. R.; Meijer, E. W. Orthogonal Self-Assembly in Folding Block Copolymers. *J. Am. Chem. Soc.* **2013,** *135*, 501-10.

(59) Altintas, O.; Artar, M. g.; ter Huurne, G.; Voets, I. K.; Palmans, A. R.; Barner-Kowollik, C.; Meijer, E. Design and Synthesis of Triblock Copolymers for Creating Complex Secondary Structures by Orthogonal Self-Assembly. *Macromolecules* **2015,** *48*, 8921-8932.

(60) Ter Huurne, G. M.; Voets, I. K.; Palmans, A. R. A.; Meijer, E. W. Effect of Intra- Versus Intermolecular Cross-Linking on the Supramolecular Folding of a Polymer Chain. *Macromolecules* **2018,** *51*, 8853-8861.

(61) Ogura, Y.; Artar, M. g.; Palmans, A. R.; Sawamoto, M.; Meijer, E.; Terashima, T. Self-Assembly of Hydrogen-Bonding Gradient Copolymers: Sequence Control Via Tandem Living Radical Polymerization with Transesterification. *Macromolecules* **2017,** *50*, 3215-3223.

(62) Ter Huurne, G. M.; de Windt, L. N. J.; Liu, Y.; Meijer, E. W.; Voets, I. K.; Palmans, A. R. A. Improving the Folding of Supramolecular Copolymers by Controlling the Assembly Pathway Complexity. *Macromolecules* **2017,** *50*, 8562-8569.

(63) Noll, D. M.; Mason, T. M.; Miller, P. S. Formation and Repair of Interstrand Cross-Links in DNA. *Chem. Rev.* **2006,** *106*, 277-301.

(64) Mavila, S.; Rozenberg, I.; Lemcoff, N. G. A General Approach to Mono- and Bimetallic Organometallic Nanoparticles. *Chem. Sci.* **2014,** *5*, 4196-4203.

(65) Zhang, Y.; Wang, W.; Fu, W.; Zhang, M.; Tang, Z.; Tan, R.; Yin, D. Titanium(Iv)-Folded Single-Chain Polymeric Nanoparticles as Artificial Metalloenzyme for Asymmetric Sulfoxidation in Water. *Chem. Commun.* **2018,** *54*, 9430-9433.

(66) Garmendia, S.; Lawrenson, S. B.; Arno, M. C.; O'Reilly, R. K.; Taton, D.; Dove, A. P. Catalytically Active N-Heterocyclic Carbene Release from Single-Chain Nanoparticles Following a Thermolysis-Driven Unfolding Strategy. *Macromol. Rapid Commun.* **2019,** *40*, e1900071.

(67) Lambert, R.; Wirotius, A.-L.; Garmendia, S.; Berto, P.; Vignolle, J.; Taton, D. Pd(II)–Nhc Coordination-Driven Formation of Water-Soluble Catalytically Active Single Chain Nanoparticles. *Polym. Chem.* **2018,** *9*, 3199-3204.

(68) Chen, J.; Wang, J.; Bai, Y.; Li, K.; Garcia, E. S.; Ferguson, A. L.; Zimmerman, S. C. Enzyme-Like Click Catalysis by a Copper-Containing Single-Chain Nanoparticle. *J. Am. Chem. Soc.* **2018,** *140*, 13695-13702.

(69) Thanneeru, S.; Duay, S. S.; Jin, L.; Fu, Y.; Angeles-Boza, A. M.; He, J. Single Chain Polymeric Nanoparticles to Promote Selective Hydroxylation Reactions of Phenol Catalyzed by Copper. *ACS Macro Lett.* **2017,** *6*, 652-656.

(70) Sanchez-Sanchez, A.; Arbe, A.; Colmenero, J.; Pomposo, J. A. Metallo-Folded Single-Chain Nanoparticles with Catalytic Selectivity. *ACS Macro Lett.* **2014,** *3*, 439-443.

(71) Liu, Y.; Turunen, P.; de Waal, B. F. M.; Blank, K. G.; Rowan, A. E.; Palmans, A. R. A.; Meijer, E. W. Catalytic Single-Chain Polymeric Nanoparticles at Work: From Ensemble Towards Single-Particle Kinetics. *Mol. Syst. Des. Eng.* **2018,** *3*, 609-618.

(72) Willenbacher, J.; Altintas, O.; Trouillet, V.; Knöfel, N.; Monteiro, M. J.; Roesky, P. W.; Barner-Kowollik, C. Pd-Complex Driven Formation of Single-Chain Nanoparticles. *Polym. Chem.* **2015,** *6*, 4358-4365.

(73) Knöfel, N. D.; Rothfuss, H.; Willenbacher, J.; Barner‐Kowollik, C.; Roesky, P. W. Platinum (Ii)‐Crosslinked Single‐Chain Nanoparticles: An Approach Towards Recyclable Homogeneous Catalysts. *Angew. Chem. Int. Ed.* **2017,** *56*, 4950-4954.

(74) Liu, Y.; Pujals, S.; Stals, P. J. M.; Paulohrl, T.; Presolski, S. I.; Meijer, E. W.; Albertazzi, L.; Palmans, A. R. A. Catalytically Active Single-Chain Polymeric Nanoparticles: Exploring Their Functions in Complex Biological Media. *J. Am. Chem. Soc.* **2018,** *140*, 3423-3433.

(75) Bai, Y.; Feng, X.; Xing, H.; Xu, Y.; Kim, B. K.; Baig, N.; Zhou, T.; Gewirth, A. A.; Lu, Y.; Oldfield, E. A Highly Efficient Single-Chain Metal–Organic Nanoparticle Catalyst for Alkyne–Azide "Click" Reactions in Water and in Cells. *J. Am. Chem. Soc.* **2016,** *138*, 11077-11080.

(76) Chen, J.; Li, K.; Shon, J. S. L.; Zimmerman, S. C. Single-Chain Nanoparticle Delivers a Partner Enzyme for Concurrent and Tandem Catalysis in Cells. *J. Am. Chem. Soc.* **2020,** *142*, 4565-4569.

(77) Liu, C. H.; Dugas, L. D.; Bowman, J. I.; Chidanguro, T.; Storey, R. F.; Simon, Y. C. Forcing Single-Chain Nanoparticle Collapse through Hydrophobic Solvent Interactions in Comb Copolymers. *Polym. Chem.* **2020,** *11*, 292-297.

(78) Frisch, H.; Kodura, D.; Bloesser, F. R.; Michalek, L.; Barner-Kowollik, C. Wavelength-Selective Folding of Single Polymer Chains with Different Colors of Visible Light. *Macromol. Rapid Commun.* **2020,** *41*, e1900414.

(79) Dashan, I.; Balta, D. K.; Temel, B. A.; Temel, G. Preparation of Single Chain Nanoparticles Via Photoinduced Double Collapse Process. *Macromol. Chem. Phys.* **2019,** *220*, 1900116.

(80) Chao, D.; Jia, X.; Tuten, B.; Wang, C.; Berda, E. B. Controlled Folding of a Novel Electroactive Polyolefin Via Multiple Sequential Orthogonal Intra-Chain Interactions. *Chem. Commun.* **2013,** *49*, 4178-80.

(81) Pomposo, J. A.; Perez-Baena, I.; Lo Verso, F.; Moreno, A. J.; Arbe, A.; Colmenero, J. How Far Are Single-Chain Polymer Nanoparticles in Solution from the Globular State? *ACS Macro Lett.* **2014,** *3*, 767-772.

(82) Formanek, M.; Moreno, A. J. Effects of Precursor Topology and Synthesis under Crowding Conditions on the Structure of Single-Chain Polymer Nanoparticles. *Soft Matter* **2017,** *13*, 6430-6438.

(83) Rubio-Cervilla, J.; Frisch, H.; Barner-Kowollik, C.; Pomposo, J. A. Synthesis of Single-Ring Nanoparticles Mimicking Natural Cyclotides by a Stepwise Folding-Activation-Collapse Process. *Macromol. Rapid Commun.* **2019,** *40*, e1800491.

(84) Chen, R.; Benware, S. J.; Cawthern, S. D.; Cole, J. P.; Lessard, J. J.; Crawford-Eng, I. M.; Saxena, R.; Berda, E. B. Assessing Structure/Property Relationships and Synthetic Protocols in the Fabrication of Poly(Oxanorbornene Imide) Single-Chain Nanoparticles. *Eur. Polym. J.* **2019,** *112*, 206-213.

(85) Stals, P. J. M.; Gillissen, M. A. J.; Paffen, T. F. E.; de Greef, T. F. A.; Lindner, P.; Meijer, E. W.; Palmans, A. R. A.; Voets, I. K. Folding Polymers with Pendant Hydrogen Bonding Motifs in Water: The Effect of Polymer Length and Concentration on the Shape and Size of Single-Chain Polymeric Nanoparticles. *Macromolecules* **2014,** *47*, 2947-2954.

(86) Huurne, G. M.; Vantomme, G.; Bersselaar, B. W. L.; Thota, B. N. S.; Voets, I. K.; Palmans, A. R. A.; Meijer, E. W. The Effect of Dendritic Pendants on the Folding of Amphiphilic Copolymers Via Supramolecular Interactions. *J. Polym. Sci., Part A: Polym. Chem.* **2018,** *57*, 411-421.

(87) Basasoro, S.; Gonzalez-Burgos, M.; Moreno, A. J.; Verso, F. L.; Arbe, A.; Colmenero, J.; Pomposo, J. A. A Solvent-Based Strategy for Tuning the Internal Structure of Metallo-Folded Single-Chain Nanoparticles. *Macromol. Rapid Commun.* **2016,** *37*, 1060-5.

(88) Terashima, T.; Sugita, T.; Fukae, K.; Sawamoto, M. Synthesis and Single-Chain Folding of Amphiphilic Random Copolymers in Water. *Macromolecules* **2014,** *47*, 589-600.

(89) Koda, Y.; Terashima, T.; Sawamoto, M. Multimode Self-Folding Polymers Via Reversible and Thermoresponsive Self-Assembly of Amphiphilic/Fluorous Random Copolymers. *Macromolecules* **2016,** *49*, 4534-4543.

(90) Mamusa, M.; Tempesti, P.; Bartolini, A.; Carretti, E.; Ghobadi, A. F.; Smets, J.; Aouad, Y. G.; Baglioni, P. Associative Properties of Poly(Ethylene Glycol)-Poly(Vinyl Acetate) Comb-Like Graft Copolymers in Water. *Nanoscale* **2019,** *11*, 6635-6643.

(91) Hirai, Y.; Terashima, T.; Takenaka, M.; Sawamoto, M. Precision Self-Assembly of Amphiphilic Random Copolymers into Uniform and Self-Sorting Nanocompartments in Water. *Macromolecules* **2016,** *49*, 5084-5091.

(92) Hattori, G.; Hirai, Y.; Sawamoto, M.; Terashima, T. Self-Assembly of PEG/Dodecyl-Graft Amphiphilic Copolymers in Water: Consequences of the Monomer Sequence and Chain Flexibility on Uniform Micelles. *Polym. Chem.* **2017,** *8*, 7248-7259.

(93) Shibata, M.; Matsumoto, M.; Hirai, Y.; Takenaka, M.; Sawamoto, M.; Terashima, T. Intramolecular Folding or Intermolecular Self-Assembly of Amphiphilic Random Copolymers: On-Demand Control by Pendant Design. *Macromolecules* **2018,** *51*, 3738-3745.

(94) Onbulak, S.; Rzayev, J. Synthesis and One-Dimensional Assembly of Cylindrical Polymer Nanoparticles Prepared from Tricomponent Bottlebrush Copolymers. *J. Polym. Sci., Part A: Polym. Chem.* **2017,** *55*, 3868-3874.

(95) Hokajo, T.; Terao, K.; Nakamura, Y.; Norisuye, T. Solution Properties of Polymacromonomers Consisting of Polystyrene V. Effect of Side Chain Length on Chain Stiffness. *Polym. J.* **2001,** *33*, 481-485.

(96) Lecommandoux, S.; Chécot, F.; Borsali, R.; Schappacher, M.; Deffieux, A.; Brûlet, A.; Cotton, J. P. Effect of Dense Grafting on the Backbone Conformation of Bottlebrush Polymers: Determination of the Persistence Length in Solution. *Macromolecules* **2002,** *35*, 8878-8881.

(97) Onbulak, S.; Rzayev, J. Cylindrical Nanocapsules from Photo-Cross-Linkable Core–Shell Bottlebrush Copolymers. *Polym. Chem.* **2015,** *6*, 764-771.

(98) Huang, K.; Johnson, M.; Rzayev, J. Synthesis of Degradable Organic Nanotubes by Bottlebrush Molecular Templating. *ACS Macro Lett.* **2012,** *1*, 892-895.

(99) Huang, K.; Rzayev, J. Charge and Size Selective Molecular Transport by Amphiphilic Organic Nanotubes. *J. Am. Chem. Soc.* **2011,** *133*, 16726-9.

(100) Huang, K.; Canterbury, D. P.; Rzayev, J. Organosoluble Polypyrrole Nanotubes from Core-Shell Bottlebrush Copolymers. *Chem. Commun.* **2010,** *46*, 6326-8.

(101) Huang, K.; Rzayev, J. Well-Defined Organic Nanotubes from Multicomponent Bottlebrush Copolymers. *J. Am. Chem. Soc.* **2009,** *131*, 6880-5.

(102) Van Renterghem, L. M.; Lammens, M.; Dervaux, B.; Viville, P.; Lazzaroni, R.; Du Prez, F. E. Design and Use of Organic Nanoparticles Prepared from Star-Shaped Polymers with Reactive End Groups. *J. Am. Chem. Soc.* **2008,** *130*, 10802-11.

(103) Ding, L.; Wang, C.; Jiang, R.; Wang, L.; Song, W. Preparation of Small and Photoresponsive Polymer Nanoparticles by Intramolecular Crosslinking of Reactive Star Azo-Polymers. *React. Funct. Polym.* **2016,** *109*, 56-63.

(104) Rodriguez, K. J.; Hanlon, A. M.; Lyon, C. K.; Cole, J. P.; Tuten, B. T.; Tooley, C. A.; Berda, E. B.; Pazicni, S. Porphyrin-Cored Polymer Nanoparticles: Macromolecular Models for Heme Iron Coordination. *Inorg. Chem.* **2016,** *55*, 9493-9496.

(105) Suzuki, T.; Yamamoto, T.; Tezuka, Y. Constructing a Macromolecular K(3,3) Graph through Electrostatic Self-Assembly and Covalent Fixation with a Dendritic Polymer Precursor. *J. Am. Chem. Soc.* **2014,** *136*, 10148-55.

(106) Thota, B. N.; Urner, L. H.; Haag, R. Supramolecular Architectures of Dendritic Amphiphiles in Water. *Chem. Rev.* **2016,** *116*, 2079-102.

(107) Zimmerman, S. C.; Wendland, M. S.; Rakow, N. A.; Zharov, I.; Suslick, K. S. Synthetic Hosts by Monomolecular Imprinting inside Dendrimers. *Nature* **2002,** *418*, 399-403.

(108) Lemcoff, N. G.; Spurlin, T. A.; Gewirth, A. A.; Zimmerman, S. C.; Beil, J. B.; Elmer, S. L.; Vandeveer, H. G. Organic Nanoparticles Whose Size and Rigidity Are Finely Tuned by Cross-Linking the End Groups of Dendrimers. *J. Am. Chem. Soc.* **2004,** *126*, 11420-1.

(109) Yang, S. K.; Zimmerman, S. C. Polyglycerol-Dendronized Perylenediimides as Stable, Water-Soluble Fluorophores. *Adv. Funct. Mater.* **2012,** *22*, 3023-3028.

(110) Li, Y.; Bai, Y.; Zheng, N.; Liu, Y.; Vincil, G. A.; Pedretti, B. J.; Cheng, J.; Zimmerman, S. C. Crosslinked Dendronized Polyols as a General Approach to Brighter and More Stable Fluorophores. *Chem. Commun.* **2016,** *52*, 3781-4.

(111) Asenjo-Sanz, I.; Verde-Sesto, E.; Pomposo, J. A. Valuable Structure-Size Relationships for Tadpole-Shaped Single-Chain Nanoparticles with Long and Short Flexible Tails Unveiled. *Phys. Chem. Chem. Phys.* **2019,** *21*, 10884-10887.

(112) Li, W.; Thanneeru, S.; Kanyo, I.; Liu, B.; He, J. Amphiphilic Hybrid Nano Building Blocks with Surfactant-Mimicking Structures. *ACS Macro Lett.* **2015,** *4*, 736-740.

(113) Zhou, F.; Xie, M.; Chen, D. Structure and Ultrasonic Sensitivity of the Superparticles Formed by Self-Assembly of Single Chain Janus Nanoparticles. *Macromolecules* **2013,** *47*, 365-372.

(114) Li, W.; Kuo, C.-H.; Kanyo, I.; Thanneeru, S.; He, J. Synthesis and Self-Assembly of Amphiphilic Hybrid Nano Building Blocks Via Self-Collapse of Polymer Single Chains. *Macromolecules* **2014,** *47*, 5932-5941.

(115) Zhang, Y.; Zhao, H. Surface-Tunable Colloidal Particles Stabilized by Mono-Tethered Single-Chain Nanoparticles. *Polymer* **2015,** *64*, 277-284.

(116) Wen, J.; Zhang, J.; Zhang, Y.; Yang, Y.; Zhao, H. Controlled Self-Assembly of Amphiphilic Monotailed Single-Chain Nanoparticles. *Polym. Chem.* **2014,** *5*, 4032.

(117) Wen, J.; Yuan, L.; Yang, Y.; Liu, L.; Zhao, H. Self-Assembly of Monotethered Single-Chain Nanoparticle Shape Amphiphiles. *ACS Macro Lett.* **2013,** *2*, 100-106.

(118) Zhang, J.; Tanaka, J.; Gurnani, P.; Wilson, P.; Hartlieb, M.; Perrier, S. Self-Assembly and Disassembly of Stimuli Responsive Tadpole-Like Single Chain Nanoparticles Using a Switchable Hydrophilic/Hydrophobic Boronic Acid Cross-Linker. *Polym. Chem.* **2017,** *8*, 4079-4087.

(119) Thanneeru, S.; Li, W.; He, J. Controllable Self-Assembly of Amphiphilic Tadpole-Shaped Polymer Single-Chain Nanoparticles Prepared through Intrachain Photo-Cross-Linking. *Langmuir* **2019,** *35*, 2619-2629.

(120) Wen, W.; Huang, T.; Guan, S.; Zhao, Y.; Chen, A. Self-Assembly of Single Chain Janus Nanoparticles with Tunable Liquid Crystalline Properties from Stilbene-Containing Block Copolymers. *Macromolecules* **2019,** *52*, 2956-2964.

(121) Frisch, H.; Bloesser, F. R.; Barner-Kowollik, C. Controlling Chain Coupling and Single-Chain Ligation by Two Colours of Visible Light. *Angew. Chem. Int. Ed.* **2019,** *58*, 3604-3609.

(122) Matsumoto, M.; Terashima, T.; Matsumoto, K.; Takenaka, M.; Sawamoto, M. Compartmentalization Technologies Via Self-Assembly and Cross-Linking of Amphiphilic Random Block Copolymers in Water. *J. Am. Chem. Soc.* **2017,** *139*, 7164-7167.

(123) Kozawa, S. K.; Matsumoto, K.; Suzuki, A.; Sawamoto, M.; Terashima, T. Self‐Assembly of Amphiphilic Aba Random Triblock Copolymers in Water. *J. Polym. Sci., Part A: Polym. Chem.* **2018,** *57*, 313-321.

(124) Claus, T. K.; Zhang, J.; Martin, L.; Hartlieb, M.; Mutlu, H.; Perrier, S.; Delaittre, G.; Barner-Kowollik, C. Stepwise Light-Induced Dual Compaction of Single-Chain Nanoparticles. *Macromol. Rapid Commun.* **2017,** *38*, 1700264.

(125) Cui, Z.; Cao, H.; Ding, Y.; Gao, P.; Lu, X.; Cai, Y. Compartmentalization of an Abc Triblock Copolymer Single-Chain Nanoparticle Via Coordination-Driven Orthogonal Self-Assembly. *Polym. Chem.* **2017,** *8*, 3755-3763.

(126) Cui, Z.; Huang, L.; Ding, Y.; Zhu, X.; Lu, X.; Cai, Y. Compartmentalization and Unidirectional Cross-Domain Molecule Shuttling of Organometallic Single-Chain Nanoparticles. *ACS Macro Lett.* **2018,** *7*, 572-575.

(127) Zhang, J.; Gody, G.; Hartlieb, M.; Catrouillet, S.; Moffat, J.; Perrier, S. Synthesis of Sequence-Controlled Multiblock Single Chain Nanoparticles by a Stepwise Folding–Chain Extension–Folding Process. *Macromolecules* **2016,** *49*, 8933-8942.

(128) Ji, X.; Zhang, Y.; Zhao, H. Amphiphilic Janus Twin Single-Chain Nanoparticles. *Chem. Eur. J.* **2018,** *24*, 3005-3012.

(129) Jiang, L.; Xie, M.; Dou, J.; Li, H.; Huang, X.; Chen, D. Efficient Fabrication of Pure, Single-Chain Janus Particles through Their Exclusive Self-Assembly in Mixtures with Their Analogues. *ACS Macro Lett.* **2018,** *7*, 1278-1282.

(130) Xiang, D.; Jiang, B.; Liang, F.; Yan, L.; Yang, Z. Single-Chain Janus Nanoparticle by Metallic Complexation. *Macromolecules* **2020,** *53*, 1063-1069.

(131) Xiang, D.; Chen, X.; Tang, L.; Jiang, B.; Yang, Z. Electrostatic-Mediated Intramolecular Cross-Linking Polymers in Concentrated Solutions. *CCS Chem.* **2019,** *1*, 407-430.

(132) Harth, E.; Van Horn, B.; Lee, V. Y.; Germack, D. S.; Gonzales, C. P.; Miller, R. D.; Hawker, C. J. A Facile Approach to Architecturally Defined Nanoparticles via Intramolecular Chain Collapse. *J. Am. Chem. Soc.* **2002,** *124*, 8653-60.

(133) Schultz, L. G.; Zhao, Y.; Zimmerman, S. C. Synthesis of Cored Dendrimers with Internal Cross-Links. *Angew. Chem. Int. Ed.* **2001,** *40*, 1962-1966.

(134) Gröschel, A. H.; Schacher, F. H.; Schmalz, H.; Borisov, O. V.; Zhulina, E. B.; Walther, A.; Müller, A. H. E. Precise Hierarchical Self-Assembly of Multicompartment Micelles. *Nat. Commun.* **2012,** *3*, 710.

(135) Dobson, C. M. Protein Folding and Misfolding. *Nature* **2003,** *426*, 884-90.

(136) Treat, N. J.; Sprafke, H.; Kramer, J. W.; Clark, P. G.; Barton, B. E.; Read de Alaniz, J.; Fors, B. P.; Hawker, C. J. Metal-Free Atom Transfer Radical Polymerization. *J. Am. Chem. Soc.* **2014,** *136*, 16096-101.

(137) Chen, M.; Zhong, M.; Johnson, J. A. Light-Controlled Radical Polymerization: Mechanisms, Methods, and Applications. *Chem. Rev.* **2016,** *116*, 10167-211.

(138) Asandei, A. D. Photomediated Controlled Radical Polymerization and Block Copolymerization of Vinylidene Fluoride. *Chem. Rev.* **2016,** *116*, 2244-74.

(139) Wang, S.; Chao, D.; Berda, E. B.; Jia, X.; Yang, R.; Wang, X.; Jiang, T.; Wang, C. Fabrication of Electroactive Oligoaniline Functionalized Poly(Amic Acid) Nanofibers for Application as an Ammonia Sensor. *RSC Adv.* **2013,** *3*, 4059.

(140) Garmendia, S.; Dove, A. P.; Taton, D.; O'Reilly, R. K. Reversible Ionically-Crosslinked Single Chain Nanoparticles as Bioinspired and Recyclable Nanoreactors for N-Heterocyclic Carbene Organocatalysis. *Polym. Chem.* **2018,** *9*, 5286-5294.

(141) Perez-Baena, I.; Loinaz, I.; Padro, D.; García, I.; Grande, H. J.; Odriozola, I. Single-Chain Polyacrylic Nanoparticles with Multiple Gd(Iii) Centres as Potential Mri Contrast Agents. *J. Mater. Chem.* **2010,** *20*, 6916.

(142) Sanchez-Sanchez, A.; Akbari, S.; Etxeberria, A.; Arbe, A.; Gasser, U.; Moreno, A. J.; Colmenero, J.; Pomposo, J. A. "Michael" Nanocarriers Mimicking Transient-Binding Disordered Proteins. *ACS Macro Lett.* **2013,** *2*, 491-495.

(143) He, J.; Tremblay, L.; Lacelle, S.; Zhao, Y. Preparation of Polymer Single Chain Nanoparticles Using Intramolecular Photodimerization of Coumarin. *Soft Matter* **2011,** *7*, 2380.

(144) Fan, W.; Tong, X.; Farnia, F.; Yu, B.; Zhao, Y. CO_2-Responsive Polymer Single-Chain Nanoparticles and Self-Assembly for Gas-Tunable Nanoreactors. *Chem. Mater.* **2017,** *29*, 5693-5701.

(145) Gillissen, M. A. J.; Voets, I. K.; Meijer, E. W.; Palmans, A. R. A. Single Chain Polymeric Nanoparticles as Compartmentalised Sensors for Metal Ions. *Polym. Chem.* **2012,** *3*, 3166.

(146) Tuten, B. T.; Bloesser, F. R.; Marshall, D. L.; Michalek, L.; Schmitt, C. W.; Blanksby, S. J.; Barner-Kowollik, C. Polyselenoureas Via Multicomponent Polymerizations Using Elemental Selenium as Monomer. *ACS Macro Lett.* **2018,** *7*, 898-903.

(147) Hanlon, A. M.; Chen, R.; Rodriguez, K. J.; Willis, C.; Dickinson, J. G.; Cashman, M.; Berda, E. B. Scalable Synthesis of Single-Chain Nanoparticles under Mild Conditions. *Macromolecules* **2017,** *50*, 2996-3003.

(148) Cole, J. P.; Lessard, J. J.; Rodriguez, K. J.; Hanlon, A. M.; Reville, E. K.; Mancinelli, J. P.; Berda, E. B. Single-Chain Nanoparticles Containing Sequence-Defined Segments: Using Primary Structure Control to Promote Secondary and Tertiary Structures in Synthetic Protein Mimics. *Polym. Chem.* **2017,** *8*, 5829-5835.

(149) Lyon, C. K.; Hill, E. O.; Berda, E. B. Zipping Polymers into Nanoparticles via Intrachain Alternating Radical Copolymerization. *Macromol. Chem. Phys.* **2016,** *217*, 501-508.

(150) Prasher, A.; Loynd, C. M.; Tuten, B. T.; Frank, P. G.; Chao, D.; Berda, E. B. Efficient Fabrication of Polymer Nanoparticles Via Sonogashira Cross-Linking of Linear Polymers in Dilute Solution. *J. Polym. Sci., Part A: Polym. Chem.* **2016,** *54*, 209-217.

(151) Hanlon, A. M.; Martin, I.; Bright, E. R.; Chouinard, J.; Rodriguez, K. J.; Patenotte, G. E.; Berda, E. B. Exploring Structural Effects in Single-Chain "Folding" Mediated by Intramolecular Thermal Diels–Alder Chemistry. *Polym. Chem.* **2017,** *8*, 5120-5128.

(152) Berkovich, I.; Mavila, S.; Iliashevsky, O.; Kozuch, S.; Lemcoff, N. G. Single-Chain Polybutadiene Organometallic Nanoparticles: An Experimental and Theoretical Study. *Chem. Sci.* **2016,** *7*, 1773-1778.

(153) Mecerreyes, D.; Lee, V.; Hawker, C. J.; Hedrick, J. L.; Wursch, A.; Volksen, W.; Magbitang, T.; Huang, E.; Miller, R. D. A Novel Approach to Functionalized Nanoparticles: Self-Crosslinking of Macromolecules in Ultradilute Solution. *Adv. Mater.* **2001,** *13*, 204-208.

(154) Jiang, J.; Thayumanavan, S. Synthesis and Characterization of Amine-Functionalized Polystyrene Nanoparticles. *Macromolecules* **2005,** *38*, 5886-5891.

(155) Dirlam, P. T.; Kim, H. J.; Arrington, K. J.; Chung, W. J.; Sahoo, R.; Hill, L. J.; Costanzo, P. J.; Theato, P.; Char, K.; Pyun, J. Single Chain Polymer Nanoparticles via Sequential Atrp and Oxidative Polymerization. *Polym. Chem.* **2013,** *4*, 3765.

(156) Zhou, Y.; Qu, Y.; Yu, Q.; Chen, H.; Zhang, Z.; Zhu, X. Controlled Synthesis of Diverse Single-Chain Polymeric Nanoparticles Using Polymers Bearing Furan-Protected Maleimide Moieties. *Polym. Chem.* **2018,** *9*, 3238-3247.

(157) Cole, J. P.; Lessard, J. J.; Lyon, C. K.; Tuten, B. T.; Berda, E. B. Intra-Chain Radical Chemistry as a Route to Poly(Norbornene Imide) Single-Chain Nanoparticles: Structural Considerations and the Role of Adventitious Oxygen. *Polym. Chem.* **2015,** *6*, 5555-5559.

(158) Chatterjee, A. K.; Morgan, J. P.; Scholl, M.; Grubbs, R. H. Synthesis of Functionalized Olefins by Cross and Ring-Closing Metatheses. *J. Am. Chem. Soc.* **2000,** *122*, 3783-3784.

(159) Binder, W. H.; Kluger, C. Combining Ring-Opening Metathesis Polymerization (ROMP) with Sharpless-Type "Click" Reactions: An Easy Method for the Preparation of Side Chain Functionalized Poly (Oxynorbornenes). *Macromolecules* **2004,** *37*, 9321-9330.

(160) D'Annibale, A.; Ciaralli, L.; Bassetti, M.; Pasquini, C. Synthesis of Alkyl-Substituted Six-Membered Lactones through Ring-Closing Metathesis of Homoallyl Acrylates. An Easy Route to Pyran-2-ones, Constituents of Tobacco Flavor. *J. Org. Chem.* **2007,** *72*, 6067-6074.

(161) Bilel, H.; Hamdi, N.; Zagrouba, F.; Fischmeister, C.; Bruneau, C. Cross-Metathesis Transformations of Terpenoids in Dialkyl Carbonate Solvents. *Green Chemistry* **2011,** *13*, 1448-1452.

(162) Tuten, B. T.; Chao, D.; Lyon, C. K.; Berda, E. B. Single-Chain Polymer Nanoparticles via Reversible Disulfide Bridges. *Polym. Chem.* **2012,** *3*, 3068.

(163) Kroger, A. P. P.; Hamelmann, N. M.; Juan, A.; Lindhoud, S.; Paulusse, J. M. J. Biocompatible Single-Chain Polymer Nanoparticles for Drug Delivery-a Dual Approach. *ACS Appl. Mater. Interfaces* **2018,** *10*, 30946-30951.

(164) Gandhi, A.; Paul, A.; Sen, S. O.; Sen, K. K. Studies on Thermoresponsive Polymers: Phase Behaviour, Drug Delivery and Biomedical Applications. *Asian J. Pharm.* **2015,** *10*, 99-107.

(165) Lee, L.-C.; Lu, J.; Weck, M.; Jones, C. W. Acid–Base Bifunctional Shell Cross-Linked Micelle Nanoreactor for One-Pot Tandem Reaction. *ACS Catal.* **2016,** *6*, 784-787.

(166) Lu, A.; O'Reilly, R. K. Advances in Nanoreactor Technology Using Polymeric Nanostructures. *Curr. Opin. Biotechnol.* **2013,** *24*, 639-45.

(167) Zhang, P.; Sundberg, D. C.; Tsavalas, J. G. Polymerization Induced Phase Separation in Composite Latex Particles During Seeded Emulsion Polymerization. *Ind. Eng. Chem. Res.* **2019,** *58*, 21118-21129.

(168) Utama, R. H.; Drechsler, M.; Förster, S.; Zetterlund, P. B.; Stenzel, M. H. Synthesis of Ph-Responsive Nanocapsules Via Inverse Miniemulsion Periphery Raft Polymerization and Post-Polymerization Reaction. *ACS Macro Lett.* **2014,** *3*, 935-939.

(169) Hattori, G.; Takenaka, M.; Sawamoto, M.; Terashima, T. Nanostructured Materials Via the Pendant Self-Assembly of Amphiphilic Crystalline Random Copolymers. *J. Am. Chem. Soc.* **2018,** *140*, 8376-8379.

(170) Alaboalirat, M.; Qi, L.; Arrington, K. J.; Qian, S.; Keum, J. K.; Mei, H.; Littrell, K. C.; Sumpter, B. G.; Carrillo, J.-M. Y.; Verduzco, R.; Matson, J. B. Amphiphilic Bottlebrush Block Copolymers: Analysis of Aqueous Self-Assembly by Small-Angle Neutron Scattering and Surface Tension Measurements. *Macromolecules* **2018,** *52*, 465-476.

(171) Gratton, S. E.; Williams, S. S.; Napier, M. E.; Pohlhaus, P. D.; Zhou, Z.; Wiles, K. B.; Maynor, B. W.; Shen, C.; Olafsen, T.; Samulski, E. T.; Desimone, J. M. The Pursuit of a Scalable Nanofabrication Platform for Use in Material and Life Science Applications. *Acc. Chem. Res.* **2008,** *41*, 1685-95.

(172) Perry, J. L.; Herlihy, K. P.; Napier, M. E.; Desimone, J. M. Print: A Novel Platform toward Shape and Size Specific Nanoparticle Theranostics. *Acc. Chem. Res.* **2011,** *44*, 990-8.

(173) Wong, E. H. H.; Qiao, G. G. Factors Influencing the Formation of Single-Chain Polymeric Nanoparticles Prepared via Ring-Opening Polymerization. *Macromolecules* **2015,** *48*, 1371-1379.

(174) Wong, E. H. H.; Lam, S. J.; Nam, E.; Qiao, G. G. Biocompatible Single-Chain Polymeric Nanoparticles via Organo-Catalyzed Ring-Opening Polymerization. *ACS Macro Lett.* **2014,** *3*, 524-528.

(175) Perez-Baena, I.; Barroso-Bujans, F.; Gasser, U.; Arbe, A.; Moreno, A. J.; Colmenero, J.; Pomposo, J. A. Endowing Single-Chain Polymer Nanoparticles with Enzyme-Mimetic Activity. *ACS Macro Lett.* **2013,** *2*, 775-779.

(176) Ke, Y.; Ji, R.; Wei, T.; Lee, S.; Huang, S.; Huang, M.; Chen, C.; Luh, T. Well-Defined Condensation Polymers with Narrow Polydispersity via Unsymmetrical Ladderphanes by Sequential Polymerization. *Macromolecules* **2013,** *46*, 6712-6722.

(177) Zhou, Z.; Palermo, E. F. Templated Ring-Opening Metathesis (TROM) of Cyclic Olefins Tethered to Unimolecular Oligo(Thiophene)S. *Macromolecules* **2018,** *51*, 6127-6137.

(178) Połowiński, S. Template Polymerisation and Co-Polymerisation. *Prog. Polym. Sci.* **2002,** *27*, 537-577.

(179) Ames, D. E.; Grey, T. F. The Synthesis of Some N-hydroxyimides. *J. Chem. Soc.* **1955,** 631.

(180) Akiyama, M.; Shimizu, K.; Aiba, S.; Banba, F. Synthesis of N-hydroxymaleimide and N-hydroxyitaconimide and Their Related Derivatives. *J. Chem. Soc., Perkin Trans. 1* **1980,** 2122.

(181) Sati, G. C.; Crich, D. Facile Synthesis of 3-N-Alkyl Pyrimidin-2,4-Diones from N-Sulfonyloxy Maleimides and Amines. *Org. Lett.* **2015,** *17*, 4122-4.

(182) Li, Y.; Zhang, J.; Li, D.; Chen, Y. Metal-Free C(Sp(3))-H Allylation via Aryl Carboxyl Radicals Enabled by Donor-Acceptor Complex. *Org. Lett.* **2018,** *20*, 3296-3299.

(183) Inomata, T.; Eguchi, H.; Funahashi, Y.; Ozawa, T.; Masuda, H. Adsorption Behavior of Microbes on a Qcm Chip Modified with an Artificial Siderophore-Fe^{3+} Complex. *Langmuir* **2012,** *28*, 1611-7.

(184) More, S. S.; Vince, R. Design, Synthesis and Biological Evaluation of Glutathione Peptidomimetics as Components of Anti-Parkinson Prodrugs. *J. Med. Chem.* **2008,** *51*, 4581-8.

(185) Shiner, V.; Martin, B. The Mechanism of Decarboxylation of Glycidic Acids. *J. Am. Chem. Soc.* **1962,** *84*, 4824-4827.

(186) Jiang, Y.; Liang, M.; Svejkar, D.; Hart-Smith, G.; Lu, H.; Scarano, W.; Stenzel, M. H. Albumin-Micelles Via a One-Pot Technology Platform for the Delivery of Drugs. *Chem. Commun.* **2014,** *50*, 6394-7.

(187) Jiang, Y.; Wong, S.; Chen, F.; Chang, T.; Lu, H.; Stenzel, M. H. Influencing Selectivity to Cancer Cells with Mixed Nanoparticles Prepared from Albumin–Polymer Conjugates and Block Copolymers. *Bioconjugate Chem.* **2017,** *28*, 979-985.

(188) Samanta, S. R.; Cai, R.; Percec, V. A Rational Approach to Activated Polyacrylates and Polymethacrylates by Using a Combination of Model Reactions and SET-LRP of Hexafluoroisopropyl Acrylate and Methacrylate. *Polym. Chem.* **2015,** *6*, 3259-3270.

(189) Jochum, F. D.; Theato, P. Thermo- and Light Responsive Micellation of Azobenzene Containing Block Copolymers. *Chem. Commun.* **2010,** *46*, 6717-9.

(190) Cubbon, R. The Free Radical and Anionic Polymerization of Some N-Substituted Maleimides. *Polymer* **1965,** *6*, 419-426.

(191) Onimura, K.; Tsutsumi, H.; Oishi, T. Asymmetric Anionic Polymerization of N-Substituted Maleimides with Et_2Zn and Chiral Bisoxazolines. *Chem. Lett.* **1998,** *27*, 791-792.

(192) Hagiwara, T.; Someno, T.; Hamana, H.; Narita, T. Anionic Polymerization of N‐Substituted Maleimide. Ii. Polymerization of N‐Ethylmaleimide. *J. Polym. Sci., Part A: Polym. Chem.* **1988,** *26*, 1011-1020.

(193) Hagiwara, T.; Shimizu, T.; Someno, T.; Yamagishi, T.; Hamana, H.; Narita, T. Anionic Polymerization of N-Substituted Maleimide. 4." Living" Characteristics of Anionic Polymerization of N-Phenylmaleimide. *Macromolecules* **1988,** *21*, 3324-3327.

(194) Azechi, M.; Toyota, N.; Yamabuki, K.; Onimura, K.; Oishi, T. Anionic Polymerization of N-Substituted Maleimide with Achiral and Chiral Amines as an Initiator. *Polym. Bull.* **2011,** *67*, 631-640.

(195) Yoshida, Y.; Endo, T. Synthesis and Thermal Properties of Vinyl Copolymers with Phenyl Vinylethylene Carbonate and N-Substituted Maleimides Undergoing Color Change with Acid–Base Switching. *Polym. Chem.* **2016,** *7*, 6770-6778.

(196) Yoshida, Y.; Endo, T. Color Change of Alternating Copolymers with Phenyl Vinylethylene Carbonate and N-Phenylmaleimide in a Solution and in the Solid-State, Depending on Their Structure. *RSC Adv.* **2017,** *7*, 9373-9380.

(197) Haas, H. C.; MacDonald, R. L. Maleimide Polymers. I. A Polymeric Color Reaction. *J. Polym. Sci., Part A: Polym. Chem.* **1973,** *11*, 327-343.

(198) Labbé, A. l.; Brocas, A.-L.; Ibarboure, E.; Ishizone, T.; Hirao, A.; Deffieux, A.; Carlotti, S. p. Selective Ring-Opening Polymerization of Glycidyl Methacrylate: Toward the Synthesis of Cross-Linked (Co)Polyethers with Thermoresponsive Properties. *Macromolecules* **2011,** *44*, 6356-6364.

(199) Billouard, C.; Carlotti, S.; Desbois, P.; Deffieux, A. “Controlled” High-Speed Anionic Polymerization of Propylene Oxide Initiated by Alkali Metal Alkoxide/Trialkylaluminum Systems. *Macromolecules* **2004,** *37*, 4038-4043.

(200) Herzberger, J.; Niederer, K.; Pohlit, H.; Seiwert, J.; Worm, M.; Wurm, F. R.; Frey, H. Polymerization of Ethylene Oxide, Propylene Oxide, and Other Alkylene Oxides: Synthesis, Novel Polymer Architectures, and Bioconjugation. *Chem. Rev.* **2016,** *116*, 2170-243.

(201) Carlotti, S. p.; Labbé, A. l.; Rejsek, V.; Doutaz, S. p.; Gervais, M.; Deffieux, A. Living/Controlled Anionic Polymerization and Copolymerization of Epichlorohydrin with Tetraoctylammonium Bromide−Triisobutylaluminum Initiating Systems. *Macromolecules* **2008,** *41*, 7058-7062.

(202) Rejsek, V.; Sauvanier, D.; Billouard, C.; Desbois, P.; Deffieux, A.; Carlotti, S. Controlled Anionic Homo- and Copolymerization of Ethylene Oxide and Propylene Oxide by Monomer Activation. *Macromolecules* **2007,** *40*, 6510-6514.

(203) Roos, K.; Dolci, E.; Carlotti, S.; Caillol, S. Activated Anionic Ring-Opening Polymerization for the Synthesis of Reversibly Cross-Linkable Poly(Propylene Oxide) Based on Furan/Maleimide Chemistry. *Polym. Chem.* **2016,** *7*, 1612-1622.

(204) Herzberger, J.; Leibig, D.; Langhanki, J.; Moers, C.; Opatz, T.; Frey, H. "Clickable PEG" via Anionic Copolymerization of Ethylene Oxide and Glycidyl Propargyl Ether. *Polym. Chem.* **2017,** *8*, 1882-1887.

(205) Gervais, M.; Brocas, A.-L.; Cendejas, G.; Deffieux, A.; Carlotti, S. Synthesis of Linear High Molar Mass Glycidol-Based Polymers by Monomer-Activated Anionic Polymerization. *Macromolecules* **2010,** *43*, 1778-1784.

(206) Müller, S. S.; Moers, C.; Frey, H. A Challenging Comonomer Pair: Copolymerization of Ethylene Oxide and Glycidyl Methyl Ether to Thermoresponsive Polyethers. *Macromolecules* **2014,** *47*, 5492-5500.

(207) Ying, Q.; Chu, B. Overlap Concentration of Macromolecules in Solution. *Macromolecules* **1987,** *20*, 362-366.

(208) Mardles, E. W. J. Viscosity of Suspensions and the Einstein Equation. *Nature* **1940,** *145*, 970-970.

(209) Das, A.; Theato, P. Multifaceted Synthetic Route to Functional Polyacrylates by Transesterification of Poly(Pentafluorophenyl Acrylates). *Macromolecules* **2015,** *48*, 8695-8707.

(210) Koch, A. S.; Feng, A. S.; Hopkins, T. A.; Streitwieser, A. Nucleophilic Reactions of Pyridines and Imidazoles with Vinyl and Aromatic Halides. *J. Org. Chem.* **1993,** *58*, 1409-1414.

(211) Weiss, R.; Pomrehn, B.; Hampel, F.; Bauer, W. First‐Ever Per (Onio) Substitution of Benzene: The Role of the Counterion. *Angew. Chem. Int. Ed.* **1995,** *34*, 1319-1321.

(212) Pühlhofer, F. G.; Weiss, R. Sasapos Cascades of Perfluorinated Aromatic Carboxylic Acids: Low‐Temperature Decarboxylation Triggered by Electrostatic Effects of Polycationic Ligand Sets. *Eur. J. Org. Chem.* **2004,** *2004*, 1002-1007.

(213) Tuten, B. T. Modular and Dynamic Approaches to the Formation of Single-Chain Polymer Nanoparticles. **2016,** Doctoral Dissertations. 2242. University of New Hampshire.

(214) Rost, D.; Porta, M.; Gessler, S.; Blechert, S. A Hexafluorobenzene Promoted Ring-Closing Metathesis to Form Tetrasubstituted Olefins. *Tetrahedron Lett.* **2008,** *49*, 5968-5971.

(215) Grandbois, A.; Collins, S. K. Enantioselective Synthesis of [7]Helicene: Dramatic Effects of Olefin Additives and Aromatic Solvents in Asymmetric Olefin Metathesis. *Chem. Eur. J.* **2008,** *14*, 9323-9.

(216) Liu, F.; Long, Y.; Zhao, Q.; Liu, X.; Qiu, G.; Zhang, L.; Ling, Q.; Gu, H. Gallol-Containing Homopolymers and Block Copolymers: Romp Synthesis and Gelation Properties by Metal-Coordination and Oxidation. *Polymer* **2018,** *143*, 212-227.

(217) Love, J. A.; Morgan, J. P.; Trnka, T. M.; Grubbs, R. H. A Practical and Highly Active Ruthenium-Based Catalyst That Effects the Cross Metathesis of Acrylonitrile. *Angew. Chem. Int. Ed.* **2002,** *41*, 4035-4037.

APPENDIX

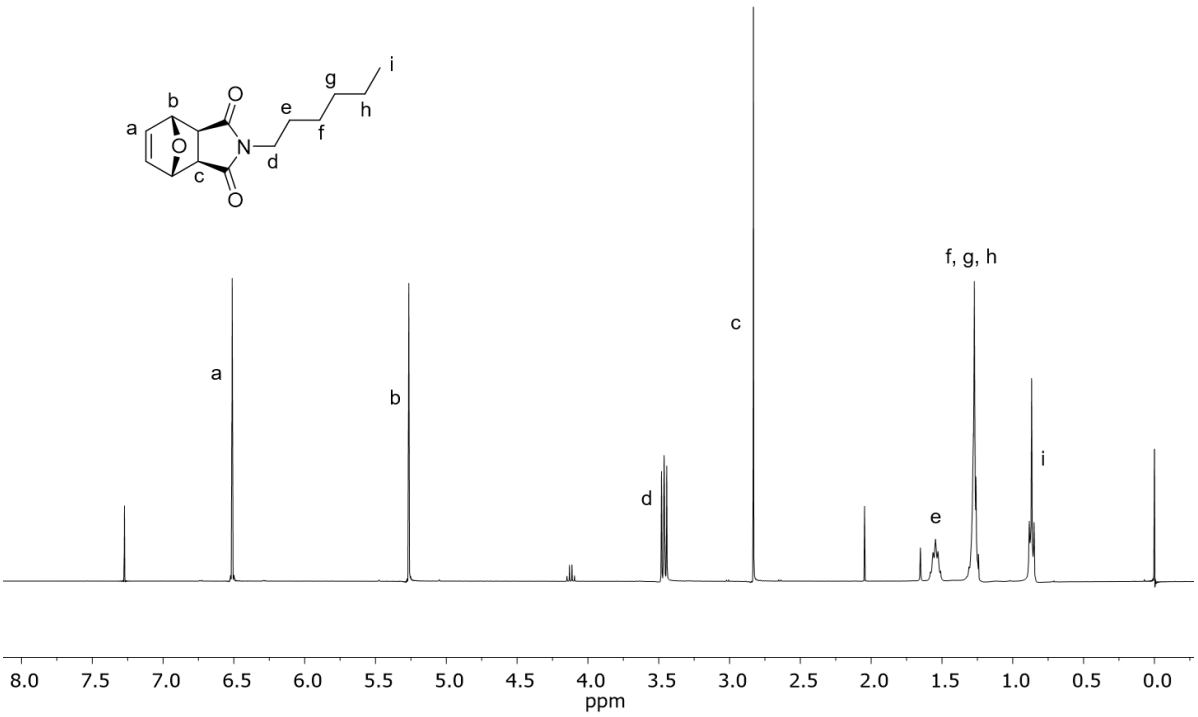

*Figure A 1. ^{1}H NMR spectrum of **M1**.*

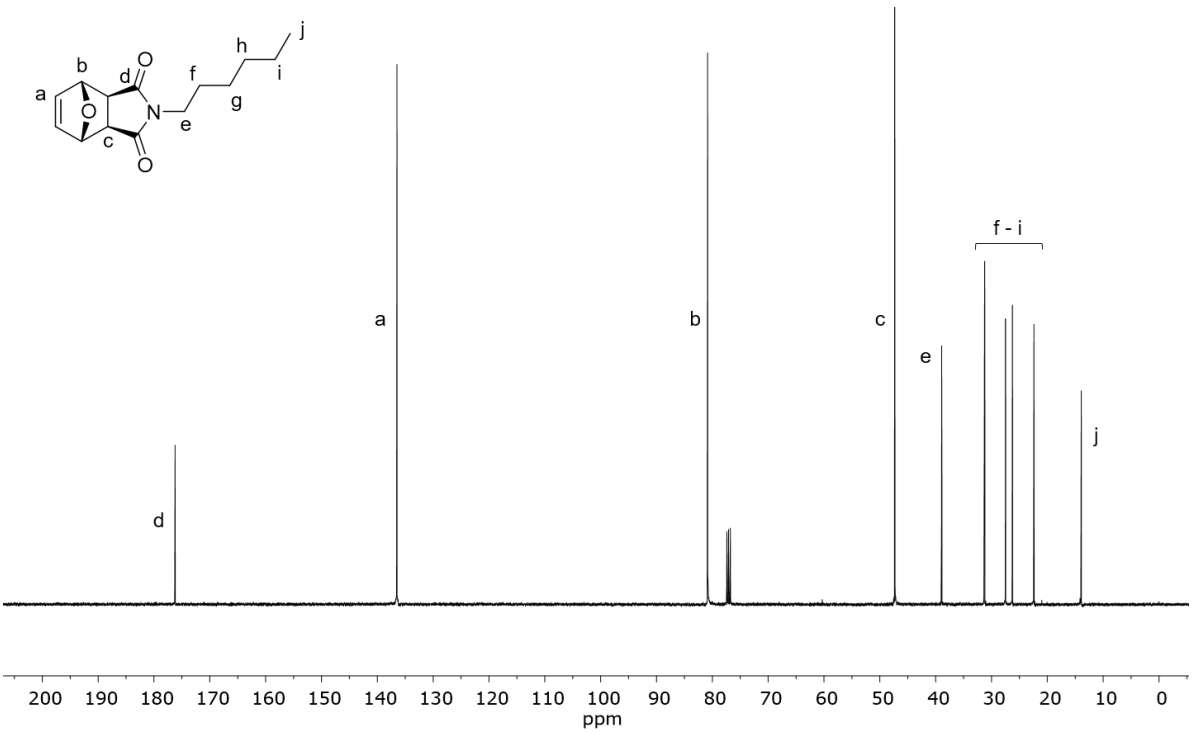

*Figure A 2. ^{13}C NMR spectrum of **M1**.*

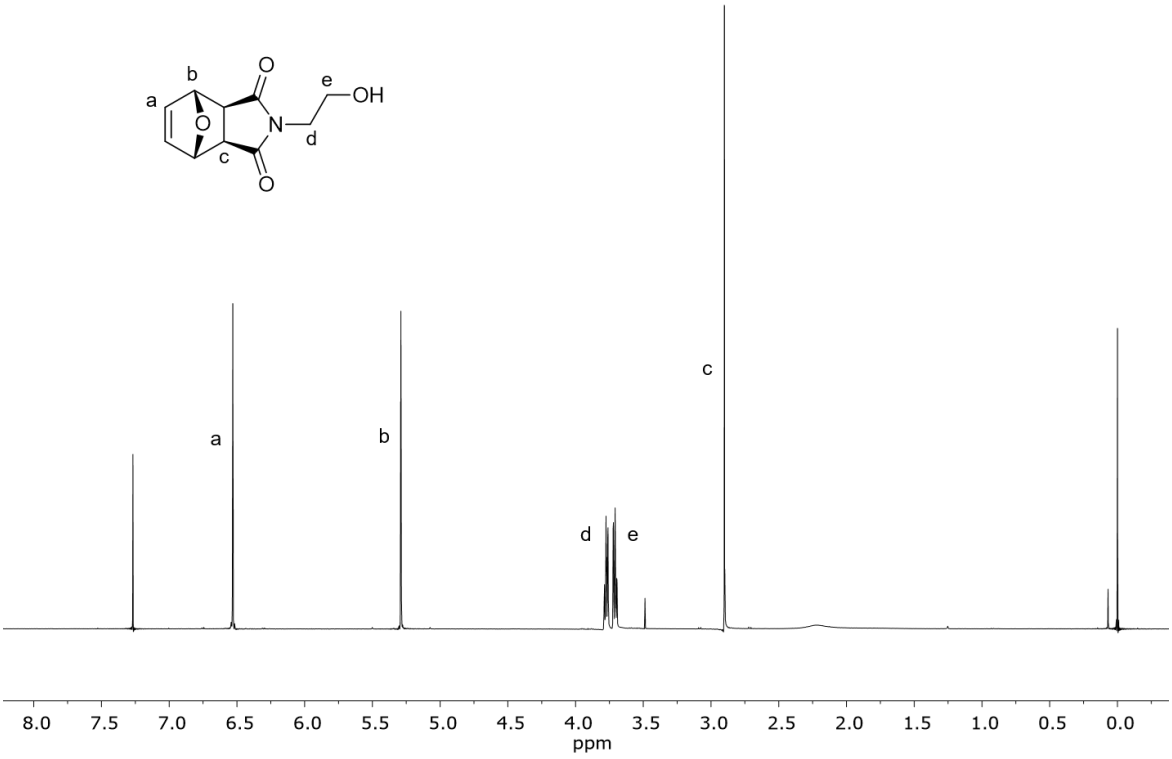

*Figure A 3. [1]H NMR spectrum of **M2-0***

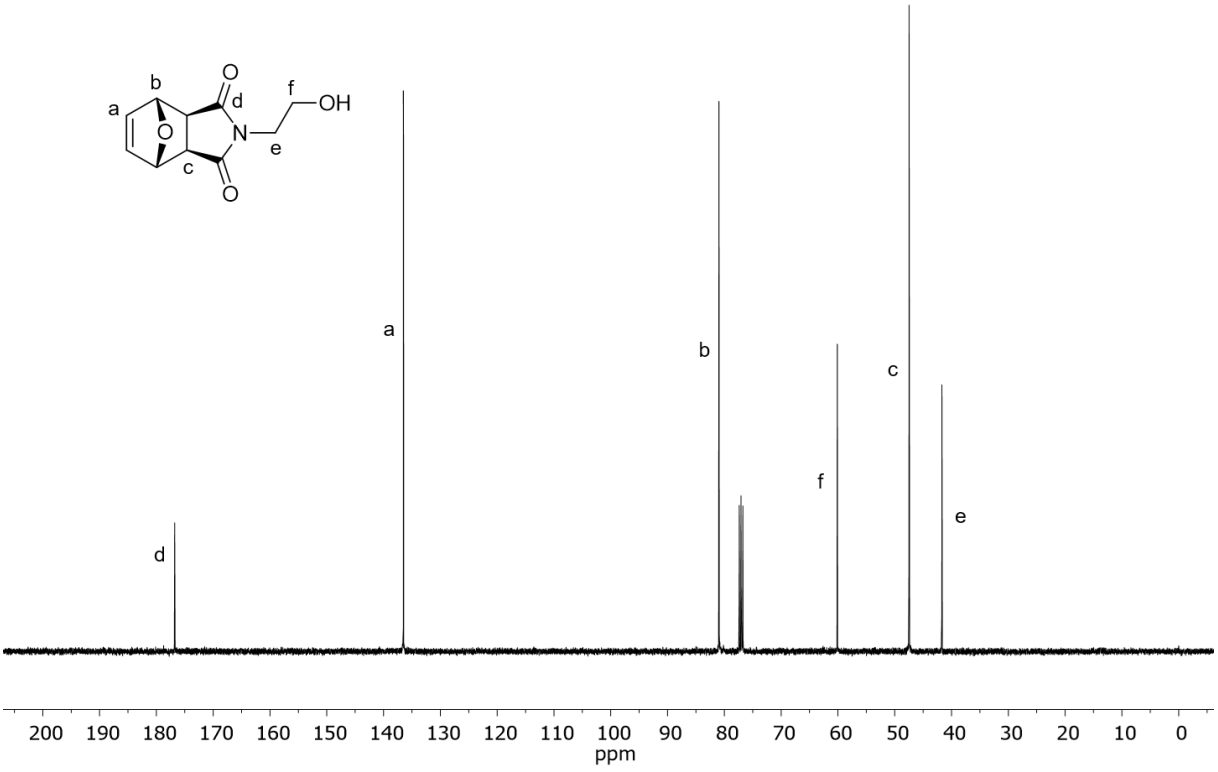

*Figure A 4. [13]C NMR spectrum of **M2-0***

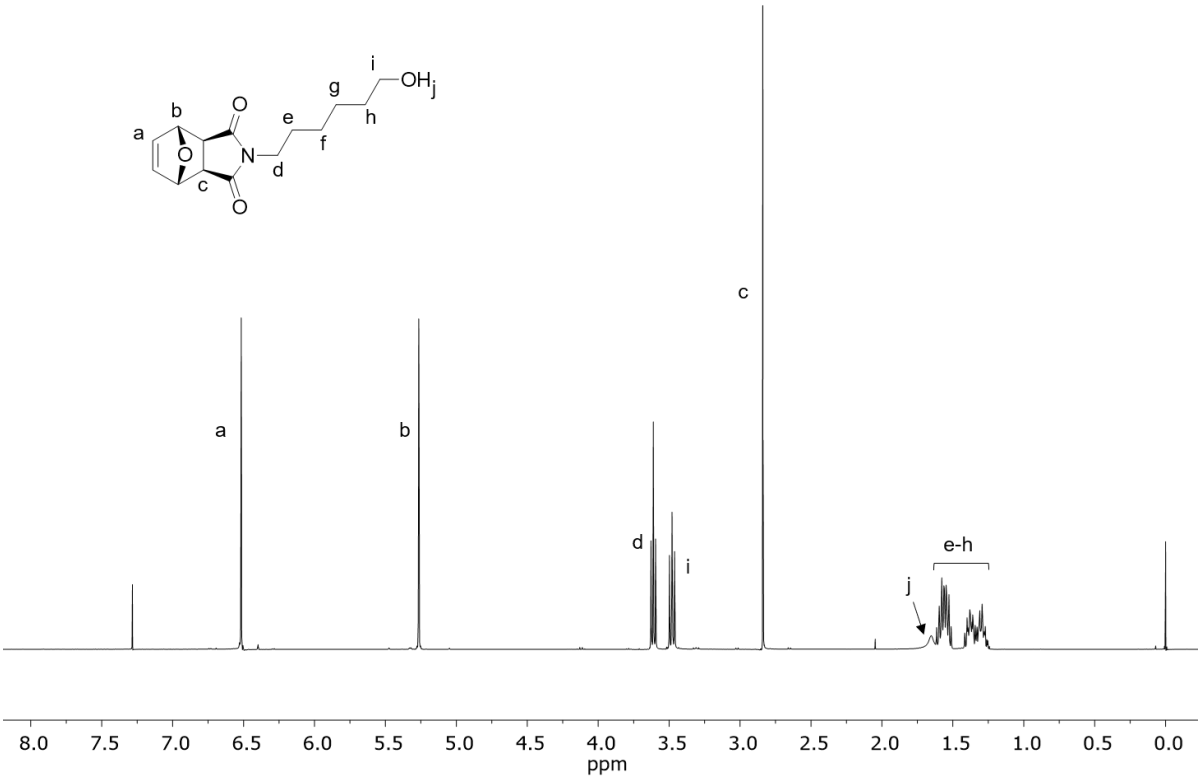

*Figure A 5. [1]H NMR spectrum of **M3-0**.*

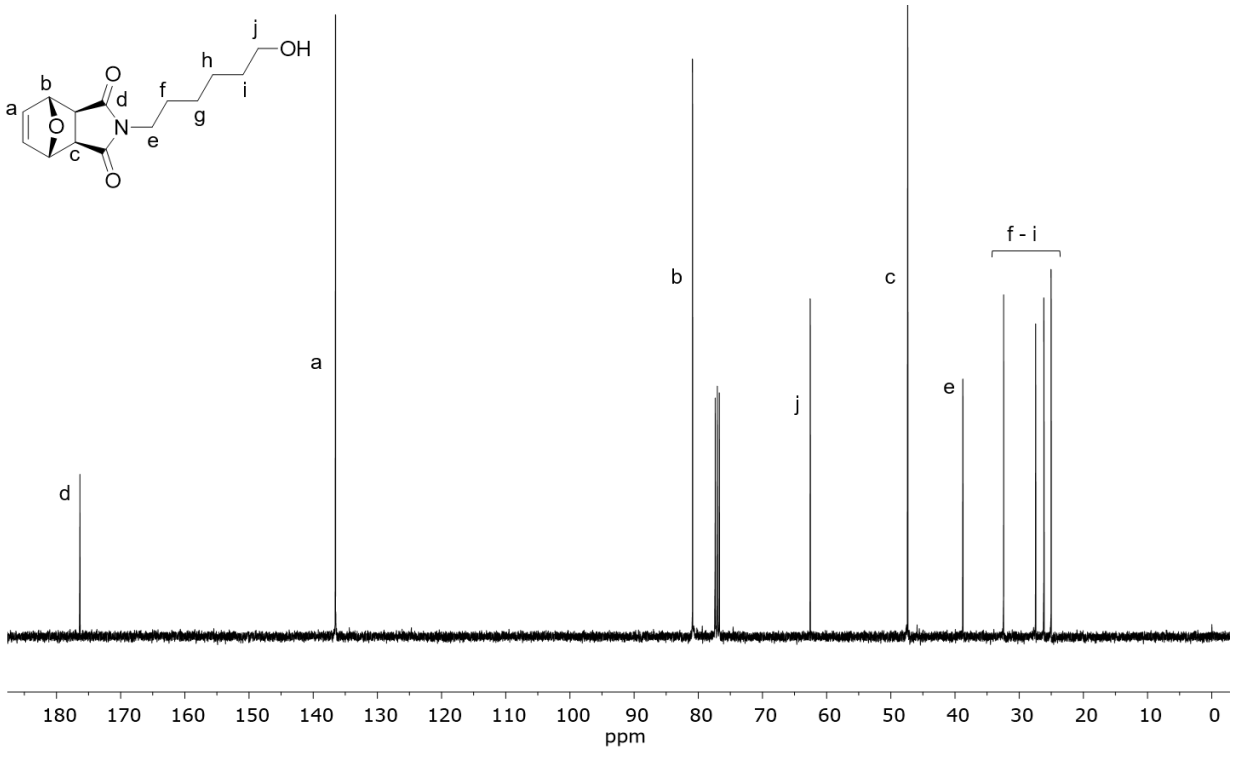

*Figure A 6. [13]C NMR spectrum of **M3-0***

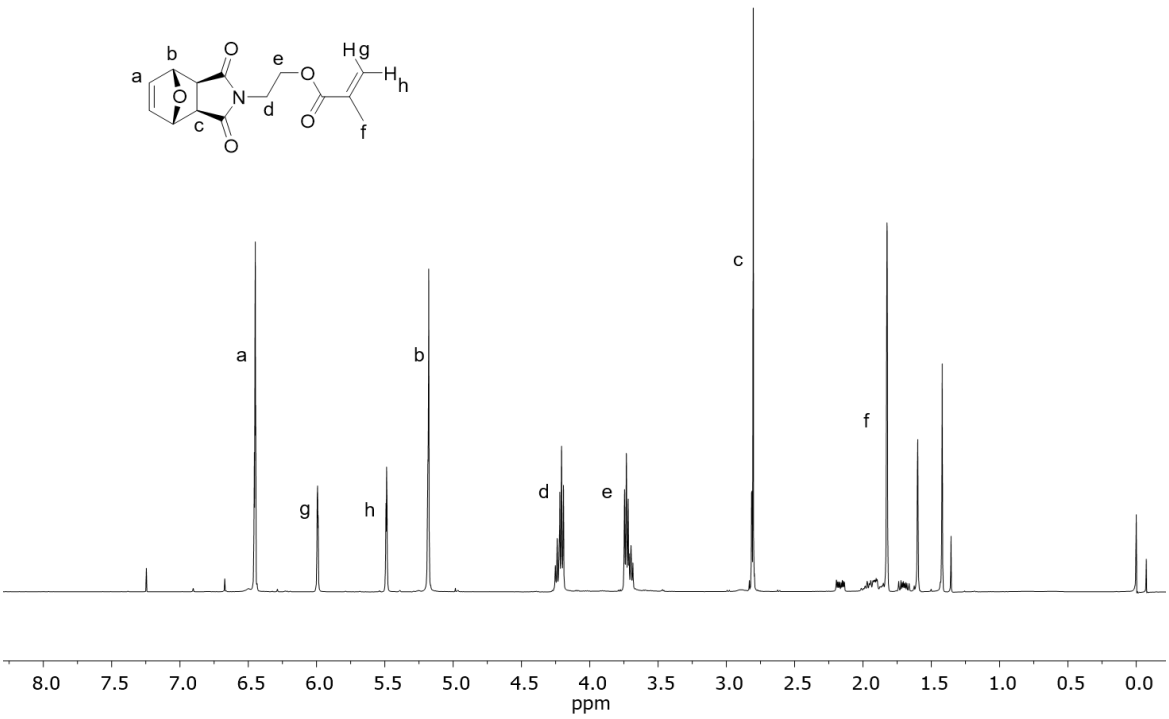

*Figure A 7. [1]H NMR spectrum of **M2.***

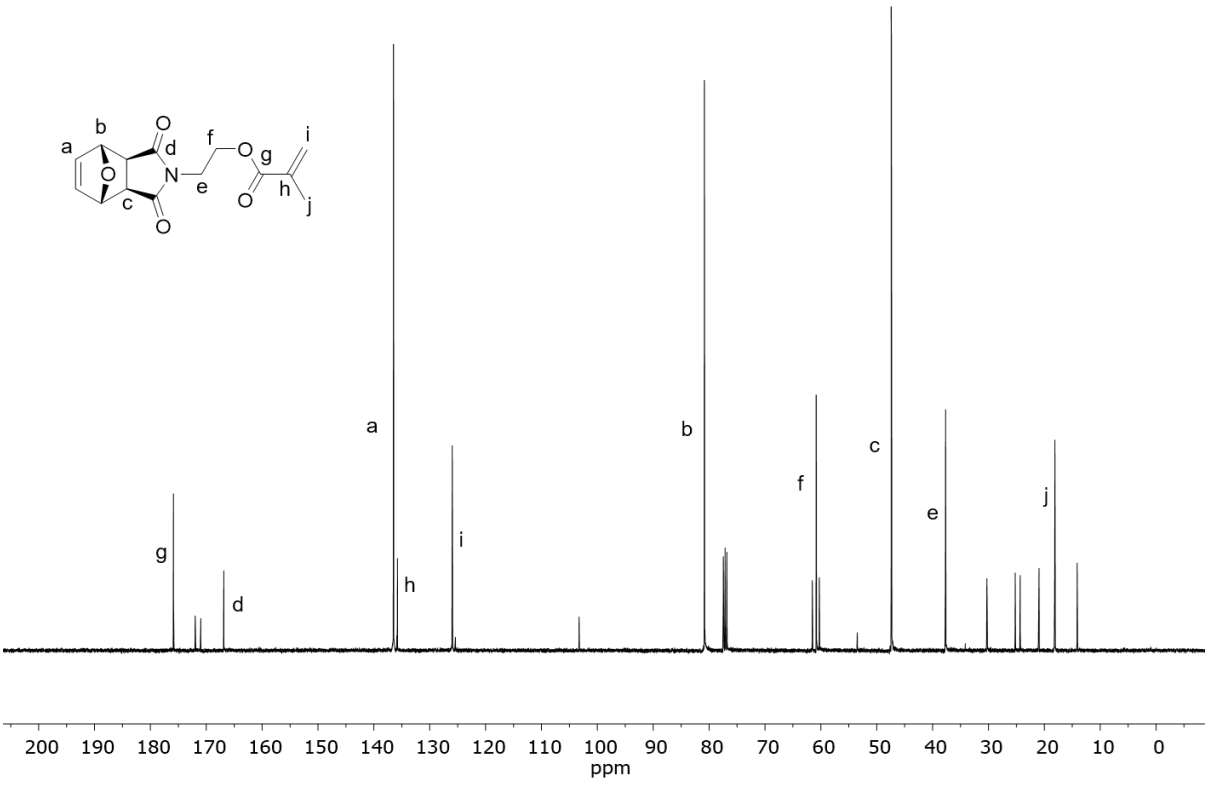

*Figure A 8. [13]C NMR spectrum of **M2**.*

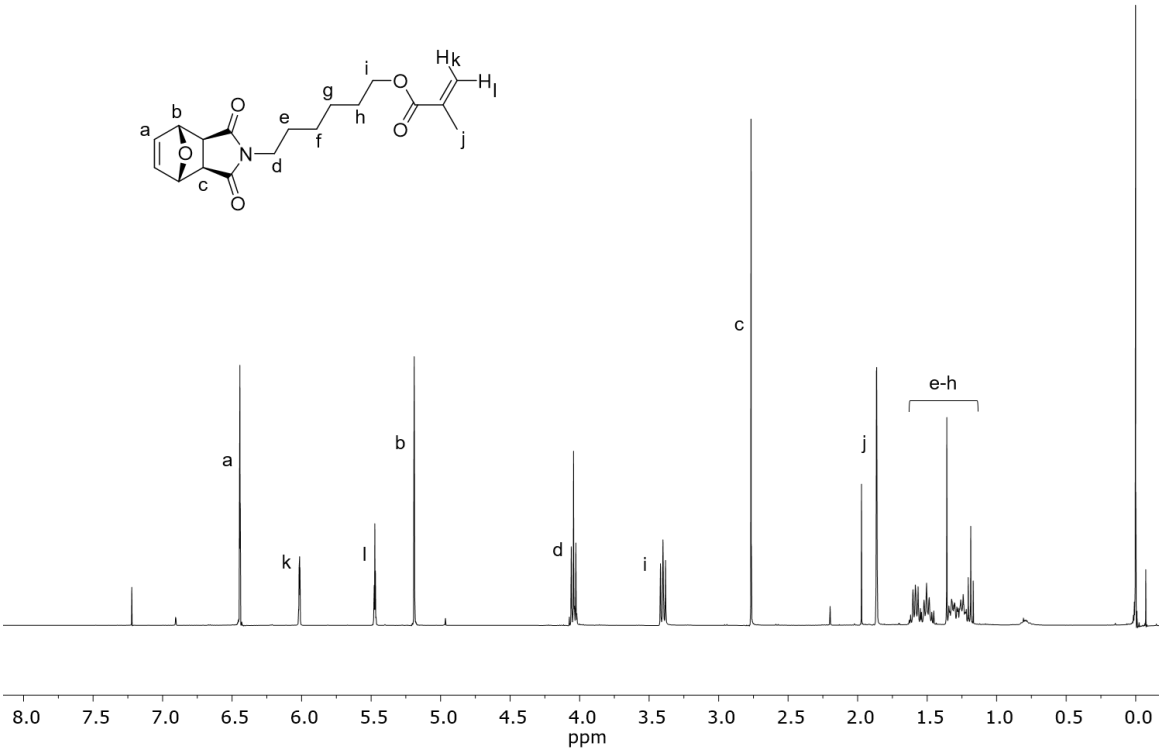

*Figure A 9. [1]H NMR spectrum of **M3**.*

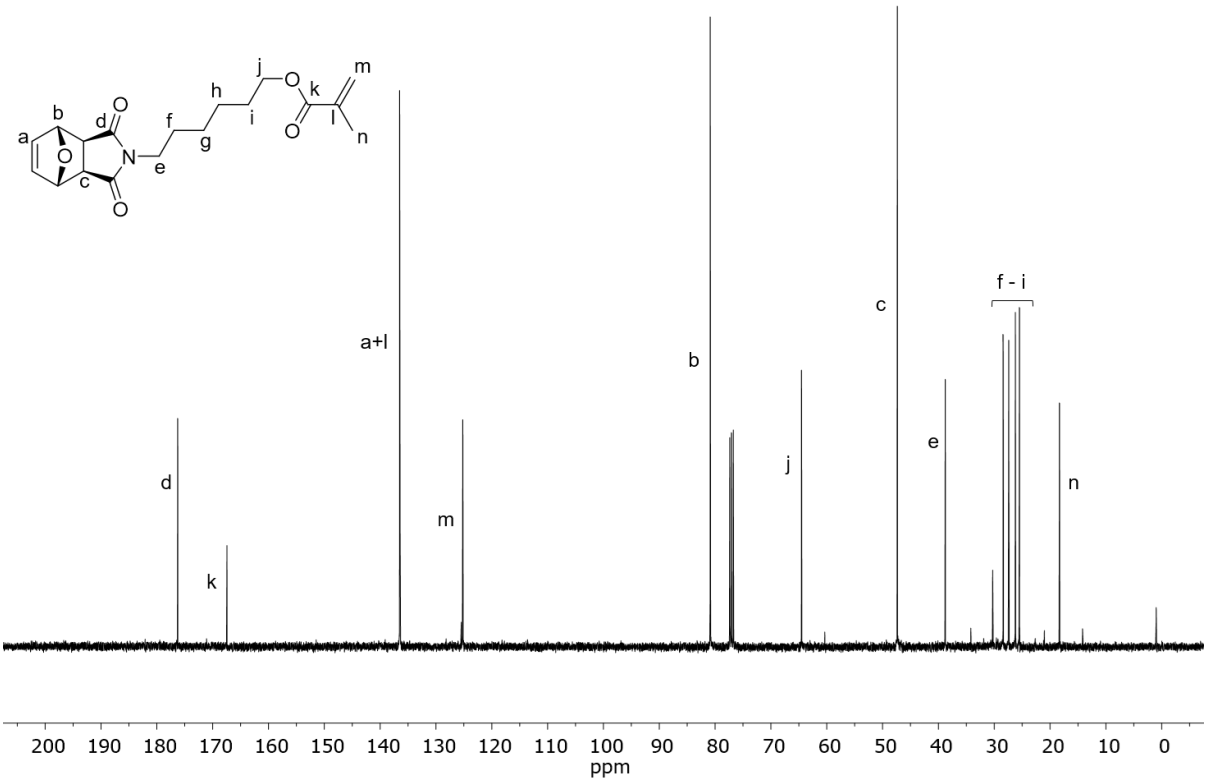

*Figure A 10. [13]C NMR spectrum of **M3**.*

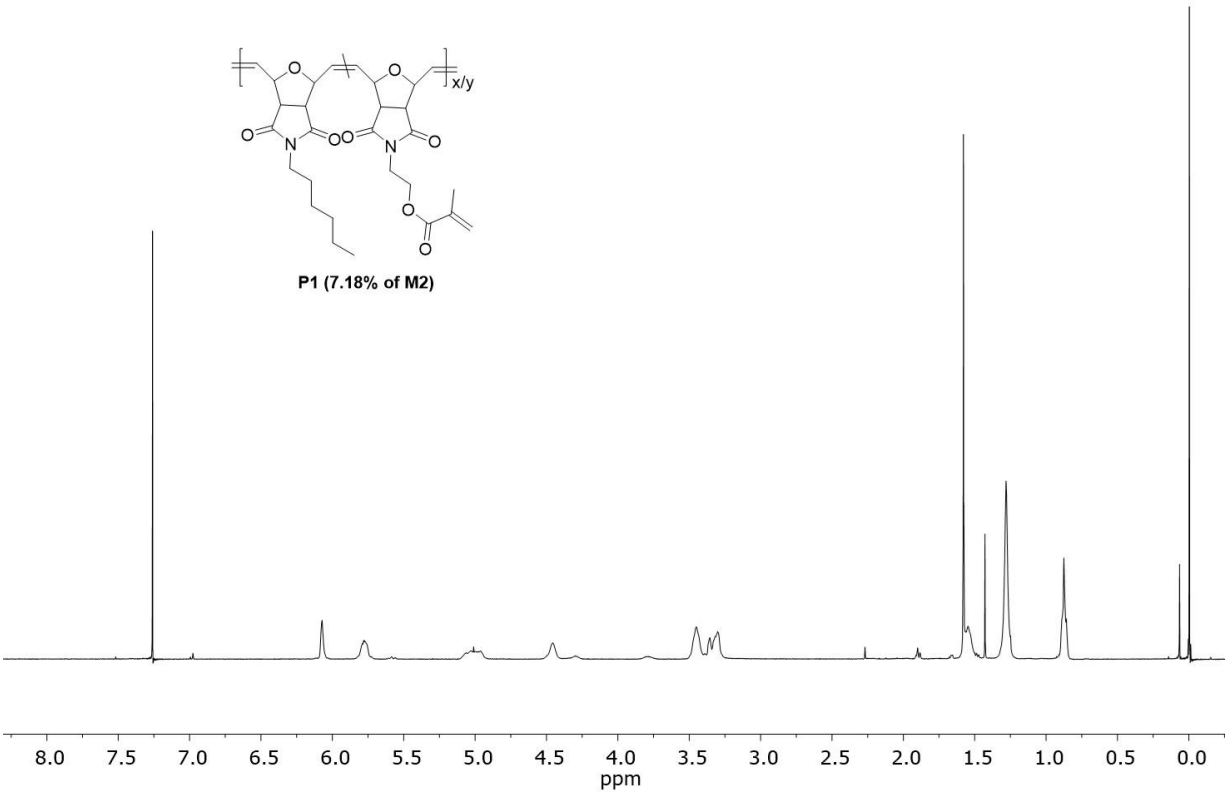

*Figure A 11. [1]H NMR spectrum of polymer **P1**.*

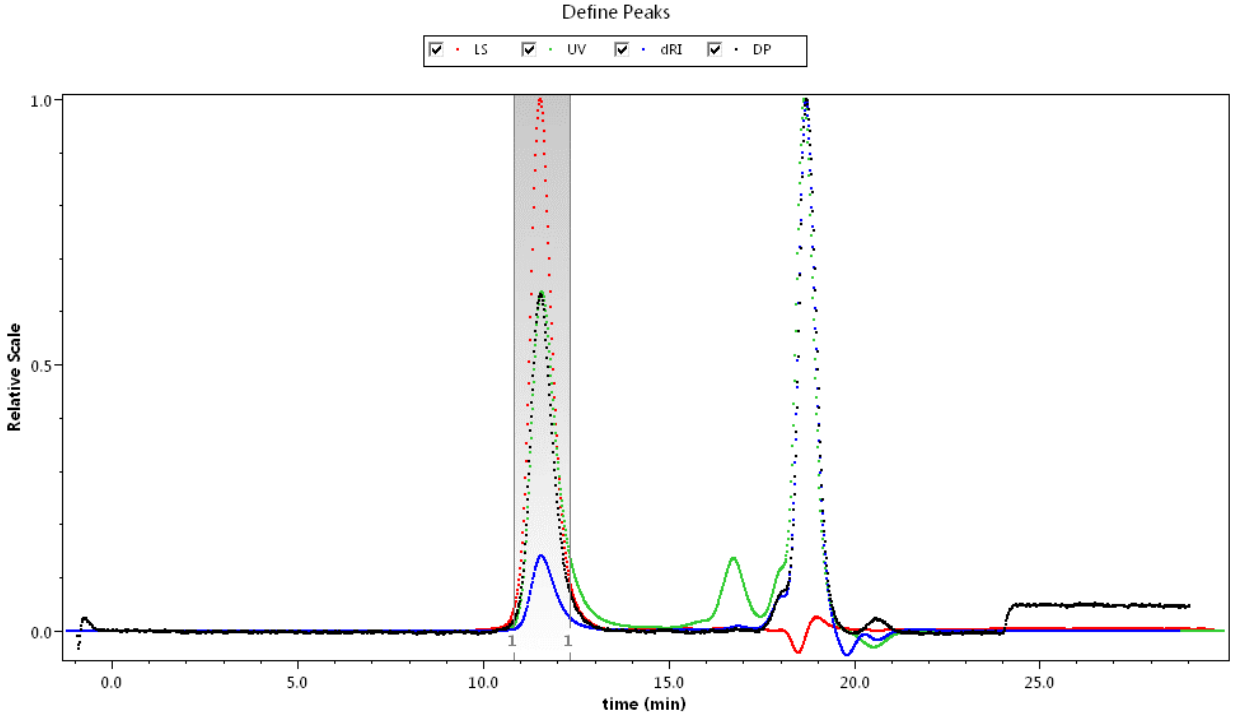

*Figure A 12. GPC trace of polymer **P1**.*

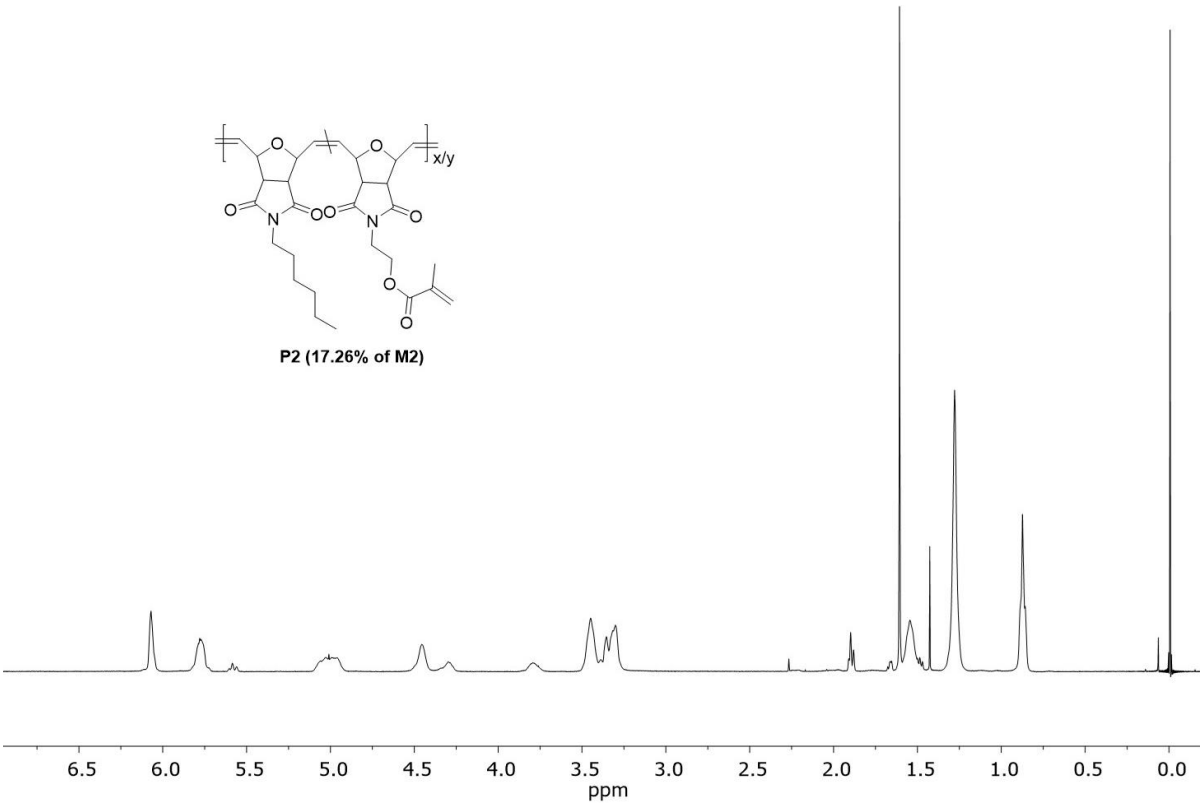

*Figure A 13. ^{1}H NMR spectrum of polymer **P2**.*

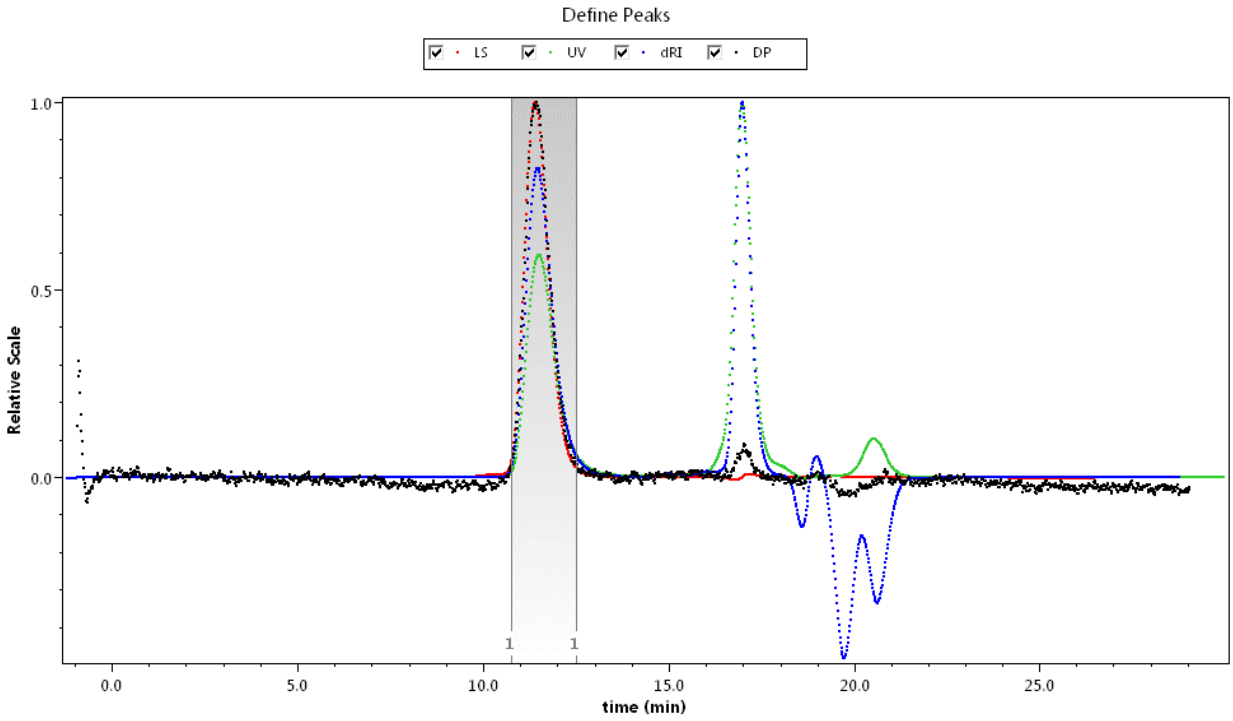

*Figure A 14. GPC trace of polymer **P2**.*

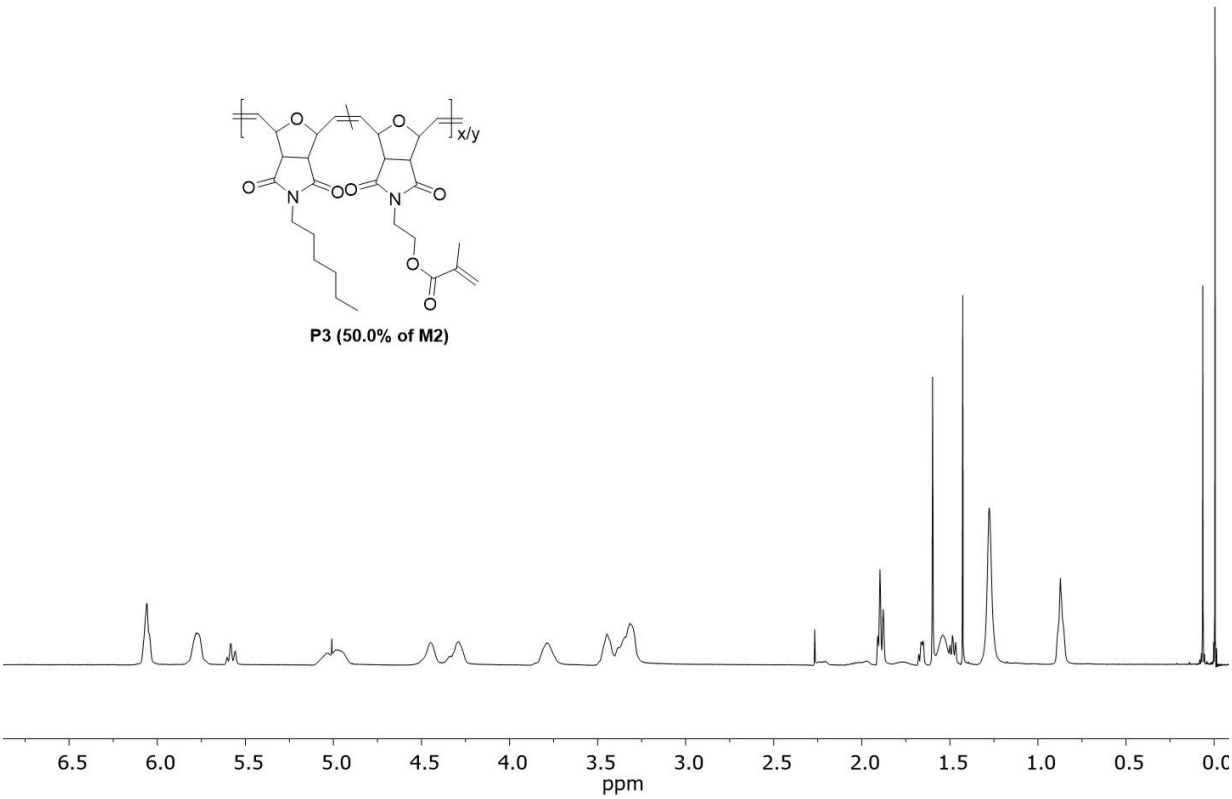

*Figure A 15. ^{1}H NMR spectrum of polymer **P3**.*

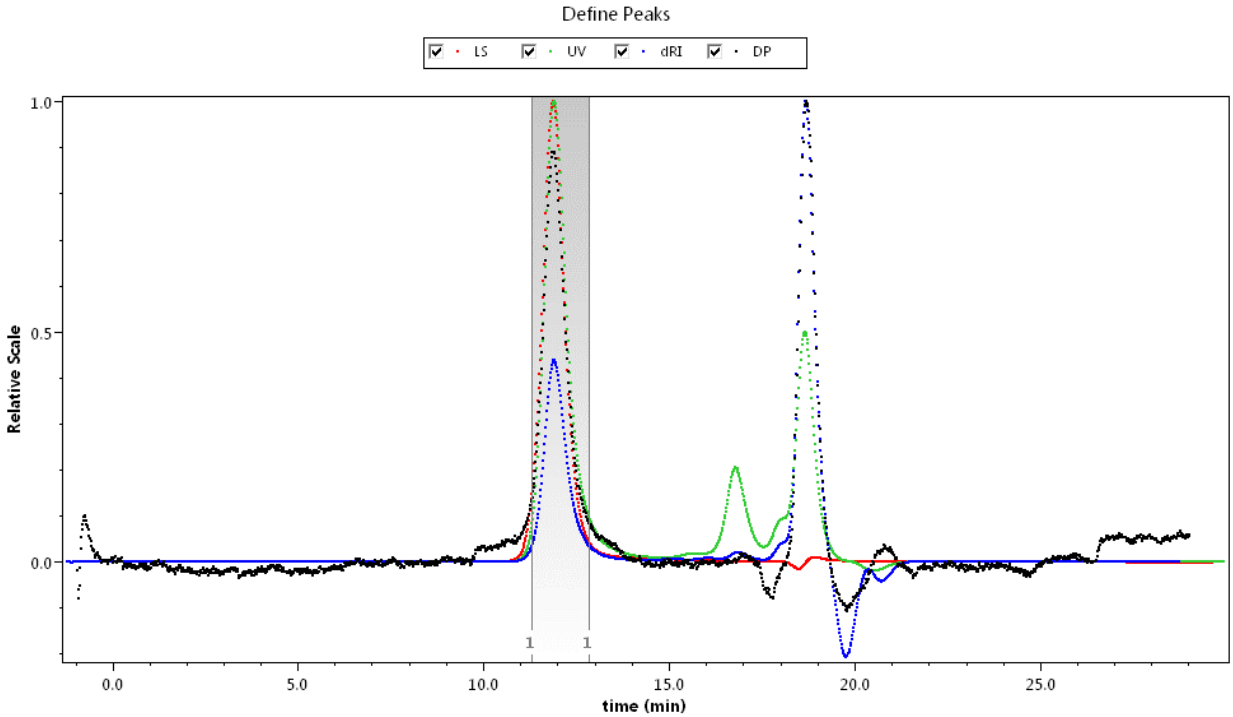

*Figure A 16. GPC trace of polymer **P3**.*

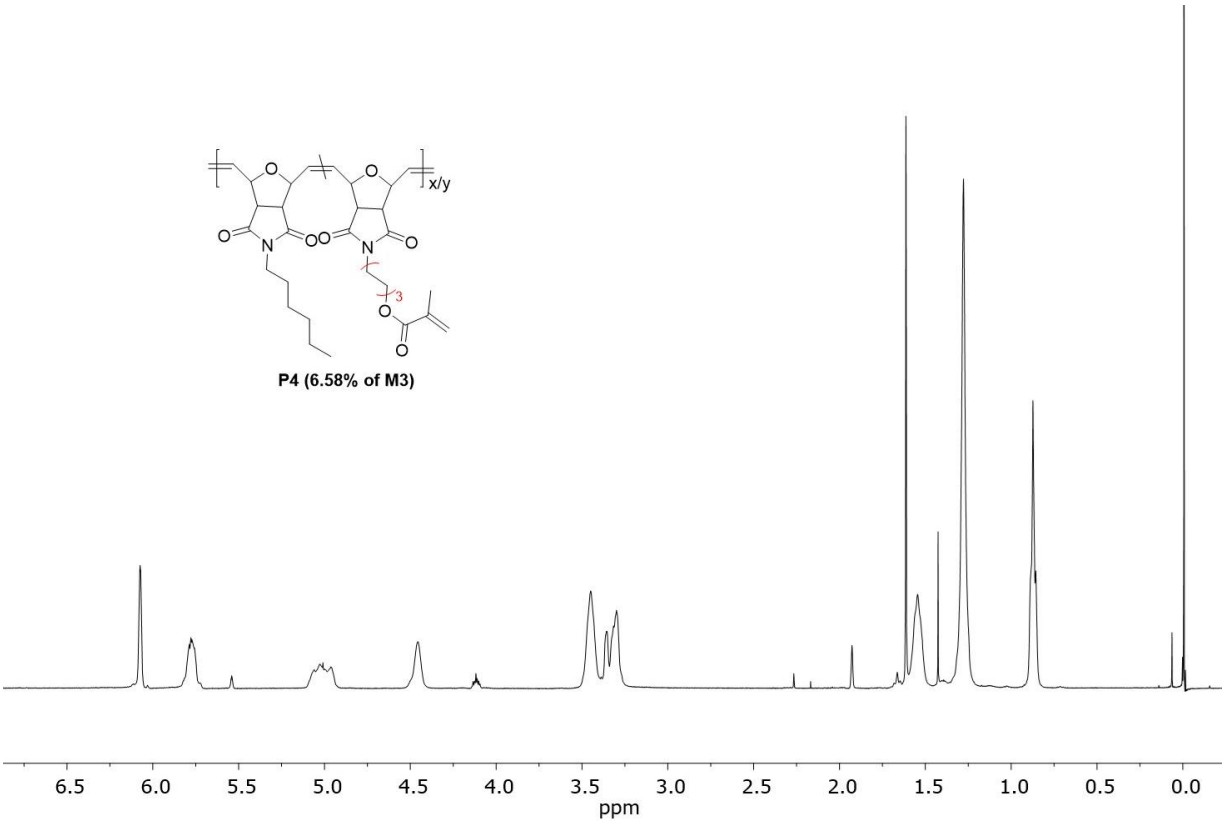

*Figure A 17. ^{1}H NMR spectrum of polymer **P4**.*

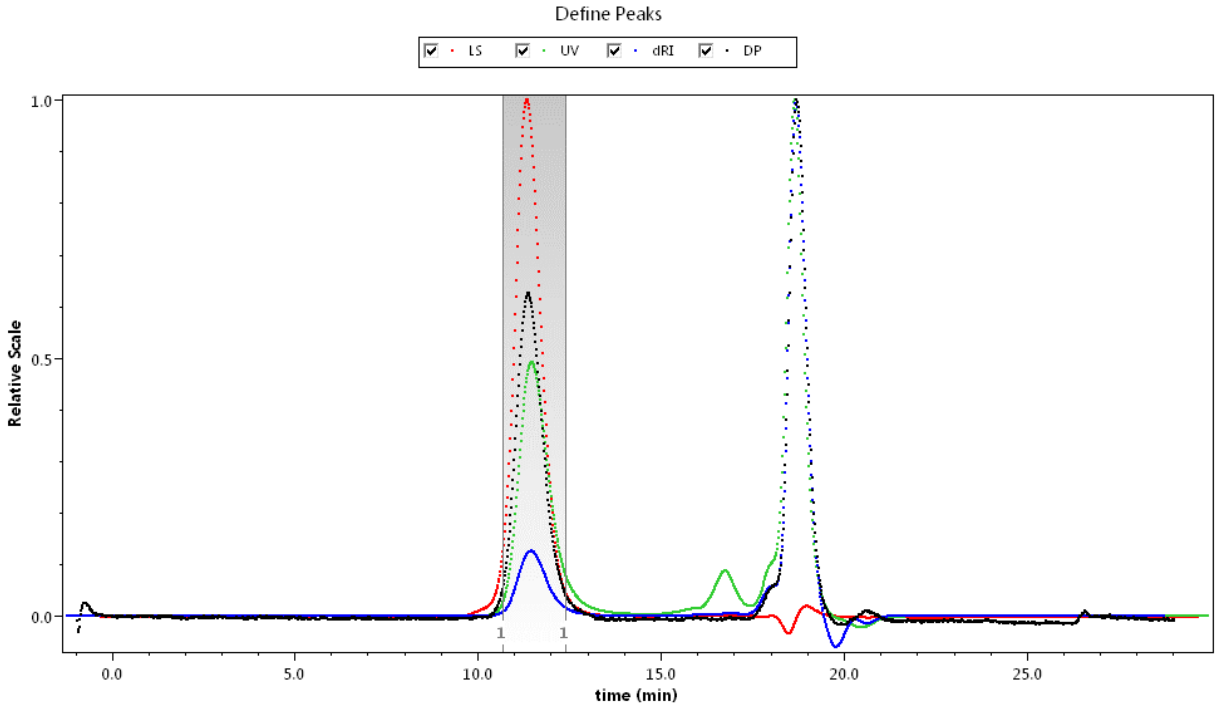

*Figure A 18. GPC trace of polymer **P4**.*

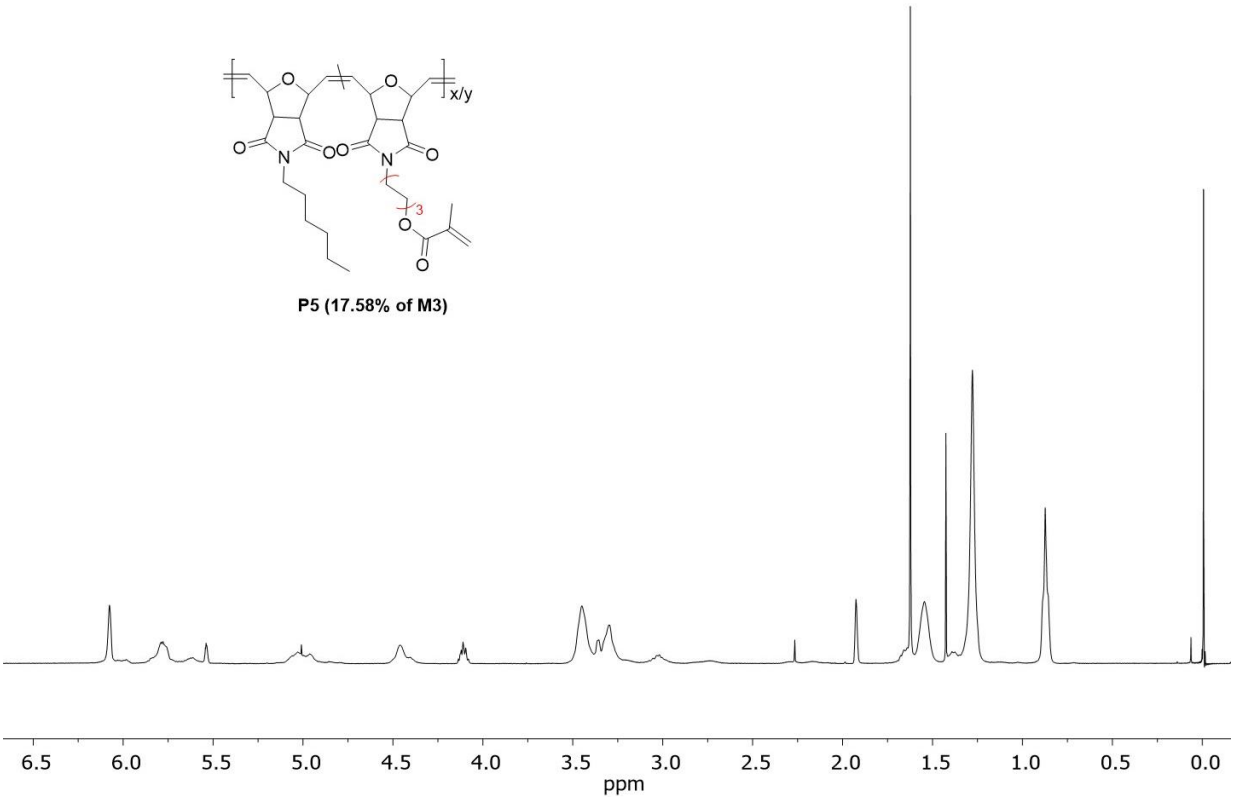

*Figure A 19. ^{1}H NMR spectrum of polymer **P5**.*

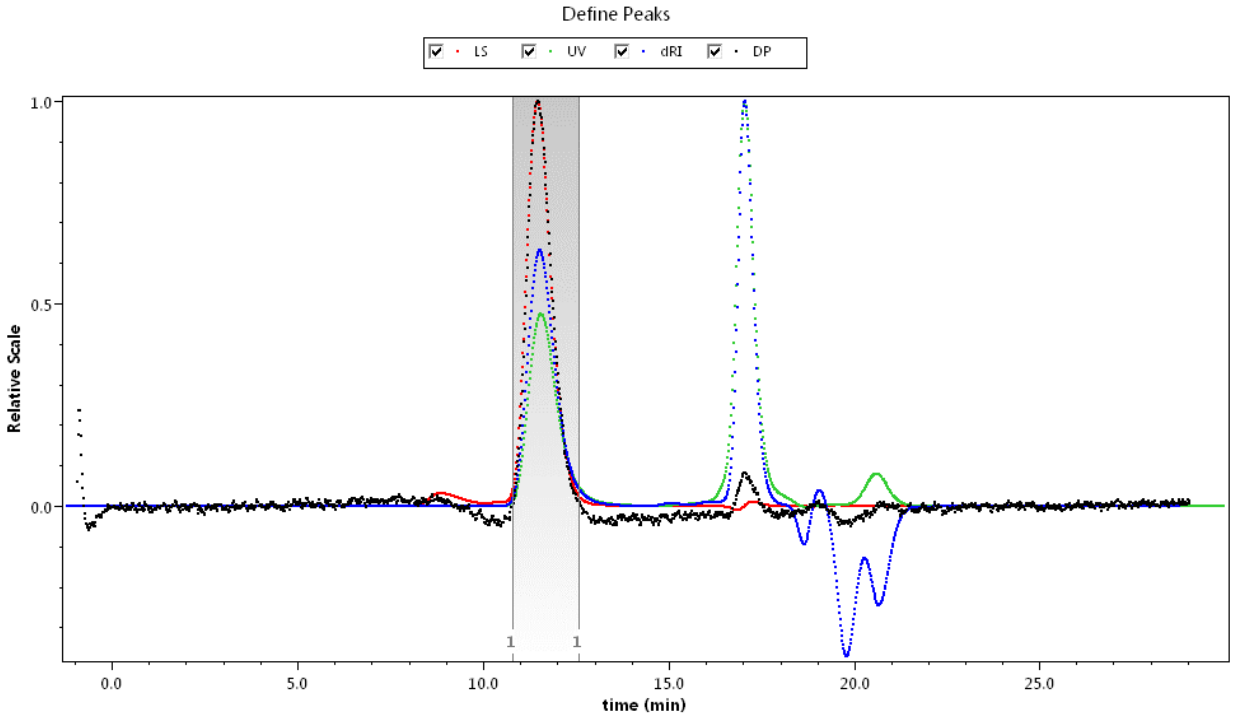

*Figure A 20. GPC trace of polymer **P5**.*

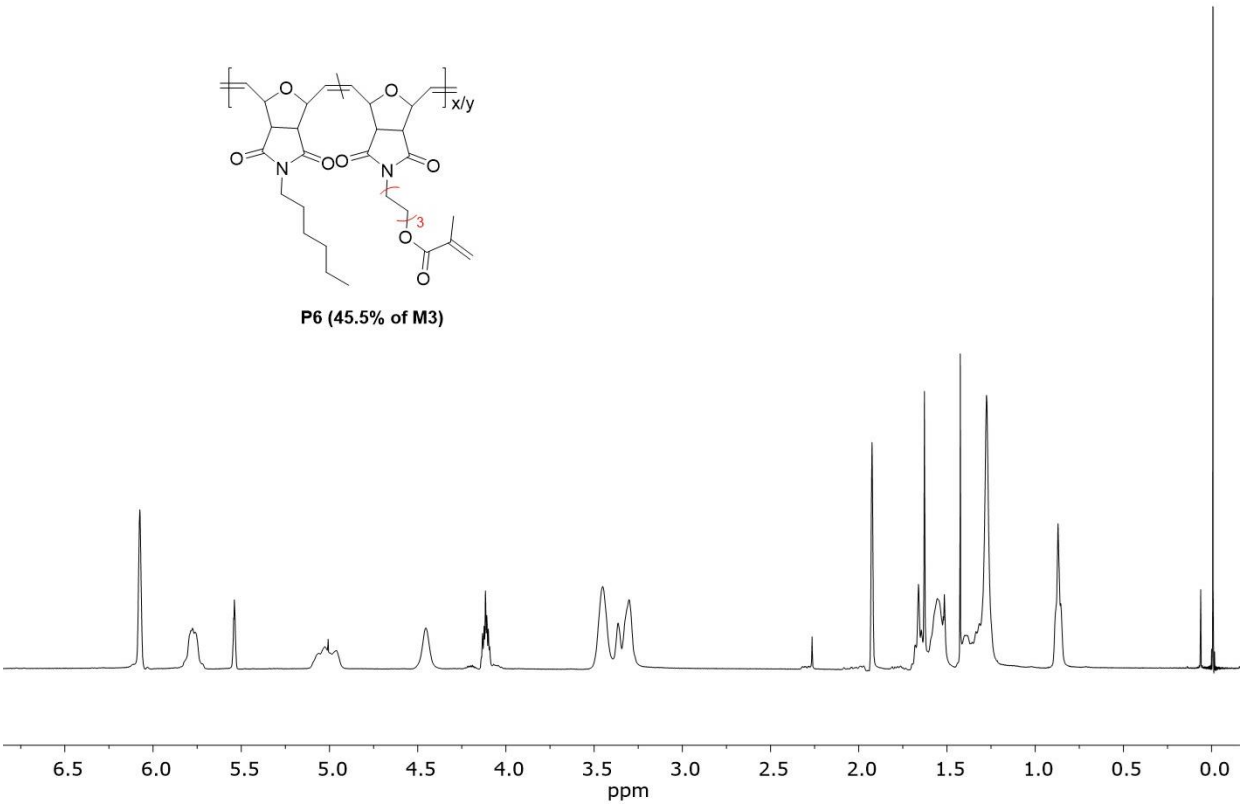

*Figure A 21. ^{1}H NMR spectrum of polymer **P6**.*

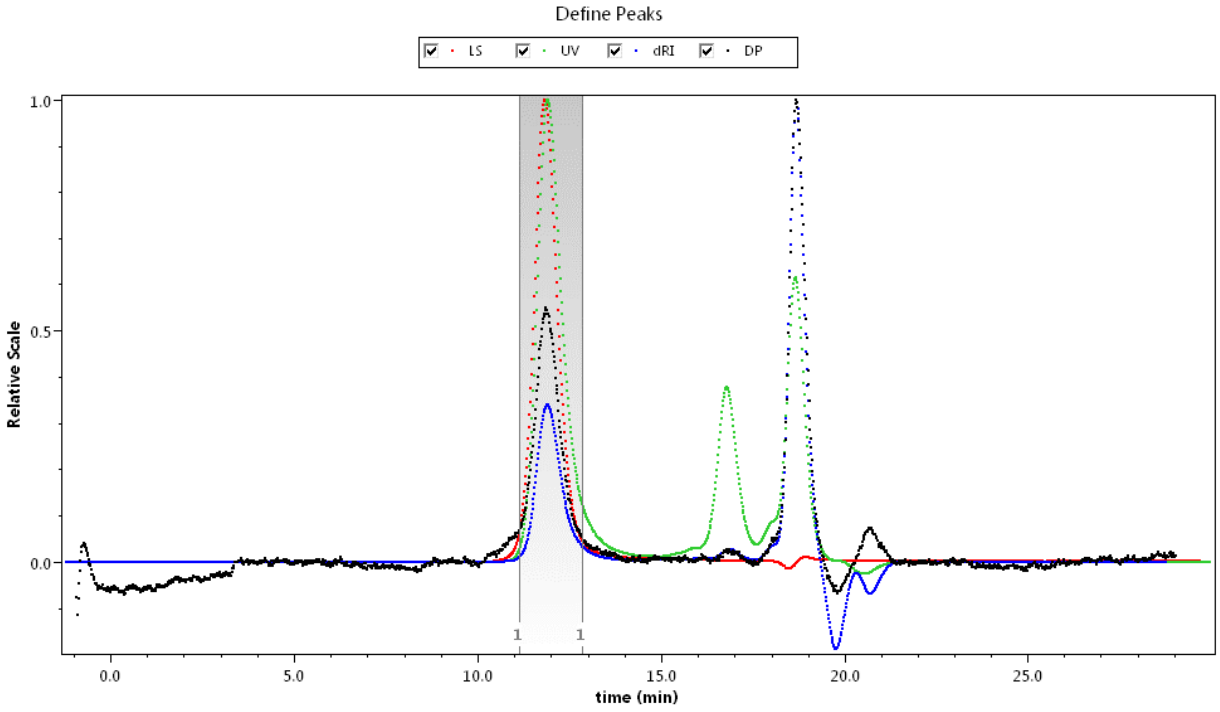

*Figure A 22. GPC trace of polymer **P6**.*

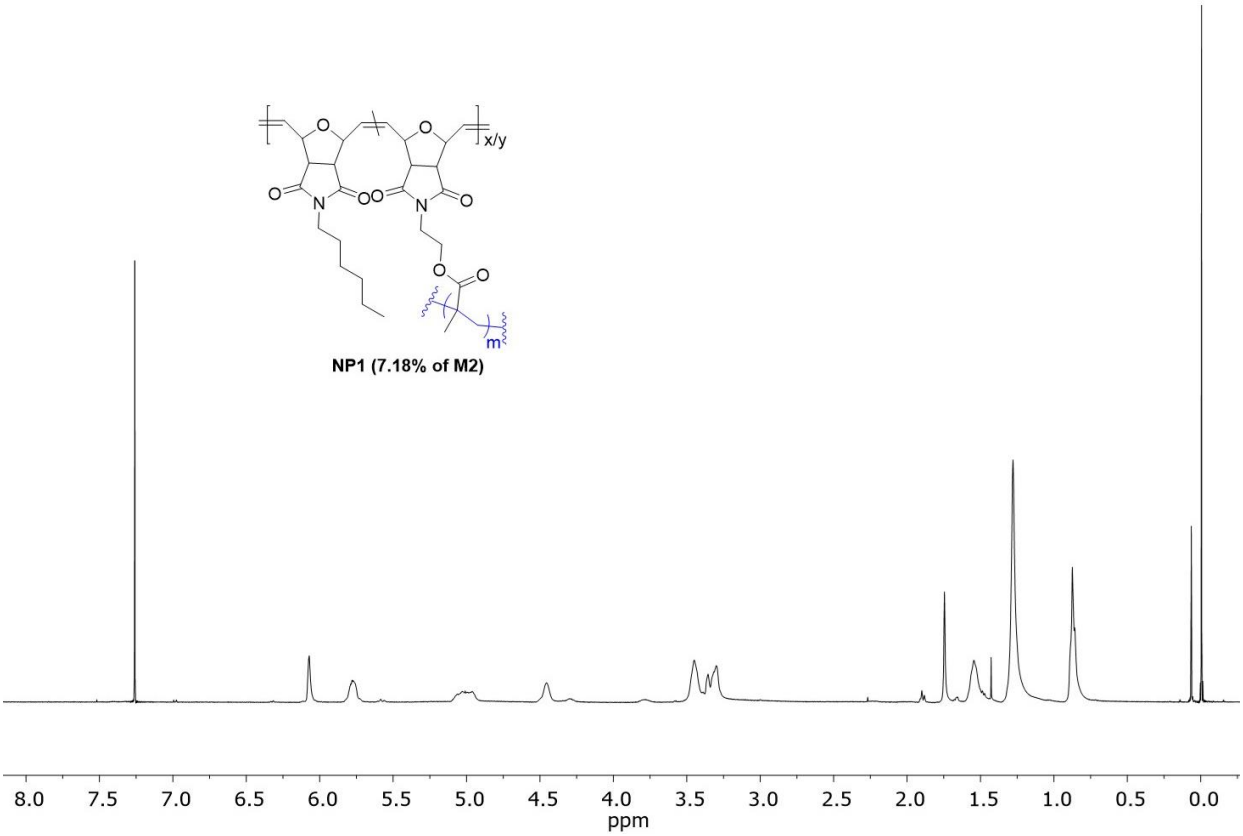

*Figure A 23. ^{1}H NMR spectrum of nanoparticle **NP1**.*

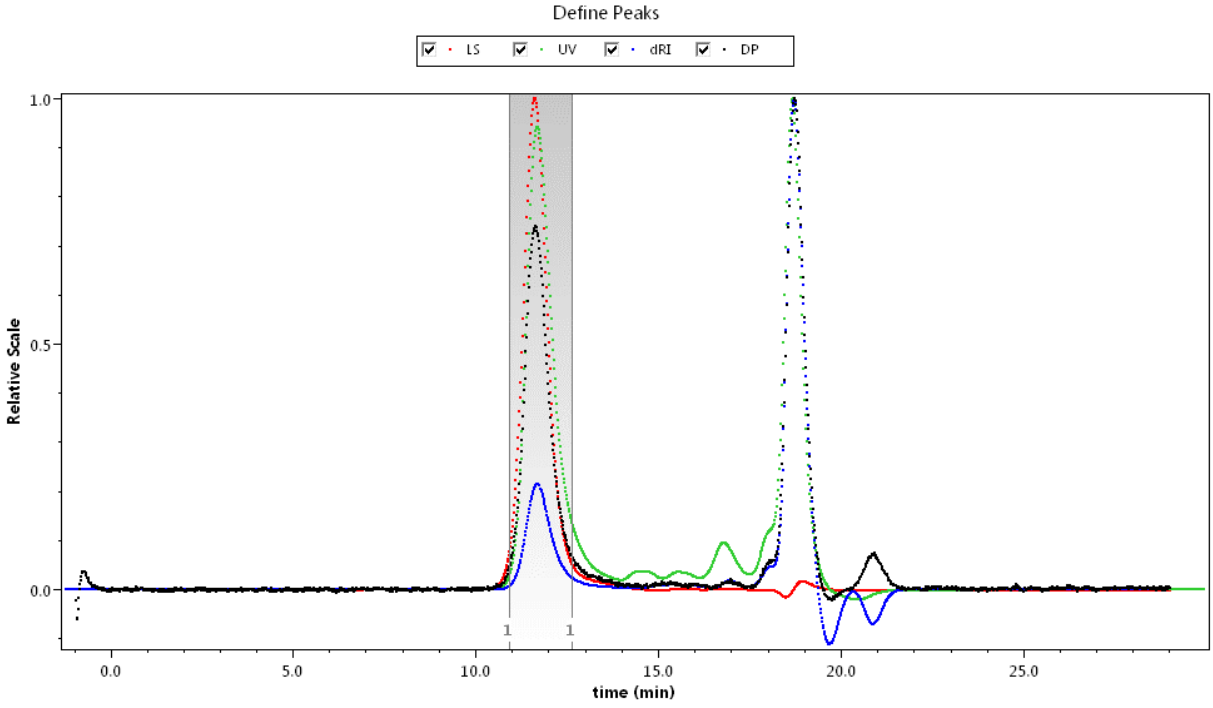

*Figure A 24. GPC trace of nanoparticle **NP1**.*

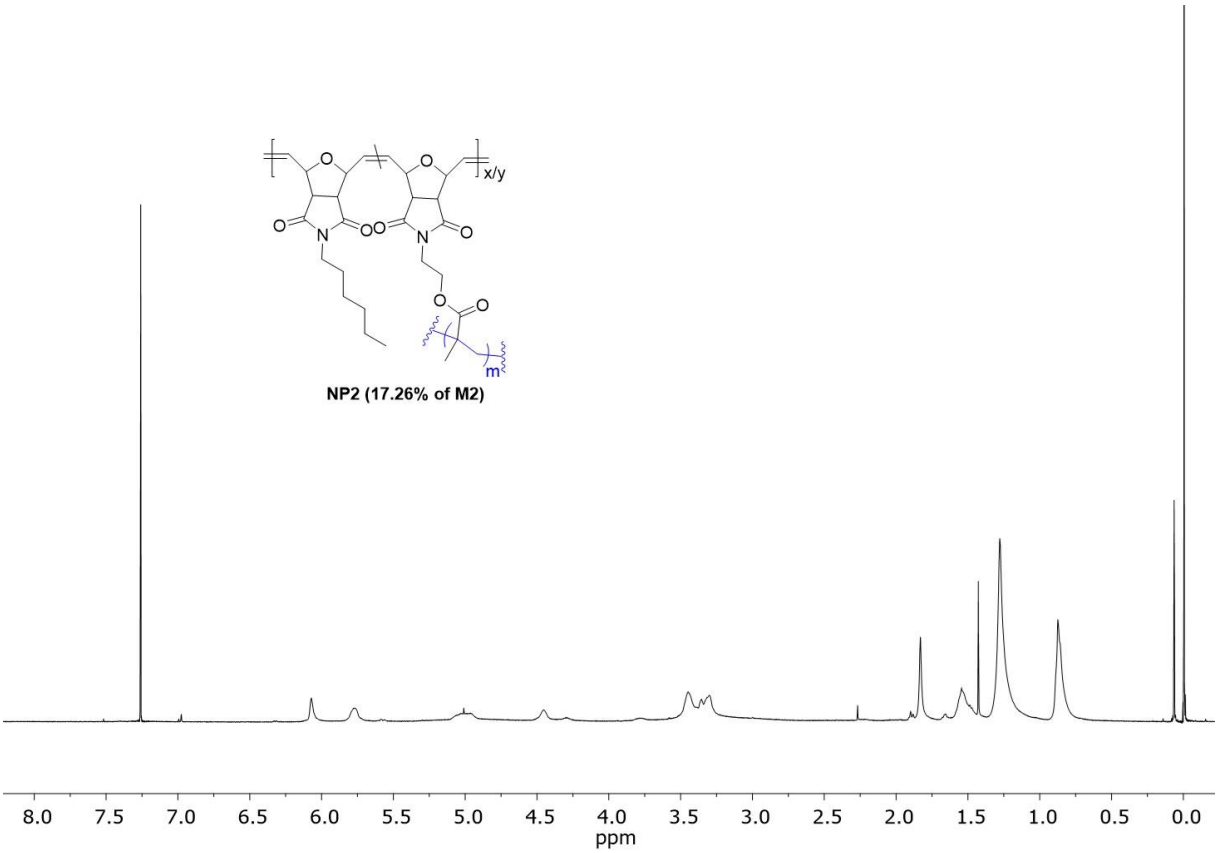

*Figure A 25. ^{1}H NMR spectrum of nanoparticle **NP2**.*

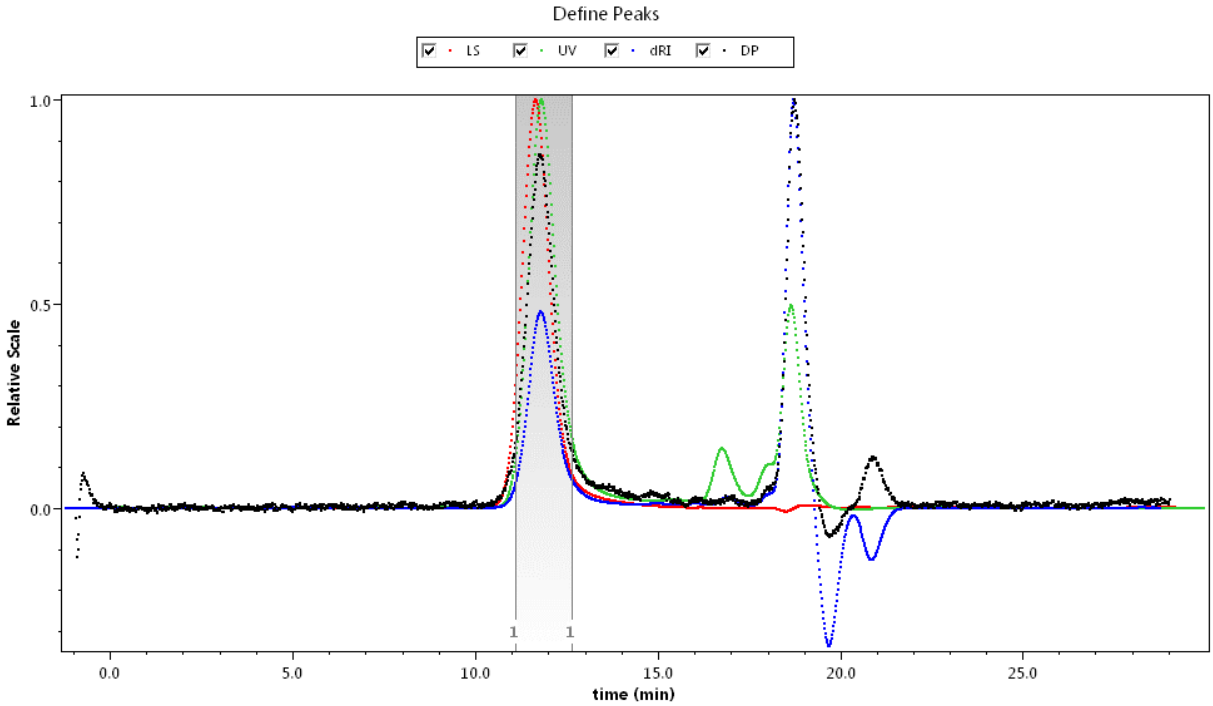

*Figure A 26. GPC trace of nanoparticle **NP2**.*

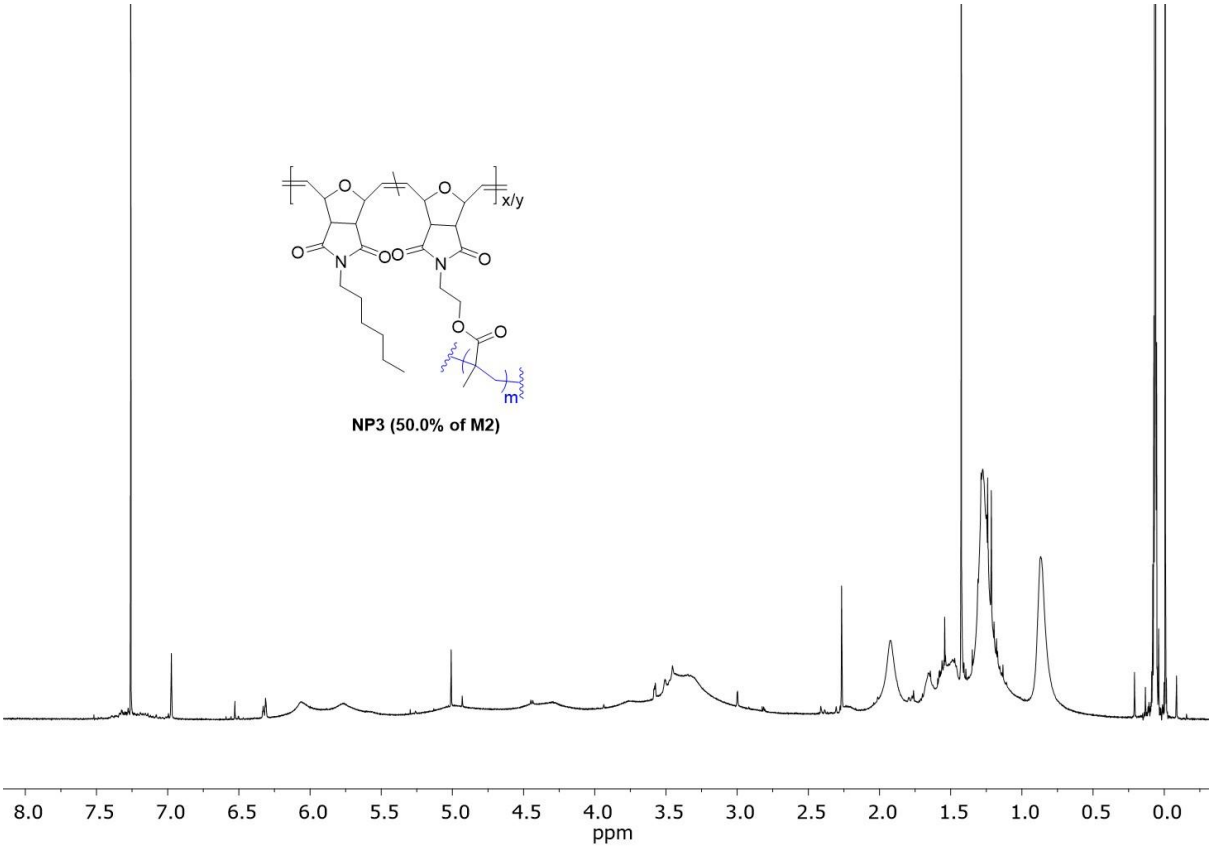

*Figure A 27. ^{1}H NMR spectrum of nanoparticle **NP3**.*

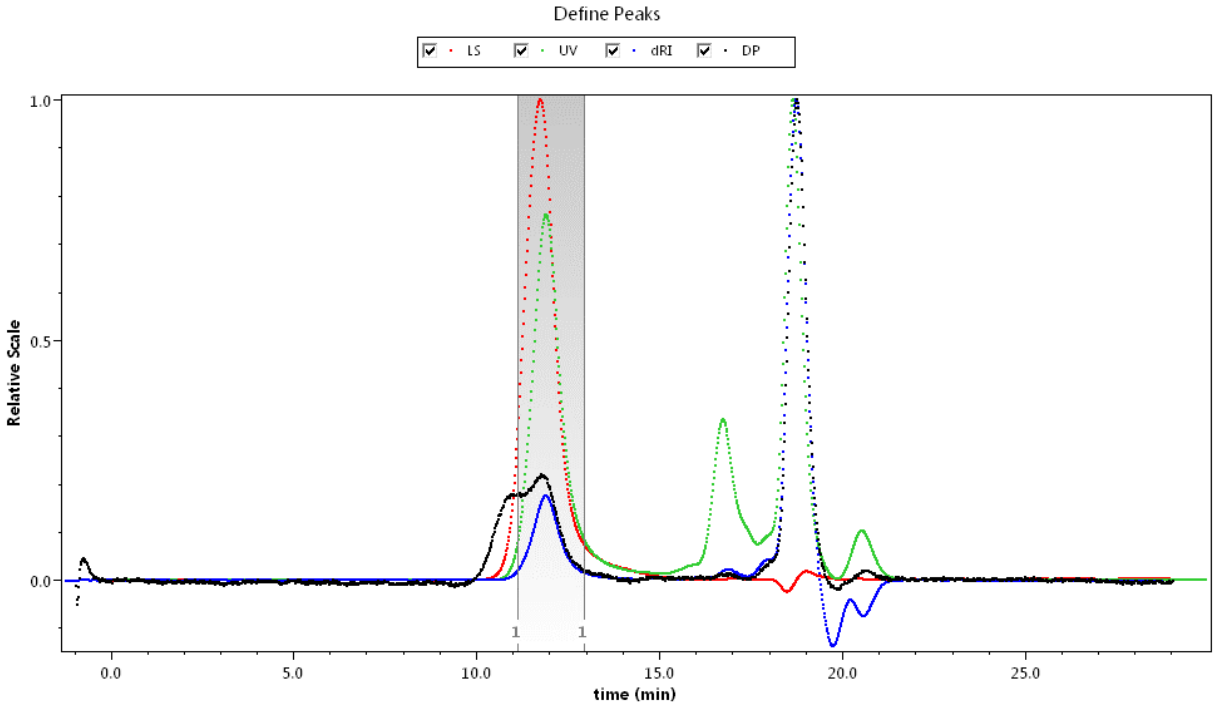

*Figure A 28. GPC trace of nanoparticle **NP3**.*

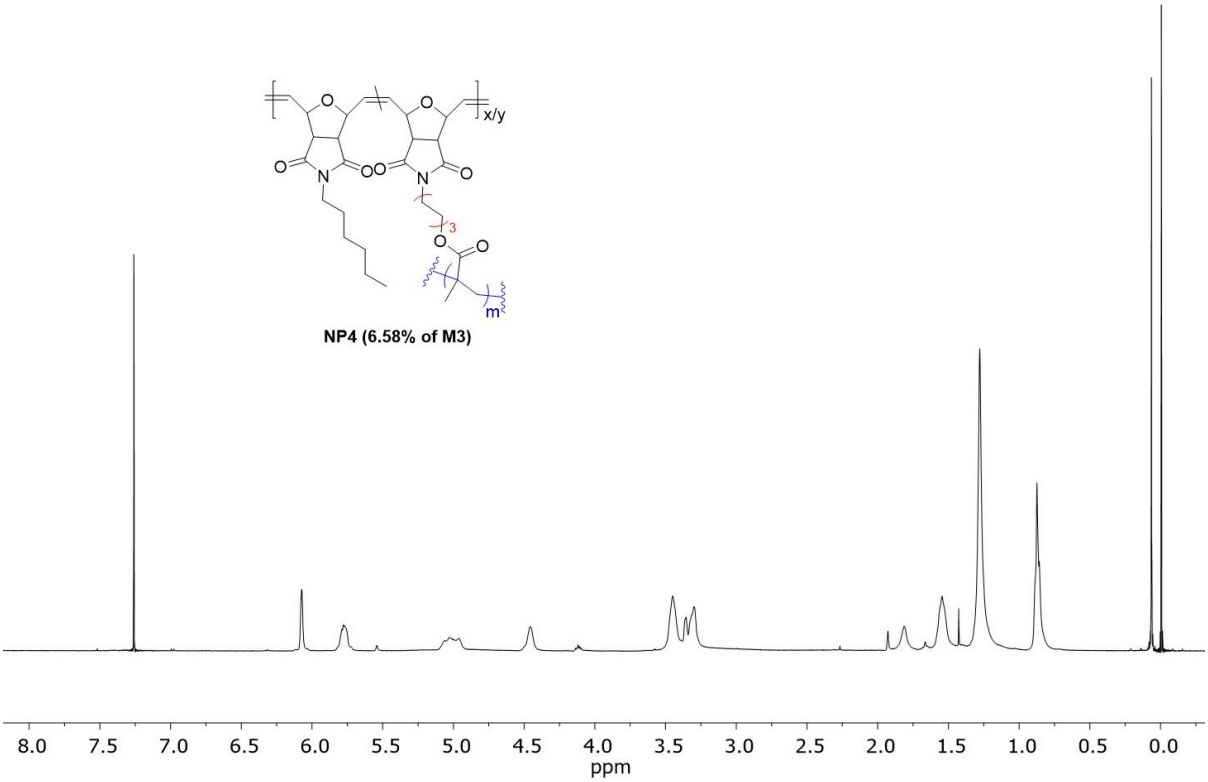

*Figure A 29. [1]H NMR spectrum of nanoparticle **NP4**.*

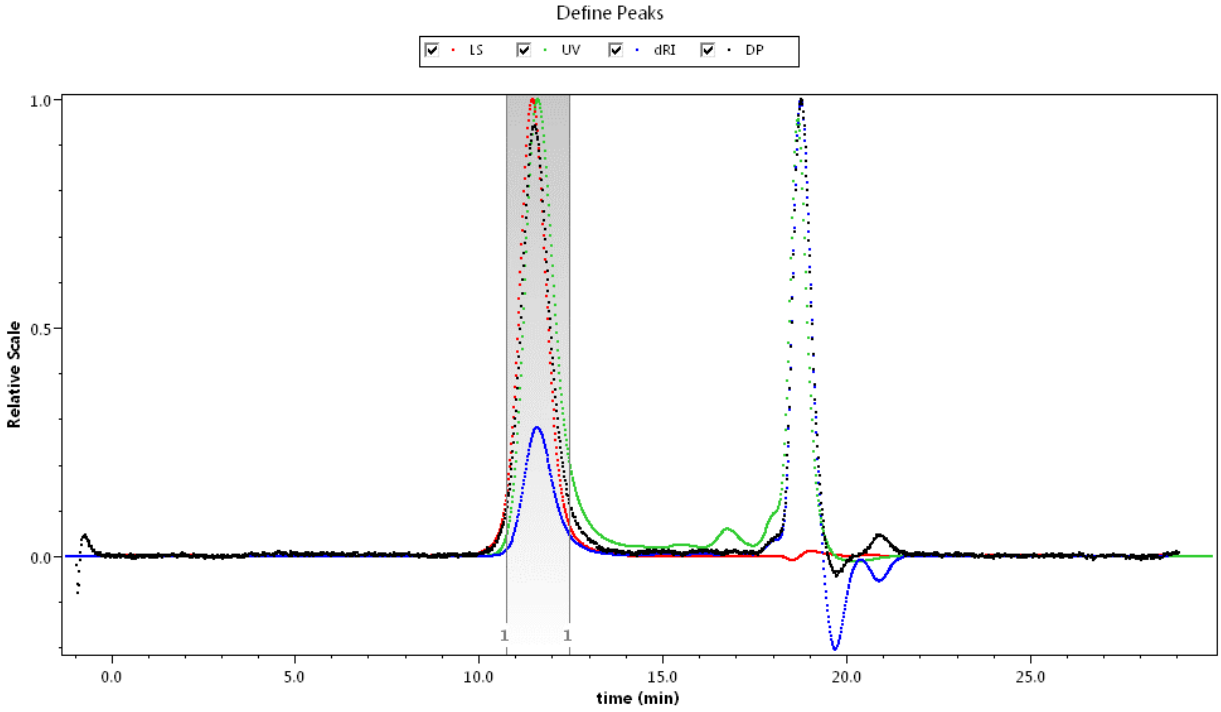

*Figure A 30. GPC trace of nanoparticle **NP4**.*

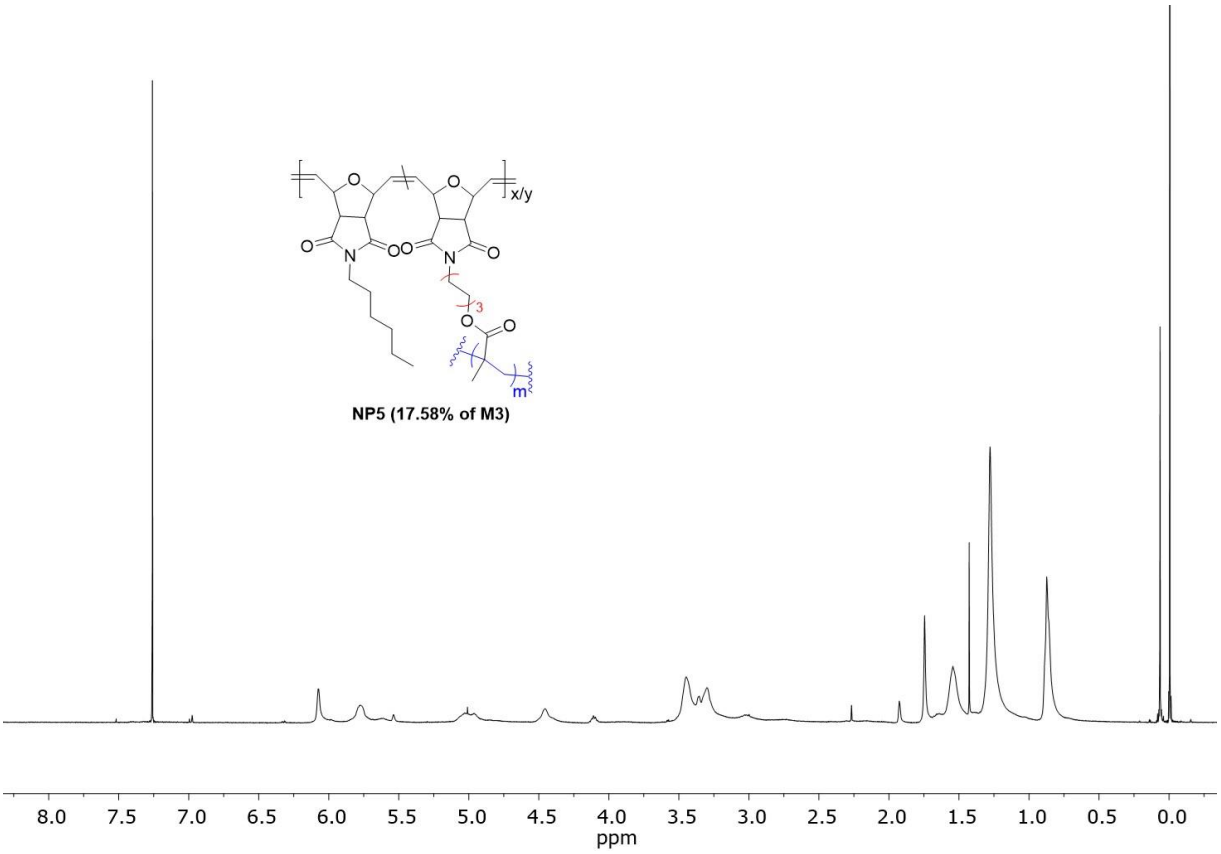

*Figure A 31. ^{1}H NMR spectrum of nanoparticle **NP5**.*

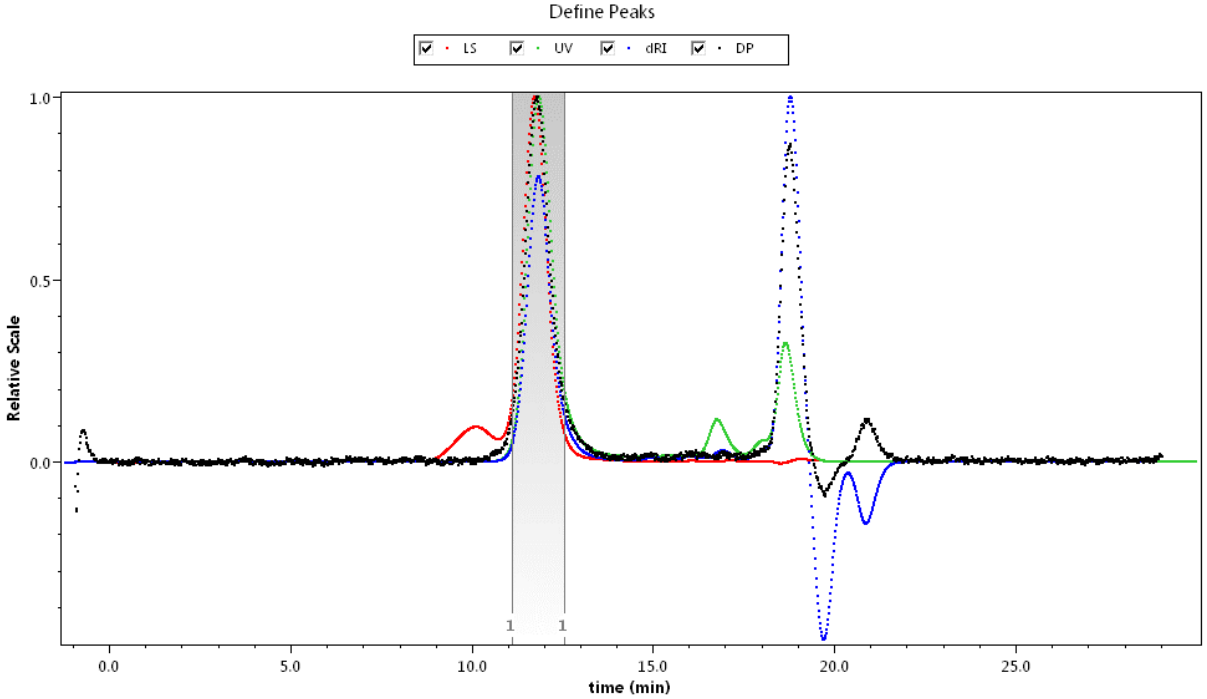

*Figure A 32. GPC trace of nanoparticle **NP5**.*

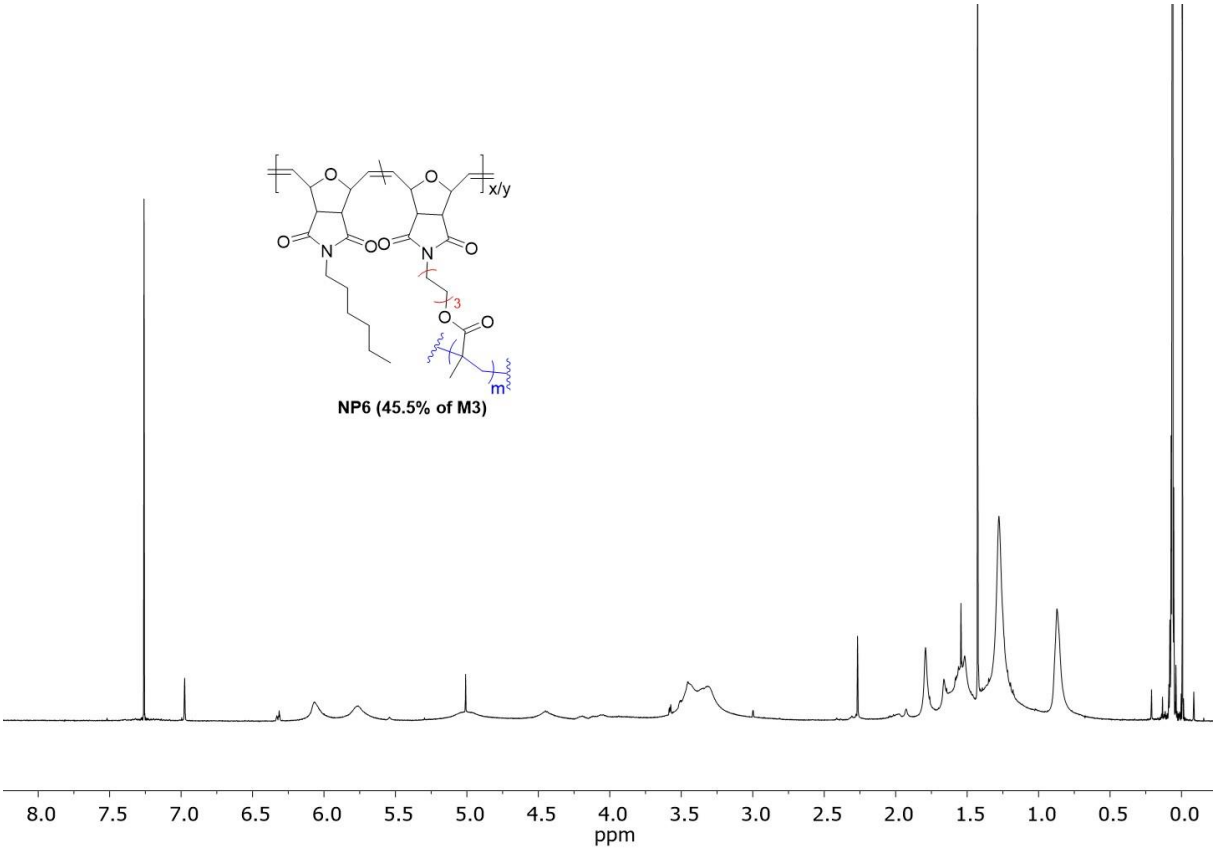

*Figure A 33. ^{1}H NMR spectrum of nanoparticle **NP6**.*

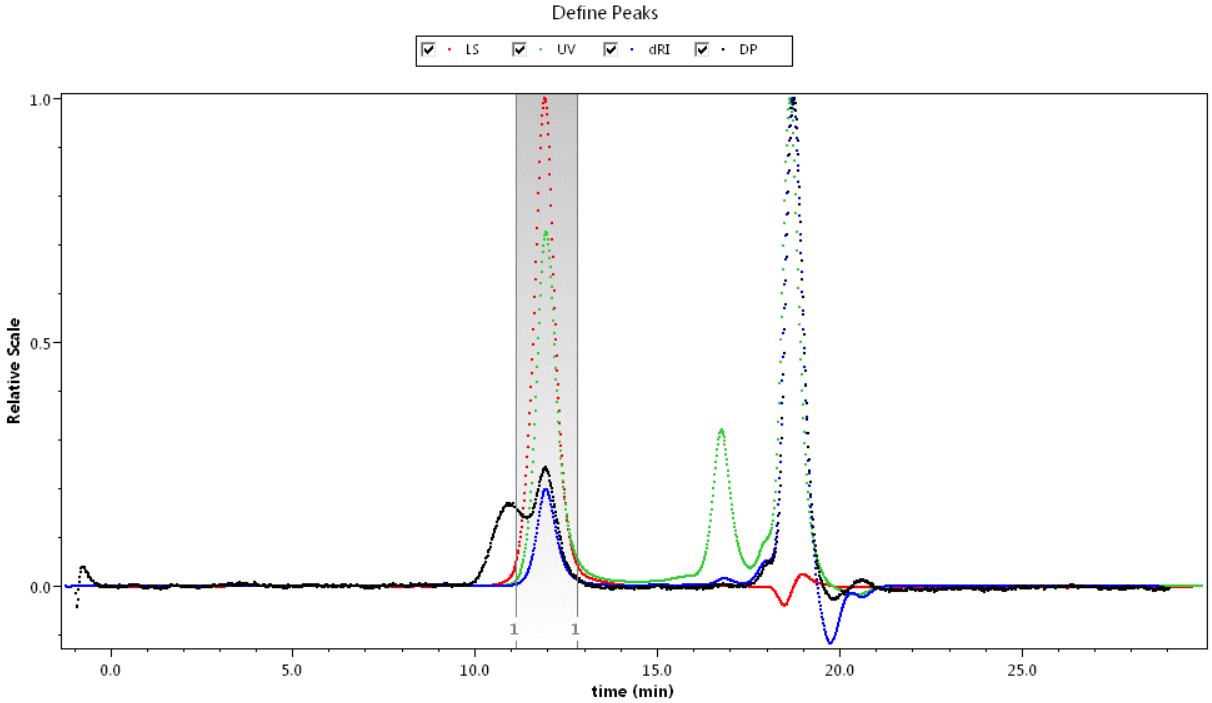

*Figure A 34. GPC trace of nanoparticle **NP6**.*

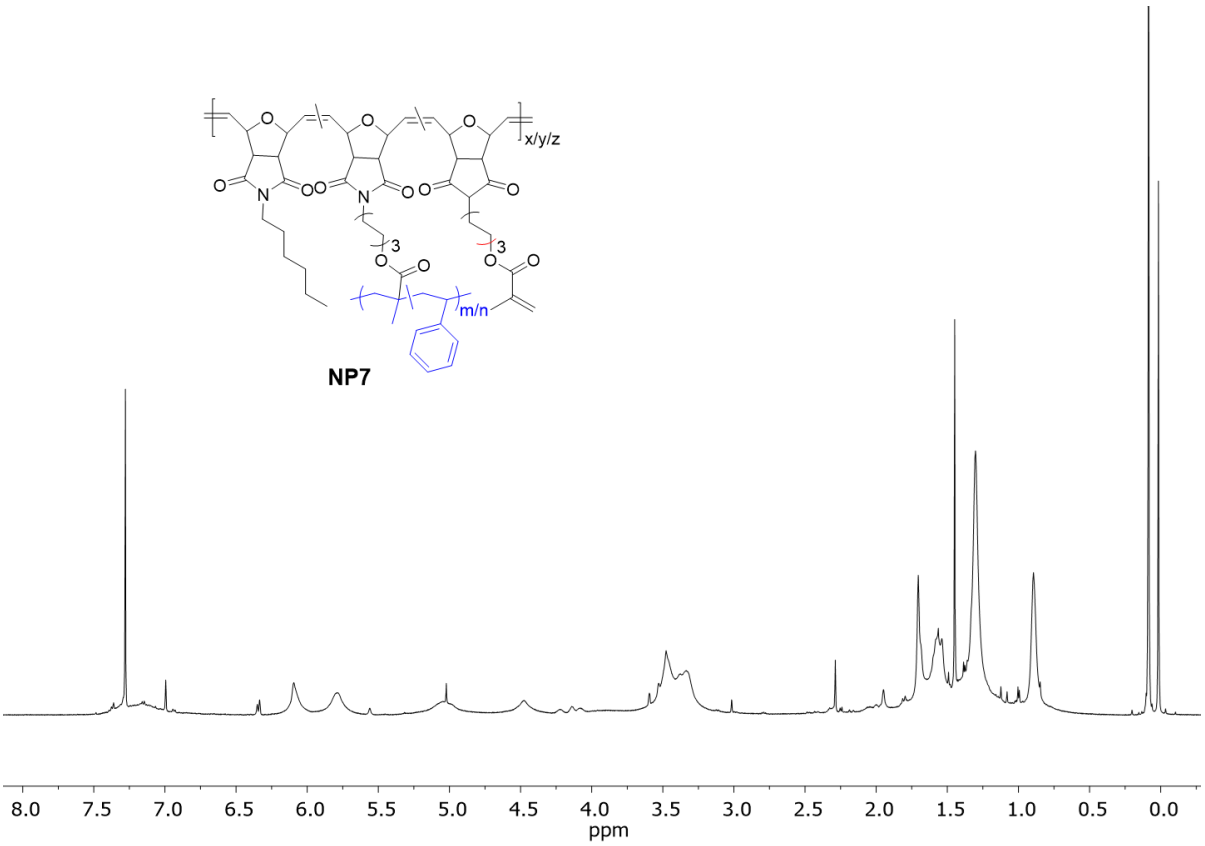

*Figure A 35. ^{1}H NMR spectrum of nanoparticle **NP7**.*

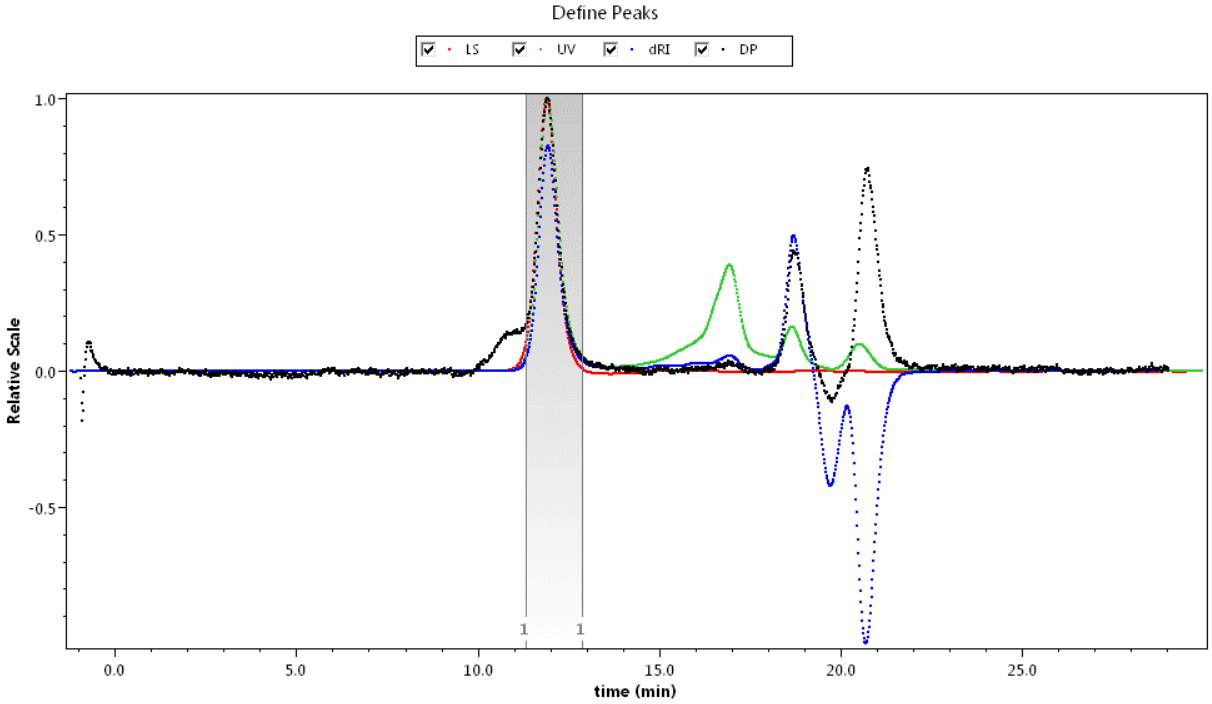

*Figure A 36. GPC trace of nanoparticle **NP7**.*

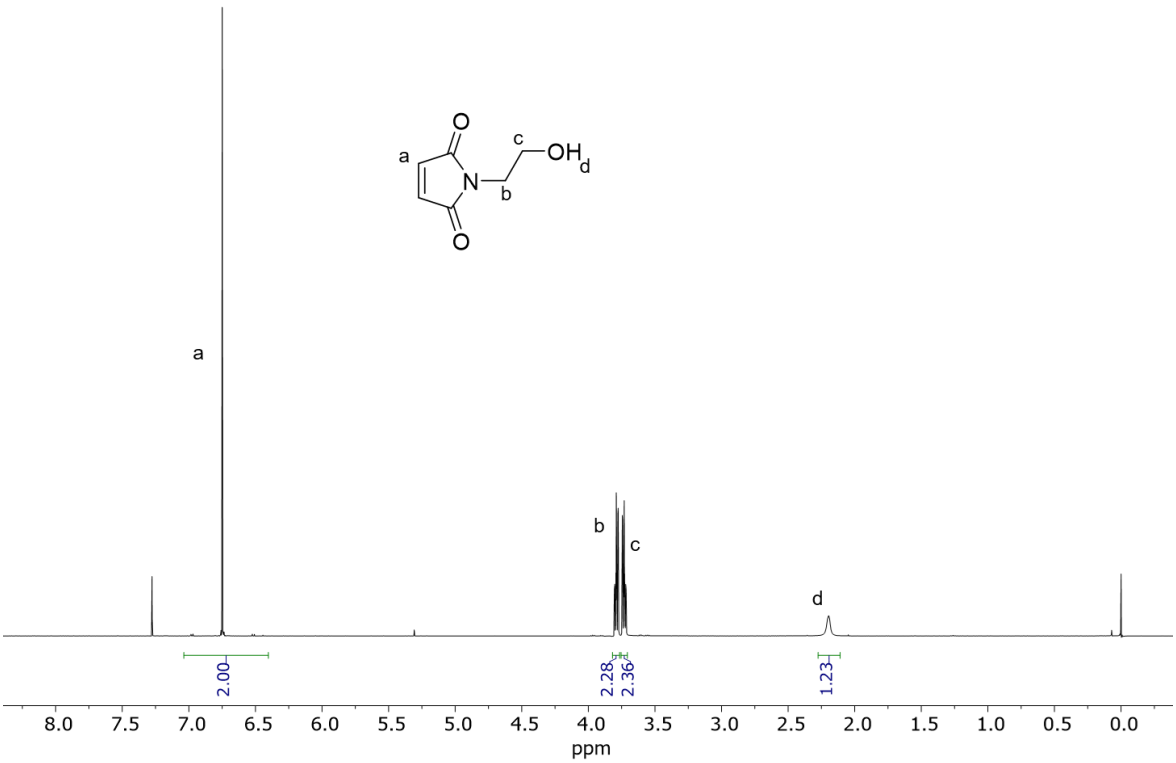

Figure A 37. [1]H NMR spectrum of M3.2.

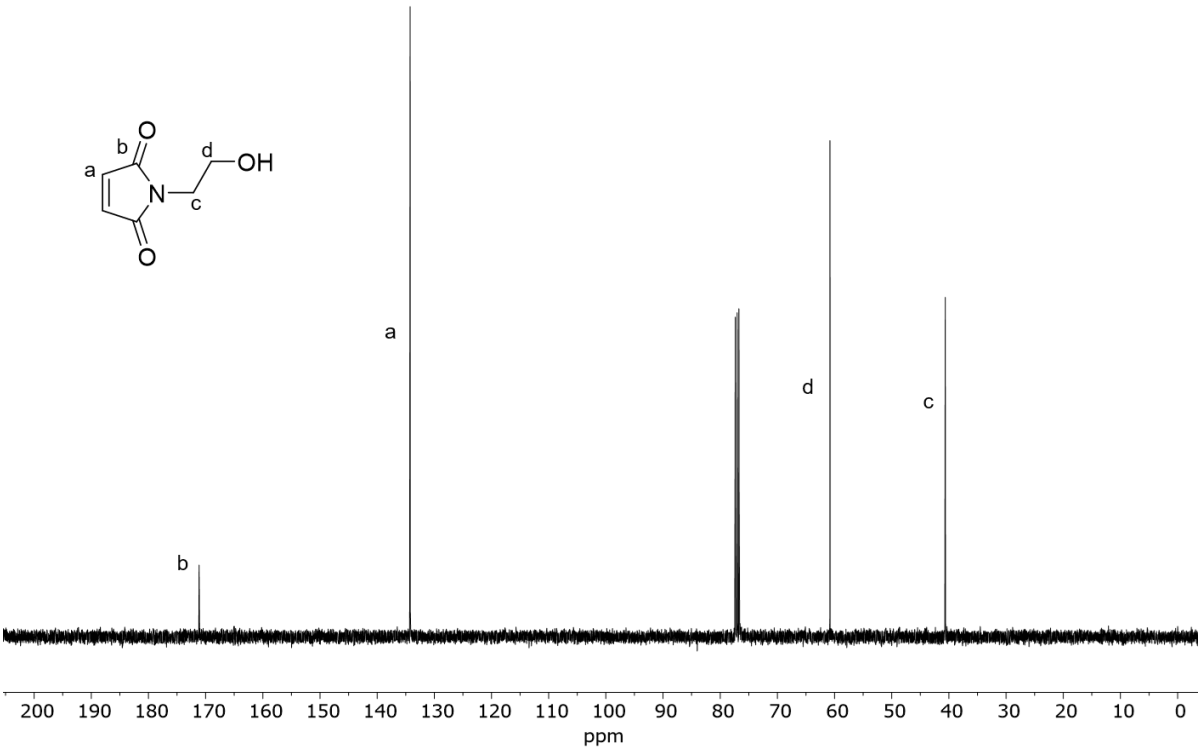

Figure A 38. [13]C NMR spectrum of M3.2.

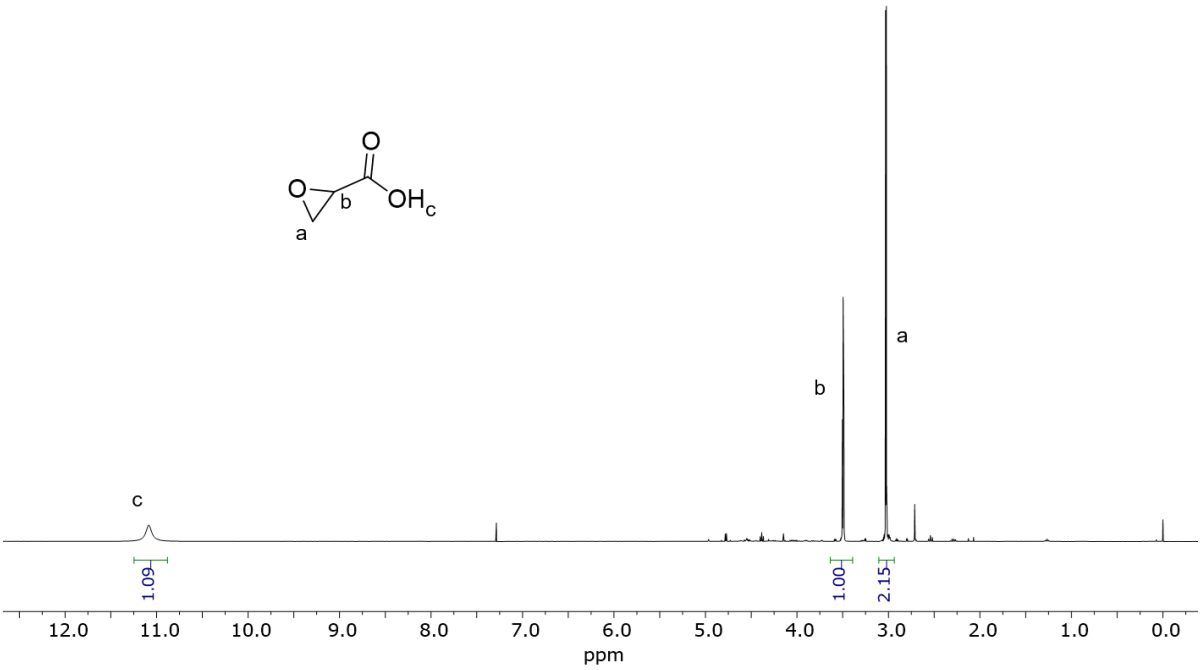

Figure A 39. ^{1}H NMR spectrum of glycidic acid.

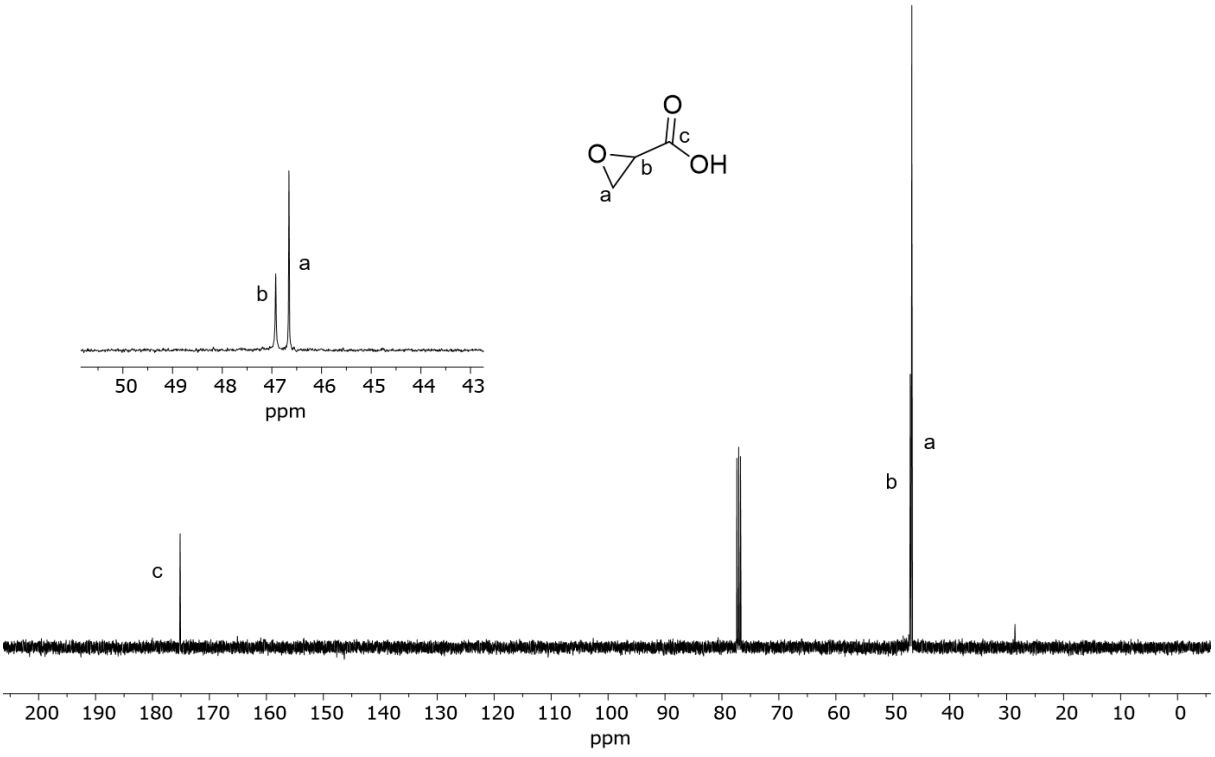

Figure A 40. ^{13}C NMR spectrum of glycidic acid.

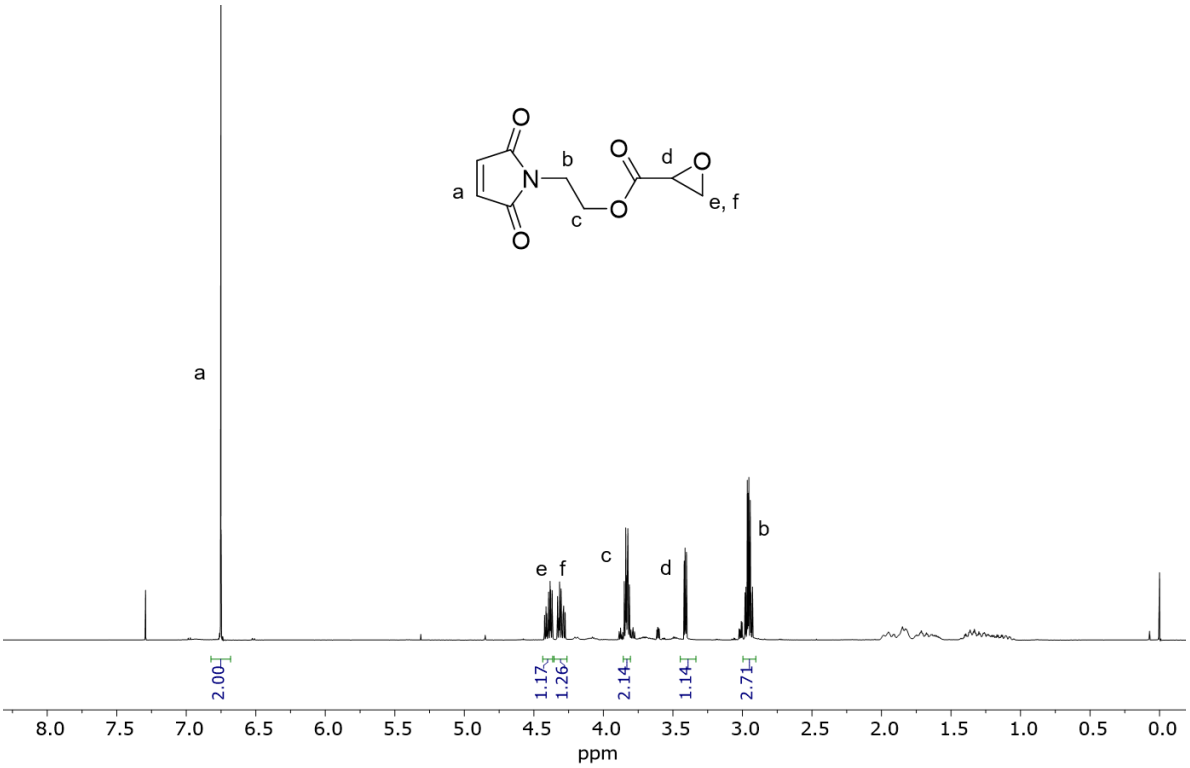

Figure A 41. [1]H NMR spectrum of M3.0b.

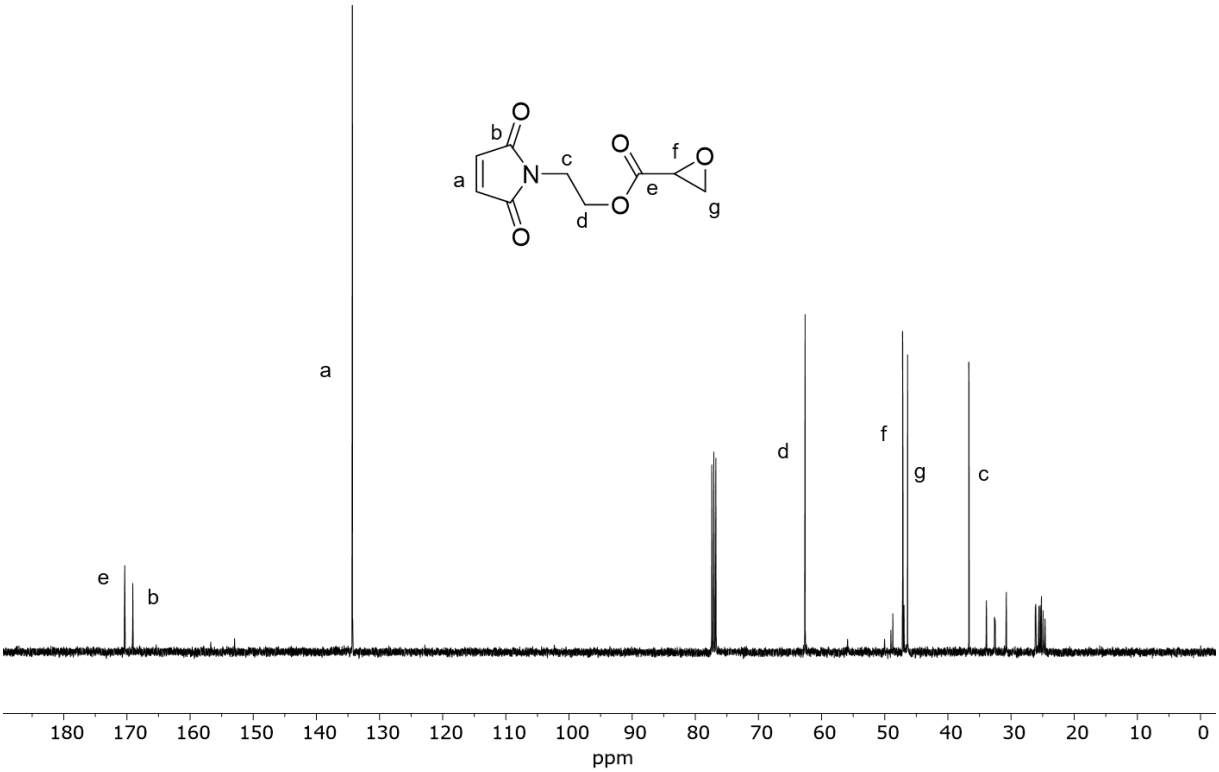

Figure A 42. [13]C NMR spectrum of M3.0b.

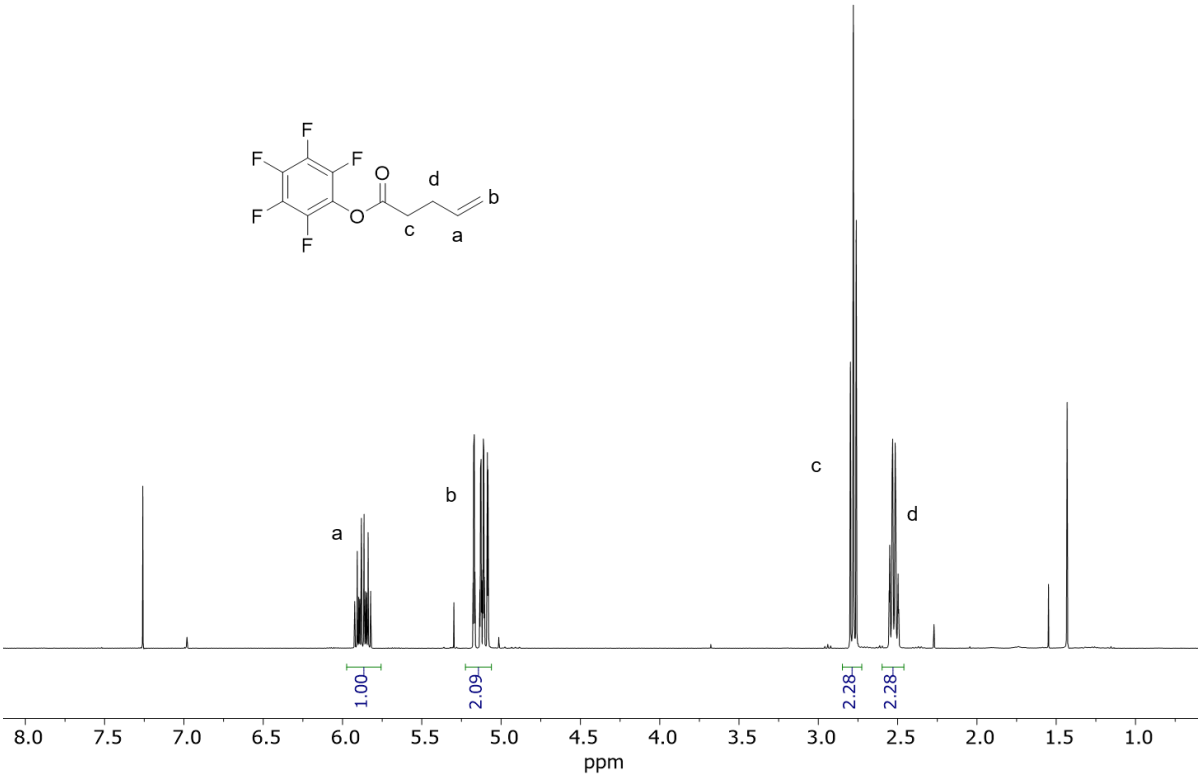

Figure A 43. [1]H NMR spectrum of M3.3.

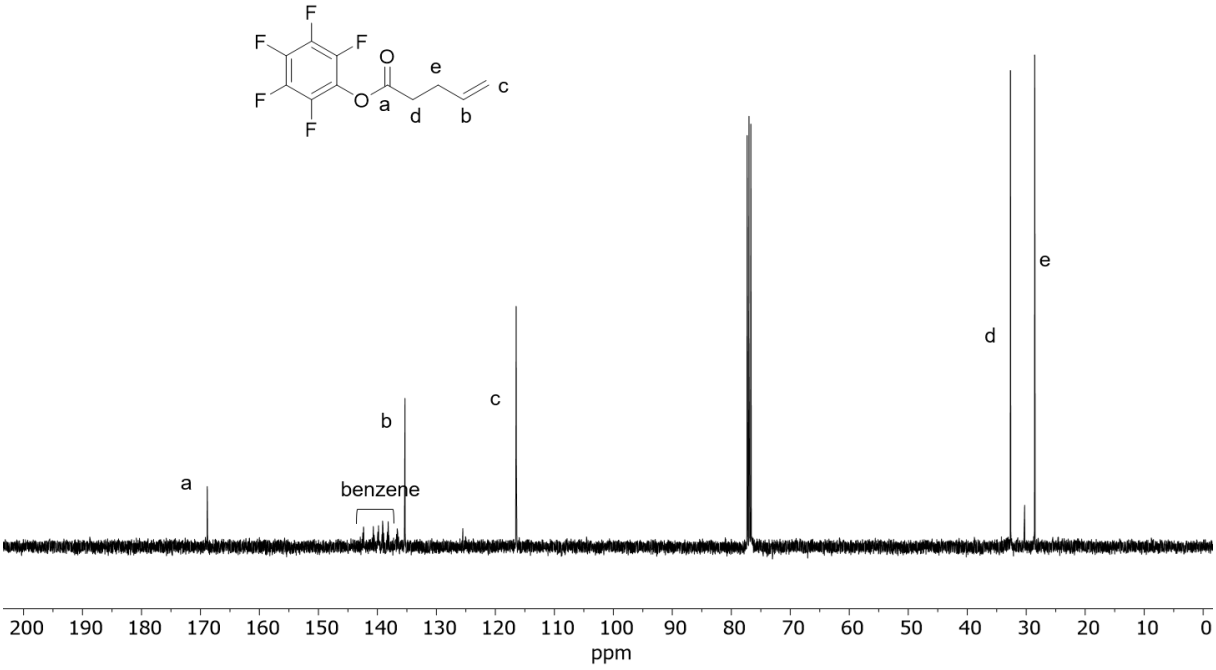

Figure A 44. [13]C NMR spectrum of M3.3.

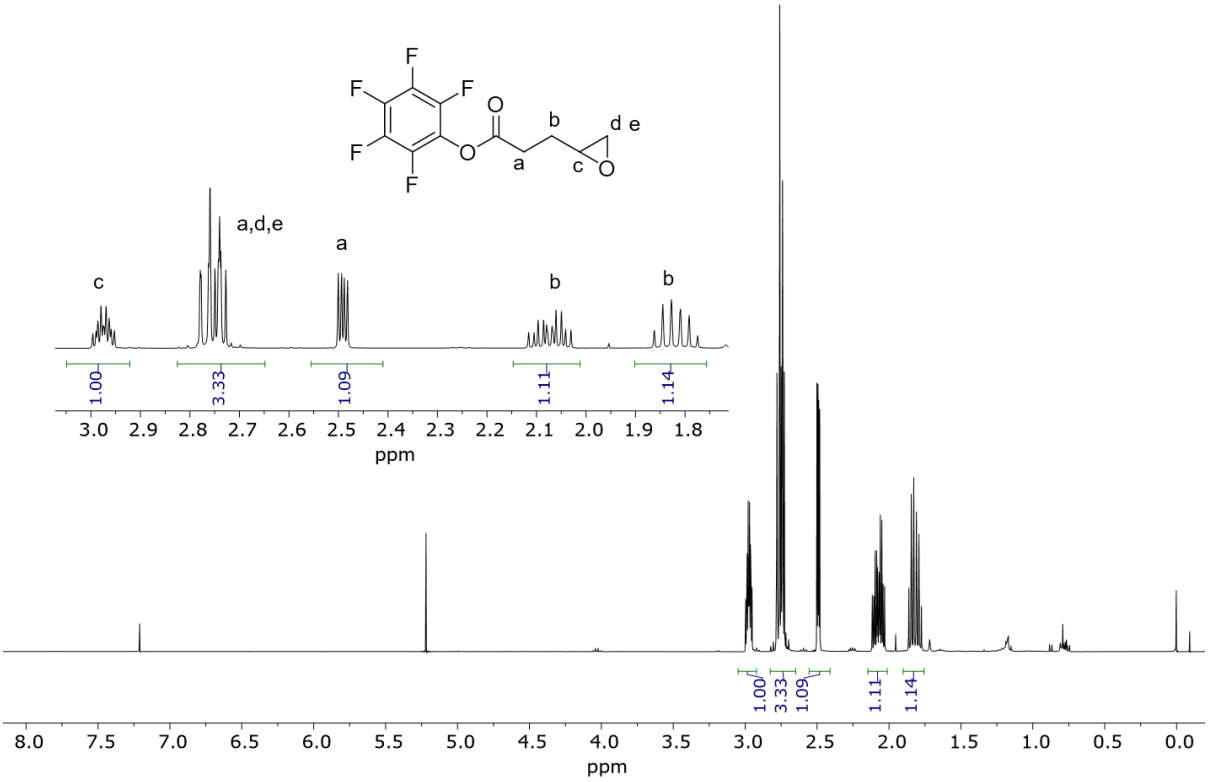

Figure A 45. [1]H NMR spectrum of M3.4.

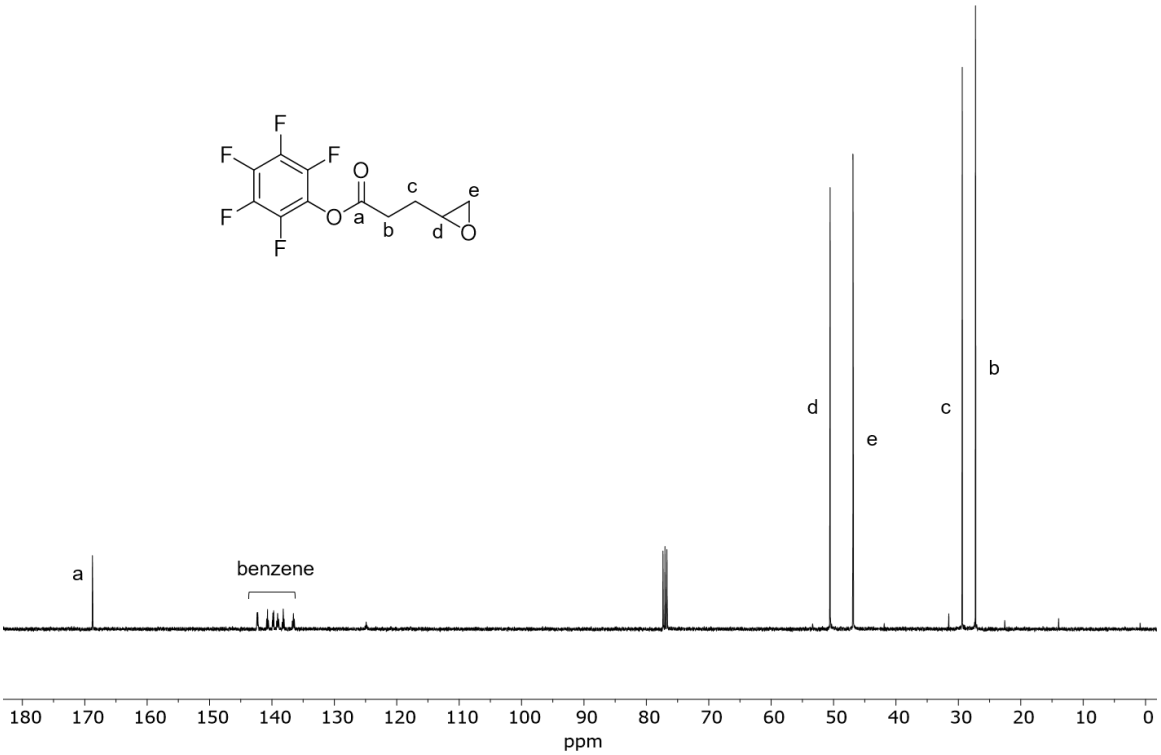

Figure A 46. [13]C NMR spectrum of M3.4.

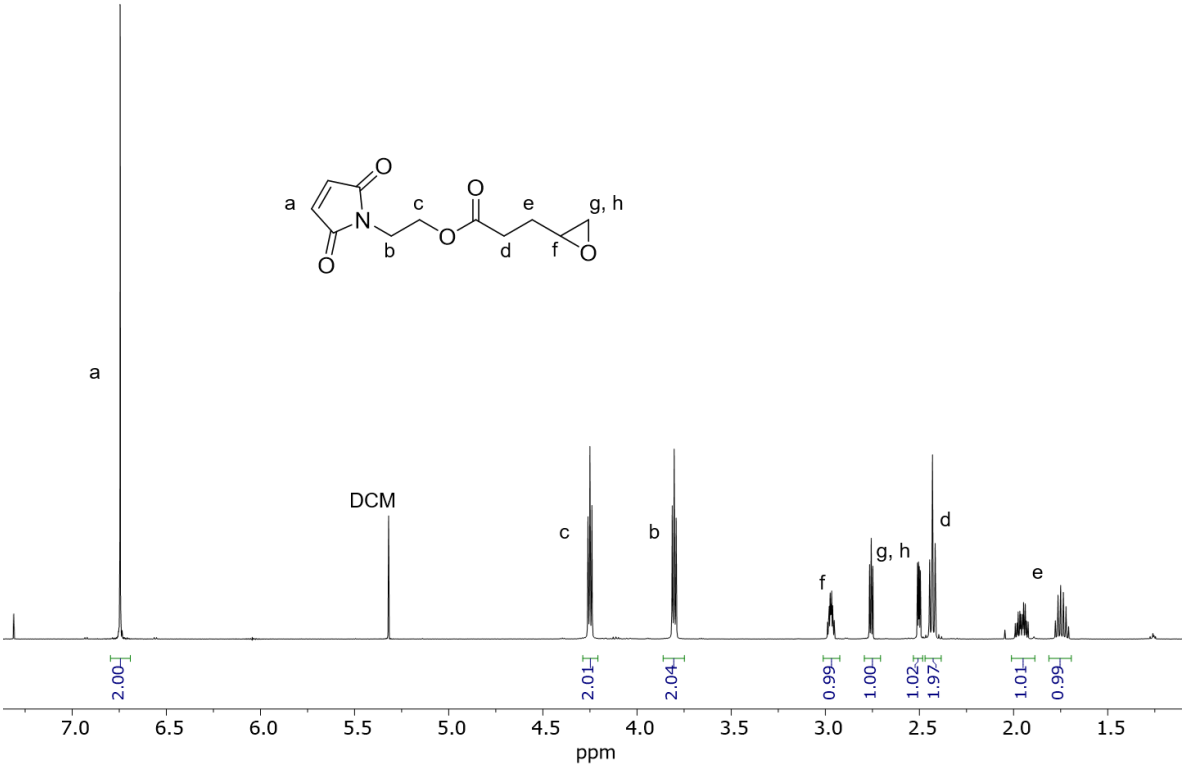

Figure A 47. [1]H NMR spectrum of M3.5.

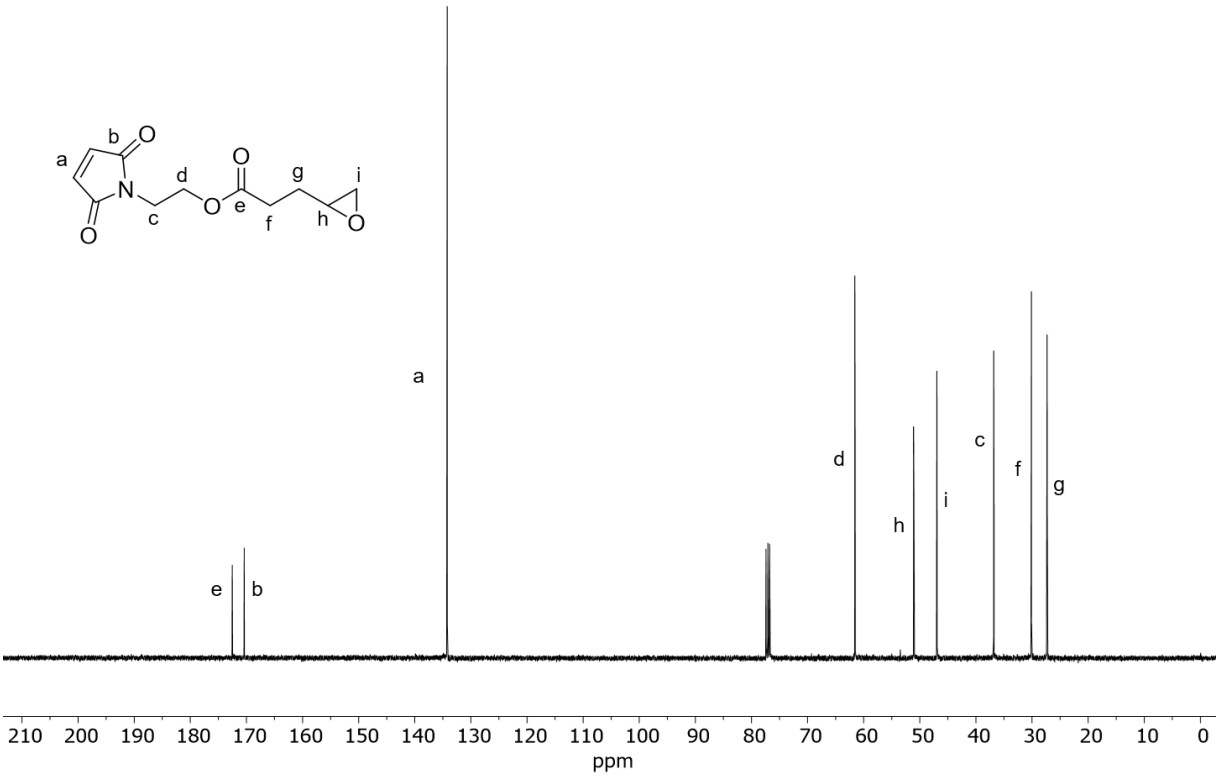

Figure A 48. [13]C NMR spectrum of M3.5.

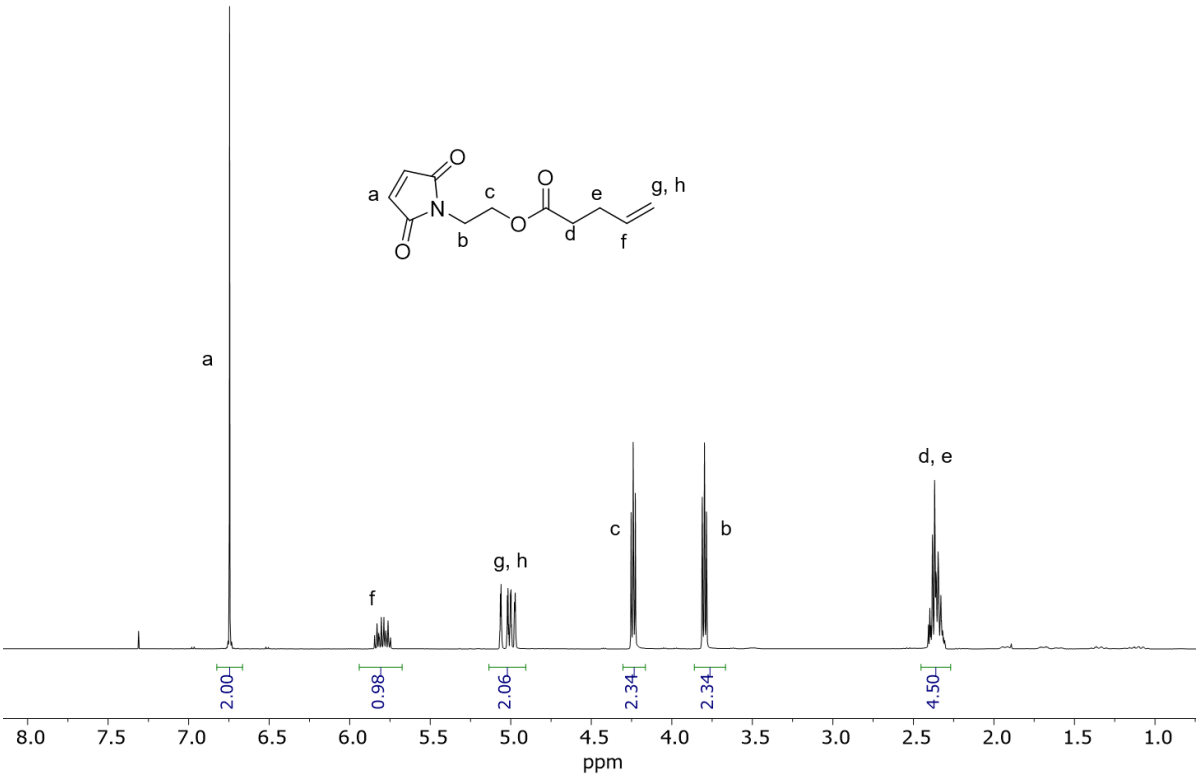

Figure A 49. [1]H NMR spectrum of M3.6.

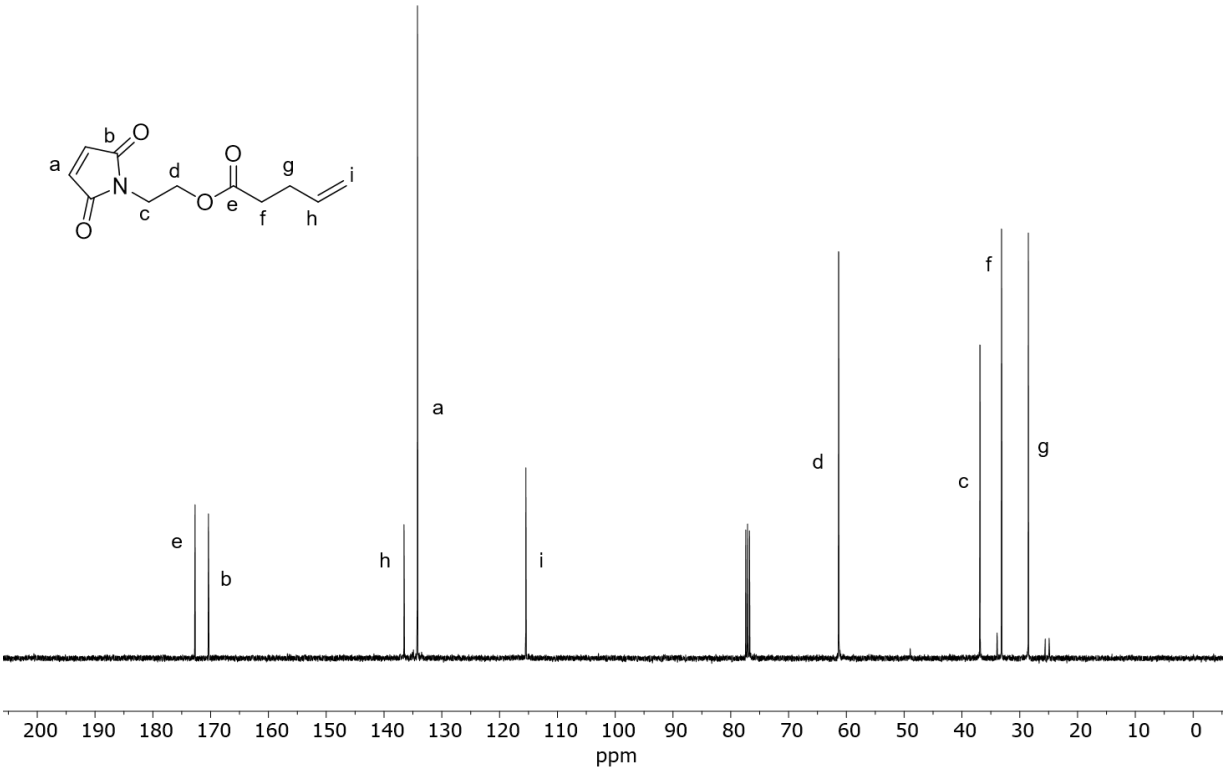

Figure A 50. [13]C NMR spectrum of M3.6.

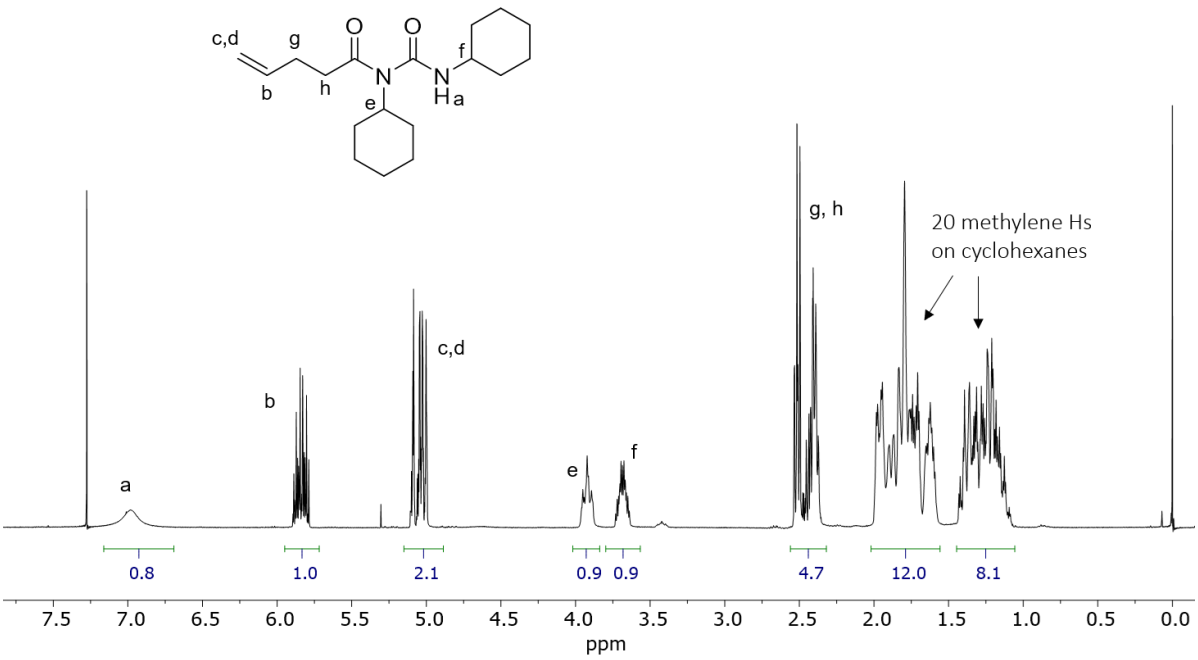

Figure A 51. ^{1}H NMR spectrum of the rearrangement product during Steglich esterification of 4-pentenoic acid and M3.2.

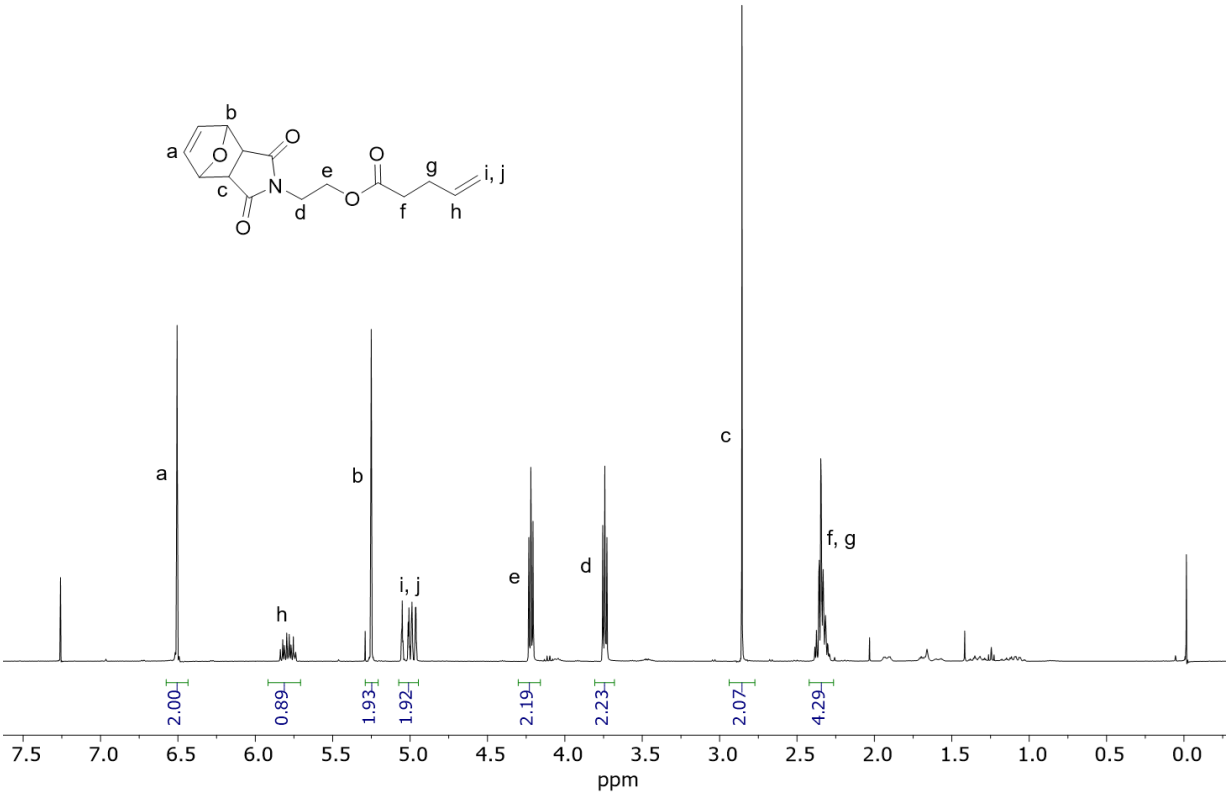

Figure A 52. ^{1}H NMR spectrum of M3.7.

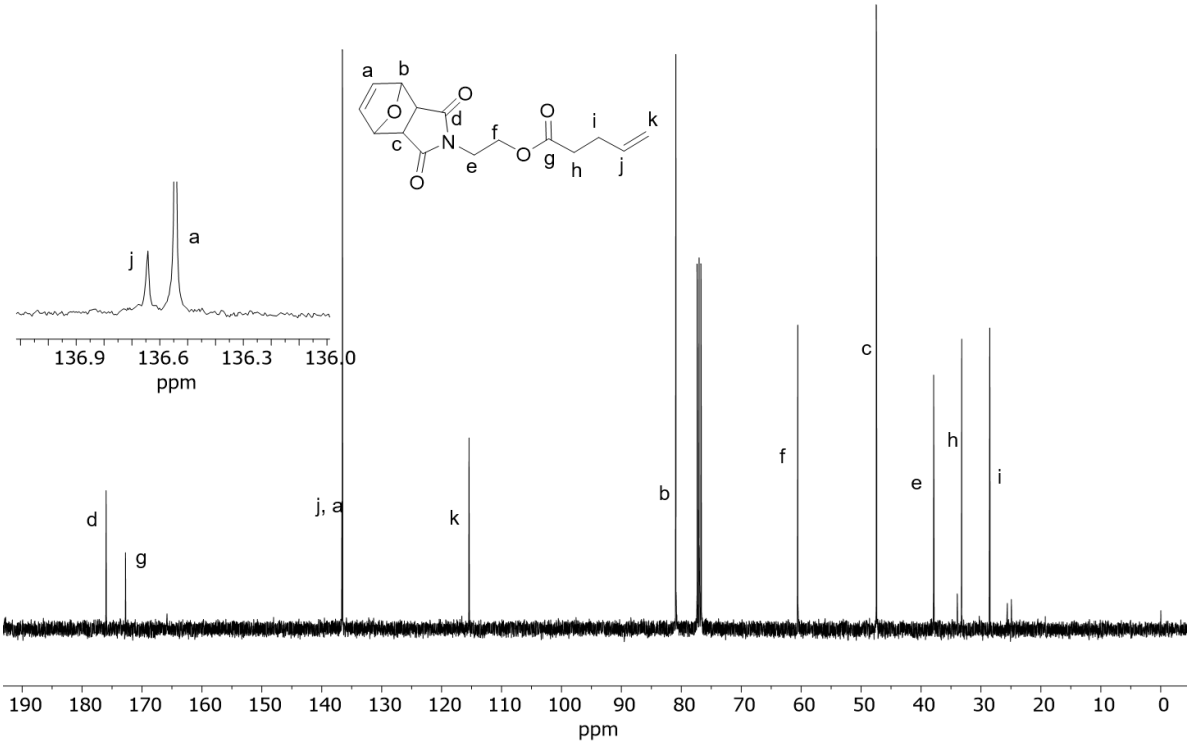

Figure A 53. [13]C NMR spectrum of M3.7.

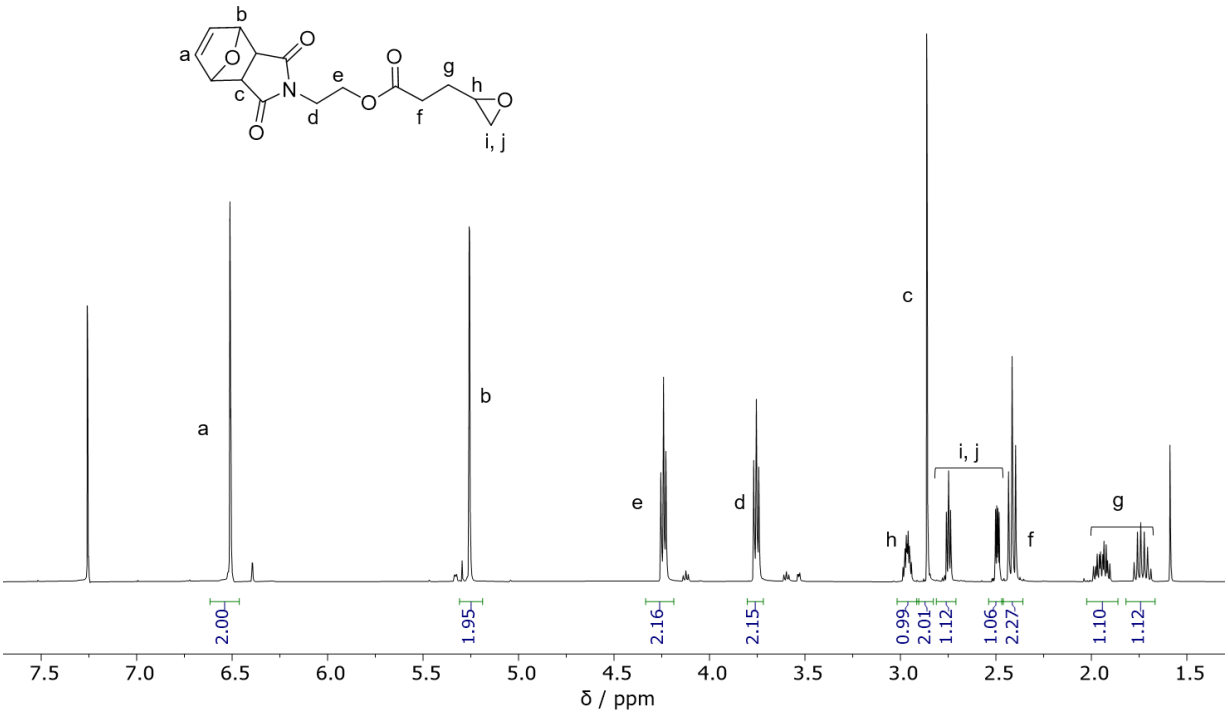

Figure A 54. [1]H NMR spectrum of M3.8.

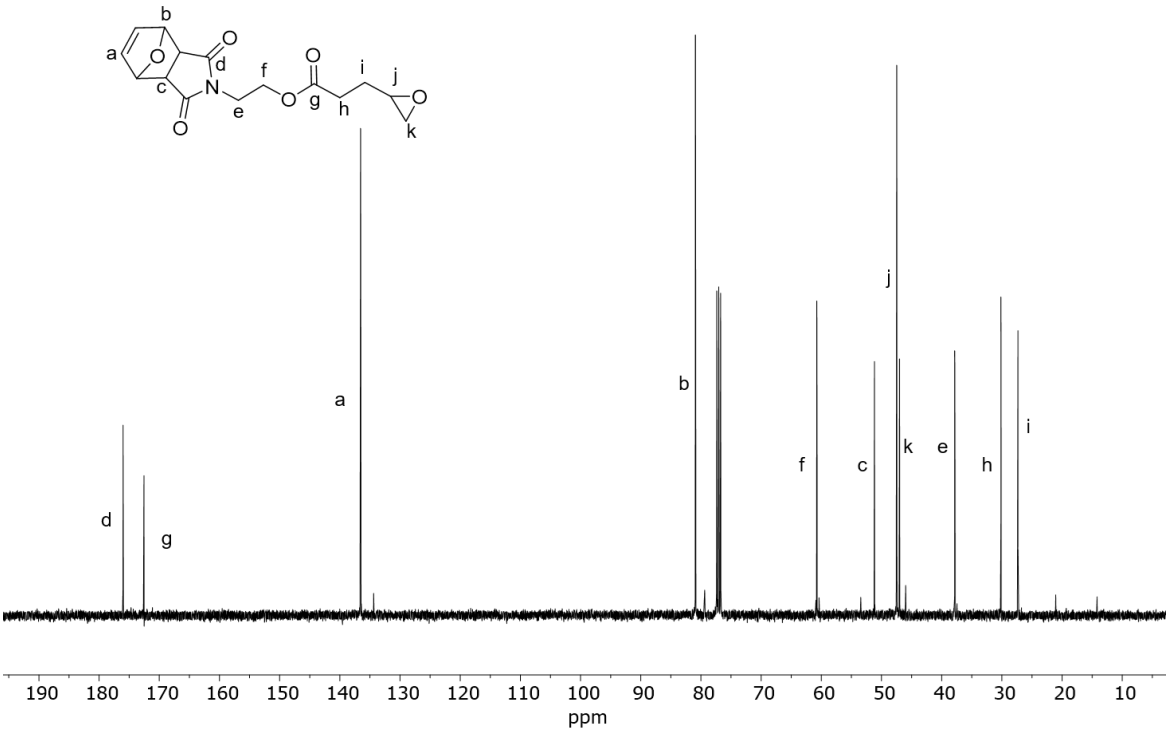

Figure A 55. ^{13}C NMR spectrum of M3.8.

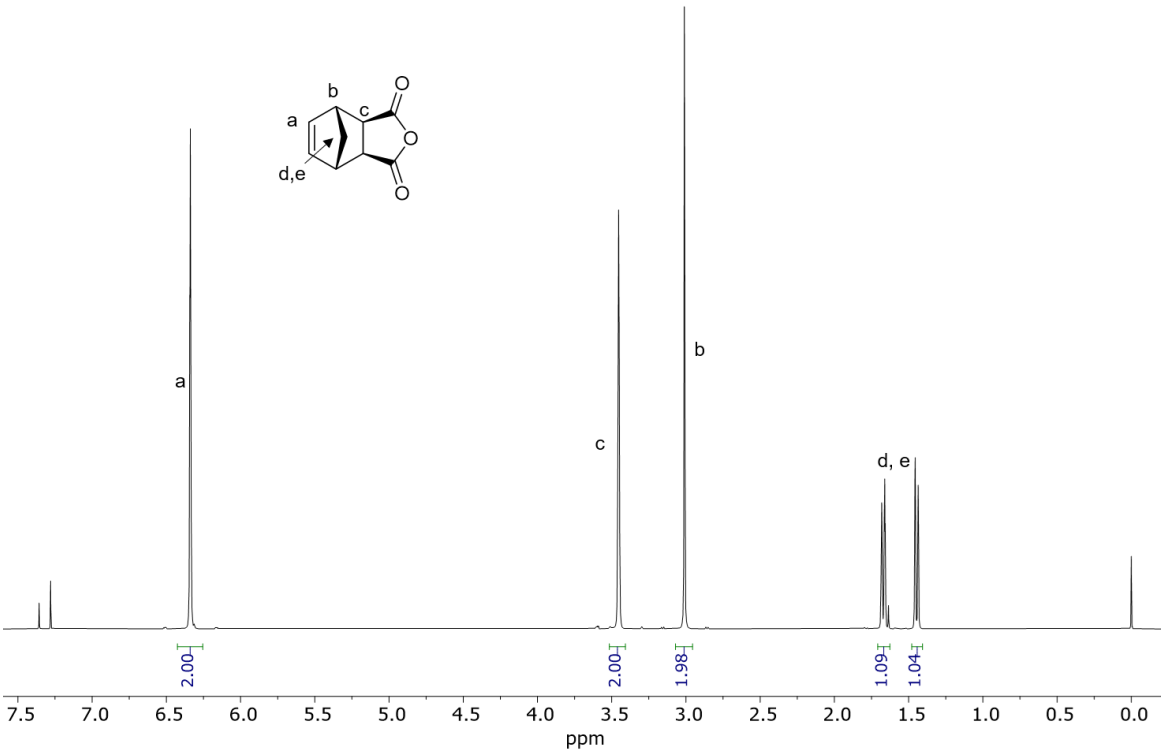

Figure A 56. ^{1}H NMR spectrum of exo-norbornene dicarboxylic anhydride.

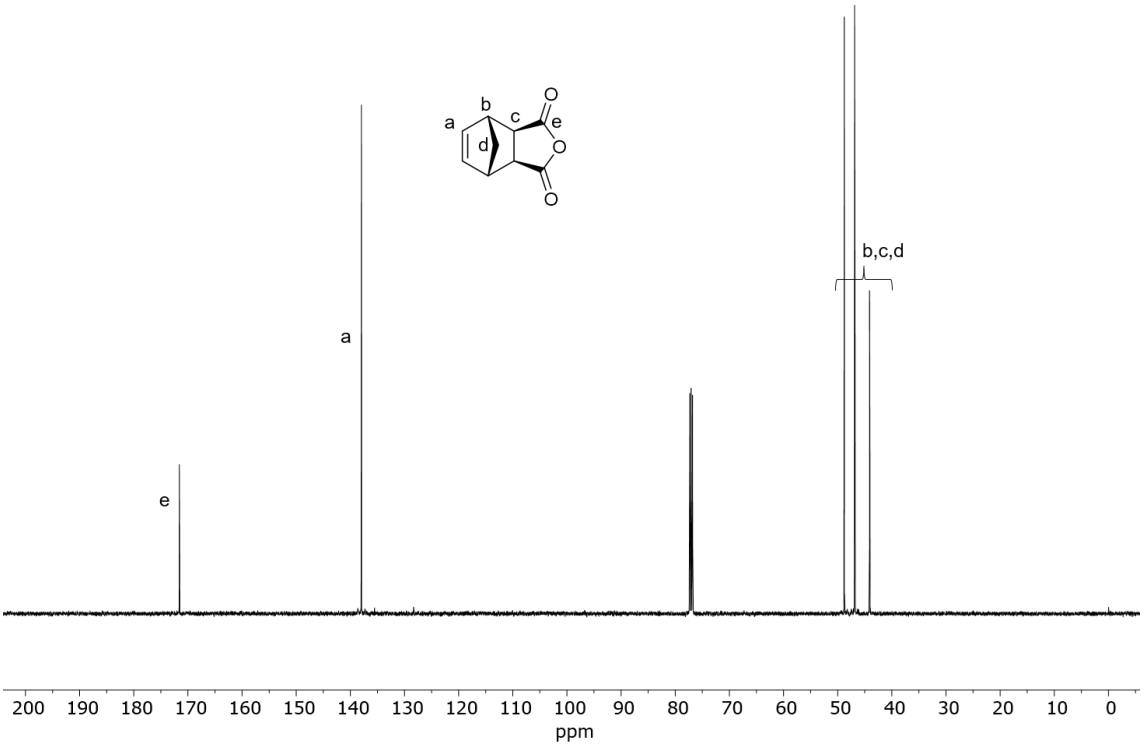

Figure A 57. ^{13}C NMR spectrum of exo-norbornene dicarboxylic anhydride.

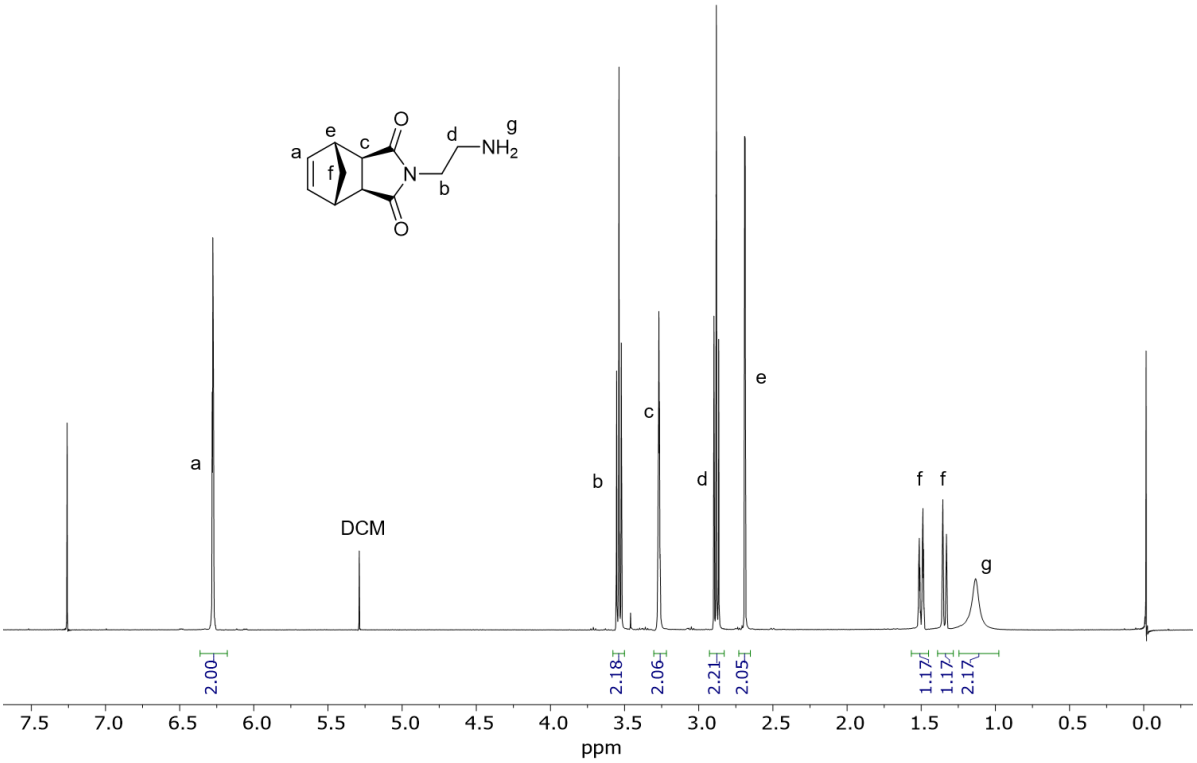

Figure A 58. ^{1}H NMR spectrum of NBI-NH_2.

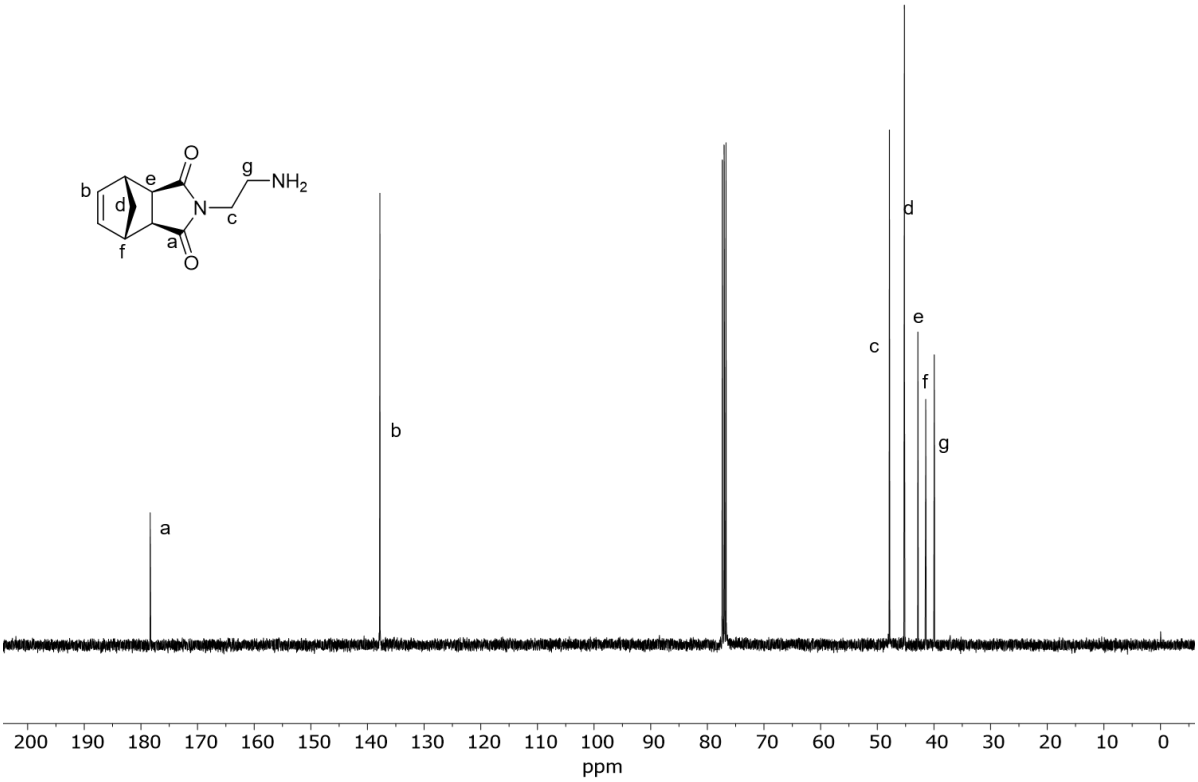

Figure A 59. ^{13}C NMR spectrum of NBI-NH_2.

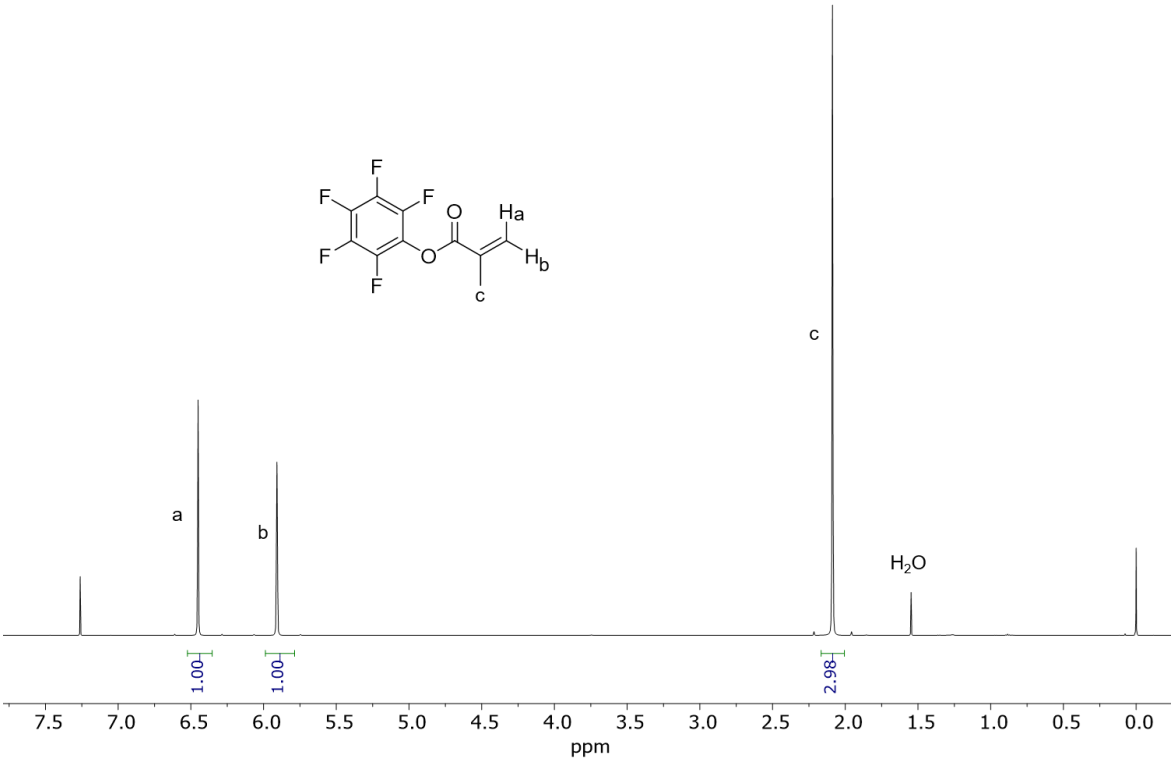

Figure A 60. ^{1}H NMR spectrum of PFP-MA.

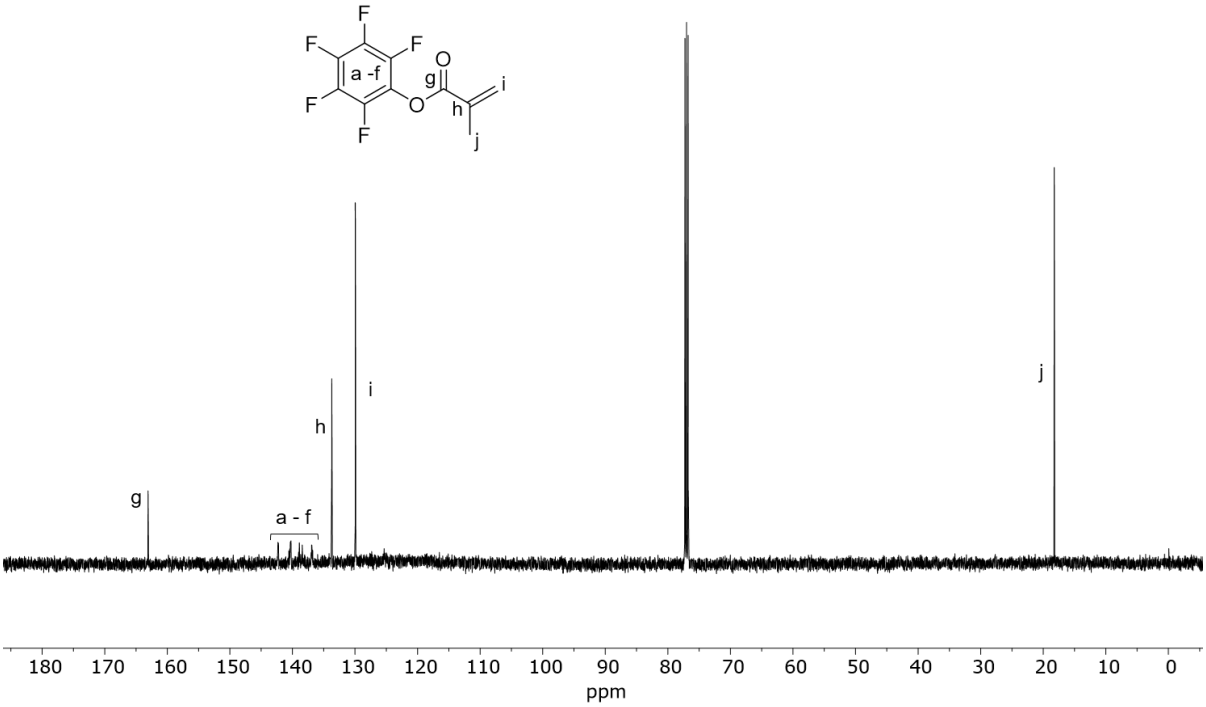

Figure A 61. [13]C NMR spectrum of PFP-MA.

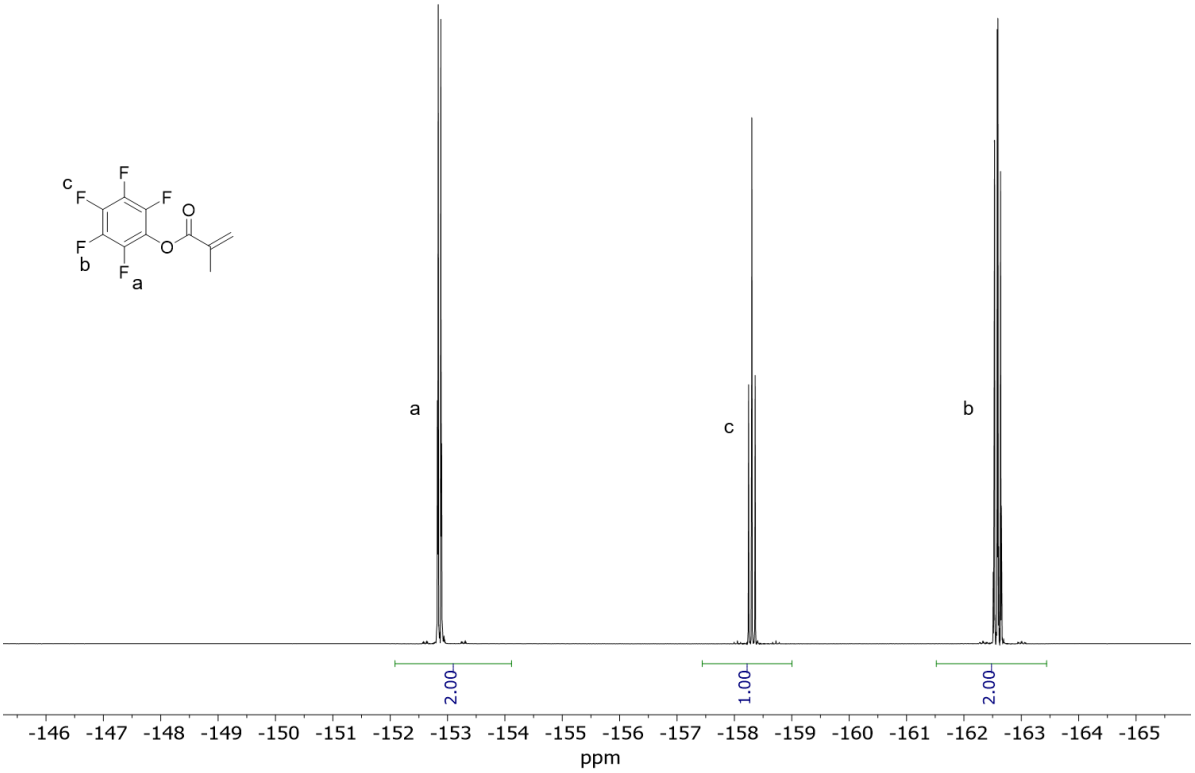

Figure A 62. [19]F NMR spectrum of PFP-MA.

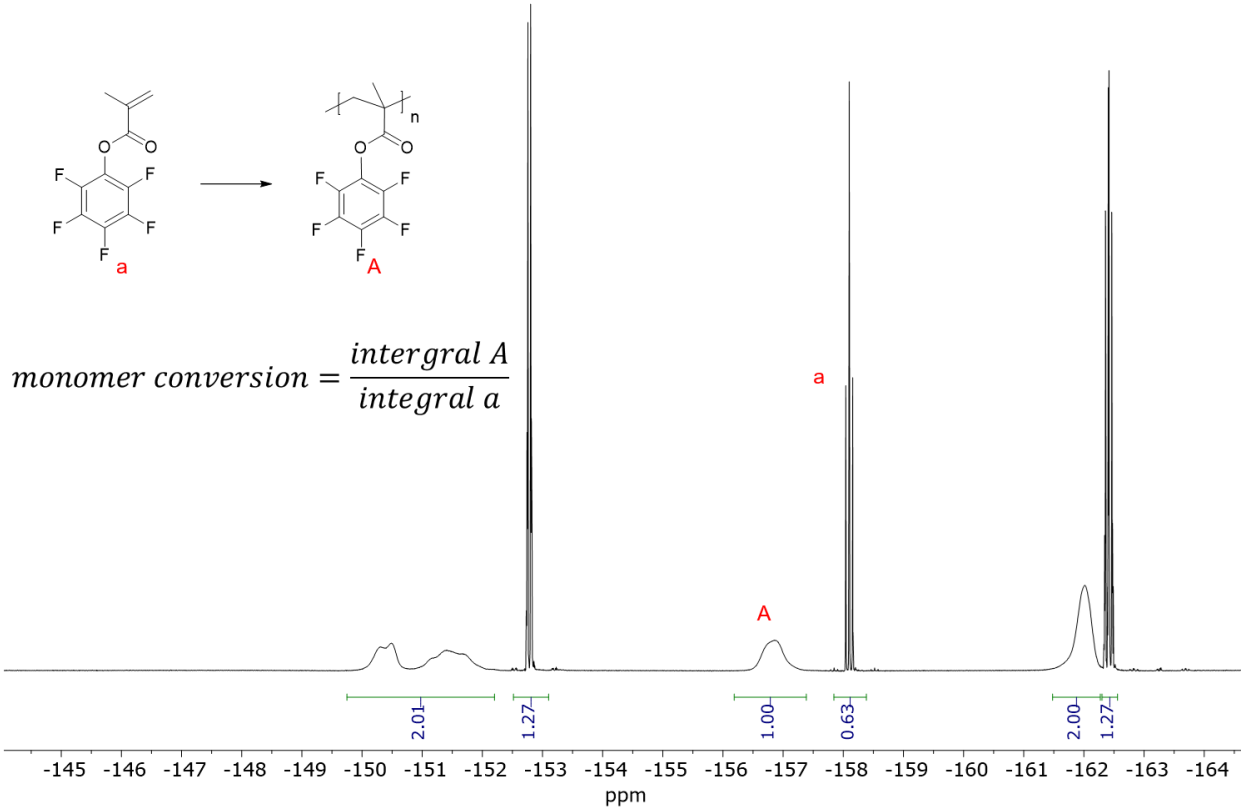

Figure A 63. Calculation of PFP-MA monomer conversion from ^{19}F NMR spectrum.